12-2016

Synthesis, Reactivity, and NMR Trends of Early Transition Metal Compounds

Tabitha Marie Cook
University of Tennessee, Knoxville, tcallawa@vols.utk.edu

To the Graduate Council:

I am submitting herewith a dissertation written by Tabitha Marie Cook entitled "Synthesis, Reactivity, and NMR Trends of Early Transition Metal Compounds." I have examined the final electronic copy of this dissertation for form and content and recommend that it be accepted in partial fulfillment of the requirements for the degree of Doctor of Philosophy, with a major in Chemistry.

Ziling Xue, Major Professor

We have read this dissertation and recommend its acceptance:

Michael Best, Craig Barnes, Hong Guo

Accepted for the Council:
Carolyn R. Hodges

Vice Provost and Dean of the Graduate School

(Original signatures are on file with official student records.)

Synthesis, Reactivity, and NMR Trends of Early Transition Metal Compounds

A Dissertation Presented for the

Doctor of Philosophy

Degree

The University of Tennessee, Knoxville

Tabitha Marie Cook

December 2016

Dedication

I would like to dedicate this dissertation to my family, both the Callaways and the Cooks, as well as to my loving husband, Matthew Cook. Without your support, I would not have made it this far.

Acknowledgments

I would like to recognize and thank the people who have given me help and support while I have been at graduate school.

First and foremost, I would like to thank my Ph. D. advisor Dr. Zi-Ling (Ben) Xue for all the time, patience, and guidance he has given to me. His enthusiasm for chemistry is an inspiration. I would like to thank Dr. Maozhong Miao who helped me get started with the tungsten project, and Dr. Adam Lamb for his help on the zirconium/hafnium project. I would also like to thank Drs. Zi-Ling Xue and Adam Lamb with their involvement in Part 5. Dr. Xue noticed the trends in a small number of complexes and conceived the concept of studying the literature. We, along with Dr. Adam C. Lamb, searched the literature and provided the interpretation of the trends. I would also like to thank Drs. Michael Richmond and David Hrovat at the University of North Texas for doing DFT calculations for the NMR shifts of Cp_2MMe_2 complexes in Table C14 in Appendix C.

I would also like to thank my other committee members, Drs. Michael Best, Craig Barnes, and Hong Guo for their advice in the various defenses I have presented to them. I also had the pleasure of taking classes from Drs. Zi-Ling Xue, Michael Best, Craig Barnes, David Jenkins, Jon Camden, Carlos Steren, and George Schweitzer. It was an honor to be a student of each of these professors. I learned a great deal in each of their classes. I would also like to thank Drs. Liguo Song and Stephen Gibson for their help in teaching me how to use the mass spectrometer. To Dr. Stephen Gibson, thank

you for your enthusiasm about isotopic patterns in my samples. I would also like to thank Dr. Yvette Yang for her guidance in teaching. Thank you for allowing me to be one of your teaching assistants and your head teaching assistant for general chemistry. I learned a lot from that experience. Thank you as well to Dr. Zi-Ling Xue for allowing me to be teacher's assistant to your advanced inorganic lab as well as your graduate class.

While working as a graduate student, I had some amazing lab mates, who helped made graduate school easier to survive and a lot more fun. To past members, Kendhl Witt as well as Drs. Adam Lamb, Samuel Rosolina, and Jonathan Fong, I miss our hilarious lunch conversations and our walks to lunch. I would also like to thank Dr. Maozhong Miao for helping me get started in the Xue group and showing me the ropes around the lab. I would also like to thank other past members of the Xue group, Drs. Stephanie Bragg, Bhavna Sharma, and Seth Hunter for their support. I would also like to thank my current lab mates, Roberto Federico-Perez, Duncan Moseley, Shelby Stavretis, and Thomas Carpenter. I wish you all the best of luck! You all are wonderful, and I am excited to see where you go in life. Thank you to Dr. Gaya Elpitiya, a postdoc in the Jenkins lab, for your wonderful personality and always making me smile. I would also like to thank Lena Elenchin in the Barnes group. You were my roommate when we first visited UTK, and I'm so glad we remained good friends throughout our time as graduate students. You are an amazing and hilarious person. Thanks for your support through the good and bad times.

I would also like to thank Dr. Carlos Steren for his help with the NMR instruments. I would also like to thank Bo Bishop for being an amazing glassblower and

for his sense of humor, as well as Tim Free for always keeping our pumps functional and his stories about UTK's past. I would also like to thank Bill Gurley who was always willing to help us with any electronic problems and for his friendship. To Neal Fischer, manager of the general chemistry labs, I will miss our hallway conversations. Thanks for always checking in on me. Thank you as well to Dr. Patrick Hillesheim for showing me some new tricks to solving crystal structures.

I would also like to thank my chemistry professors at Berry College, Drs. Kenneth Martin, Alice Suroviec, Kevin Hoke, and Charles Earnest. Your help and enthusiasm helped me prepare for graduate school. To my undergraduate academic and research advisor, Dr. Kenneth Martin, thank you for your patience and time with me and showing me me how cool crystals are. I continued using crystallography though graduate school, and the tricks you taught me were instrumental.

I would like to thank my friends and family for all their support while I have been in graduate school. To my previous roommates, Amanda Faint and Julie Beaton, thank you for being willing to listen to me when things got hard and laugh with me when times were easy. I would also like to thank my family at Cornerstone Church of Knoxville for all their patience, love, and support. I could not have gotten this far without my family. To my mother, Heidi Callaway, you are an amazing mom and a wonderful woman. To my brother, James Callaway, and my grandmother, Mary Cameron, thanks for always being there for me to chat while I drove home after work. To my grandparents, Michael and Virginia Callaway, thank you for being there always for me. I would also like to thank my husband's family. To his parents, Gary and Kathy Cook, thank you for accepting me into your family. To my brothers- and sisters-in-law, Brandon and Melody

Cook, and Jeremy and Nichoal Cook, thank you also for being there for me. To my husband, Matthew Cook, I could not ask for a better life partner. Thank you for your love and help that you have given me.

I would lastly like to thank UTK for accepting me and hosting me as a graduate student and the National Science Foundation (NSF) for funding my research.

Abstract

This dissertation focuses of three different subjects. The first is the synthesis and characterization of heptacoordinate amidinate compounds. Heptacoordinate compounds are not common, but their structures have been studied. Group 4 amidinate compounds have been used as precursors in the CVD/ ALD processes. Ancillary ligands, such as amidinates, have been used to reduce air-sensitivity of complexes. Reactions of these complexes with water have been used to make metal oxide thin films.

In the first study, the complexes $Zr[MeC(N^iPr)_2]_3Cl$ [zirconium trisamidinate chloride], $Hf[MeC(N^iPr)_2]_3Cl$ [hafnium trisamidinate chloride], $Zr[MeC(N^iPr)_2]_3Me$ [zirconium trisamidinate methyl], $Hf[MeC(N^iPr)_2]_3Me$ [hafnium trisamidinate methyl], $Zr[MeC(N^iPr)_2]_3Et$ [zirconium trisamidinate ethyl], and $Hf[MeC(N^iPr)_2]_3Me$ [hafnium trisamidinate methyl] have been synthesized and characterized. The three amidinate ligands bind to the metal centers in a propeller-like fashion. This allows for Λ [lambda] and Δ [delta] enantiomers, which undergo fast exchange in solution. All of these complexes were also found to react with water in air to form $Zr[MeC(N^iPr)_2]_3OH$ [zirconium trisamidinate hydroxyl] or $Hf[MeC(N^iPr)_2]_3OH$ [hafnium trisamidinate hydroxyl] complexes.

The second portion of the dissertation focuses on the reactions of tungsten alkylidyne complexes with water. When $W(\equiv CSiMe_3)(CH_2SiMe_3)_3$ [tungsten neosilyl neosilylidyne] is reacted with water at room temperature, a tungsten trimer was formed

and characterized via NMR spectroscopies and single-crystal X-ray diffraction. The reaction of a second complex, W(≡C^{t}Bu)(O^{t}Bu)$_3$ [tungsten alkoxide neopentylidyne] with water was studied via NMR and mass spectrometries. While only one complex formed via the NMR-scale reactions, several more were identified using the DART ionizer to react W(≡C^{t}Bu)(O^{t}Bu)$_3$ [tungsten alkoxide neopentylidyne] with water in air before being analyzed via MS.

The last subject focuses on the chemical shift trends of d^0 [d0] metal complexes. Two trends have been identified and will be discussed in Part 5. The first trend, usually pertaining to hydride and alkyl complexes, is a downfield shift in the peaks of the α [alpha] atoms in first- and third-row metals from those of the second-row analogs. The first trend, which usually relates to alkylidene, alkylidyne, oxo, and fluoro complexes, is an upfield shift in the peaks of the α atoms in first- and third-row metals from those of the second-row analogs.

Table of Contents

List of Tables

List of Figures

List of Schemes

Numbering Scheme of Compounds in the Text

1 $Zr[MeC(N^{i}Pr)_2]_3Cl$

2 $Hf[MeC(N^{i}Pr)_2]_3Cl$

3 $Zr[MeC(N^{i}Pr)_2]_3Me$

4 $Hf[MeC(N^{i}Pr)_2]_3Me$

5 $EtMgCl$

6 $Zr[MeC(N^{i}Pr)_2]_3Et$

7 $Hf[MeC(N^{i}Pr)_2]_3Et$

8 $Zr[MeC(N^{i}Pr)_2]_3OH$

9 $Hf[MeC(N^{i}Pr)_2]_3OH$

10 $W(\equiv C^{t}Bu)(O^{t}Bu)_3$

11 $W(\equiv CSiMe_3)(CH_2SiMe_3)_3$

12 $[(\mu\text{-}O)W(CH_2SiMe_3)_2(=O)(THF)]_3$

13 $W(CH_2{}^{t}Bu)(O^{t}Bu)_3(=O)$

14 $W(\equiv C^{t}Bu)(O^{t}Bu)(=O)$

15 $W(\equiv C^{t}Bu)(O^{t}Bu)_2(OH)$

16 $W(=CH^{t}Bu)(O^{t}Bu)_2(=O)$

17 $W(CH_2{}^{t}Bu)(O^{t}Bu)(=O)_2$

18 $W(CH_2{}^{t}Bu)(OH)(=O)_2$

Nomenclature and Abbreviations

ALD	Atomic Layer Deposition
CVD	Chemical Vapor Deposition
DART	Data Analysis in Real Time
DEPT	Distortionless Enhancement by Polarization Transfer
DFT	Density Functional Theory
GC	Gas Chromatography
HQSC	Heteronuclear Single Quantum Correlation
MS	Mass Spectrometry
NMR	Nuclear Magnetic Resonance
ORTEP	Oak Ridge Thermal Ellipsoid Plot
SOC	Spin-Orbital Coupling
TOF	Time-of-Flight
VT	Variable-Temperature

Part 1

Introduction and Background

This dissertation covers three areas of my Ph. D. research: (1) Synthesis, characterization, and reactions of heptacoordinated Group 4 complexes; (2) Reactions of W alkylidyne complexes with water; (3) Overview of two NMR trends observed in d^0 transition metal complexes. This part provides a brief introduction to these three parts.

1.1. Introduction

1.1.1. Heptacoordinated Complexes

There are relatively few heptacoordinated complexes. In the Chemical Structural Database (CSD), these complexes represent >2% of all complexes.[1,2] The active sites of a few metalloproteins have heptacoordinated metals. These include the Cd center in cellobiose oxidase,[3] Mo centers in the oxidized form of DMSO oxidase,[4] and Mn atoms in glutamine synthetase.[5] This coordination number is also found in the chemistry of d^4 Mo and W complexes containing carbon monoxide ligands.[6]

The studies on heptacoordinate complexes mostly pertain to their unique geometries.[2,7] There is no regular polyhedron which can adequately describe coordination sphere of these complexes.[2] Heptacoordinate complexes usually take one of three stereochemistries: pentagonal bipyramid, capped octahedron, and the capped trigonal prism (Figure 1.1). Among these three geometries, the pentagonal bipyramid is the most common.[2] Complexes with three bidentate ligands and one monodentate ligand, like the complexes presented in Parts 2 and 3, generally prefer the capped octahedron geometry. The bidentate ligands bind to the central metal in a propeller-like geometry similar to that of $Co(en)_3^{3+}$ (en = ethylenediamine). This forms a three-fold axis of rotation along the central axis containing the monodentate ligand.[2,7]

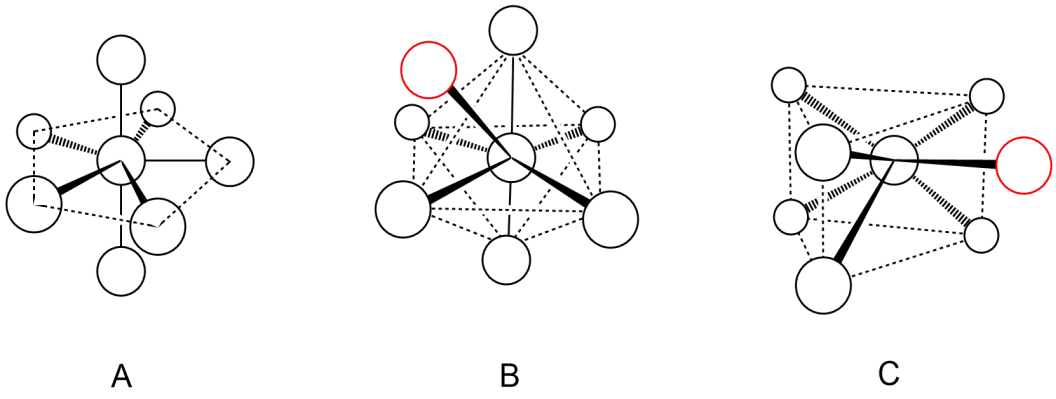

Figure 1.1. Models of the pentagonal bipyramid (A), capped octahedron (B), and the capped trigonal prism (C) geometries.[2,7] Dotted lines on A for the five, in-plane, equatorial atoms, on B for the edges on the octahedral, and on C show the edges of the trigonal prism. The 'caps' on B and C are shown in red.

1.1.2. Precursors to Metal Oxide Thin Films

Microelectronic devices such as smartphones and computers are an integral part of the present-day society. Complementary metal-oxide semiconductor (CMOS) field effect transistor (FET) (Scheme 1.1) is one of the most important parts of the integrated circuits in these devices. Improving and scaling of the CMOS have resulted in smaller, more efficient devices. Over the past 40 years, there has been steady progress in this area following Moore's law, which states the number of transistors that can fit onto an integrated circuit doubles approximately every two years.[8] To keep pace with Moore's law, new designs for the transistors as well as new materials are needed.

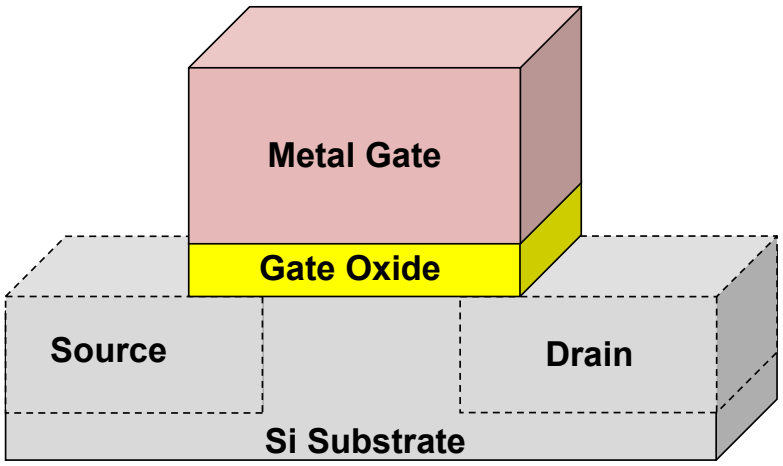

Scheme 1.1. Scheme of a transistor in a microelectronic device.

Inorganic compounds, including d^0 complexes, have been used as precursors to fabricate gate oxide layers in microelectronics. This layer separates the terminals in a transistor from the source and drain as well as acts as a channel to both the source and drain. This layer is made of dielectric materials, which is polarized when placed in an electric field.[9] Until recently, SiO_2 was used as the primary gate oxide film. SiO_2, however, has a small dielectric constant (*k*) of 3.9. As the film gets thinner (<2 nm), current leakage is larger, generating heat and wasting energy. This leakage can cause degradation of the transistor over time. Because of the high current leakage, there is a limit to how much the SiO_2 layer can be scaled down before it is no longer efficient as an insulating material.[8,10] Metal gate oxide layers made with materials with high-*k* values (Table 1.1)[10b] are better insulators and are able to be scaled down further than SiO_2 while still maintaining their insulating capabilities. For this reason, companies such as Intel™ now use HfO_2-based materials.

Table 1.1. List of metal oxides and their dielectric constants[10b]

Metal Oxide	*k*
SiO_2	3.9
Al_2O_3	9
Y_2O_3	15
La_2O_3	30
TiO_2	80
ZrO_2	25
HfO_2	25[9]
Ta_2O_5	26

Reactions of d^0 early transition metal complexes with oxygen sources, such as O_2, H_2O or O_3, have been employed to make metal oxide thin films through methods such as chemical vapor deposition (CVD) and atomic layer deposition (ALD) (Scheme 1.2).[11] Both processes are well suited for manufacturing metal gate oxides due to their ability to give uniform, high purity films.

An important factor in making metal oxide thin films is the type of inorganic precursors used. Homoleptic amide and amide imide complexes have been used as precursors for both CVD and ALD processes.[12] These complexes have good thermal stability, volatility, and decomposition characteristics required for CVD or ALD. However, these complexes are very air-sensitive, making them difficult to handle. Bulky, ancillary ligands such as cyclopentadienyl, amidinate, β-diketiminate, and guanidinate ligands have been used in precursors to make the compounds more stable.[11]

$M(NEt_2)_4 + O_2 \rightarrow MO_2$ thin films (M = Zr, Hf)[12a]

$Ta(NMe_2)_5 + O_2 \rightarrow Ta_2O_5$ thin films[12b]

$^tBuN{=}Ta(NEt_2)_3 + O_2 \rightarrow Ta_2O_5$ thin films[12c]

$Zr(NEt_2)_4 + Hf(NEt_2)_4 + H_2O \rightarrow HfZrO_x$ thin films[12d]

Scheme 1.2. Syntheses of metal-oxide thin films.[12a-d]

1.1.3. Fisher- and Schrock-type Carbyne Ligands

The study of complexes containing M≡C bonds has been active since 1973 when E. O. Fischer first reported them.[13] These complexes were initially synthesized via electrophilic abstraction of the methoxide ion from a Fischer carbene complex (Scheme 1.3).[13] Fischer-type carbyne ligands are typically found on low-oxidation-state metal centers with π-accepting ligands. The carbene/carbyne ligands are electrophilic. Soon after the discovery of Fischer-type carbene and carbyne complexes, R. R. Schrock discovered a second class of these compounds. The Schrock-type carbyne complexes are called alkylidynes. Alkylidyne complexes usually contain early transition metal centers in high-oxidation states such as W(VI) or Ta(V). These complexes also have non-π-acceptor ligands and non-π-donor R groups. One approach in synthesizing alkylidynes is to add a Grignard reagent such as RCH_2MgCl (R = CMe_3 or $SiMe_3$) to WCl_6 or $W(OMe)_3Cl_3$. Alkyne metathesis between acetylene complexes and M≡M bonds also give alkylidyne complexes. Scheme 1.4 gives examples of alkylidyne syntheses.[14]

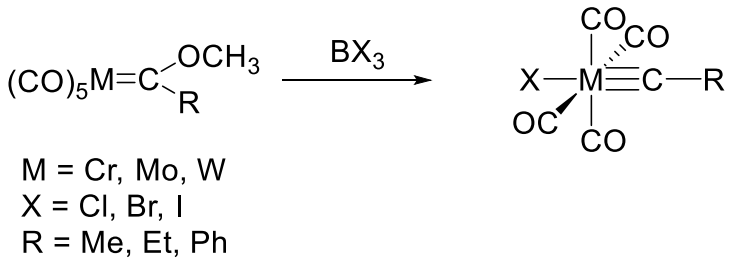

Scheme 1.3. Synthesis of a Fischer carbyne complexes.[13a]

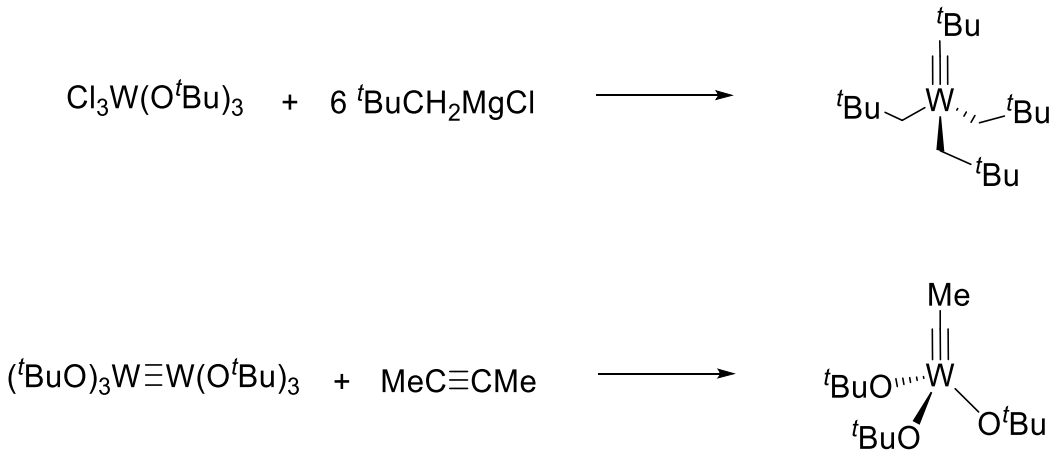

Scheme 1.4. Syntheses of alkylidyne complexes via salt metathesis (top) and alkyne metathesis (bottom).[14]

1.1.4. Analysis of Complexes via DART-TOF Mass Spectrometry

The DART (data analysis in real time) ion source was developed in 2005.[15] The DART ion source is usually coupled to a time-of-flight (TOF) mass spectrometer. A major advantage of this ion source is that it does not require sample preparation. This technique has been used in a wide range of applications to detect compounds in

substances such as biological samples[15] and fragrances.[16] It has also been applied to forensic science to identify substances such as illegal drugs.[17] NIST (National Institute of Science and Technology) has compiled thousands of substances into the DART Forensics Library.[18]

Several ionization methods can be utilized with the DART depending on the carrier gas used and the polarization.[19] For the compounds used in this dissertation, the carrier gas was He and DART was in the positive-ion mode, only detecting cations. To ionize the sample, metastable He gas is generated.[19b] These excited He atoms then collide and transfer their energy to atmospheric water molecules, which is an efficient process. The water molecules undergo several reactions with other neutral water molecules in the air, which finally results in a protonated water cluster. This cluster then transfers a proton to the analyte. This ionizes the analyte, making it able to be separated from other ions by mass and analyzed by the TOF mass spectrometer.[19b] The water molecules undergo several reactions with other neutral water molecules in the air, which finally result in a protonated water cluster. This cluster then transfers a proton to the analyte. This ionizes the analyte, making it separated from other ions and analyzed by the TOF mass spectrometer.

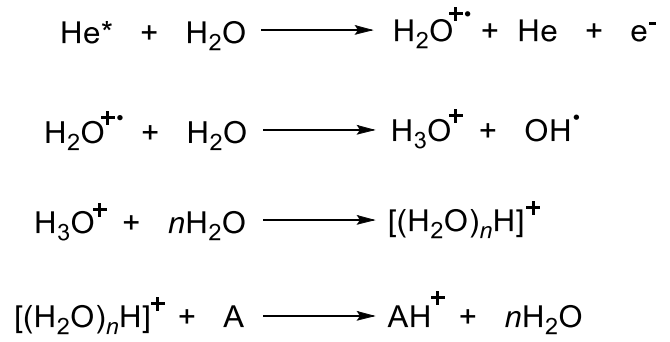

Scheme 1.5. Ionization of an analyte (A) by the DART ion source. Metastable He is denoted by the symbol *.[19]

1.1.5. NMR Spectroscopy

Nuclear Magnetic Resonance (NMR) spectroscopy has been a powerful tool to identify and characterize compounds for the last few decades. NMR involves flipping the nuclear spin (I) in an atom. Isotopes with $I = 0$ are NMR inactive.[20] The most common and easily studied isotopes via NMR are those with $I = 1/2$, e.g, ^{13}C and ^{1}H, but other nuclei with $I > 1/2$ may also be studied via NMR. Inside an external magnetic field, the degenerate $m_I = \pm 1/2$ states of the $I = 1/2$ nuclei split (Figure 1.2) and the ground state $m_I = +1/2$ may be excited to the $m_I = -1/2$ state.[20]

The resonant frequency at which this energy transfer occurs is dependent on the chemical environment and electron density of the nucleus being probed.[20] When an atom is placed in a magnetic field, the electrons circulate and generate a small magnetic field opposing the applied magnetic field. This produces a small effective magnetic field (B_{eff}) which is expressed by the equation:

$$B_{eff} = B_0 (1 - \sigma) \qquad \text{(Eq. 1.1)}$$

where σ is the shielding constant. The resonance frequency of a nucleus is proportional its shielding factor (1 - σ).[20] The chemical shift (δ), which is reported in ppm, of a nucleus is calculated by the following equation:

$$\delta = \frac{\nu_{sample} - \nu_{reference}}{\nu_{observing}} \times 10^6 \qquad \text{(Eq. 1.2)}$$

where ν_{sample} and $\nu_{reference}$ are the resonance frequencies of the nuclei in the sample and an internal standard reference, respectively, and $\nu_{observing}$ is the frequency used by the spectrometer.[20]

As the electron density around a nucleus changes, the shielding around the nucleus will change as well. If a nucleus is more shielded, the NMR peak pertaining to it will be found more upfield (lower ppm). The NMR peaks of less shielded nuclei will be found more downfield (higher ppm).

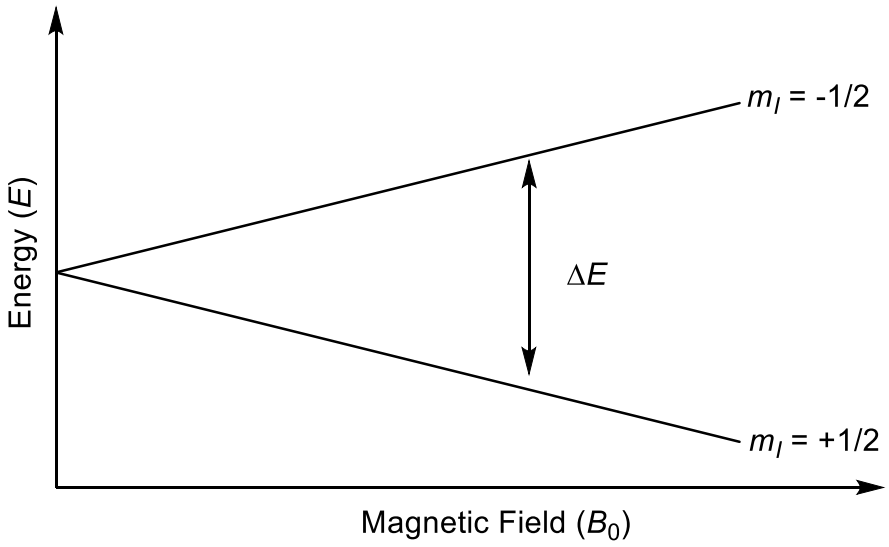

Figure 1.2. Energy differences (Δ*E*) between adjacent energy levels needed to induce a spin flip in a nucleus with *I* = 1/2.[20]

1.2 Current Dissertation

1.2.1. Part 2

Heptacoordinate amidinate chloride complexes M[MeC(N^{i}Pr)$_2$]$_3$Cl (M = Zr, **1**; Hf, **2**) have been prepared via salt metathesis reactions between MCl_4 and Li[MeC(N^{i}Pr)$_2$]. The reactions required gentle heating to proceed. These complexes have been characterized by ^{1}H and ^{13}C{^{1}H} NMR spectroscopies, single-crystal X-ray diffraction, elemental analysis, and MS. In the MS of **1** exposed to air, [**1**+H$^+$], [**8**+H$^+$], Zr[MeC(N^{i}Pr)$_2$]$_3^+$, and amidine ^{i}PrNH-C(Me)=N^{i}Pr were observed. Similarly, in the MS of **2** exposed to air, [**2**+H$^+$], [**9**+H$^+$], Hf[MeC(N^{i}Pr)$_2$]$_3^+$, and amidine ^{i}PrNH-C(Me)=N^{i}Pr were identified. The dynamic behaviors of compounds **1** and **2** in solution have been studied

using variable-temperature NMR (VT-NMR) spectroscopy. This study yielded the activation parameters $\Delta H^{\neq}$, $\Delta S^{\neq}$, and $\Delta G^{\neq}$ for both **1** and **2**.

1.2.2. Part 3

Heptacoordinate amidinate alkyl complexes M[MeC(N^{i}Pr)$_2$]$_3$Me (M = Zr, **3**; Hf, **4**) and M[MeC(N^{i}Pr)$_2$]$_3$Et (M = Zr, **6**; Hf, **7**) have been prepared. These complexes were characterized via elemental analysis and ^{1}H and ^{13}C{^{1}H} NMR spectroscopies. Compounds **6** and **7** have also been characterized by single-crystal X-ray diffraction. The alkyl ligands in **3**, **4**, **6**, and **7** were found to be too labile for the characterization by MS. In the MS of **3** or **6** exposed to air, only [**8**+H$^+$], Zr[MeC(N^{i}Pr)$_2$]$_3^+$, and amidine ^{i}PrNH-C(Me)=N^{i}Pr were observed. Similarly, in the MS of **4** or **7** exposed to air, only [**9**+H$^+$], Hf[MeC(N^{i}Pr)$_2$]$_3^+$, and amidine ^{i}PrNH-C(Me)=N^{i}Pr were observed. The thermal decomposition of **6** has also been studied between 373-388 K. The thermolysis was found to follow first-order kinetics with activation parameters $\Delta H^{\neq}$ = 29(4) kcal/mol, $\Delta S^{\neq}$ = -5(8) eu, and $\Delta G^{\neq}_{298}$ = 31(6) kcal/mol.

1.2.3. Part 4

The reaction of W(≡CSiMe$_3$)(CH$_2$SiMe$_3$)$_3$ (**11**) with H$_2$O at room temperature has been studied, yielding the trimer [(μ-O)W(CH$_2$SiMe$_3$)$_2$(=O)(THF)]$_3$ (**12**) as a crystalline product at -32 °C. The structure of **12** has been characterized by single-crystal X-ray diffraction. Reactions of water with a second alkylidyne complex, W(≡C^{t}Bu)(O^{t}Bu)$_3$ (**10**), have also been studied using NMR spectroscopy and MS. While only one product,

$W(CH_2{}^tBu)(O{}^tBu)_3(=O)$ (**13**), was found by NMR, **13** and several more W-containing products were found using MS.

1.2.4. Part 5

This part presents two trends found in the NMR spectra of d^0 complexes. Trend 1 describes the *downfield shift* of the second-row analogs of both first- and third-row transition metal complexes. This trend has been observed in the ^1H, ^{13}C and ^{29}Si shifts of the α atoms in the complexes with single-bonded ligands such as M-H, $M-CR_3$ and $M-SiR_3$, respectfully. Trend 2 pertains to the *upfield shift of* third-row transition metals are typically from those of the second-row analogs observed in ^{13}C, ^{17}O and ^{19}F NMR chemical shifts of the α atoms in the complexes containing M=CHR, M≡CR, M=O and M–F, respectfully. Scandide (d-block) and lanthanide (f-block) contractions as well as relativistic effects are believed to contribute to the NMR shifts, leading to the observed trends. NMR spectra of d^n complexes and organic compounds are compared with those of the d^0 complexes.

1.2.5. Part 6

A summary of the research in this dissertation is given. The important sections of each part are reviewed. Future directions for the research are proposed.

References

1. Haas, R. M.; Arshad, M.; Anthony, J.; Altmann, P. J.; Pöthig, A.; Köhler, F. H.; Hess, C. R. *Inorg. Chem. Front.* **2016**, 3, 616.
2. Casanova, D; Alemany, P.; Bofill, J. M.; Alvarez, S. *Chem. Eur. J.* **2003**, *9*, 1281.
3. Hallberg, B. M.; Bergfors, T.; Backbro, K.; Pettersson, G.; Henriksson, G.; Divne, C. *Structure* **2000**, *8*, 78.
4. (a) Bray, R. C.; Adams, B.; Smith, A. T.; Benett, B.; Bailey, S. *Biochemistry* **2000**, *39*, 11258. (b) McAlpine, A. S.; McEwan, A. G.; Shaw, A. L.; Bailey, S. *J. Biol. Inorg. Chem.* **1997**, *2*, 590.
5. Gill, H. S.; Eisenberg, D. *Biochemistry* **2001**, *40*, 1903.
6. Templeton, J. L.; Ward, B. C. *Inorg. Chem.* **1980**, *19,* 1753.
7. (a) Kepert, D. L. *Progr. Inorg. Chem.* **1979**, *25*, 41. (b) Drew, M. G. B. *Progr. Inorg. Chem.* **1977**, *23*, 67. (c) Hoffmann, R.; Beier, B. F.; Muetterties, E. L; Rossi, A. R. *Inorg. Chem.* **1977**, *16*, 511. (d) Lin, Z.; Bytheway, I. *Inorg. Chem.* **1996,** *35,* 594.
8. (a) Robertson, J. *Rep. Prog. Phys.* **2006**, *69*, 327. (b) Rockett, A. *The Materials Science of Semiconductors*, Springer Science+Business Media, 2008. (c) Jan, C.-H. *ECS Trans*. **2012**, *44*, 451. (d) Arghavani, R.; Miner, G. Agustin, M. *Semicond. Internal.* **2007**, *30*, 32.
9. Sah, C.-T. in *Fundamentals of Solid-State Electronics*, World Scientific Publishing Co., 1991, Ch. 6, p. 521.
10. (a) Smith, R. C.; Ma, T.; Hoilien, N.; Tsung, L. Y.; Bevan, M. J.; Colombo, L.; Roberts, J.; Campbell, S. A.; Gladfelter, W. L. *Adv. Mater. Opt. Electr.* **2000**, *10*,

105. (b) Wallace, R.; Wilk, G. D. *Crit. Rev. Solid State Mater. Sci.* **2003**, *28*, 231. (c) Wilk, G. D.; Wallace, R. M.; Anthony, J. M. J. *Appl. Phys.* **2001**, 89, 5243. (d) Jones, A. C.; Aspinall, H. C.; Chalker, P. R.; Potter, R. J.; Kukli, K.; Rahtu, A.; Ritala, M.; Leskelae, M. *J. Mater. Chem.* **2004**, *14*, 3101. (e) Walawalkar, M. G.; Kottanthrayil, A.; Rao, R.; *Syn. React. Inorg. Met.* **2009**, *39*, 331. (f) Degraeve, R.; Cartier, E.; Kauerauf, T.; Carter, R.; Pantisano, L.; Kerber, A.; Groeseneken. G. *MRS Bull*. **2002**, *27*, 222.

11. (a) Hoelbling, R. *Z. Angew. Chem.* **1927**, *40*, 655. (b) *Thin Film Processes II*, eds. Vossen J. L.; Kern, W., Academic Press, 1991. (b) Campbell, S. A. *Science and Engineering of Microelectronic Fabrication,* ed. Sedra, A. S., Oxford University Press, 2nd Ed., 2001. (c) Panda, D.; Tseng, T. –Y. *Thin Solid Films* **2013***, 531,* 1. (d) Hitchman, M. L.; Jenson, K. F. *Chemical Vapor Deposition: Principles and Applications*. eds. Hitchman, M. L.; Jenson, K. F., Academic Press, 1993, 1. (e) Jenson, K. F. *Chemical Vapor Deposition: Principles and Applications*. eds. Hitchman, M. L.; Jenson, K. F., Academic Press, 1993, 31. (f) Pierson, H. O. *Handbook of Chemical Vapor Deposition: Principles, Technology, and Applications.* eds. Bunshah, R. F.; McGuire, G. E.; Rossnagel, S. M., Noyes Publications, 1992. (g) Pierson, H. O. *Handbook of Chemical Vapor Deposition: Principles, Technology, and Applications.* eds. Bunshah, R. F.; McGuire, G. E.; Rossnagel, S. M., Noyes Publications, 1992. (h) Jones, A. C. *Adv. Mater. Opt. Electron.* **2000**, *10*, 91. (i) Conley, J. J. F.; Ono, Y.; Zhuang, W.; Tweet, D. J.; Gao, W.; Mohammed, S. K.; Solanki, R. *Electrochem. Solid State Lett.* **2002**, *5*, C57. (j) Gordon, R. G.; Becker, J.; Hausmann, D.; Suh, S. *Chem. Mater.* **2001**,

13, 2463. (k) Devi, A.; Bhakta, R.; Milanov, A.; Hellwig, M.; Barreca, D.; Tondello, E.; Thomas, R.; Ehrhart, P.; Winter, M.; Fischer, R. *Dalton Trans.* **2007**, 1671. (l) Milanov, A.; Bhakta, R.; Baunemann, A.; Becker, H.-W.; Thomas, R.; Ehrhart, P.; Winter, M.; Devi, A. *Inorg. Chem.* **2006**, *45*, 11008.

12. (a) Bastianini, A.; Battiston, G. A.; Gerbasi, R.; Porchia, M.; Daolio, S. *J. Phys. IV* **1995**, *5* (C5, Chemical Vapour Deposition, Vol. 1), C5-525. (b) Ohshita, Y.; Ogura, A.; Hoshino, A.; Hiiro, S.; Machida, H. *J. Cryst. Growth* **2001**, *233*, 292. (c) Son, K.-A.; Mao, A. Y.; Sun, Y.-M.; Kim, B. Y.; Liu, F.; Kamath, A.; White, J. M.; Kwong, D. L.; Roberts, D. A.; Vrtis, R. N. *Appl. Phys. Lett.* **1998**, *72*, 1187. (d) Chiu, H.-T.; Wang, C.-N.; Chuang, S.-H. *Chem. Vap. Deposition* **2000**, *6*, 223. (e) Shi, X.; Tielens, H.; Takeoka, S.; Nakabayashi, T.; Nyns, L.; Adelmann, C.; Delabie, A.; Schram, T.; Ragnarsson, L.; Schaekers, M.; Date, L.; Schreutelkamp, R.; Van Elshocht, S. *J. Electrochem. Soc.* **2011**, *158*, H69. (f) Milanov, A. P.; Fischer, R. A.; Devi, A. *Inorg. Chem.* **2008**, *47*, 11405. (g) Hausman, D. M.; Kim, E.; Becker, J.; Gordon, R. G. *Chem. Mater.* **2002**, *14*, 4350.

13. Fischer, E. O.; Kreis, G.; Kreiter, C.G.; Miiller, J.; Huttner, G.; Lorenz, H. *Angew. Chem. Int. Ed.* **1973**, *I2*, 564. (b) Fischer, E. O.; Maasbol. A. *Angew. Chem. Int. Ed.* **1964**, *3*, 580. (c) Fischer, H.; Kreissl, F. R.; Schubert, U.; Hofmann, P.; Dotz, K. H.; Weiss, K. *Transition Metal Carbene Complexes*, 1984, VCH.

14. (a) McLain, S. J.; Wood C. D.; Messerle, L. W.; Schrock R. R. *J. Am. Chem. Soc.* **1978**, *100*, 5962. (b) Schrock, R. R. *J. Organomet. Chem.* **1986**, *300*, 249. (b) Schrock, R. R. *J. Am. Chem. Soc.* **1974**, *96*, 6796. (c) Listemann, M. L.; Schrock,

R. R. *Organometallics* **1985**, *4*, 74. (d) Schrock, R. R.; Fellmann, J. D. *J. Am. Chem. Soc.* **1978**, *100*, 3359. (e) Schrock, R. R.; Clark, D. N.; Sancho, J.; Wengrovius, J. H.; Rocklage, S. M.; Pedersen, S. F. *Organometallics* **1982**, *1*, 1645.

15. (a) Song, Y.-Q.; Liao, J.; Zha, C.; Wang, B.; Liu, C. C. *Anal. Methods* **2015**, *7*, 1600. (b) Wang, C.; Zhu, H.; Cai, Z.; Song, F.; Liu, Z.; Liu, S. *Anal. Bioanal. Chem.* **2013**, *405*, 3159.

16. (a) Saitoh, K. *Aroma Res.* **2007**, *8*, 366. (b) Haefliger, O. P.; Jeckelmann, N. *Rapid Comm. Mass Spectrom.* **2007**, *21*, 1361.

17. (a) Lesiak, A. D. *Bioanal.* **2014**, *6*, 819. (b) LaPointe, J.; Musselman, B.; O'Neill, T.; Shepard, J. R. E. *J. Am. Soc. Mass Spectrom.* **2015**, *26*, 159.

18. *"NIST DART Forensics Library".* http://chemdata.nist.gov/mass-spc/ms-search/DART_Forensic.html. Accessed on June 30, 2016.

19. (a) Cody, R. B.; Laramée, J. A.; Durst, H. D. *Anal. Chem.* **2005**, *77*, 2297. (b) Cody, R. B.; Laramée, J. A.; Nilles, J. M.; Durst, H. D. *JEOL News Col*. **2005**, *40*, 8.

20. Friebolin, H. *Basic One- and Two-Dimensional NMR Spectroscopy,* 3rd Ed.; Wiley-VCH, 1998.

Part 2

Synthesis and Characterization of Heptacoordinate Zirconium and Hafnium Amidinate Chloride Complexes

Abstract

Heptacoordinate amidinate chloride complexes M[MeC(N^{i}Pr)$_2$]$_3$Cl (M = Zr, **1**; Hf, **2**) have been prepared via salt metathesis and purified by crystallization. These complexes have been characterized by ^{1}H and ^{13}C{^{1}H} NMR spectroscopies, single-crystal X-ray diffraction, and MS. **1-2** show broad features in their ^{1}H NMR spectra at room temperature and variable-temperature NMR studies have been conducted to probe their dynamic behaviors. The activation parameters $\Delta H^{\neq}$, $\Delta S^{\neq}$, and $\Delta G^{\neq}$ have been determined for both **1** and **2**.

2.1. Introduction

Many d^0 early transition metal complexes are sensitive to air and they are usually handled in an inert gas environment.[1] The reactions of O_2 and water with many of these complexes differ from those of d^n late transition metal complexes.[1-2] The reactions of d^0 early transition metal complexes with oxygen sources, such as with O_2, H_2O, or O_3, have been used to synthesize metal oxide (MO_n) thin films via chemical vapor deposition (CVD) or atomic layer deposition (ALD) processes.[3] CVD and ALD processes require precursors to have a sufficient temperature window between evaporation and decomposition so that the precursor does not decompose prematurely.[3d,j,k] Bulky, ancillary ligands such as amidinates, guanidinates, and β-diketiminates (Figure 2.1) have been used to add stability as well as to decrease the reactivity of the complexes.[3k,4]

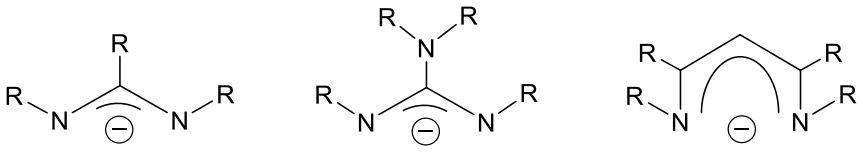

Figure 2.1. Bidentate, nitrogen donating ancillary ligands.

Amidinate ligands offer advantages over commonly used η^5-cyclopentadienyl (Cp) ligands in that the former are more easily modified, allowing their electronic and steric properties to be finely tuned. Though sterically similar to Cp, amidinate ligands

are isoelectronic with π-allyl ligands.[4,5] The amidinate ligands bond to metals via two bonds, one dative and one covalent. Through conjugation, the bonds to the metal center are equivalent. Amidinate complexes have been used for a variety of applications including polymerization,[4b,5a] hydroamination,[6] Si-C/Si-Cl bond activations,[7] and as CVD/ALD precursors.[3k,4,8] Devi and coworkers have studied the preparation of HfO_2 thin films using the reaction of a hafnium amidinate with O_2 in CVD (Scheme 2.1).[8f] Pallem and Dussarrat have investigated the formation of ZrO_2 thin films using a zirconium amidinate with its reaction with H_2O via ALD (Scheme 2.1).[8i]

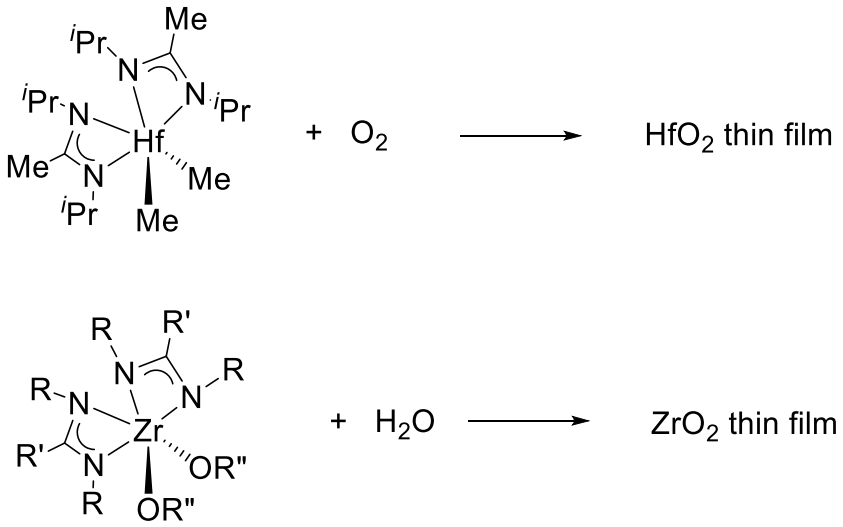

Scheme 2.1. Reactions of amidinate complexes with O_2 and H_2O to give metal oxide films.[8i,f]

Our group has synthesized and studied group 4 amidinate complexes from MCl_4 (M = Ti, Hf, Zr). The Ti amide amidinate complex, $Ti[MeC(NCy)_2]_2(NMe_2)_2$, was

prepared in a two-step process. Reacting $TiCl_4$ with 2 equiv of $LiNMe_2$ yielded $Ti(NMe_2)_2Cl_2$, which was then reacted with 2 equiv of $Li[MeC(NCy)_2]$ to give $Ti[MeC(NCy)_2]_2(NMe_2)_2$. In the preparation of Hf and Zr amide amidinate complexes $M[MeC(N^iPr)_2]_2(NR_2)_2$ (M = Zr, R = Me, Et; M = Hf, R = Me), at least two methods have been used.[9-11] MCl_4 was mixed with 2 equiv of $Li[MeC(NCy)_2]$, followed by the addition of 2 equiv of LNR_2 to yield the products.[9] Our group has also synthesized analogous amide amidinate complexes $Zr[MeC(N^iPr)_2]_2(NR_2)_2$ (R = Me, Et) via aminolysis from the reactions of 2 equiv of $^iPrN(H)CMe=N^iPrZr(NR_2)_4$ with $Zr(NR_2)_4$.[10]

In comparison to tetra-, penta-, and hexacoordinated transition metal complexes, metal centers with the coordination number of seven or higher occur much less often because of the steric and electronic restrictions.[12,13] However, the heptacoordinated complexes are important as, e.g., intermediates in associative reactions of hexacoordinate complexes,[14] in the active sites of metalloproteins in biological systems, and as polymerization catalysts.[12,14-16] Herein, we report the preparation and characterization of rare d^0 heptacoordinated Zr and Hf amidinate chloride complexes $Zr[MeC(N^iPr)_2]_3Cl$ (**1**) and $Hf[MeC(N^iPr)_2]_3Cl$ (**2**). These complexes have been used to synthesize several alkyl analogs and show reactivity with H_2O, which will be discussed in Part 3.

2.2. Results and Discussion

2.2.1. Synthesis and Characterizations of $Zr[MeC(N^iPr)_2]_3Cl$ (1)

The synthesis of $Zr[MeC(N^iPr)_2]_3Cl$ (**1**) was accomplished via the salt metathesis $Li[MeC(N^iPr)_2]$ and $ZrCl_4$. $Li[MeC(N^iPr)_2]$ was synthesized via the literature procedure

from the addition of MeLi to the carbodiimide ^{i}Pr-N=C=N-^{i}Pr (Scheme 2.2).[17] Compound **1** was prepared by adding 3 equiv of Li[MeC(N^{i}Pr)$_2$] to freshly sublimed $ZrCl_4$ in a 2:1 hexanes:THF solution at -30 °C (Scheme 2.3). After the mixture was warmed to 23 °C, it was heated to 35 °C for 24 h. After volatiles were removed in vacuo, the crude product was extracted with pentane. After filtration, the volume of the pentane solution was reduced. The flask was then placed in a -32 °C freezer to give yellow crystals of **1** in 61% yield.

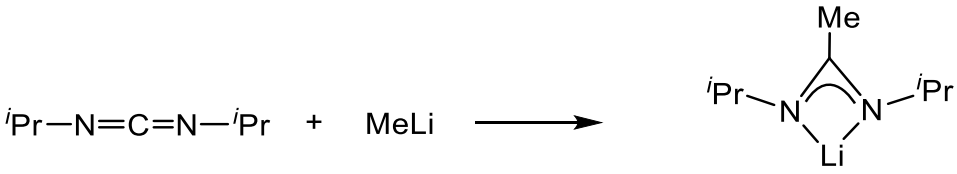

Scheme 2.2. Synthesis of Li[MeC(N^{i}Pr)$_2$].

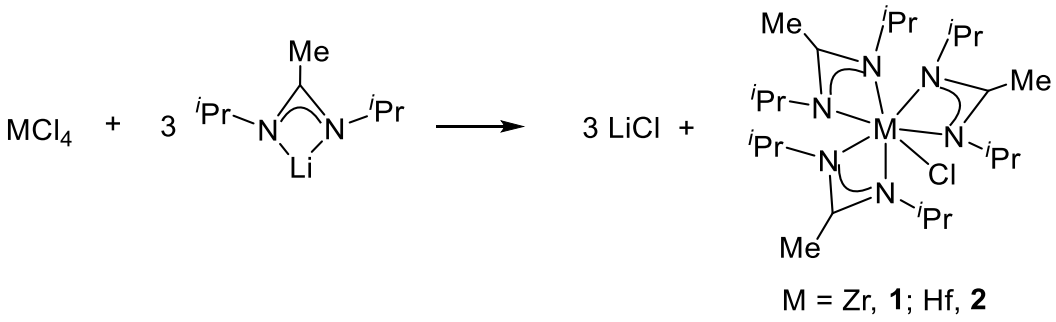

Scheme 2.3. Preparation of **1** and **2.**

The ^{1}H NMR spectrum of **1** in benzene-d_6 (Figure 2.2) shows a singlet at 1.62 ppm assigned to the methyl group on the amidinate ligands. A multiplet for the C*H* in the isopropyl groups appears at 3.53 ppm. A broad peak at 1.34 ppm is assigned to the CH(*Me*)$_2$ groups. This observation suggests that **1** has dynamic behavior in solution, undergoing rapid exchanges at room temperature via a pseudo-Bailar twist mechanism (Scheme 2.4).[18] The Bailar twist mechanism occurs when two enantiomers (Δ and Λ) of an octahedral complex undergo exchange via a trigonal prismatic intermediate. Our group has studied the twisting mechanism with bisamidinate bisamide complexes Zr[MeC(NR)$_2$]$_2$(NMe$_2$)$_2$ (R = Cy, ^{i}Pr). A variable-temperature NMR (VT-NMR) study was conducted on **1** and will be discussed further in Section 2.2.2. In the ^{13}C{^{1}H} NMR spectrum of **1** (Figure 2.3), the peaks for –*C*(Me)- and –C(*Me*)– groups on the amidinate were assigned to 174.68 and 12.80 ppm, respectively. The CH*Me*$_2$ groups on the isopropyl groups appear at 23.94 ppm. The *C*HMe$_2$ carbon atom is observed at 48.29 ppm.

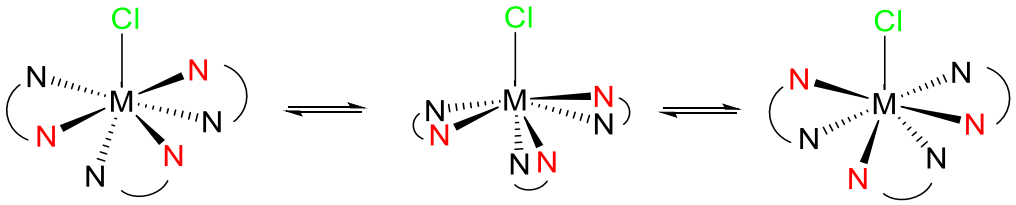

Scheme 2.4. Exchange between the Δ and Λ enantiomers of **1** and **2.**

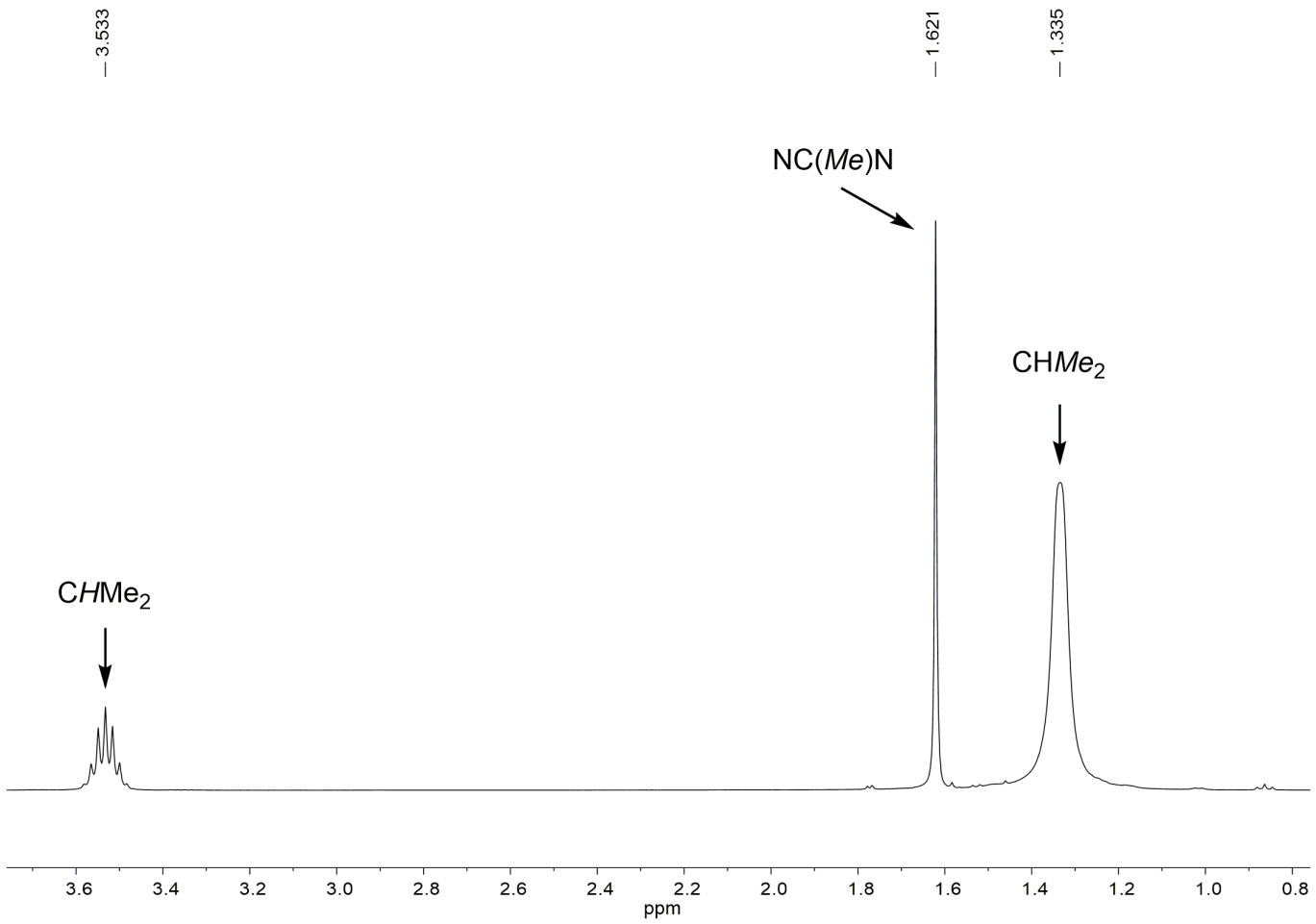

Figure 2.2. ^{1}H NMR spectrum of **1** in benzene-d_6 at 23 °C.

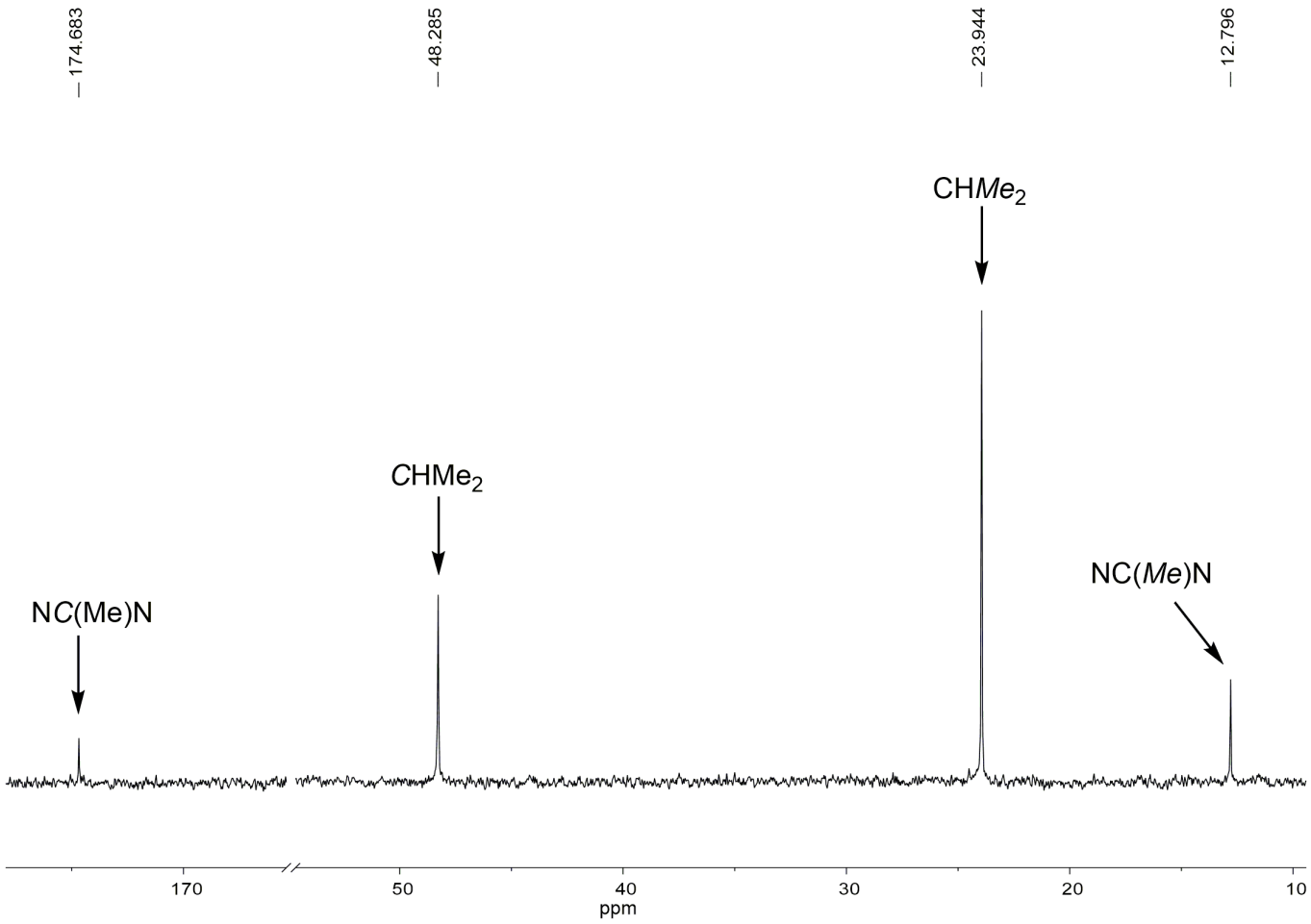

Figure 2.3. $^{13}C\{^{1}H\}$ NMR spectrum of **1** in benzene-d_6 at 23 °C.

The crystals of **1** were suitable for single-crystal X-ray diffraction studies. A molecular drawing, crystallographic data, and selected bond distances and angles of **1** are given in Figure 2.4, Table 2.1 and Table 2.2, respectively. The complete lists of crystallographic data are given in Appendix A. **1** adopts mono-capped octahedron geometry.[12,19] Both the Δ and Λ enantiomers are present in the crystals. The Zr(1)-Cl(1) bond length of 2.5125(5) Å is longer than those of reported octahedral complexes $Zr[NRC(R')_2]_2Cl_2$ (R = Me, Ph; R' = Cy, ^{i}Pr), but is similar to the Zr-Cl bond in the heptacoordinated guanidinate compound $[PhNC(NMe_2)NSiMe_3]_3ZrCl$, where the Zr-Cl bond is 2.512 Å.[11,16]

Compound **1** was also characterized by mass spectrometry (MS) with an *m*/*z* = 549.29 [**1**+H$^+$]. Zirconium has five stable isotopes (^{90}Zr, ^{91}Zr, ^{92}Zr, ^{94}Zr, and ^{96}Zr; Table 2.3). Since these isotopes have different abundances, the pattern made by a monomer zirconium center is easy to recognize. In addition to the zirconium isotopes, chlorine also has two stable isotopes (^{35}Cl and ^{37}Cl, Table 2.4). With these isotopes, the MS spectrum of **1** is expected to show a unique pattern. Solid powders of **1** were placed in a heated He stream (200 °C) by utilizing the sealed end of a capillary tube. Both the calculated and experimental spectra of [**1**+H$^+$] are shown in Figure 2.5. Since the Cl ligand is very labile, the major observed species was the cation, $Zr[NMeC(^iPr)_2]_3^+$ (*m*/*z* = 513.32). Both the observed and calculated MS spectrum of $Zr[NMeC(^iPr)_2]_3^+$ are given in Figure 2.6.

In addition to [**1**+H$^+$], MS spectrum of the powders of **1** exposed to air showed the presence of [**8**+H$^+$], $Zr[MeC(N^iPr)_2]_3^+$, and amidine ^{i}PrNH-C(Me)=N^{i}Pr. Their formation is discussed below in Section 3.2.7, along with the MS of **3** and **6**, alkyl analogs of **1**.

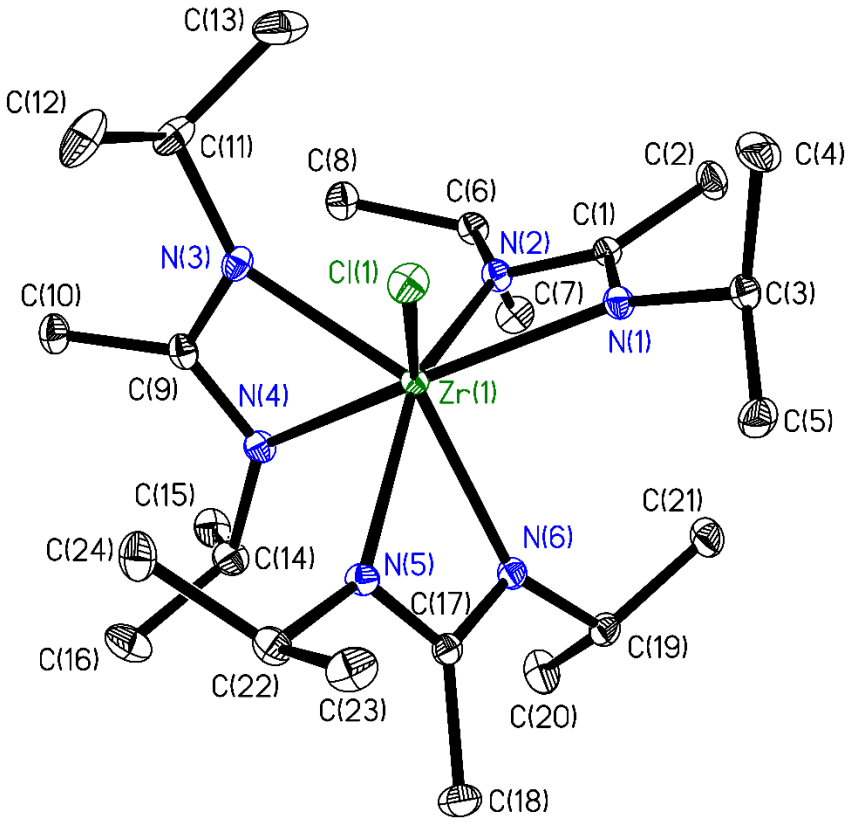

Figure 2.4. ORTEP of **1** at 100(2) K. Thermal ellipsoids are 30% probability level. Hydrogen atoms were removed for clarity.

Table 2.1. Crystal data and structure refinement for **1**

Empirical formula	$C_{24}H_{51}N_6ClZr$	
Formula weight	550.37	
Temperature	100(2) K	
Wavelength	0.71073 Å	
Crystal System	Monoclinic	
Space Group	$P2_1/n$	
Unit cell dimensions	a = 10.447(2) Å	α = 90°
	b = 16.453(3) Å	β = 93.334°
	c = 17.100(3) Å	γ = 90°
Volume	2934.5(8) Å^3	
Z	4	
Density (calculated)	1.246 g/cm^3	
Absorption coefficient	0.487 mm^{-1}	
F(000)	1176	
Crystal size	0.358 x 0.219 x 0.203 mm^3	
Theta range for data collection	2.23 to 27.91°	
Index ranges	$-13 \le h \le 13$, $0 \le k \le 21$, $0 \le l \le 22$	
Reflections collected	6921	
Independent reflections	6921 [R_{int} = 0.000]	
Completeness to theta = 27.91°	98.4%	
Max. and min. transmission	0.746 and 0.658	
Refinement method	Full-matrix least-squares on F^2	
Absorption correction	Semi-empirical from equivalents	
Data / restraints / parameters	6921 / 0 / 305	
Goodness-of-fit on F^2	1.031	

Table 2.1. Continued

Final *R* indices [$I > 2\sigma(I)$]	$R1 = 0.0269$, $wR2 = 0.0639$
R indices (all data)	$R1 = 0.0307$, $wR2 = 0.0662$
Largest diff. peak and hole	0.51 and -0.40 eÅ^{-3}

[a] $R1 = \Sigma \, ||F_o| - |F_c|| \, / \, \Sigma |F_o|$; $wR2 = [\Sigma \, w(F_o^2 - F_c^2)^2 \, / \, \Sigma \, w(F_o^2)^2]^{1/2}$;

$w = 1/[\sigma^2(F_o) + (aP)^2 + bP]$; $P = [2Fc^2 + \mathrm{Max}(F_o^2, 0)]/3$

Table 2.2. Selected distances (Å) and angles (°) in **1**

Distances			
Zr(1)-Cl(1)	2.5125(5)	Zr(1)-N(4)	2.2814(13)
Zr(1)-N(1)	2.2141(14)	Zr(1)-N(5)	2.2172(13)
Zr(1)-N(2)	2.3154(14)	Zr(1)-N(6)	2.3175(13)
Zr(1)-N(3)	2.2015(14)		

Angles			
N(1)-Zr(1)-Cl(1)	82.71(4)	N(3)-Zr(1)-N(4)	58.96(5)
N(2)-Zr(1)-Cl(1)	123.82(4)	N(3)-C(9)-N(4)	111.82(14)
N(1)-Zr(1)-N(2)	58.64(5)	N(5)-Zr(1)-Cl(1)	84.72(3)
N(1)-C(1)-N(2)	112.78(14)	N(6)-Zr(1)-Cl(1)	125.68(4)
N(3)-Zr(1)-Cl(1)	84.96(4)	N(5)-Zr(1)-N(6)	58.57(5)
N(4)-Zr(1)-Cl(1)	132.45(4)	N(5)-C(17)-N(6)	112.79(14)

Table 2.3. Stable isotopes of zirconium

Isotope	Accurate Mass	% Natural Abundance
^{90}Zr	89.9047026(26)	51.45(2)
^{91}Zr	90.9056439(26)	11.22(2)
^{92}Zr	91.9050386(28)	17.15(1)
^{94}Zr	93.9063148(28)	17.38(2)
^{96}Zr	95.908275(4)	2.80(1)

Table 2.4. Stable isotopes of chlorine

Isotope	Accurate Mass	% Natural Abundance
^{35}Cl	34.968852721(69)	75.78(4)
^{37}Cl	36.96590262(11)	24.22(4)

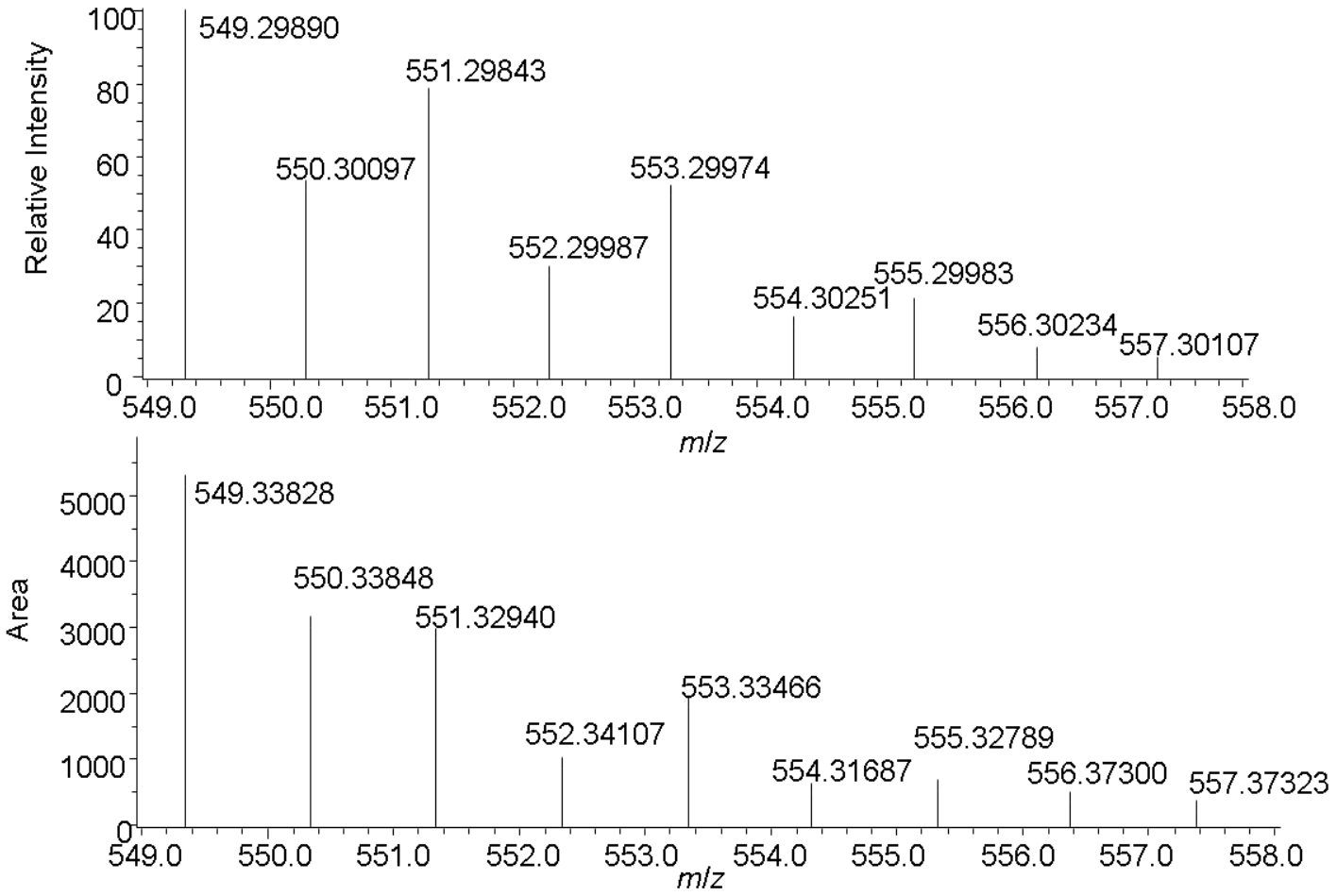

Figure 2.5. (Top) Calculated and (Bottom) Observed MS for [**1**+H^+].

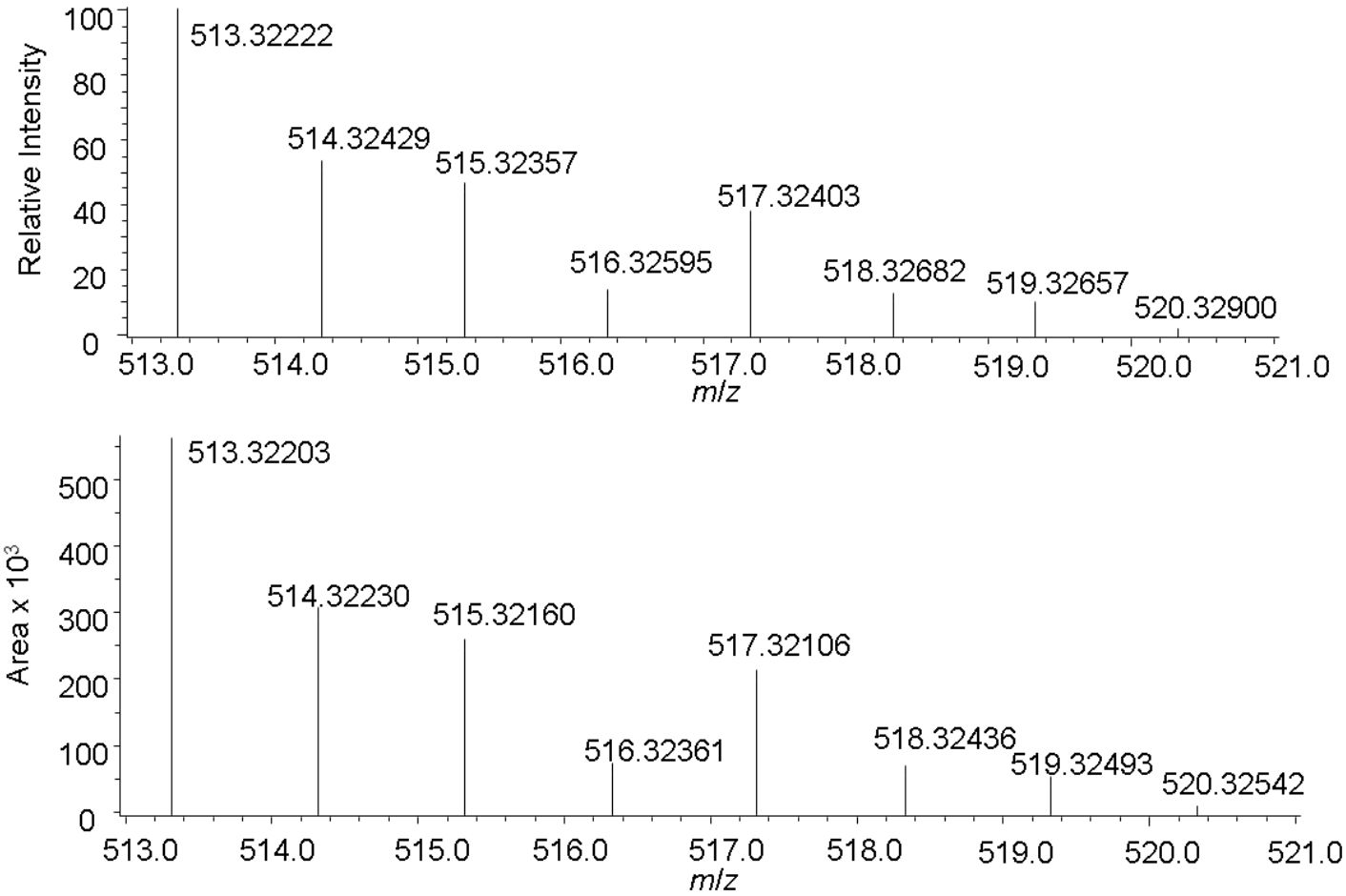

Figure 2.6. (Top) Calculated and (Bottom) Observed MS for $Zr[MeC(N^{i}Pr)_2]_3^+$.

2.2.2. Variable-Temperature NMR Studies of Zr[MeC(N^{i}Pr)$_2$]$_3$Cl (1)

Since the ^{1}H NMR spectrum of **1** showed a broad peak, we have studied the dynamic behavior in solution using variable-temperature NMR (VT-NMR). As the temperature of **1** in solution was lowered to 193 K, de-coalescence of the isopropyl CH and methyl groups occurred. Two multiplets located at 3.52 and 3.35 ppm appeared for CH_AMe$_2$ and CH_BMe$_2$.

At low temperatures, rotations are significantly slowed. The spectrum shows four sets doublets located at 1.64, 1.51, 1.16, and 1.13 ppm for the two sets of methyl groups Me_GMe_H and Me_EMe_F for the isopropyl groups CHMe_EMe_F and CHMe_GMe_H, respectively. As the temperature was slowly raised, the rates of the rotations of the methyl groups on the isopropyl groups increase until they reach coalescence, or where the Me groups are equivalent. Since these two methyl rotations are of the same type, it is not surprising that their temperature ranges are similar at 203-238 K and 208-243 K, respectively.

The next exchange observed was the pseudo-Bailar twist, which racemizes the Δ and Λ enantiomers and requires higher temperatures than the simple methyl rotations discussed above. The Bailar twist was observed in the coalescences between the two isopropyl groups CHMe_GMe_H and CHMe_EMe_F (labeled as $Me_{E\text{-}F}Me_{G\text{-}H}$) as well as the H atoms (labeled as H_AH_B) of the isopropyl groups CH$_A$$Me_EMe_F$ (or CH_AMe$_2$) and CH$_B$$Me_EMe_F$ (or CH_BMe$_2$). The CH_AMe$_2$ and CH_BMe$_2$ peaks coalesced at 268(1) K, and the two sets of CHMe_2 peaks coalesced into a broad singlet at 283(1) K, which became a doublet at 308(1) K due to the coupling to the H atoms in the CHMe_2 groups. Figure 2.7 shows the partial ^{1}H NMR spectra of the CHMe$_2$ and CHMe_2 regions. The rate

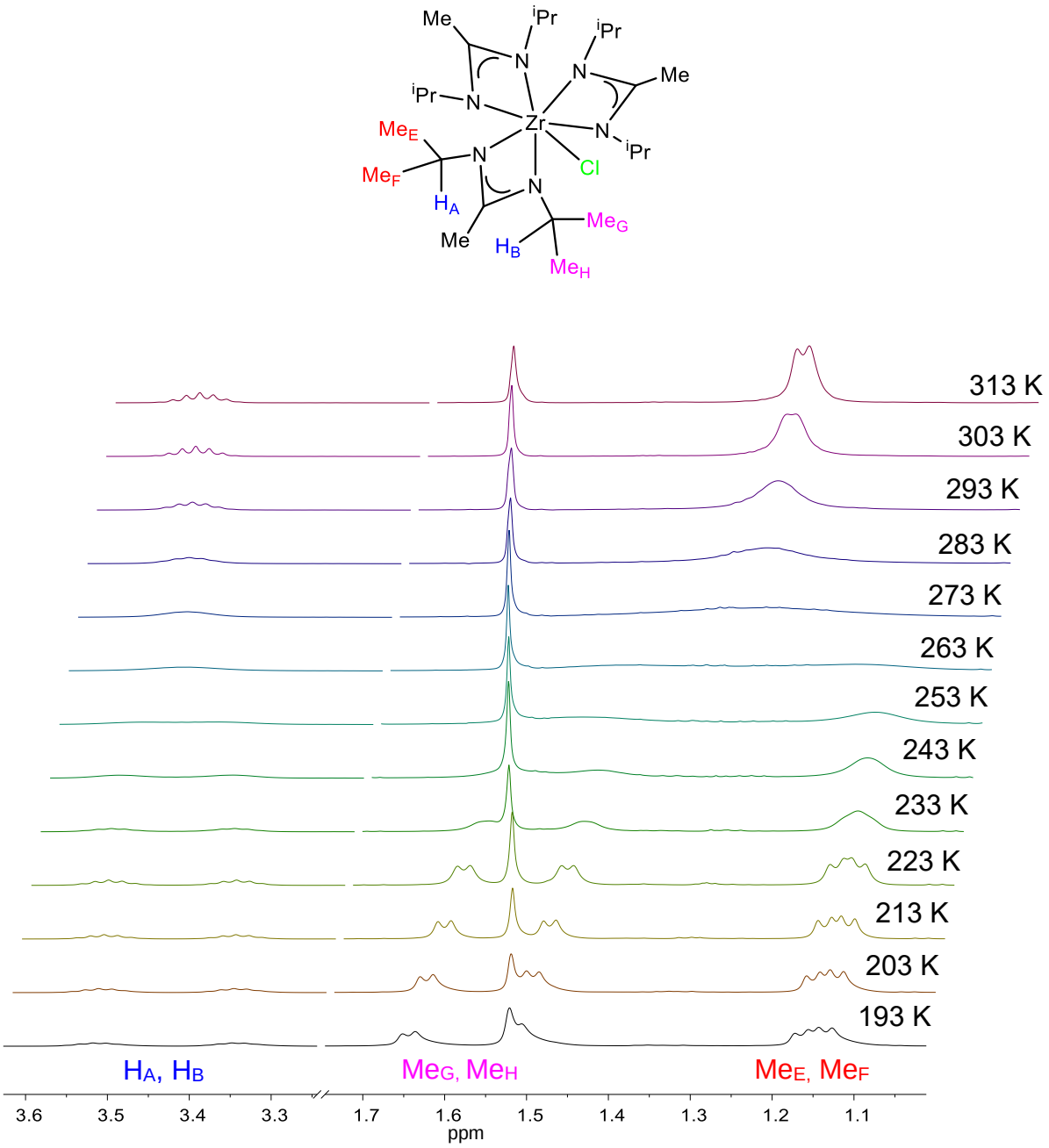

Figure 2.7. Partial ^{1}H NMR spectra of **1** at several temperatures showing the de-coalesce of the methyl and H atom peaks pertaining to the CHMe$_2$ groups as the temperature is lowered from room temperature to 193 K. As the temperature is raised to 313 K, the broad peak for the CH*Me*$_2$ groups becomes a doublet.

constants of this interconversion at different temperatures were calculated from Eq. 2.1.

$$k = \pi\sqrt{2(\Delta\nu_0^2 - \Delta\nu^2)} \qquad \text{(Eq. 2.1)}$$

where $\Delta\nu_0$ and $\Delta\nu$ are frequency differences (Hz) between the sites of the slow exchange limit and the exchange-broadened sites at the temperature (*T*), respectively.[20-23]

The rate constants and activation parameters for each exchange are given in Tables 2.5 and 2.6, respectively. The frequency differences were taken from the CH*Me*$_2$ groups and used in Eq. 2.1. The activation parameters of the exchanges were determined from Eyring plots (Figures 2.8, 2.9, 2.10 and 2.11). A common feature among the four sets of activation parameters is that $\Delta H^{\neq}$ is relatively low and $\Delta S^{\neq}$ is largely negative. $\Delta S^{\neq}$ in these exchanges are, however, much more negative than those in typical unimolecular chemical reactions, and the values of $T\Delta S^{\neq}$ are, in fact, much larger contributors to the activation free energy $\Delta G^{\neq}$. These results reflect the fact that no bonds were broken in the exchanges, but the bulkiness of the amidinate groups makes the exchanges difficult.

The *Me*$_E$*Me*$_F$ and *Me*$_G$*Me*$_H$ exchanges are the slow rotations of the two methyl groups on the same isopropyl groups in Zr[MeC(N^{i}Pr)$_2$]$_3$Cl (**1**). These methyl rotations reach coalescence first at the rather low temperatures of 238(1) and 253(1) K with

Table 2.5. Rate constants of the interconversions in **1**

T (K)	k (s^{-1}) for H_AH_B[b]	k (s^{-1}) for Me_EMe_F	k (s^{-1}) for Me_GMe_H	k (s^{-1}) for $Me_{E\text{-}F}Me_{G\text{-}H}$
203(1)		7.86(7)		
208(1)		10.7(4)	28.0(1)	
213(1)		14.51(7)	37.4(7)	
218(1)		18.3(4)	48(2)	
223(1)		25.2(6)	55(1)	
228(1)	131(2)	34(1)	69(3)	
233(1)	143(3)	46(1)	84.8(2)	
238(1)	154(3)	52.3(9)	112(5)	297.9(6)
243(1)	177(3)		152(2)	333(3)
248(1)	211(6)			365(16)
253(1)	249(5)			431(8)
258(1)	279(1)			482(11)
263(1)	301(1)			573(15)
268(1)				688(3)
273(1)				745(3)

[a] The total uncertainties $\delta k/k$ were calculated from $\delta k_{ran}/k$ from each column and $\delta k_{sys}/k$ = 0.050. (1) H_AH_B: $\delta k_{ran}/k$ = 0.027, $\delta k/k$ = 0.057; (2) Me_EMe_F: $\delta k_{ran}/k$ = 0.039, $\delta k/k$ = 0.063; (3) Me_GMe_H: $\delta k_{ran}/k$ = 0.045, $\delta k/k$ = 0.067; (4) $Me_{E\text{-}F}Me_{G\text{-}H}$: $\delta k_{ran}/k$ = 0.043, $\delta k/k$ = 0.066.

Table 2.6. Activation parameters of the interconversions in **1**

	H_AH_B[a]	Me_EMe_F	Me_GMe_H	$Me_{E\text{-}F}Me_{G\text{-}H}$[b]
$\Delta H^{\neq}$ (kcal/mol)	2.6(3)	4.9(3)	4.1(3)	3.0(3)
$\Delta S^{\neq}$ (eu)	-37(1)	-29(1)	-31(1)	-34(1)

[a] H_A,H_B refers to the H atoms on the isopropyl groups. $Me_{E\text{-}F}$,$Me_{G\text{-}H}$ refers to the interconversion between Me_E,Me_F and Me_G,Me_H after they each have coalesced.

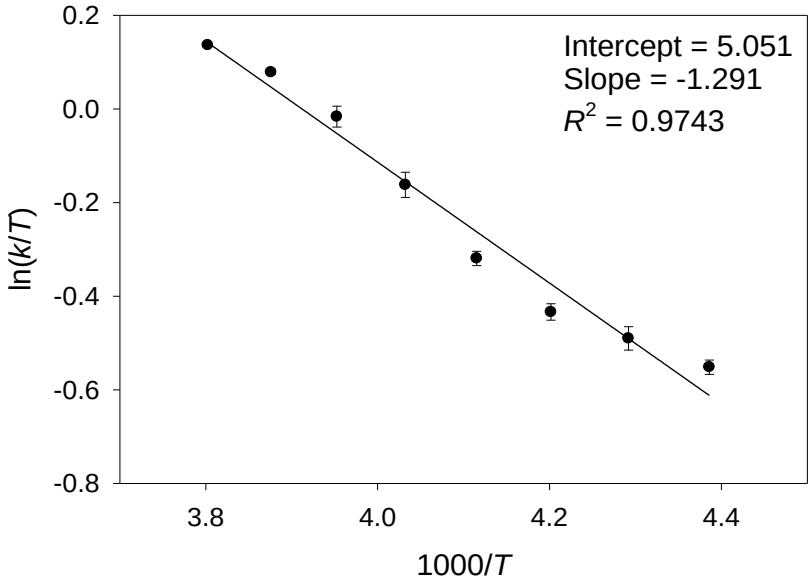

Figure 2.8. Eyring plot of the H_AH_B exchange in **1** yielding activation parameters for the exchange.

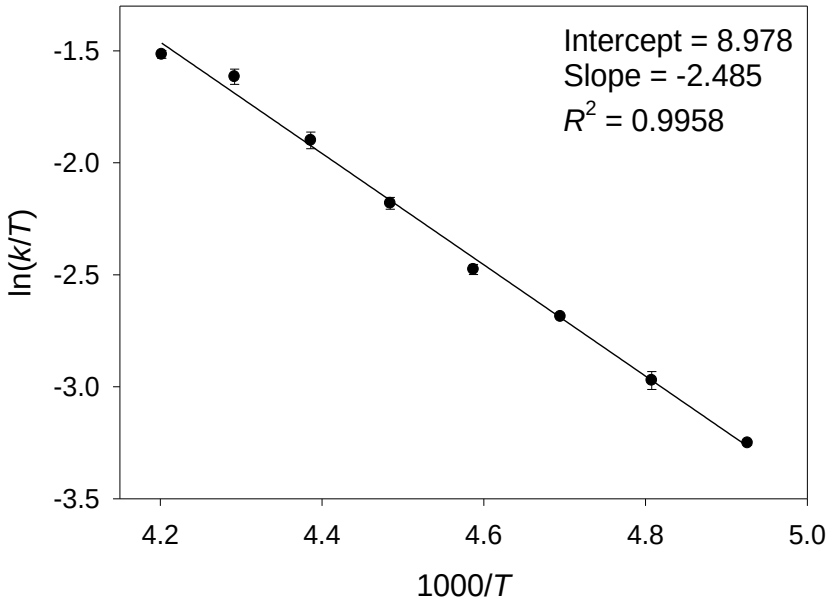

Figure 2.9. Eyring plot of the Me_EMe_F exchange in **1** yielding activation parameters for the exchange.

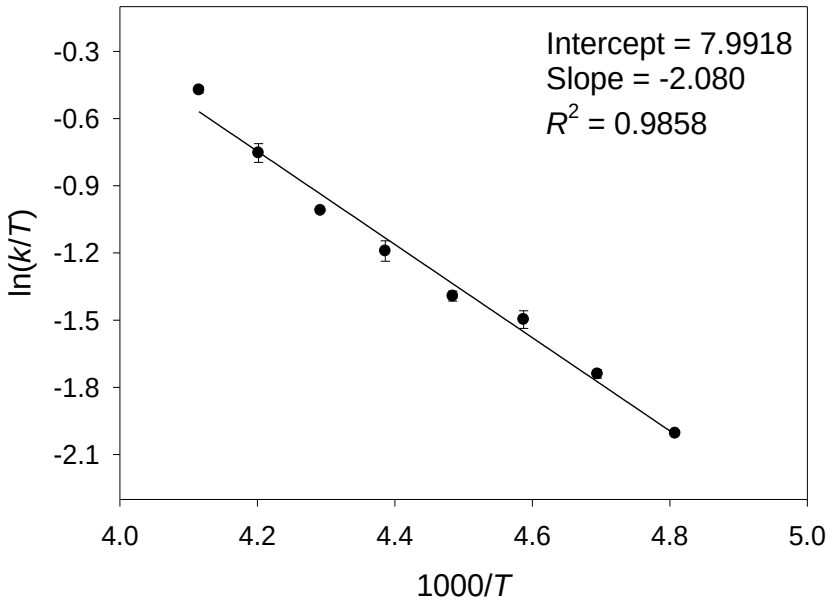

Figure 2.10. Eyring plot of the Me_GMe_H exchange in **1** yielding activation parameters for the exchange.

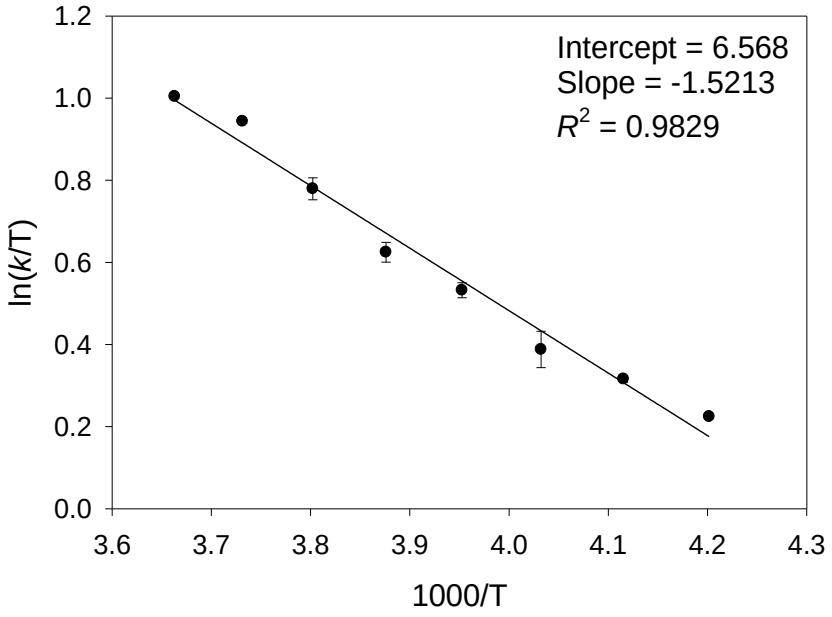

Figure 2.11. Eyring plot of the $Me_{E\text{-}F}Me_{G\text{-}H}$ exchange in **1** yielding activation parameters for the exchange.

similar activation parameters $\Delta H^{\neq}$ = 4.9(3) and 4.1(3) kcal/mol and $\Delta S^{\neq}$ = -29(1) and -31(1) eu for Me_EMe_F and Me_GMe_H, respectively.

Both the H exchange of H_AH_B and the exchange of the two isopropyl groups $Me_{E\text{-}F}Me_{G\text{-}H}$ refer to the same pseudo-Bailar twist. Thus their exchange temperature ranges and activation parameters are similar: $\Delta H^{\neq}$ = 2.6(3) kcal/mol and $\Delta S^{\neq}$ = −37(1) eu for the former and $\Delta H^{\neq}$ = 3.0(3) kcal/mol and $\Delta S^{\neq}$ = −34(1) eu for the latter.

The values of $\Delta H^{\neq}$ and $\Delta S^{\neq}$ values for **1** for the rotations of the methyl groups on the isopropyl groups (Me_EMe_F and Me_GMe_H) as well as the exchange between them ($Me_{E\text{-}F}Me_{G\text{-}H}$) are very similar to those of the methyl groups on the isopropyl groups on the guanidinate ligands of $Zr[^iPrNC(NEt_2)N^iPr]_2(NEt_2)_2$.[1x] Though in the hexacoordinate geometry, the molecules of this compound have difficulty rotating because of the bulky guanidinate and ethyl amide ligands.

2.2.3. Synthesis and Characterization of $Hf[MeC(N^iPr)_2]_3Cl$ (2)

$Hf[MeC(N^iPr)_2]_3Cl$ (**2**) was synthesized by a method similar to the preparation of **1** (Schemes 2.4). Reaction of 3 equiv of $Li[MeC(N^iPr)_2]$ with freshly sublimed $HfCl_4$ in a 2:1 hexanes:THF solution at -30 °C, followed by warming the mixture to 23 °C, and then heating it at 35 °C for 24 h, gave the product. After the volatiles were removed, pentane was used to extract the crude product. Filtration and cooling the concentrated solution at -30 °C afforded yellow crystals of **2** at 48% yield.

The ^{1}H NMR spectrum of **2** in benzene-d_6 at 23 °C (Figure 2.12) shows a multiplet for the C*H* moieties in the isopropyl groups at 3.65 ppm. A singlet at 1.62 ppm

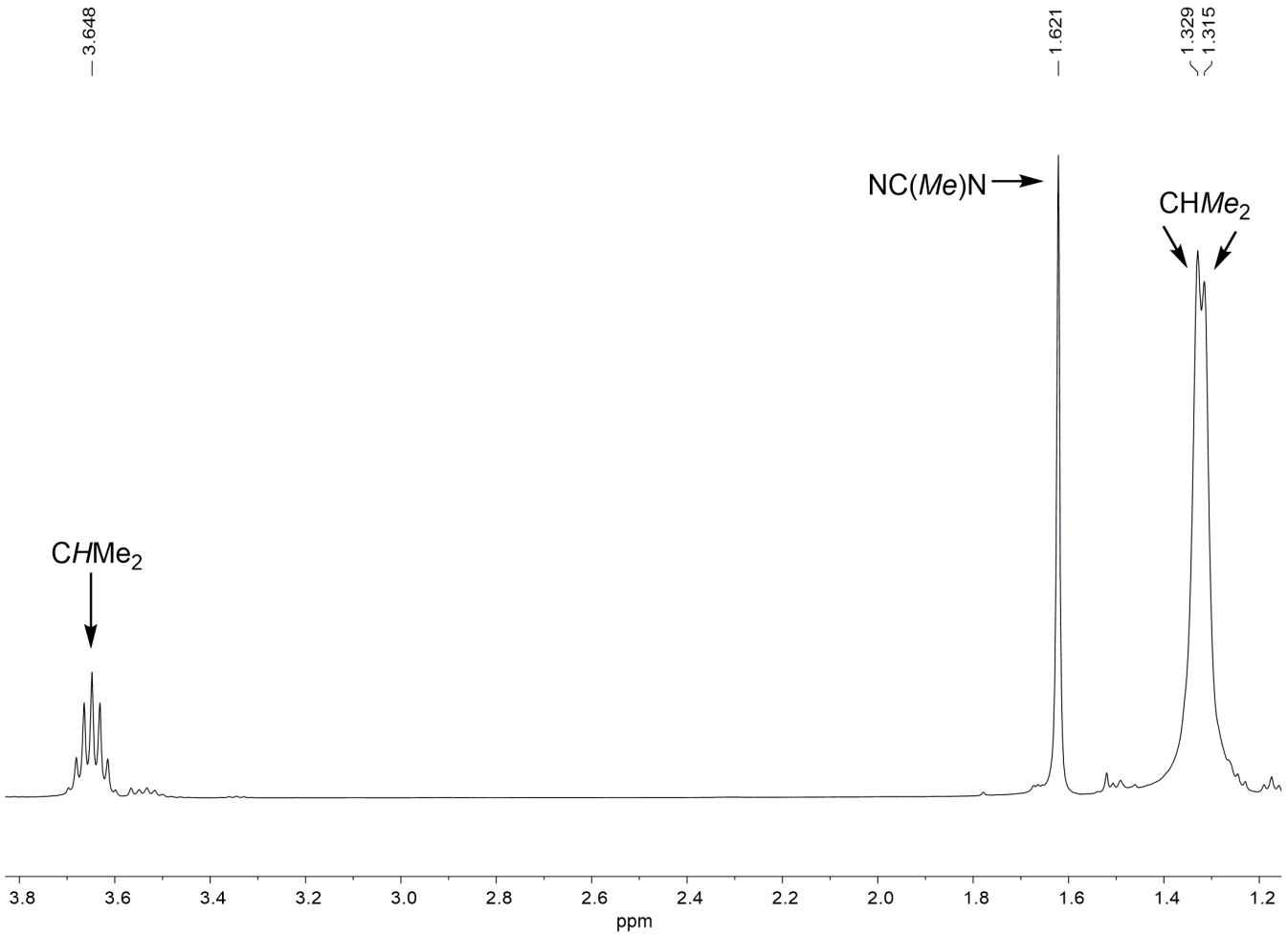

Figure 2.12. ^{1}H NMR spectrum of **2** in benzene-d_6 at 23 °C.

assigned to the methyl group on the amidinate ligands. A broad doublet at 1.34 ppm is assigned to the CH*Me*$_2$ groups. The presence of the broad doublet at room temperature suggests that the exchange between the Δ and Λ enantiomers is faster for **2** than for **1**. A VT-NMR study was also conducted on **2** and is discussed in Section 2.2.4. In the $^{13}C\{^1H\}$ NMR spectrum of **2** (Figure 2.13), the *C*HMe$_2$ atom is observed at 47.98 ppm. The peaks for –*C*(Me)- and –C(*Me*)– groups on the amidinate were assigned to 174.08 and 13.32 ppm, respectively. The CH*Me*$_2$ groups on the isopropyl groups appear at 24.03 ppm.

The crystals of **2** were suitable for single-crystal X-ray diffraction studies. The ORTEP, crystallographic data, and selected bond distances and angles of **2** are given in Figure 2.14, Table 2.7 and Table 2.8, respectively. Complete lists of crystallographic data are given in Appendix A. **2** also adopts a pseudo-capped octahedron geometry, and both Λ and Δ enantiomers are found in the unit cell. The Hf(1)-Cl(1) bond in **2** is 2.5014 Å, which is shorter than the Zr(1)-Cl bond (2.5125 Å), but longer than the reported Hf-Cl bonds (2.422 and 2.413 Å) in Hf[NMeC(^{i}Pr)$_2$]$_2$Cl$_2$ reported by Devi and coworkers.[8f] The bite angles of the amidinate ligands of **2** (59.2°, 58.9°, and 59.2°) are slightly smaller than those of Hf[NMeC(^{i}Pr)$_2$]$_2$Cl$_2$ (61.29° and 60.66°).[8f]

Compound **2** was also characterized by MS with an *m*/*z* = 635.36 [**2**+H$^+$]. Hafnium has six stable isotopes (^{174}Hf, ^{176}Hf, ^{177}Hf, ^{178}Hf, ^{179}Hf, and ^{180}Hf; Table 2.9). Along with the two stable isotopes of chlorine (^{35}Cl and ^{37}Cl, Table 2.4), the MS of **2** is expected to show a unique pattern. Solid powders of **2** were placed in a heated He stream (200 °C) by utilizing the sealed end of a capillary tube. Both the calculated and

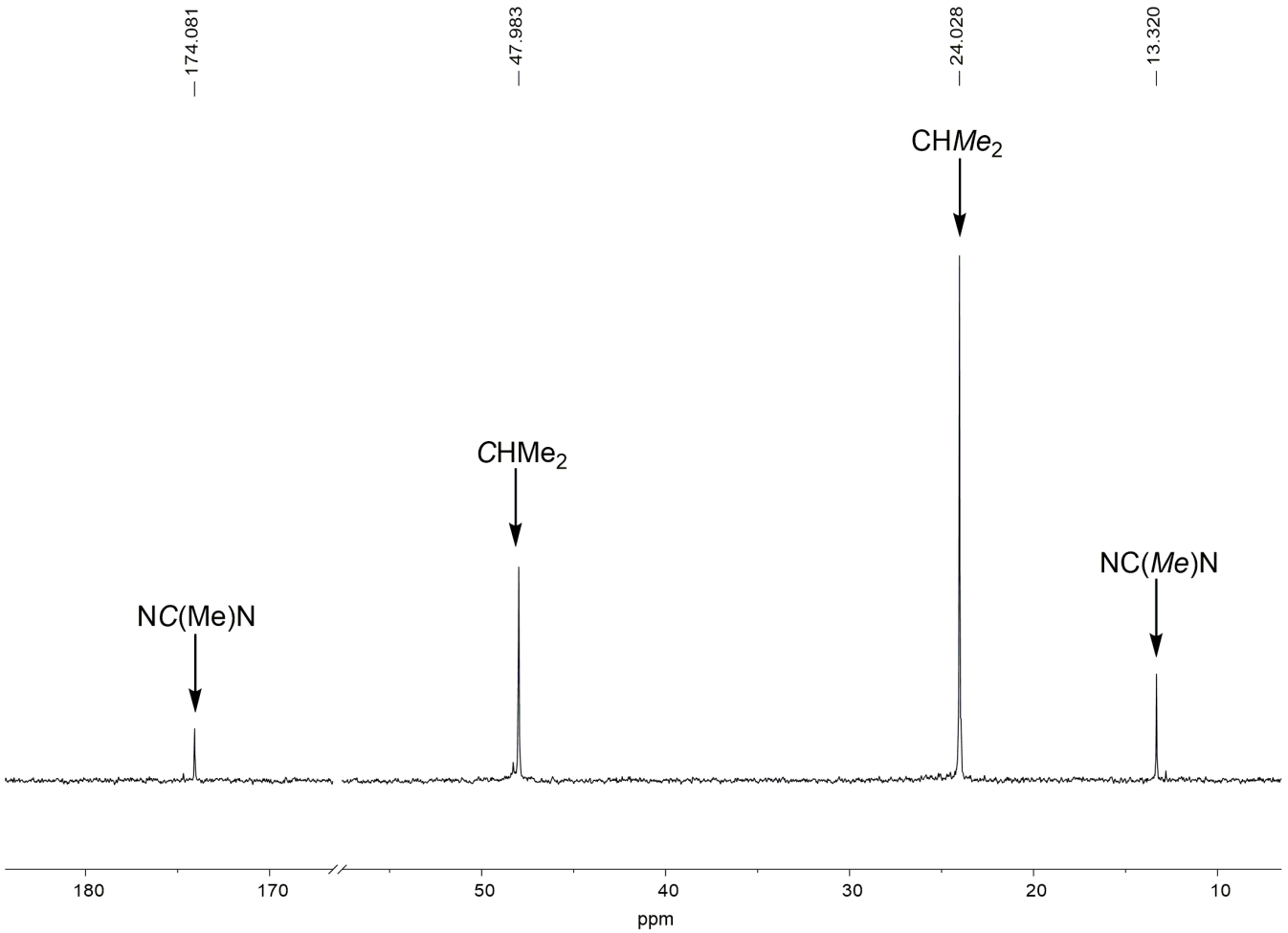

Figure 2.13. $^{13}C\{^{1}H\}$ NMR spectrum of **2** in benzene-d_6 at 23 °C.

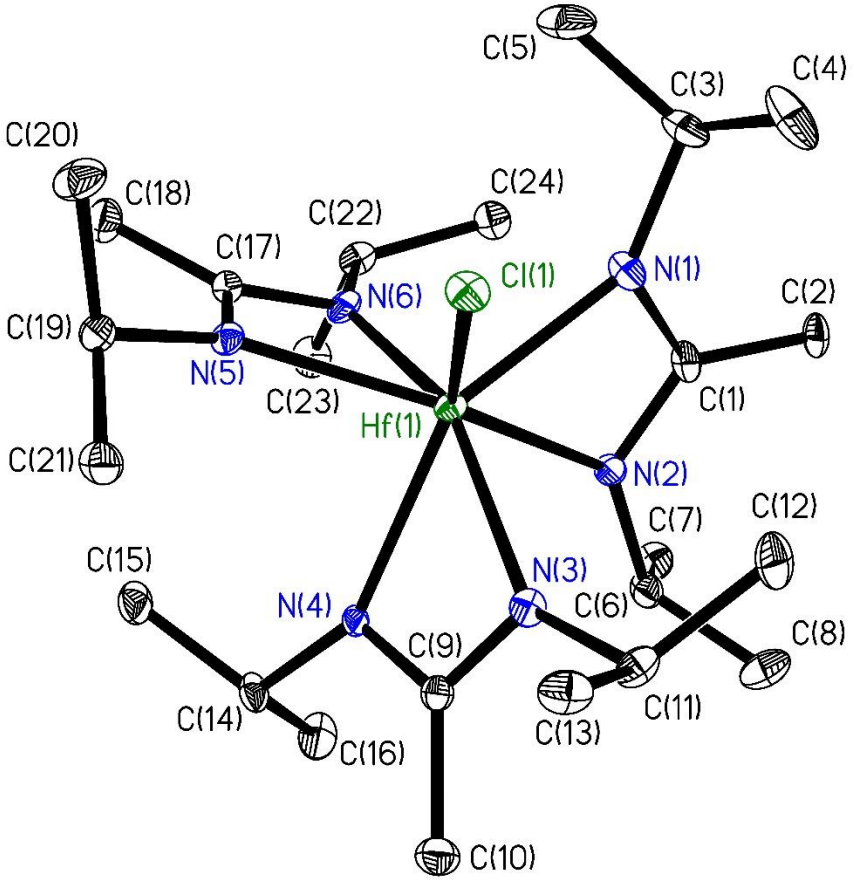

Figure 2.14. ORTEP of **2** at 100(2) K. Thermal ellipsoids are 30% probability level. Hydrogen atoms were removed for clarity.

Table 2.7. Crystal data and structure refinement for **2**

Empirical formula	$C_{24}H_{51}N_6ClHf$
Formula weight	637.64
Temperature	100(2) K
Wavelength	0.71073 Å
Crystal System	Monoclinic
Space Group	$P2_1/n$
Unit cell dimensions	a = 10.4324(15) Å α = 90°
	b = 16.447(2) Å β = 93.053(2)°
	c = 17.091(2) Å γ = 90°
Volume	2928.3(7) Å^3
Z	4
Density (calculated)	1.446 g/cm^3
Absorption coefficient	3.675 mm^{-1}
F(000)	1304.0
Crystal size	0.271 × 0.251 × 0.233 mm^3
Theta range for data collection	2.24 to 27.94°
Index ranges	$-13 \le h \le 13$, $0 \le k \le 21$, $0 \le l \le 22$
Reflections collected	6975
Independent reflections	6975 [R_{int} = 0.000]
completeness to theta = 27.94°	93.0%
Max. and min. transmission	0.745 and 0.491
Refinement method	Full-matrix least-squares on F^2
Absorption correction	Semi-empirical from equivalents
Data / restraints / parameters	6975 / 0 / 305
Goodness-of-fit on F^2	1.186

Table 2.7. Continued

Final R indices [$I > 2\sigma(I)$]	$R1$ = 0.0445, w$R2$ = 0.1177
R indices (all data)	$R1$ = 0.0525, w$R2$ = 0.1213
Largest diff. peak and hole	5.33 and -2.24 eÅ^{-3}

[a] $R1 = \Sigma\ ||F_o| - |F_c|| / \Sigma|F_o|$; $wR2 = [\Sigma\ w(F_o^2 - F_c^2)^2 / \Sigma\ w(F_o^2)^2]^{1/2}$;

$w = 1/[\sigma^2(F_o) + (aP)^2 + bP]$; $P = [2Fc^2 + \text{Max}(F_o^2, 0)]/3$

Table 2.8. Selected distances (Å) and angles (°) in **2**

Distances			
Hf(1)-Cl(1)	2.5014(16)	Hf(1)-N(4)	2.306(6)
Hf(1)-N(1)	2.183(6)	Hf(1)-N(5)	2.202(6
Hf(1)-N(2)	2.259(5)	Hf(1)-N(6)	2.293(6)
Hf(1)-N(3)	2.199(6)		

Angles			
N(1)-Hf(1)-Cl(1)	84.30(16)	N(3)-Hf(1)-N(4)	58.9(2)
N(2)-Hf(1)-Cl(1)	132.08(16)	N(3)-C(9)-N(4)	112.6(6)
N(1)-Hf(1)-N(2)	59.2(2)	N(5)-Hf(1)-Cl(1)	82.36(16)
N(1)-C(1)-N(2)	110.3(6)	N(6)-Hf(1)-Cl(1)	123.58(15)
N(3)-Hf(1)-Cl(1)	84.52(15)	N(5)-Hf(1)-N(6)	59.2(2)
N(4)-Hf(1)-Cl(1)	125.58(17)	N(5)-C(17)-N(6)	112.6(6)

Table 2.9. Stable isotopes of hafnium

Isotope	Accurate Mass	% Natural Abundance
^{174}Hf	173.940044(4)	0.16(1)
^{176}Hf	175.941406(4)	5.26(7)
^{177}Hf	176.943217(3)	18.60(9)
^{178}Hf	177.943696(3)	27.28(7)
^{179}Hf	178.9458122(29)	13.62(2)
^{180}Hf	179.9465457(30)	35.08(16)

experimental spectra of [**2**+H^+] are shown in Figure 2.15. Since the Cl ligand is very labile, the major species that was observed was the cation, Hf[NMeC(^{i}Pr)$_2$]$_3^+$, which has *m*/*z* = 599.36. Both the observed and calculated MS spectra of Hf[NMeC(^{i}Pr)$_2$]$_3^+$ are given in Figure 2.16.

In addition to [**2**+H^+], MS spectrum of the powders of **2** exposed to air showed the presence of [**9**+H^+], Hf[MeC(N^{i}Pr)$_2$]$_3^+$, and amidine ^{i}PrNH-C(Me)=N^{i}Pr. Their formation is discussed below in Section 3.2.7, along with the MS of **4** and **7**, alkyl analogs of **2**.

2.2.4. Variable-Temperature NMR Study of Hf[MeC(N^{i}Pr)$_2$]$_3$Cl (2)

Since there was a broad doublet in the ^{1}H NMR spectrum of **2**, we have also studied its dynamic behavior by VT-NMR. At 190 K, the rotations in **2** are greatly slowed. This resulted in the de-coalescence of the CH*Me*$_2$ on the isopropyl groups.

The ^{1}H spectrum of **2** at 190 K showed four doublets at 1.64, 1.51, 1.14, and 1.12 ppm for the two sets of methyl groups in CH*Me*$_E$*Me*$_F$ and CH*Me*$_G$*Me*$_H$, respectively. The doublets at 1.14 and 1.12 ppm overlapped. As the temperature was raised slowly, the rates of the methyl rotations increased until these groups became equivalent and their peaks coalesced. *Me*$_G$*Me*$_H$ and *Me*$_E$*Me*$_F$ have the temperature ranges of 200-235 K and 215-250 K, respectively.

The next exchange observed was the pseudo-Bailar twist, which is the interconversion between Δ and Λ enantiomers. This process is more difficult than the simple methyl rotations. This is reflected in the coalescence of the groups CH*Me*$_G$*Me*$_H$ and CH*Me*$_E$*Me*$_F$ (labeled as *Me*$_{E\text{-}F}$*Me*$_{G\text{-}H}$) at 270(1) K, which is higher than the

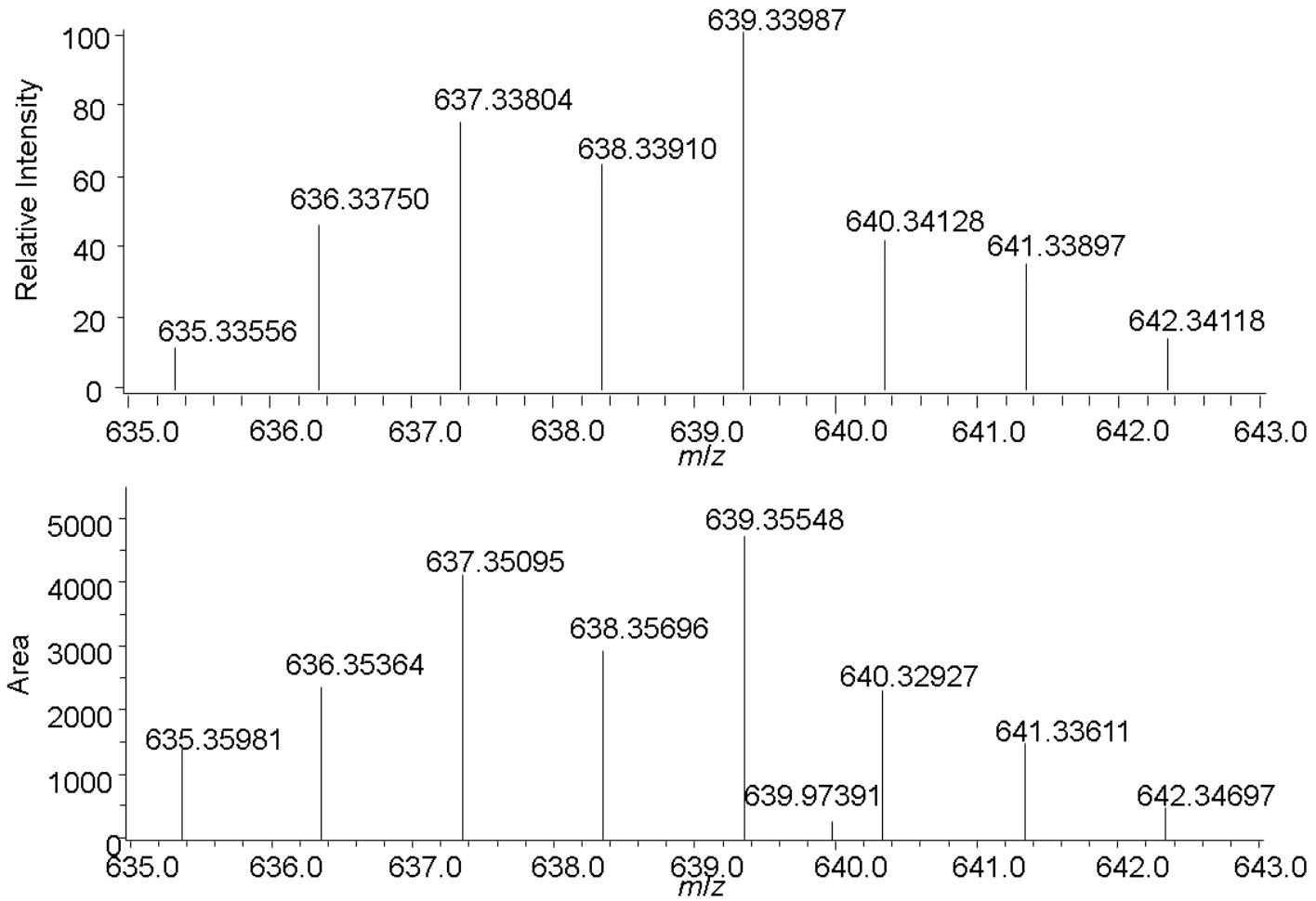

Figure 2.15. (Top) Calculated and (Bottom) Observed MS for [**2**+H^+]

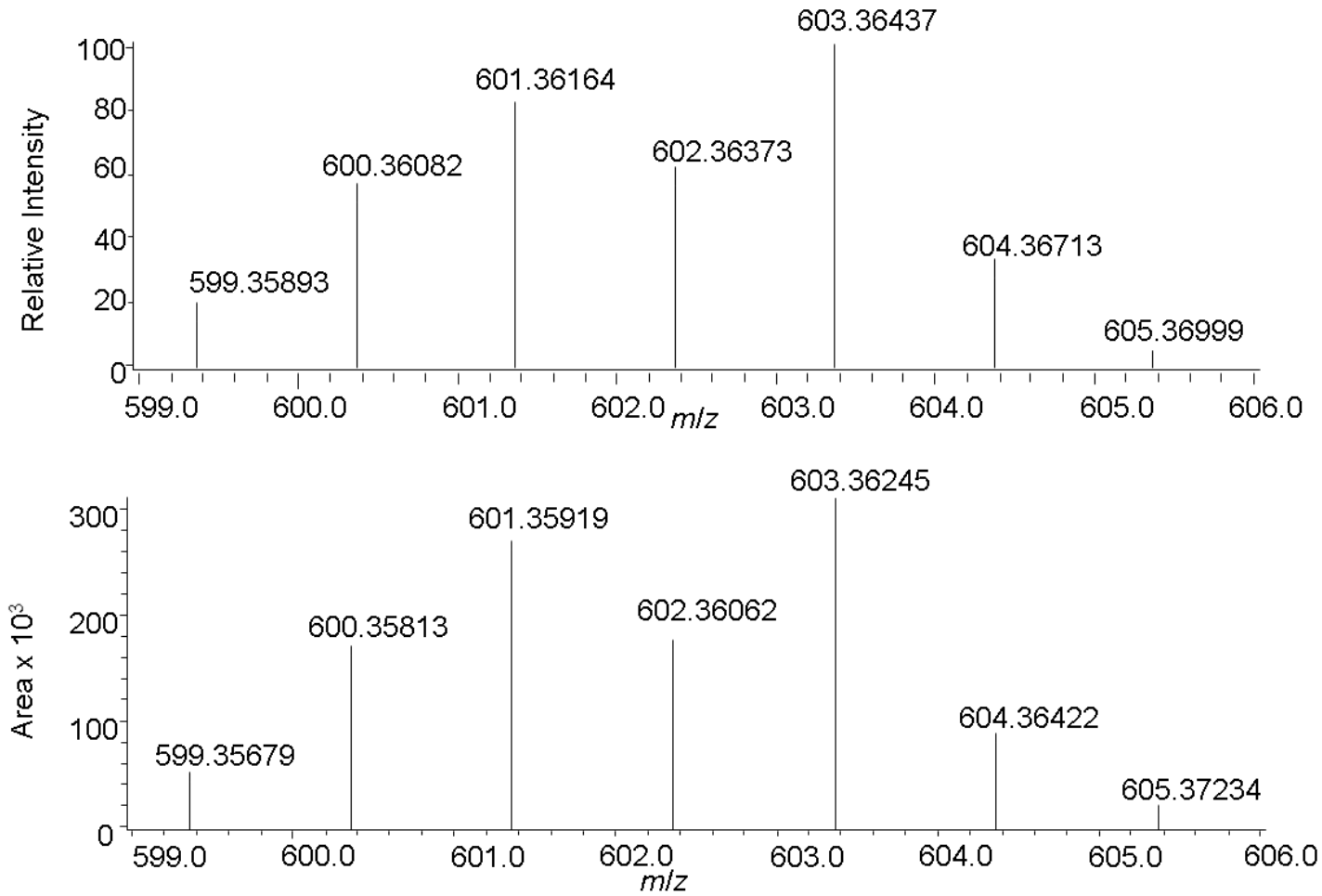

Figure 2.16. (Top) Calculated and (Bottom) Observed MS for $Hf[MeC(N^{i}Pr)_2]_3^+$.

coalescence temperatures for the methyl rotations. At 300(1) K, the CH*Me*$_2$ groups became a doublet due to the coupling to the H atoms in the CH*Me*$_2$ groups. Though the C*H*Me$_2$ multiplet greatly broadened at 190 K and became a sharp multiplet as the temperature rose, this peak never de-coalesced into C*H*$_A$Me$_2$ and C*H*$_B$Me$_2$ as in **1**

Figure 2.17 shows the partial VT-NMR spectra of the CH*Me$_2$ and* C*H*Me$_2$ regions. The frequency differences were taken from the CH*Me$_2$* groups and used in Eq. 2.1 in order to obtain the rate constants.[19-22] The rate constants and activation parameters $\Delta H^{\neq}$ and $\Delta S^{\neq}$ for the exchanges are given in Tables 2.10 and 2.11, respectively. The rate constants of the exchanges were used to generate Eyring plots (Figures 2.18, 2.18, and 2.20).

Similar to **1**, a common feature among the activation parameters for the exchanges in **2** is that $\Delta H^{\neq}$ is relatively low and $\Delta S^{\neq}$ is largely negative. $\Delta S^{\neq}$ in these exchanges are, however, much more negative than those in typical unimolecular chemical reactions, and the values of $T\Delta S^{\neq}$ are much larger contributors to the activation free energy $\Delta G^{\neq}$. These results reflect the fact that no bonds were broken in the exchanges, but the bulkiness and the number of the amidinate groups makes the exchanges difficult.

The *Me*$_E$*Me*$_F$ and *Me*$_G$*Me*$_H$ exchanges are the rotations of the two methyl groups on the same isopropyl groups in Zr[MeC(N^{i}Pr)$_2$]$_3$Cl (**1**). These methyl rotations reach coalescence first at the rather low temperatures of 235(1) and 250(1) K with activation parameters $\Delta H^{\neq}$ = 2.84(3) and 4.6(4) kcal/mol and $\Delta S^{\neq}$ = -39(1) and -29(1) eu for *Me*$_E$*Me*$_F$ and *Me*$_G$*Me*$_H$, respectively. The rates of the rotations of the methyl groups as well as the rates of the interconversions between the enantiomers were slightly faster

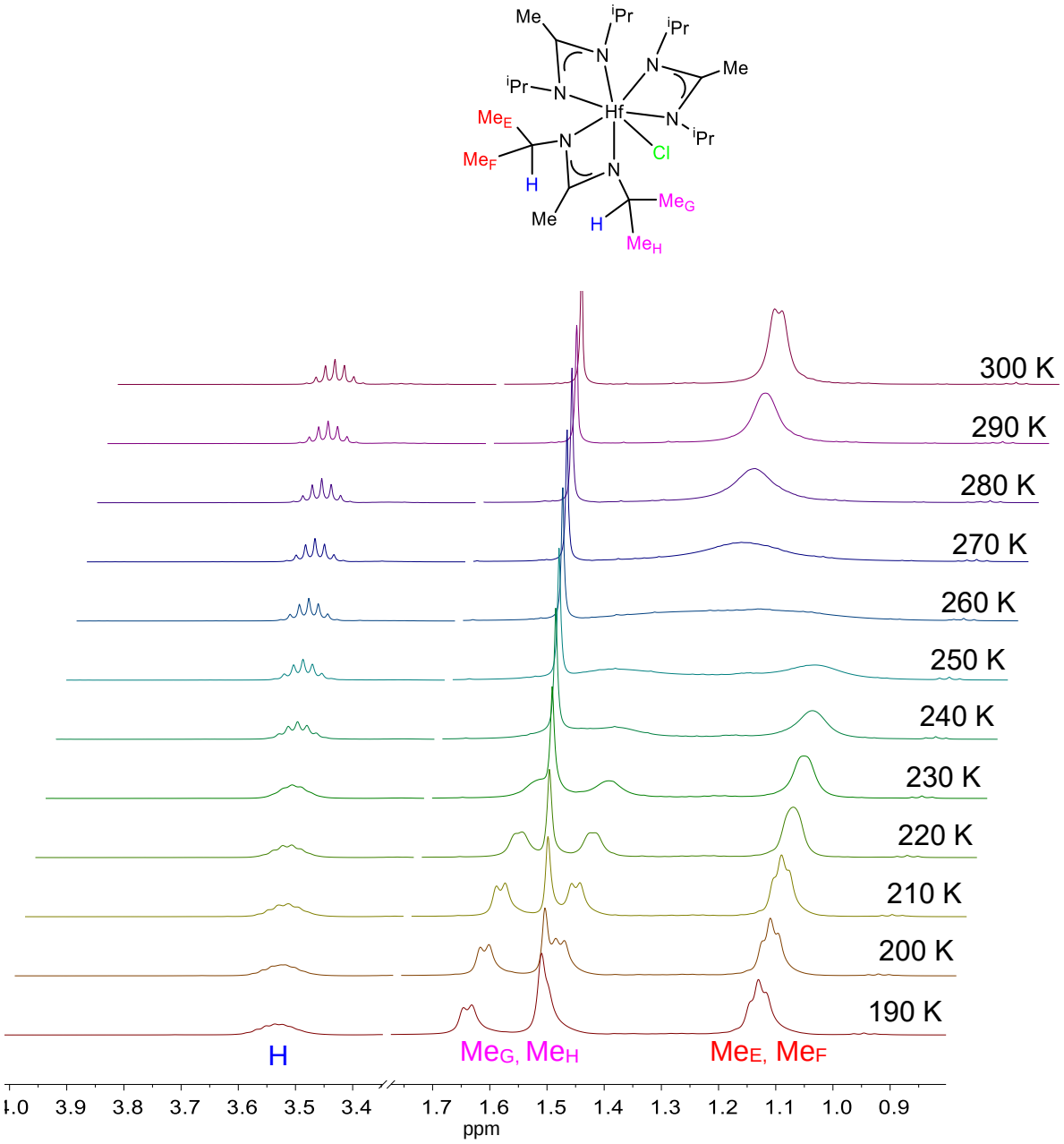

Figure 2.17. Partial ^{1}H NMR spectra of **2** at several temperatures showing the de-coalesce of the methyl and H atom peaks pertaining to the CHMe$_2$ groups as the temperature is lowered from room temperature to 190 K. As the temperature is raised to 300 K, the broad peak for the CH*Me*$_2$ groups becomes a doublet.

Table 2.10. Rate constants for the interconversions in **2**

T **(K)**	***k*** **(s^{-1}) for *Me*$_E$*Me*$_F$**	***k*** **(s^{-1}) for *Me*$_G$*Me*$_H$**	***k*** **(s^{-1}) for *Me*$_{E\text{-}F}$*Me*$_{G\text{-}H}$**
200(1)	7.4(1)		
205(1)	8.44(4)		
210(1)	10.54(0)		
215(1)	13.0(2)	51.3(9)	
220(1)	15.0(4)	61(3)	
225(1)	16.9(5)	76.9(6)	
230(1)	20.3(5)	102(2)	287(6)
235(1)	26.01(0)	141(6)	318.4(6)
240(1)		169(5)	373(2)
245(1)		222.0(6)	425(13)
250(1)		236.6(7)	485(18)
255(1)			610(17)
260(1)			702(6)
265(1)			765(6)

[a] The total uncertainties $\delta k/k$ were calculated from $\delta k_{ran}/k$ from each column and $\delta k_{sys}/k$ = 0.050. (1) *Me*$_E$*Me*$_F$: $\delta k_{ran}/k$ = 0.029, $\delta k/k$ = 0.058; (2) *Me*$_G$*Me*$_H$: $\delta k_{ran}/k$ = 0.065, $\delta k/k$ = 0.081; (3) *Me*$_{E\text{-}F}$*Me*$_{G\text{-}H}$: $\delta k_{ran}/k$ = 0.038, $\delta k/k$ = 0.063.

Table 2.11. Activation parameters for the interconversions in **2**

***T* (K)**	***k* (s^{-1}) for Me_EMe_F**	***k* (s^{-1}) for Me_GMe_H**	***k* (s^{-1}) for $Me_{E\text{-}F}Me_{G\text{-}H}$**
$\Delta H^{\neq}$ (kcal/mol)	2.84(3)	4.6(4)	3.1(3)
$\Delta S^{\neq}$ (eu)	-39(1)	-29(1)	-33(1)

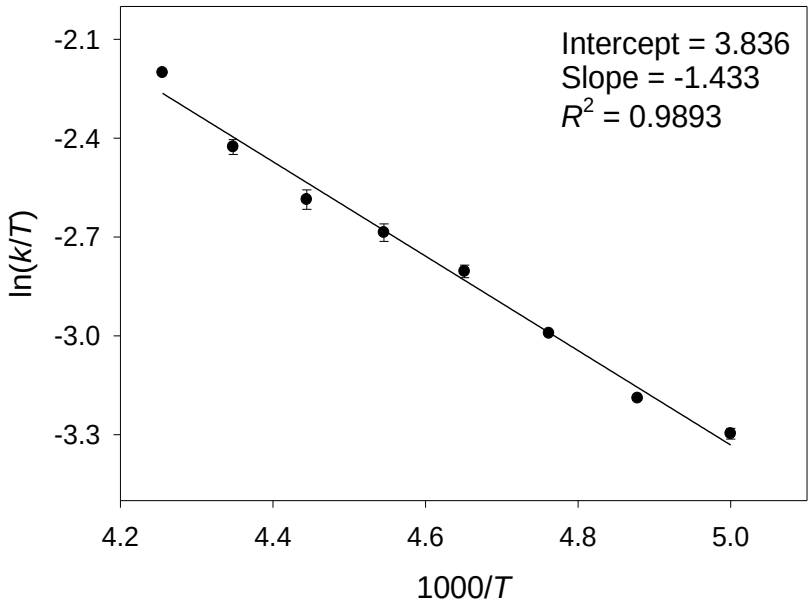

Figure 2.18. Eyring plot of the Me_EMe_F exchange in **2** yielding activation parameters for the exchange.

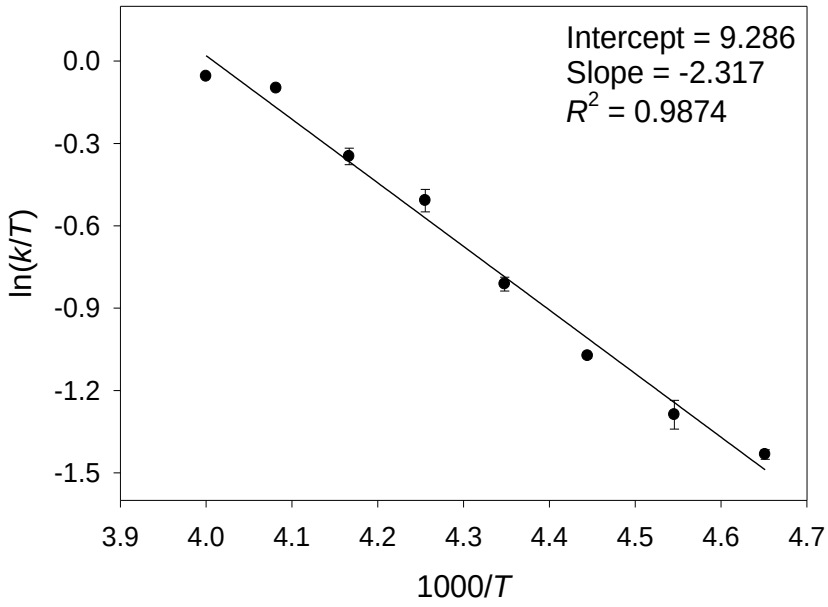

Figure 2.19. Eyring plot of the Me_GMe_H exchange in **2** yielding activation parameters for the exchange.

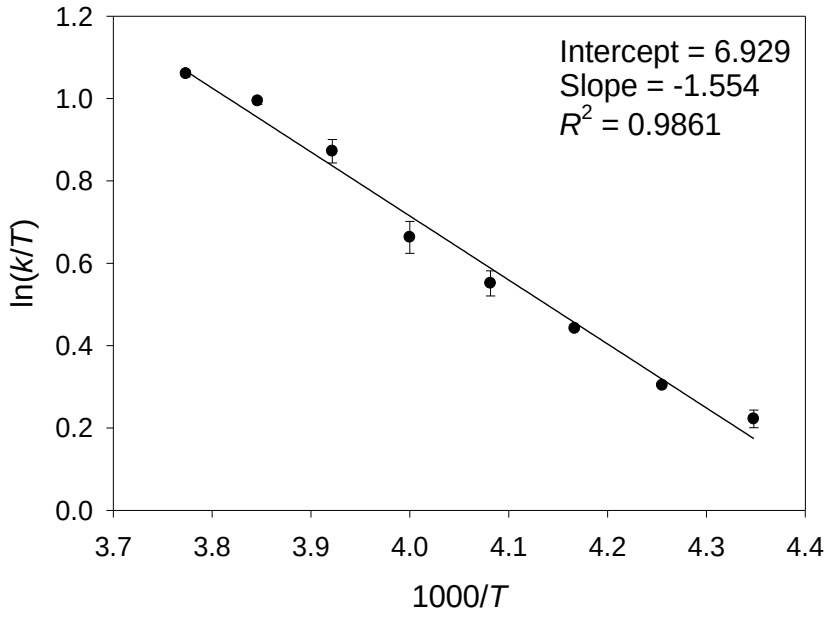

Figure 2.20. Eyring plot of the $Me_{E\text{-}F}Me_{G\text{-}H}$ exchange in **2** yielding activation parameters for the exchange.

for **2** than for **1**. The activation parameters of the two complexes are similar, showing difficulty in rotation because of the bulky amidinate ligands.

2.3. Concluding Remarks

In this chapter, two heptacoordinate amidinate chloride complexes, **1** and **2**, were prepared. The complexes were characterized via ^{1}H and ^{13}C NMR spectroscopies, singe crystal X-ray diffraction, and DART-MS. **1** and **2** were found to undergo fast exchange between Δ and Λ enantiomers which was studied via VT-NMR spectroscopy. It was found that the exchange rate of **2** was faster than that of **1**. Chloride complexes are useful as precursors to other complexes. Compounds **1** and **2** will be the starting materials to make alkyl analogues in Part 3

2.4. Experimental Section

All manipulations were carried out under a dry nitrogen atmosphere with the use of either a glovebox or standard Schlenk techniques. All glassware was flamed dried under vacuum. Hexanes, THF, and pentane were purified by distillation from potassium benzophenone ketyl. NMR solvents were dried and stored over 5 Å molecular sieves. N,N'-Diisopropylcarbodiimide and MeLi (1.6 M in Et_2O) were purchased from Acros and used without further purification. $ZrCl_4$ (Strem) was sublimed at 170 °C before use. $Li[MeC(N^{i}Pr)_2]$ was prepared by the reaction of N,N'-diisopropylcarbodiimide with MeLi by an approach similar to that of Hessen and coworkers.[17] ^{1}H, $^{13}C\{^{1}H\}$, HSQC, and VT-NMR spectra were recorded on a Bruker Avance 400 MHz or Varian VNMRS-500 spectrometer. Elemental analyses were conducted by Complete Analysis Laboratories,

Inc., Parsippany, NJ. Mass spectra were recorded on a JEOL AccuTOF™ DART Mass Spectrometer.

2.4.1. Preparation of $Zr[MeC(N^iPr)_2]_3Cl$ (1)

Freshly sublimed $ZrCl_4$ (0.889 g, 0.00381 mol) was stirred in a 2:1 (v/v) hexanes/THF solution (30 mL) at -40 °C to form a slurry. The slurry was allowed to warm to room temperature and to stir overnight. The slurry was then cooled to 0 °C. $Li[MeC(N^iPr)_2]$ (1.715 g, 0.0116 mol) was dissolved in 2:1 (v/v) hexanes/THF (10 mL) and added dropwise to the $ZrCl_4$ slurry. The solution was allowed to warm to room temperature over 2 h, and then heated at 35 °C for 24 h. Volatiles were removed in vacuo, and crude product was extracted with pentane (10-15 mL). The product was filtered, giving a bright yellow solution. The volume of the solution containing the crude product was reduced to ~5 mL. The solution was then put into a -32 °C freezer to afford light yellow crystals of **1** (1.280 g, 0.00233 mol, 61% yield based on $ZrCl_4$). ^{1}H NMR (benzene-d_6, 399.92 MHz, 23 °C): δ 3.53 (m, 6H, C*H*Me$_2$), 1.62 (s, 9H, NC(*Me)*N), 1.34 (br s, 36H, CH*Me$_2$*); ^{13}C{^{1}H} NMR (benzene-d_6, 100.56 MHz, 23 °C): δ 174.68 (N*C*(Me)N), 48.2 (*C*HMe$_2$), 23.94 (CH*Me$_2$*), 12.80 (NC(*Me*)N); ^{1}H NMR (toluene-d_8, 399.92 MHz, 23 °C): δ 3.52 (m, 6H, C*H*Me$_2$), 1.64 (s, 9H, NC(*Me)*N), 1.31 (br s, 36H, CH*Me$_2$*); ^{13}C{^{1}H} NMR (toluene-d_8, 100.56 MHz, 23 °C): δ 174.63 (N*C*(Me)N), 48.33 (*C*HMe$_2$), 23.93 (CH*Me$_2$*), 12.70 (NC(*Me*)N); ^{1}H NMR (toluene-d_8, 399.92 MHz, -80 °C) δ 3.52 (m, 3H, C*H*Me$_2$), 3.35 (m, 3H, C*H*Me$_2$), 1.64 (d, 9H, CH*Me$_2$*), 1.52 (s, 9H, NC(*Me)*N), 1.51 (d, 9H, CH*Me$_2$*), 1.16 (d, 9H, CH*Me$_2$*), 1.13 (d, 9H, CH*Me$_2$*), 1.335 (d, 9H, CH*Me$_2$*);^{13}C{^{1}H} NMR (toluene-d_8, 399.92 MHz, -80 °C): δ 174.45 (N*C*(Me)N), 48.15

(*C*HMe$_2$), 47.57 (*C*HMe$_2$), 23.73 (CH*Me*$_2$), 23.58 (CH*Me*$_2$), 12.80 (NC(*Me*)N). ^{1}H and ^{13}C{^{1}H} NMR assignments were confirmed by HSQC experiments (Figure A1). Anal. Calcd: C, 52.37; H, 9.34; N, 15.27. Found: C, 51.99; H, 9.13; N, 15.17. DART-MS: Calcd *m*/z = 549.2989 [**1**+H$^+$], Found *m*/z = 549.33828 [**1**+H$^+$].

2.4.2. Preparation of Hf[MeC(N^{i}Pr)$_2$]$_3$Cl (2)

A 2:1 (v/v) hexanes/THF solution (30 mL) was added to freshly sublimed $HfCl_4$ (1.201 g, 0.00375 mol) at -40 °C to form a slurry and allowed to stir overnight. The slurry was cooled to 0 °C. Li[MeC(N^{i}Pr)$_2$] (1.692 g, 0.0114 mol) was dissolved in a 2:1 (v/v) hexanes/THF (10 mL). The Li[MeC(N^{i}Pr)$_2$] solution was added to the slurry dropwise. The solution was allowed to reach room temperature over 2 h, and then heated to 35 °C for 24 h. The volatiles were removed in vacuo, and the crude product extracted with pentane. The solution was filtered, and the volume reduced to ~5 mL. The solution flask was placed in a -32 °C freezer to give pale yellow crystals of **2** (1.153 g, 0.00181 mol, 48% yield based on $HfCl_4$). ^{1}H NMR (benzene-d_6, 399.92 MHz, 23 °C): δ 3.65 (m, 6H, C*H*Me$_2$), 1.62 (s, 9H, NC(*Me)*N), 1.32 (d, 36H, CH*Me*$_2$); ^{13}C{^{1}H} NMR (benzene-d_6, 100.56 MHz, 23 °C): δ 174.08 (N*C*(Me)N), 47.98 (*C*HMe$_2$), 24.03 (CH*Me*$_2$), 13.33 (NC(*Me*)N). ^{1}H NMR (toluene-d_8, 399.92 MHz, 29 °C): δ 3.63 (m, 6H, C*H*Me$_2$), 1.64 (s, 9H, NC(*Me)*N), 1.29 (d, 36H, CH*Me*$_2$); ^{13}C{^{1}H} NMR (toluene-d_8, 100.56 MHz, 29 °C): δ 174.03 (N*C*(Me)N), 48.03 (*C*HMe$_2$), 24.02 (CH*Me*$_2$), 13.23 (NC(*Me*)N); ^{1}H NMR (toluene-d_8, 399.92 MHz, -83 °C): δ 3.54 (br m, 3H, C*H*Me$_2$), 1.64 (d, 9H, CH*Me*$_2$), 1.51 (s, 9H, NC(*Me)*N), 1.51 (d, 9H, CH*Me*$_2$), 1.14 (d, 9H, CH*Me*$_2$), 1.12 (d, 9H, CH*Me*$_2$), 1.335 (d, 9H, CH*Me*$_2$);^{13}C{^{1}H} NMR (toluene-d_8, 399.92 MHz, -83 °C): δ 173.82

(NC(Me)N), 47.89 (*C*HMe$_2$), 47.20 (*C*HMe$_2$), 23.96 (CH*Me*$_2$), 23.51 (CH*Me*$_2$), 12.66 (NC(*Me*)N). ^{1}H and ^{13}C{^{1}H} NMR assignments were confirmed by HSQC experiments (Figure A2). Anal. Calcd: C, 45.21; H, 8.06; N, 13.18. Found: C, 45.11; H, 7.98; N, 12.97. DART-MS: DART-MS: Calcd *m*/z = 635.33556 [**2**+H$^+$], Found *m*/z = 635.35981 [**2**+H$^+$].

2.4.3. Calculating Errors in Variable-Temperature NMR Studies

The activation parameters for **1** and **2** determined from their Eyring plots were obtained by using the average rate constants which were obtained through two separate experiments at a given temperature. The averages are listed in Tables 2.5 and 2.10. The maximum random uncertainty in the rate constants was combined with the estimated systematic uncertainty of 5%. The total uncertainties in the rate constants *k* were used in the ln(k_{eq}/*T*) vs. 1000/*T* plot in Figures 2.8, 2.9, 2.10, 2.11, 2.18, 2.19, 2.20, and error calculations. The NMR probe temperature measurements contribute to an estimated uncertainty of 1 K. The uncertainties in $\Delta H^{\neq}$ and $\Delta S^{\neq}$ were calculated from the following error formulas derived from $R\ln(kh/k_bT) = -\Delta H^{\neq}/T + \Delta S^{\neq}$.[25]

$$(\sigma\Delta H^{\neq})^2 = \frac{R^2 T_{max}^2 T_{min}^2}{\Delta T^2}\left\{\left(\frac{\sigma T}{T}\right)^2\left[\left(1+T_{min}\frac{\Delta L}{\Delta T}\right)^2+\left(1+T_{max}\frac{\Delta L}{\Delta T}\right)^2\right]+2\left(\frac{\sigma k}{k}\right)^2\right\}$$

$$(\sigma\Delta S^{\neq})^2 = \frac{R^2}{\Delta T^2}\left\{\left(\frac{\sigma T}{T}\right)^2\left[T_{max}^2\left(1+T_{min}\frac{\Delta L}{\Delta T}\right)^2+T_{min}^2\left(1+T_{max}\frac{\Delta L}{\Delta T}\right)^2\right]+\left(\frac{\sigma k}{k}\right)^2\left(T_{max}^2+T_{min}^2\right)\right\}$$

where $\Delta L = [\ln(k_{max}/T_{max}) - \ln(k_{min}/T_{min})]$ and $\Delta T = (T_{max} - T_{min})$.

2.4.4. Determination of the X-ray Crystal Structures of 1 and 2

The X-ray structures of **1** and **2** were determined on a Bruker ASX Smart 1000 X-ray diffractometer equipped with a CCD area detector and a graphite-monochromated Mo source (*K*α radiation, 0.71073 Å) and fitted with an upgraded Nicolet LT-2 low temperature device. A suitable crystal was chosen from a batch and was coated paratone oil (Exxon). The crystal was mounted onto the diffractometer using a fiber loop under a stream of nitrogen at 100(2) K. The structure was solved by direct methods, and all non-hydrogen atoms were refined anisotropically using Olex2 software. Since the crystals for both **1** and **2** were twinned, TWINABS was used for the absorption corrections. The twin laws (TWIN -1 0 -0.071 0 -1 0 0 0 1, and BASF 0.0839) and (TWIN -1 0 0 0 -1 0 0.175 0 1, and BASF 0.3297) were used for **1** and **2**, respectively, to solve the twinning by merohdry. Global refinements for the unit cells and data reduction were performed using the Saint program (Version 6.02). Calculations of atom positions were done using SHELXTL (Version 5.1) proprietary software package and Olex2.[26,27]

2.4.5. Mass Spectrometry Studies of 1 and 2

Mass spectra were recorded on a JEOL AccuTOF™ DART Mass Spectrometer. The closed end of a capillary tube was inserted into either solid powders or a solution (in pentane) of the samples. The tube was then placed into a heated stream of He (200 °C) in the spectrometer. The spectra were referenced to a polyethylene glycol (PEG) standard.

References

1. (a) Stanciu, C.; Jones, M. E.; Fanwick, P. E.; Abu-Omar, M. M. *J. Am. Chem. Soc.* **2007**, *129*, 12400. (b) Tilley, T. D. *Organometallics*, **1985**, *4*, 1452. (c) Blackburn,T. F.; Labinger, J. A.; Schwartz, J. *Tetrahedron Lett.* **1975**, *16*, 3041. (d) Lubben, T. V.; Wolczanski, P. T. *J. Am. Chem. Soc.* **1987**, *109*, 424. (e) Wang, R.; Folting,K.; Huffman, J. C.; Chamberlain, L. R.; Rothwell, I. P. *Inorg. Chim. Acta* **1986**, *120*,81. (f) Gibson, V. C.; Redshaw, C.; Walker, G. L. P.; Howard, J. A. K.; Hoy, V. J.; Cole, J. M.; Kuzmina, L. G.; De Silva, D. S. *Dalton Trans.* **1999**, 161. (g) Schaverien, C. J.; Orpen, A. G. *Inorg. Chem.* **1991**, *30*, 4968. (h) Liu, X.; Cui, D. *Dalton Trans.* **2008**, 3747. (i) Van Asselt, A.; Trimmer, M. S.; Henling, L. M.; Bercaw, J. E. *J. Am. Chem. Soc.* **1988**, *110*, 8254. (j) Brindley, P. B.; Hodgson, J.C. *J. Organomet. Chem.* **1974**, *65*, 57. (k) Boro, B. J.; Lansing, R.; Goldberg, K. I.; Kemp, R. A. *Inorg. Chem. Comm.* **2011**, *14*, 531. (l) Lu, F.; Zarkesh, R. A.; Heyduk, A. F. *Eur. J. Inorg. Chem.* **2012**, *3*, 467. (m) Chisholm, M. H.; Hammond, C. E.; Huffman, J. C. *Chem. Comm.* **1987**, 1423. (n) Wang, R.-T.; Zhang, X.-H.; Chen, S.-J.; Yu, X.-H.; Wang, C.-S.; Beach, D. B.; Wu, Y.-D.; Xue, Z.-L. *J. Am. Chem. Soc.* **2005**, *127*, 5204. (o) Chen, S.-J.; Zhang, X.-H.; Yu, X.; Qiu, H.; Yap, G. P. A.; Guzei, I. A.; Lin, Z.; Wu, Y. D.; Xue, Z.-L. *J. Am. Chem. Soc.* **2007**, *129*, 14408. (p) Chen, S.-J.; Zhang, J.; Yu, X.; Bu, X.; Chen, X.-T.; Xue, Z.-L. *Inorg. Chem.* **2010**, *49*, 4017. (q) Morton, L. A.; Miao, M.; Callaway, T. M.; Chen, T.; Chen, S.-J.; Tuinman, A. A.; Yu, X.-H.; Lu, Z.; Xue, Z.-L. *Chem. Comm.* **2013**, *49*, 9555. (r) Chen, T.-N.; Zhang, X.-H.; Wang, C.-S.; Chen, S.-J.; Wu, Z.-Z.; Li, L.- T.; Sorasaenee, K. R.; Diminnie, J. B.; Pan,

H.-J.; Guzei, I. A.; Rheingold, A. L.; Wu, Y.-D.; Xue, Z.-L. *Organometallics* **2005**, *24*, 1214. (s) Qiu, H.; Chen, S.-J.; Wang, C.-S.; Wu, Y.-D.; Guzei, I. A.; Chen, X.-T.; Xue, Z.-L. *Inorg. Chem.* **2009**, *48*, 3073. (t) Yu, X.; Chen, X.-T.; Xue, Z.-L. *Organometallics* **2009**, *28*, 6642. (u) Chen, S.-J.; Yap, G. P. A.; Xue, Z.-L. *Sci. China: Chem.* **2009**, *52*, 1583. (v) Chen, S.-J.; Zhang, X.-H.; Lin, Z.; Wu, Y.-D.; Xue, Z.-L. *Sci. China: Chem.* **2009**, *52*, 1723. (w) Chen, S.-J.; Xue, Z.-L. *Organometallics* **2010**, *29*, 5579. (x) Sharma, B.; Callaway, T. M.; Lamb, A. C.; Steren, C. A.; Chen, S.-J.; Xue, Z.-L. *Inorg. Chem.* **2013**, *52*, 11409.

2. (a) Campbell, A. N.; Stahl, S. S. *Acc. Chem. Res.* **2012**, *45*, 851. (b) Theopold, K. H.; Reinaud, O. M.; Blanchard, S.; Leelasubeharoen, S.; Hess, A.; Thyagarajan, S. *ACS Symp. Ser.* **2002**, *823*, 75. (c) Que, L.; Tolman, W. B. *Nature* **2008**, *455*, 333. (d) Himes, R. A.; Karlin, K. D. *Curr. Top. Chem. Biol.* **2009**, *13*, 119. (e) Shook, R. L.; Borovik, A. S. *Chem. Comm.* **2008**, 6095. (f) Sheldon, R. A. in *Biomimetic Oxidations Catalyzed by Transition Metal Complexes*, Meunier, B. ed., Imperial College Press, 2000, pp. 613-662. (g) *Metal-Dioxygen Complexes: A Perspective.* Special Issue, *Chem. Rev.* **1994**, *94*, Issue 3, 567-856. (h) Monillas, W. H.; Yap, G. P. A.; MacAdams, L. A.; Theopold, K. H. *J. Am. Chem. Soc.* **2007**, *129*, 8090. (i) McQuilken, A. C.; Jiang, Y.; Siegler, M. A.; Goldberg, D. P. *J. Am. Chem. Soc.* **2012**, *134*, 8758. (j) Prokop, K. A.; Goldberg, D. P. *J. Am. Chem. Soc.* **2012**, *134*, 8014. (k) Scheuermann, M. L.; Fekl, U.; Kaminsky, W.; Goldberg, K. I. *Organometallics* **2010**, *29*, 4749. (l) Boisvert, L.; Denney, M. C.; Kloek Hanson, S.; Goldberg, K. I. *J. Am. Chem. Soc.* **2009**, *131*, 15802. (m) Khusnutdinova, J. R.; Rath, N. P.; Mirica, L. M. *J. Am. Chem. Soc.* **2012**, *134*,

2414. (n) Nguyen, K. T.; Rath, S. P.; Latos-Grazynski, L.; Olmstead, M. M.; Balch, A. L. *J. Am. Chem. Soc.* **2004**, *126*, 6210. (o) Maury, J.; Feray, L.; Bazin, S.; Clement, J.-L.; Marque, S. R. A.; Siri, D.; Bertrand, M. P. *Chem. Eur. J.* **2011**, *17*, 1586. (p) Lewinski, J.; Koscielski, M.; Suwala, K.; Justyniak, I. *Angew. Chem. Int. Ed.* **2009**, *48*, 7017. (q) Mukherjee, D.; Ellern, A.; Sadow, A. D. *J. Am. Chem. Soc.* **2012**, *134*, 13018. (r) Jana, S.; Berger, R. J. F.; Fröhlich, R.; Pape, T.; Mitzel, N. W. *Inorg. Chem.* **2007**, *46*, 4293. (s) Lee, C.-M.; Chuo, C.-H.; Chen, C.-H.; Hu, C.-C.; Chiang, M.-H.; Tseng, Y.-J.; Hu, C.-H.; Lee, G.-H. *Angew. Chem. Int. Ed.* **2012**, *51*, 5427. (t) Kelley, M. R.; Rohde, J.-U. *Chem. Comm.* **2012**, *48*, 2876. (u) Brown, S. N.; Mayer, J. M. *Inorg. Chem.* **1992**, *31*, 4091. (v) Parkin, G.; Bercaw, J. E. *J. Am. Chem. Soc.* **1989**, *111*, 391.

3. (a) Campbell, S. A. *Science and Engineering of Microelectronic Fabrication,* ed. A. S. Sedra, Oxford University Press, 2nd Ed., 2001. (b) Panda, D.; Tseng, T.–Y. *Thin Solid Films* **2013***, 531,* 1. (c) Hitchman, M. L.; Jenson, K. F. in *Chemical Vapor Deposition: Principles and Applications*. eds. Hitchman, M. L.; Jenson, K. F. Academic Press, 1993, 1. (d) Jenson, K. F. in *Chemical Vapor Deposition: Principles and Applications*. eds. Hitchman, M. L.; Jenson, K. F. Academic Press, 1993, 31. (d) Pierson, H. O. in *Handbook of Chemical Vapor Deposition: Principles, Technology, and Applications.* eds. Bunshah, R. F.; McGuire, G. E.; Rossnagel, S. M., Noyes Publications, 1992. (f) Powell, C. F.; Oxley, J. H.; Blocher, J. M. *Vapor Deposition*, The Electrochemical Society, 1966. (g) Wallace, R.; Wilk, G. D. *MRS Bull*. **2002**, *27*, 192. (h) Jones, A. C.; Hitchman, M. L. *Chemical Vapour Deposition: Precursors, Processes and Applications*, Royal

Society of Chemistry, 2009, 1. (i) Ritala, M.; Niinisö, J. in *Chemical Vapour Deposition: Precursors, Processes and Applications.* eds. Jones, A. C.; Hitchman, M. L., Royal Society of Chemistry, 2009, *158.* (j) Malik, M. A.; O'Brien, P. in *Chemical Vapour Deposition: Precursors, Processes and Applications.* eds. Jones, A. C.; Hitchman, M. L., Royal Society of Chemistry, 2009, 207. (k) Jones, A. C.; Aspinall, H. C.; Chalker, P. R. in *Chemical Vapour Deposition: Precursors, Processes and Applications.* eds. Jones, A. C.; Hitchman, M. L., Royal Society of Chemistry, 2009, 357. (l) Devi, A. *Coord. Chem. Rev.* **2013***, 257,* 3332.

4. (a) Baker, R.J.; Jones, C. *J. Organomet. Chem.* **2006**, *691*, 65. (b) Barry, S.T. Coord. Chem. Rev. **2013**, *257*3, 192.
5. (a) Edelmann, F. T. *Chem. Soc. Rev.* **2012**, *41*, 7657. (b) Elkin, T.; Eisen, M. S. *Catal. Sci. Technol.* **2015**, *5*, 82.
6. Weitershaus, K.; Ward, B. D.; Kubiak, R.; Müller, C.; Wadepohl, H.; Doye, S.; Gade, L. H. *Dalton Trans.* **2009**, 4586.
7. Tiong, P. J.; Nova, A.; Clot, E.; Moundtford, P. *Chem. Comm.* **2001**, *47*, 3147.
8. (a) Krisyuk, V.; Aloui, L.; Prud'homme, N.; Sysoev, S.; Senocq, F.; Samelor, D.; Vahlas, C. *Electrochem. Solid-State Lett.* **2011**, *14*, D26. (b) Seetula, J.; Kalliorinne, K.; Koskikallio, J. *J. Photochem. Photobiol. A.: Chem.* **1988**, *43*, 31. (c) Thiede, T. B.; Krasnopolski, M.; Milanov, A. P.; Arcos, T.; Ney, A.; Becker, H.-W; Rogalla, D.; Winter, J.; Devi, A.; Fischer, R. A. *Chem. Mater.* **2011**, *23*, 1430. (d) Eleter, M.; Hubert-Pfalzgraf, L. G.; Daniele, S.; Pilet, G.; Tinant, B. *Polyhedron* **2010**, 29, 2522. (e) Li, Z.; Gordon, R. G.; Pallem, V.; Li, H.; Shenai, D. V. *Chem. Mater.* **2010**, *22*, 3060. (f) Xu, K.; Milanov, A. P.; Winter, M.;

Barreca, D.; Gasparotto, A.; Becker, H.-W.; Devi, A. *Eur. J. Inorg. Chem.* **2010**, 1679. (g) Eleter, M.; Daniele, S.; Brizé, V.; Dubourdieu, C.; Lachaud, C.; Blasco, N.; Pinchart, A. *ECS Trans.* **2009**, *25*, 151. (h) Gleizes, A. N.; Krisyuk, V. V.; Aloui, L.; Turgambaeva, A. E.; Sarapata, B.; Prud'homme, N.; Senocq, F.; Samélor, D.; Zielinska-Lipiec, A.; Dumestre, F.; Vahlas, C. *ECS Trans.* **2009**, *25*, 181. (i) Pallem, V. R.; Dussarrat, C., U.S. Pat. Appl. Publ., 2011, US 20110250354 A1 20111013. (j) Turgambaeva, A.; Prud'homme, N.; Krisyuk, V.; Vahlas, C. *J. Nanosci. Nanotechnol.* **2011**, *11*, 8198. (k) Shenai-Khatkhate, D. V.; Manzik, S. J.; Wang, Q. M., U.S. Pat. Appl. Publ., 2009, US 20090017208 A1 20090115. (l) Li, Z.; Lee, D. K.; Coulter, M.; Rodriguez, L. N. J.; Gordon, R. G. *Dalton Trans.* **2008**, 2592. (m) Li, X.-G.; Li, Z.; Li, H.; Gordon, R. G. *Eur. J. Inorg. Chem.* **2007**, 1135. (n) Li, Z.; Barry, S. T.; Gordon, R. G. *Inorg. Chem.* **2005**, *44*, 1728.

9. Sun, J.; Chen, S.-J.; Duan, Y.; Li, Y.; Chen, X.; Xue, Z.-L. *Organometallics* **2009**, *28*, 3088.

10. (a) Lamb, A. C.; Wang, Z.; Cook, T. M.; Sharma, B.; Chen, S.-J.; Lu, Z.; Steren, C. A.; Lin, Z.; Xue, Z.-L. *Polyhedron* **2016**, *103*, 2. (b) Lamb, A. C.; Lu, Z.; Xue, Z.-L. *Chem. Comm.* **2014**, *50*, 10517.

11. Ren, S.; Qiu, Z.; Xie, Z. *Organometallics* **2013**, *32*, 4292.

12. Casanova, D; Alemany, P.; Bofill, J. M.; Alvarez, S. *Chem. Eur. J.* **2003**, *9*, 1281.

13. (a) Hoffmann, R.; Beier, B. F.; Muetterties, E. L; Rossi, A. R. *Inorg. Chem.* **1977**, *16*, 511. (a) Kepert, D. L. *Progr. Inorg. Chem.* **1979**, *25*, 41. (b) Drew, M. G. B.

Progr. Inorg. Chem. **1977**, *23*, 67. (c) Lin, Z.; Bytheway, I. *Inorg. Chem.* **1996,** *35,* 594.

14. (a) Bray, R. C.; Adams, B.; Smith, A. T.; Benett, B.; Bailey, S. *Biochemistry* **2000**, *39*, 11258. (b) McAlpine, A. S.; McEwan, A. G.; Shaw, A. L.; Bailey, S. *J. Biol. Inorg. Chem.* **1997**, *2*, 590. (c) Gill, H. S.; Eisenberg, D. *Biochemistry* **2001**, *40*, 1903. (d) Johnson, K. A.; Chen, L.; Yang, H.; Roberts, M. F.; Stec, B. *Biochemistry* **2001**, *50*, 618. (e) Rao, S. T.; Satyshur, K. A.; Greaser, M. L.; Sundaralingam, M. *Acta Crystallogr. Sect. D* **1996**, *52*, 916. (f) Seemann, J. E.; Schuz, G. E. *J. Mol. Biol.* **1997**, *273*, 256.
15. Yan, L.; Wang, X.; Zhou, M. *Inorg. Chem. Comm.* **2016**, *65*, 32.
16. Zhou, M.; Tong, H.; Wei, X.; Liu, D. *J. Organomet. Chem.* **2007**, *692*, 5195.
17. Ge, S.; Meetsma, A.; Hessen, B. *Organometallics* **2008**, *27*, 3131.
18. Bailar, J. C. *J. Inorg. Nucl. Chem.* **1958**, *8*, 165.
19. Lin, Z.; Bytheway, I. *Inorg. Chem.* **1996,** *35,* 594.
20. It should be noted that this experiment used a 400 MHz NMR spectrometer. The coalescence and static spectra temperatures are dependent on the magnetic field. Thus, NMR spectra at other frequencies would show slightly different temperatures of coalescence.
21. Sandstrom, J. *Dynamic NMR Spectroscopy*; Academic Press, 1982.
22. Macomber, R. S. *A Complete Introduction to Modern NMR Spectroscopy*; Wiley, 1998; pp. 158-160.
23. The rate constants here are the chemical rate constants, and they differ from the observed magnetization transfer rate constants by a factor of 2.

24. Green, M. L. H.; Wong, L. L.; Sella, A. *Organometallics* **1992**, *11*, 2660.

25. Morse, P. M.; Spencer, M. D.; Wilson, S. R.; Girolami, G. S. *Organometallics* **1994**, *13*, 1646.

26. (a) Sheldrick, G. M. TWINABS, *A Program for Empirical Absorption Correction of Area Detector Data*; Bruker-AXS, Madison, Wisconsin, USA. 2002. (b) Sheldrick, G. M. SHELXL-97, *A Program for the Refinement of Crystal Structures*, University of Göttingen, Göttingen, Germany, 1997.

27. Dolomanov, O. V.; Bourhis, L. J.; Gildea, R. J; Howard, J. A. K.; Puschmann, H. *J. Appl. Cryst.* **2009**, *42*, 339.

Part 3

Synthesis and Characterization of Heptacoordinate Zirconium and Hafnium Amidinate Alkyl Complexes

Abstract

Amidinate alkyl complexes M[MeC(N^{i}Pr)$_2$]$_3$Me (M = Zr, **3**; Hf, **4**) and M[MeC(N^{i}Pr)$_2$]$_3$Et (M = Zr, **6**; Hf, **7**) have been synthesized via salt metathesis reactions from M[MeC(N^{i}Pr)$_2$]$_3$Cl (M = Zr, **1**; Hf, **2**). Structures of **6** and **7** have been characterized via single-crystal X-ray diffraction. Though the alkyl ligands were too labile to make characterization of **3**, **4**, **6**, or **7** by MS possible, the products of the reactions of these complexes as well as **1** and **2** with water from air have been determined. The thermal decomposition of **6** was found to follow first-order kinetics with activation parameters $\Delta H^{\neq}$ = 29(4) kcal/mol, $\Delta S^{\neq}$ = -5(8) eu, and $\Delta G^{\neq}_{298}$ = 31(6) kcal/mol.

3.1. Introduction

Formation of M-C σ bonds is an important, fundamental aspect of organometallic chemistry. Alkylation usually refers to the reaction of a metal complex containing, e.g., a halide (X) with a Grignard or alkyl lithium reagent to give an alkyl ligand. These complexes include d^0 early transition metal complexes such as WMe_6,[1] and $M(CH_2Ph)_4$ (M = Ti, Zr, Hf)[2] (Scheme 3.1) which are typically air sensitive. In the reactions to prepare d^0 alkyl complexes, proper reaction conditions, such as temperatures and molar ratios of the alkylating reagents to the starting complexes, are important.

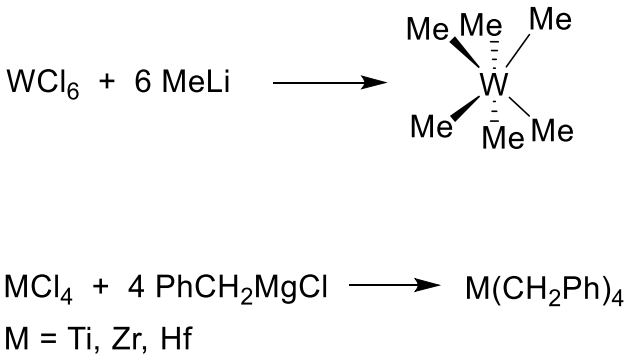

Scheme 3.1. Syntheses of organometallic complexes using Grignard or alky lithium reagents.[1,2]

Early transition metal complexes with nitrogen-containing ligands have been studied as precursors to metal oxide thin films fabricated via chemical vapor deposition (CVD) and atomic layer deposition (ALD) processes.[3-5] Until recently, SiO_2 was used as the primary gate oxide film. SiO_2, however, has a small dielectric constant (*k*) of 3.9. As

the film becomes thinner (<2 nm), current leakage is larger, generating heat and wasting energy, which can cause the transistor to degrade. Because of this high current leakage, there is a limit to how much the SiO_2 layer can be scaled down before it is no longer efficient as an insulating material.[6] Metal gate oxide layers with high-*k* values, such as HfO_2 (*k* = 25), ZrO_2 (*k* = 25), or Ta_2O_5 (*k* = 26), are better gate insulators and can be scaled down further than SiO_2 films while still maintaining their insulating capabilities.[6c]

Our group has studied the reactions of O_2, H_2O, and H_2O_2 with Group 4 amide amidinate complexes that have been used to make metal oxides. When the bis-amidinate complex $Zr[MeC(N^iPr)_2]_2(NR_2)_2$ (R = Me, Et) was reacted with O_2, a peroxo trimer $\{(\mu\text{-}\eta^2\text{:}\eta^2\text{-}O_2)Zr[MeC(N^iPr)_2]_2\}_3$, oxo dimer $\{(\mu\text{-}O)Zr[MeC(N^iPr)_2]_2\}_2$, and polymer $\{(\mu\text{ -}O)Zr[MeC(N^iPr)_2]_2\}_n$ (Scheme 3.2) were fomed. The reactions of both $Zr[MeC(N^iPr)_2]_2(NR_2)_2$ complexes with H_2O also yield $\{(\mu\text{-}O)Zr[MeC(N^iPr)_2]_2\}_2$ and $\{(\mu\text{ -}O)Zr[MeC(N^iPr)_2]_2\}_n$.[4] In this part, our syntheses and characterizations of the heptacoordinated, trisamidinate methyl complexes $M[MeC(N^iPr)_2]_3Me$ (M = Zr, **3**; Hf, **4**) and ethyl complexes $M[MeC(N^iPr)_2]_3Et$ (M = Zr, **5**; Hf, **6**) are reported. These alkyl compounds as well as the chloride complexes $M[MeC(N^iPr)_2]_3Cl$ (M = Zr, **1**; Hf, **2**) from Part 2 have been found to react with water in the air via DART-MS. We have also studied the kinetics of the thermal decomposition of **6**.

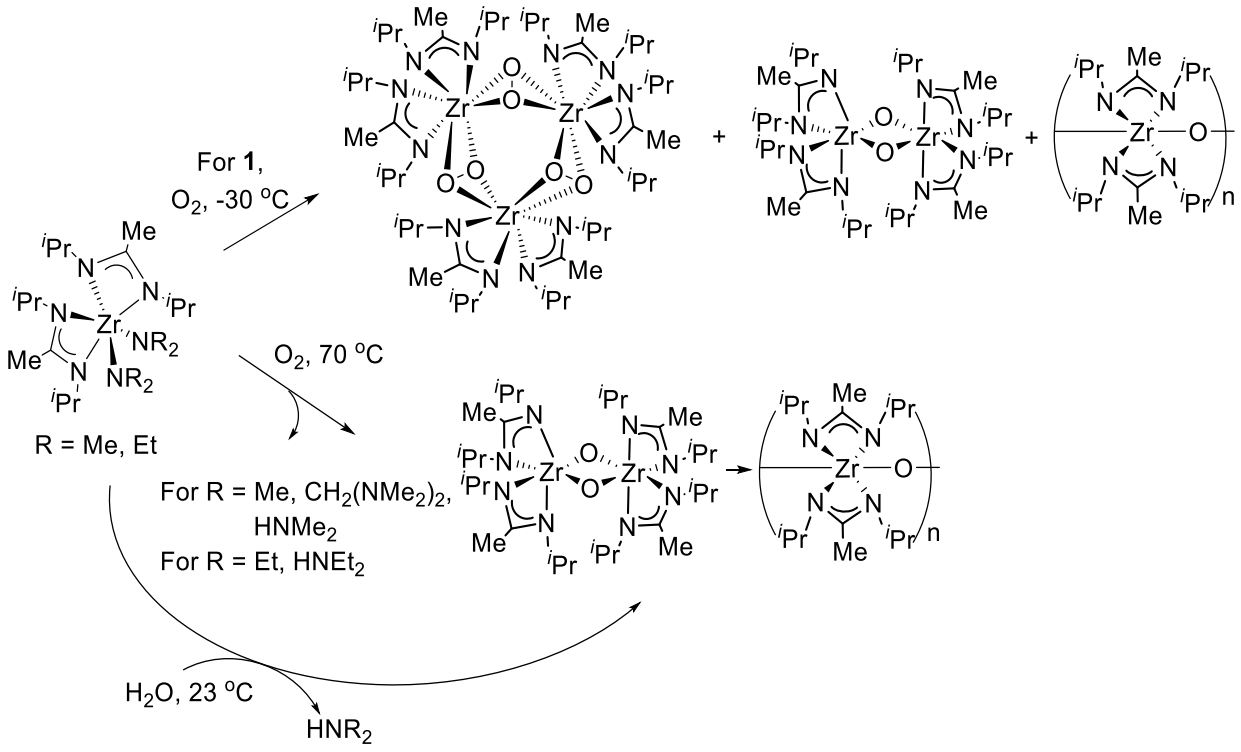

Scheme 3.2. Reactions of $Zr[MeC(N^iPr)_2]_2(NR_2)_2$ complexes with O_2 and H_2O.[5]

3.2. Results and Discussion

3.2.1. Synthesis and Characterization of $Zr[MeC(N^iPr)_2]_3Me$ (3)

$Zr[MeC(N^iPr)_2]_3Me$ (**3**) was prepared by adding 1 equiv of MeLi to $Zr[MeC(N^iPr)_2]_3Cl$ (**1**) at -40 °C in Et_2O. The solution was allowed to stir for 16 h before volatiles were removed. The product was extracted with pentane. After filtration, reducing the volume of the solution, and placing it in a freezer, white crystals of **3** formed (67% yield). Though several attempts were made to use X-ray diffraction to study this compound, the crystals were not suitable for X-ray diffraction.

The ^{1}H NMR spectrum of **3** in benzene-d_6 (Figure 3.1) shows a multiplet at 3.53 ppm and a doublet at 1.28 ppm for the C*H*Me$_2$ and CH*Me*$_2$ groups, respectively. A singlet at 1.68 ppm was assigned to the –C(*Me*) group on the amidinate. The Zr-*Me* peak was found to be at 0.81 ppm. In the ^{13}C{^{1}H} spectrum of **3** (Figure 3.2), the peaks at 12.50 and 174.30 were assigned to –C(*Me*) and –*C*(Me)- groups on the amidinate, respectively. The CH*Me*$_2$ peak appears at 24.51 ppm and *C*HMe$_2$ are at 48.00 ppm. The Zr-*Me* peak is found at 49.44 ppm, and the $J_{C\text{-}H}$ coupling constant for the Me ligand was 117 Hz.

3.2.2. Synthesis and Characterization of Hf[MeC(N^{i}Pr)$_2$]$_3$Me (4)

Synthesis of Hf[MeC(N^{i}Pr)$_2$]$_3$Me (**4**) was through the reaction of Hf[MeC(N^{i}Pr)$_2$]$_3$Cl (**2**) with 1 equiv of MeLi at -40 °C. Slowly warming the mixture in Et$_2$O to room temperature, with stirring, in 16 h gave the product. After the volatiles were removed, pentane extraction of the residue and filtration gave a solution of the crude product. Reducing the volume of the solution and cooling to -32 °C afforded clear crystals of **4** in 50% yield. Like the crystals of its Zr analog **3**, these crystals of **4** were not suitable for single X-ray diffraction.

The ^{1}H NMR spectrum of **4** in benzene-d_6 (Figure 3.3) shows a singlet at 1.65 ppm for the –C(*Me*) groups. The multiplet at 3.64 ppm and a doublet at 1.27 ppm are assigned to C*H*Me$_2$ and CH*Me*$_2$, respectively. The Hf-*Me* ligand is at 0.521 ppm, and the chemical shift is similar to 0.57 ppm (benzene-d_6) of the Hf-*Me* peak in the complex Hf[MeC(N^{i}Pr)$_2$]$_2$Me$_2$, reported by Devi and coworkers.[7]

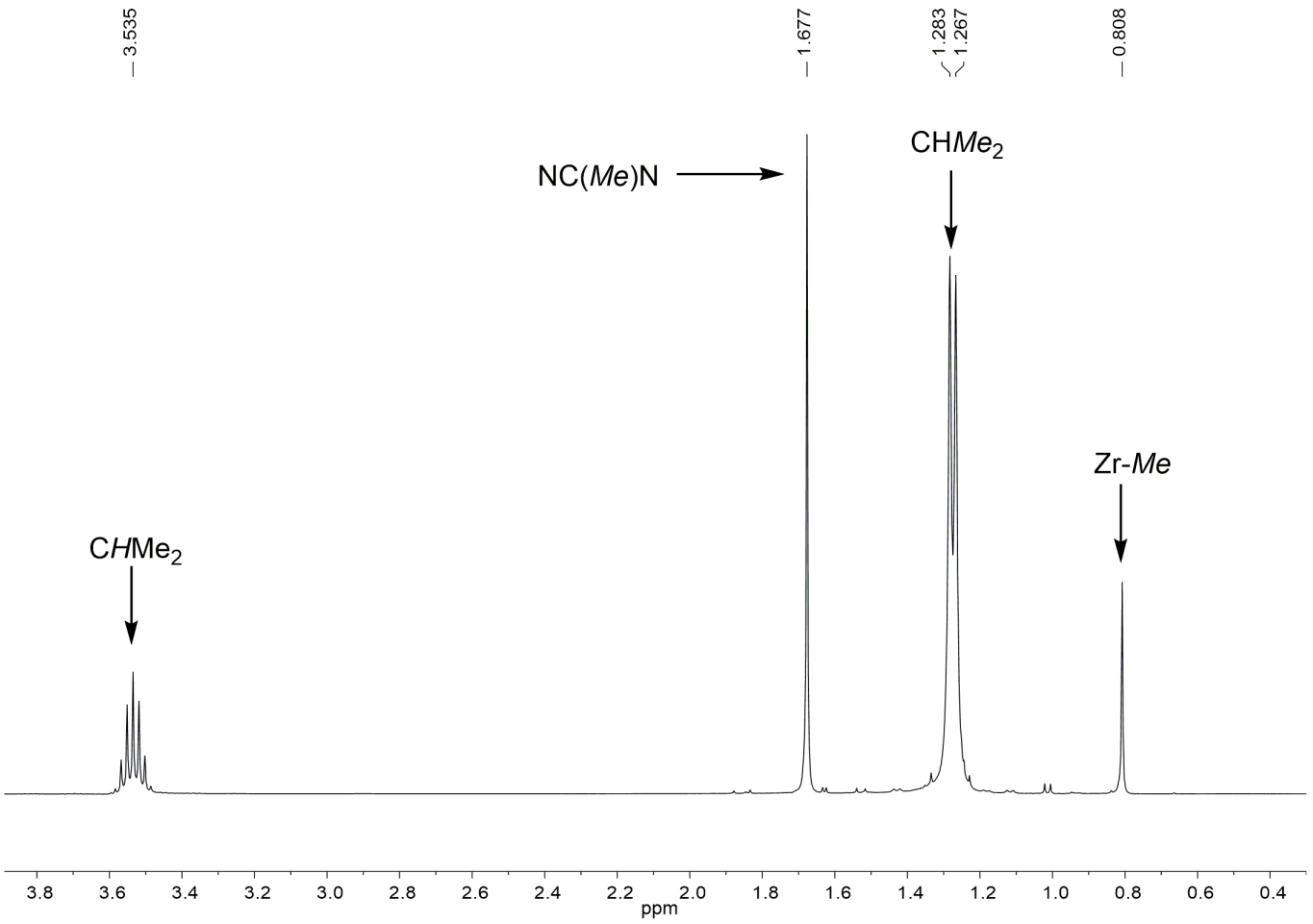

Figure 3.1. ^{1}H NMR spectrum of **3** in benzene-d_6 at 23 °C.

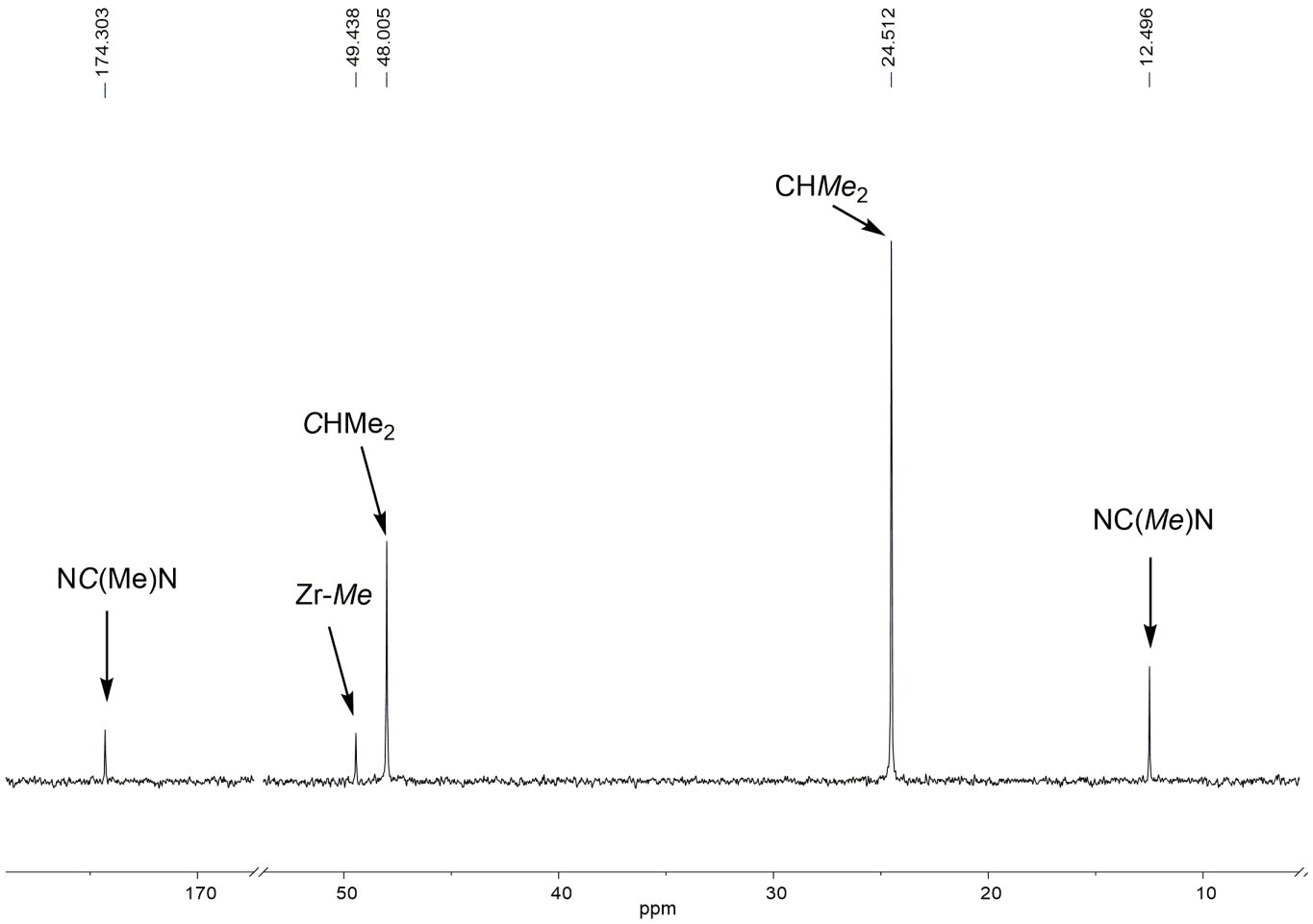

Figure 3.2. $^{13}C\{^{1}H\}$ NMR spectrum of **3** in benzene-d_6 at 23 °C.

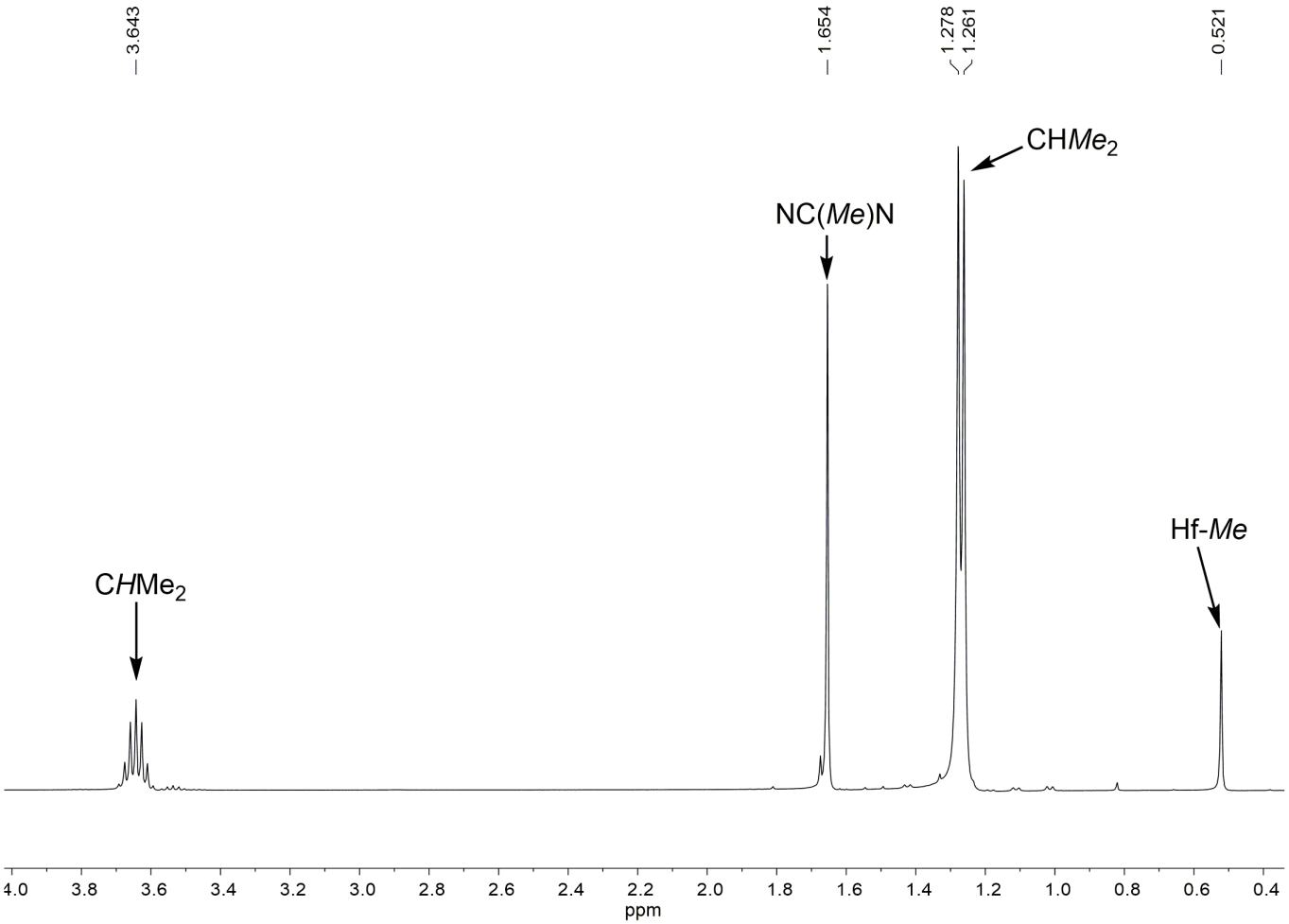

Figure 3.3. ^{1}H NMR spectrum of **4** in benzene-d_6 at 23 °C.

In the $^{13}C\{^1H\}$ NMR spectrum of **4** (Figure 3.4), the peaks at 13.14 and 173.43 ppm are assigned to –C(*Me*) and –*C*(Me)- groups on the amidinate, respectively. The CH*Me*$_2$ peak appeared at 24.50 ppm, and the 47.75 ppm is assigned to *C*HMe$_2$ the atoms. The Hf-*Me* peak at 54.71 ppm, with $J_{C\text{-}H}$ coupling constant of 111 Hz, is downfield shifted from the Zr-*Me* peak in **3** (49.44 ppm). This phenomenon will be discussed in Part 5.

3.2.3. Synthesis of EtMgCl (5)

The synthesis of Grignard reagents is well documented in the literature.[8] Our synthesis of EtMgCl (**5**) was modified from the procedure by Glöckner and coworkers to make the bromide analog EtMgBr.[8] Mg turnings were stirred vigorously in a Schleck flask containing Et$_2$O and a single crystal of I$_2$ (s). Since EtCl has a low boiling point (12.3 °C), benzene was added to the stock EtCl to make a EtCl/benzene solution which was easier to handle. The solution containing the activated Mg turnings was cooled to -50 °C. 1 equiv of EtCl in benzene was added to the Mg solution and allowed to warm to room temperature. After the reaction was completed, the solution was filtered. ^1H and $^{13}C\{^1H\}$ NMR of this compound has been previously reported in THF-d_8.[9] We have thus recorded the NMR spectra of EtMgCl (**5**) in toluene-d_8 containing both Et$_2$O and benzene. In the ^1H NMR spectrum, the C*H*$_3$ and C*H*$_2$ peaks are located at 1.62 and -0.107 ppm, respectively (Figure 2.5). In the $^{13}C\{^1H\}$ NMR spectrum (Figure 2.6), the *C*H$_2$ and *C*H$_3$ peaks are assigned to -2.00 and 13.16 ppm, respectively.

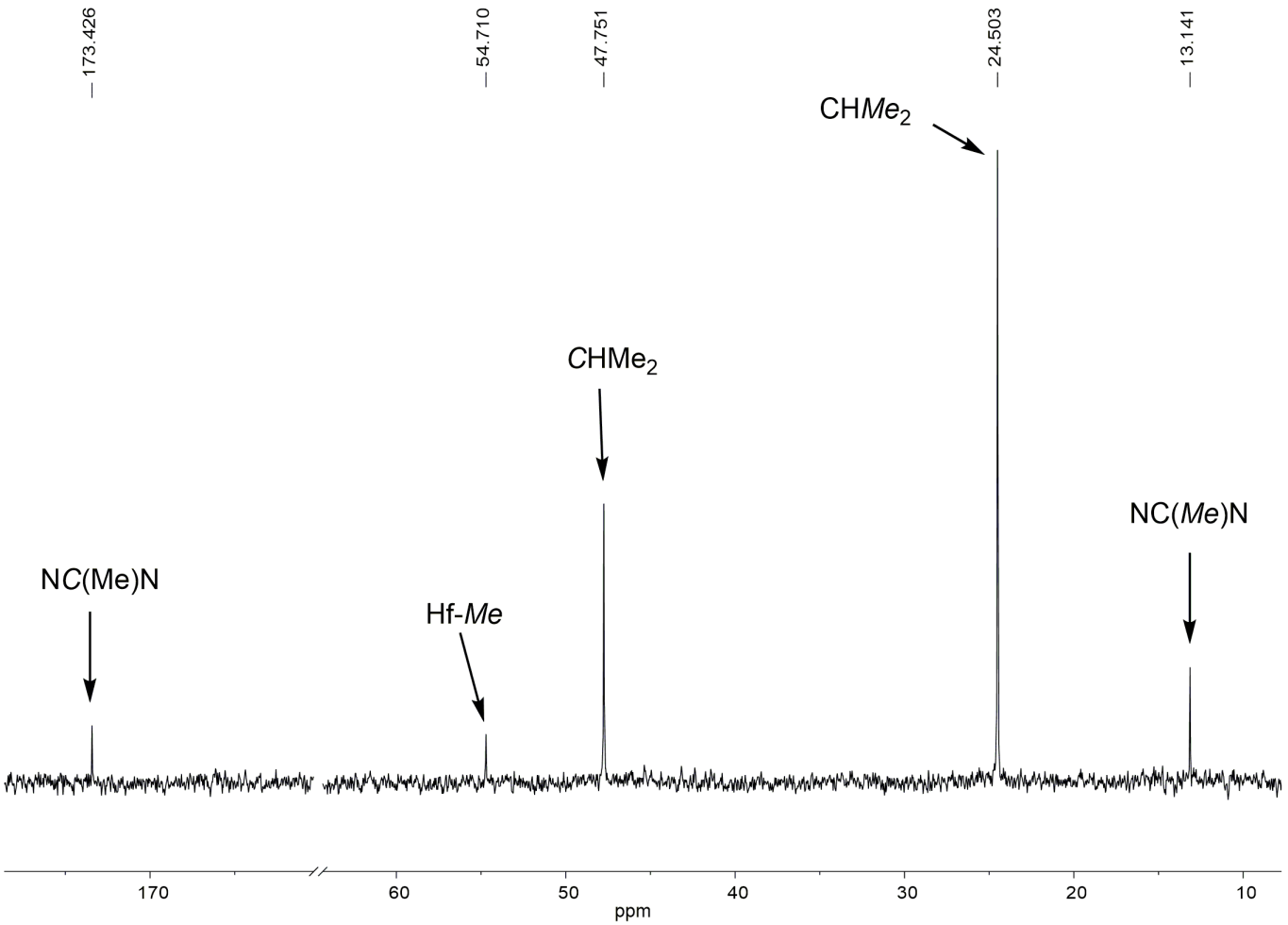

Figure 3.4. $^{13}C\{^{1}H\}$ NMR spectrum of **4** in benzene-d_6 at 23 °C.

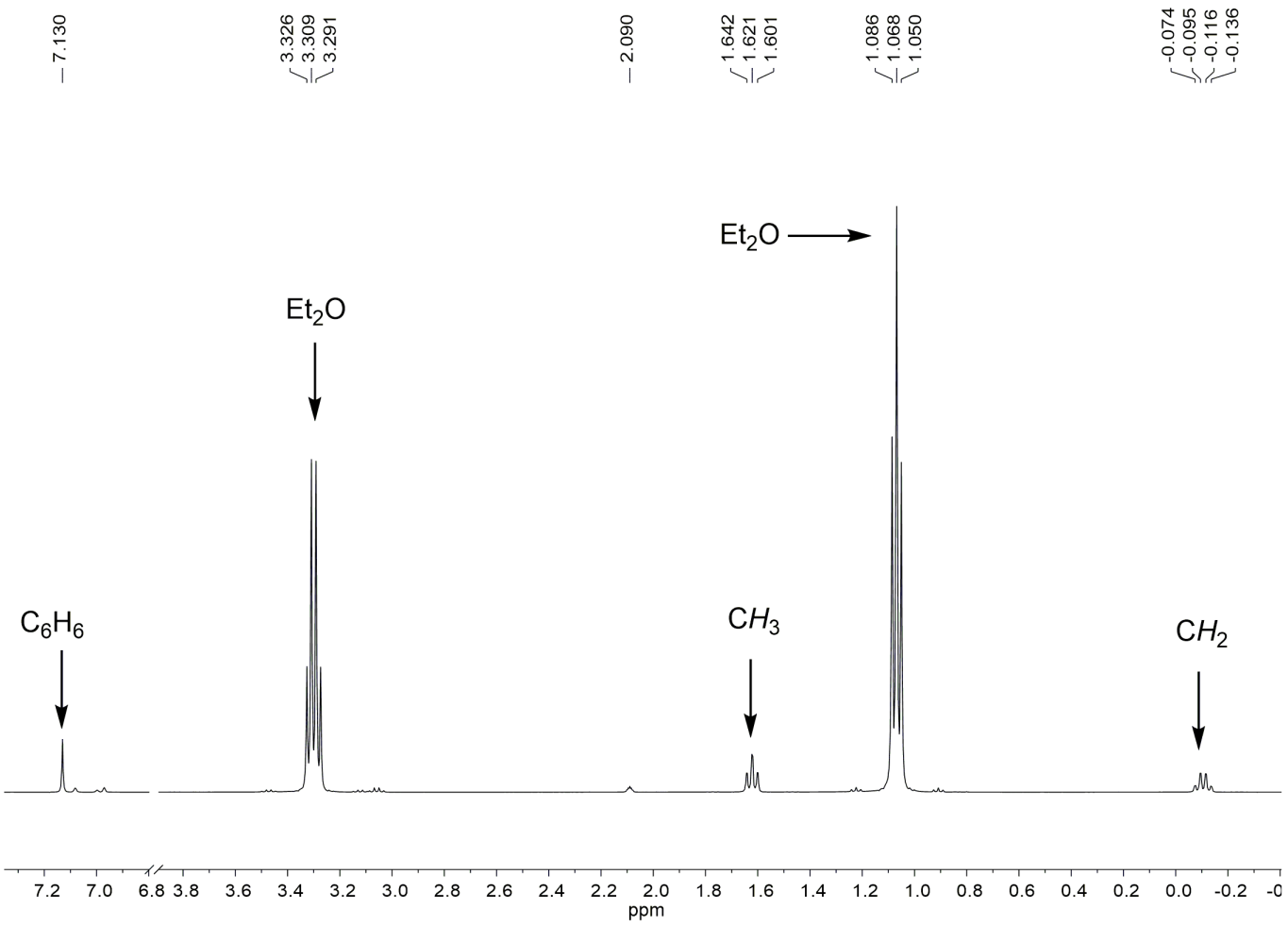

Figure 3.5. ^{1}H NMR spectrum of **5** in a benzene/Et_2O solution in toluene-d_8 at 23 °C.

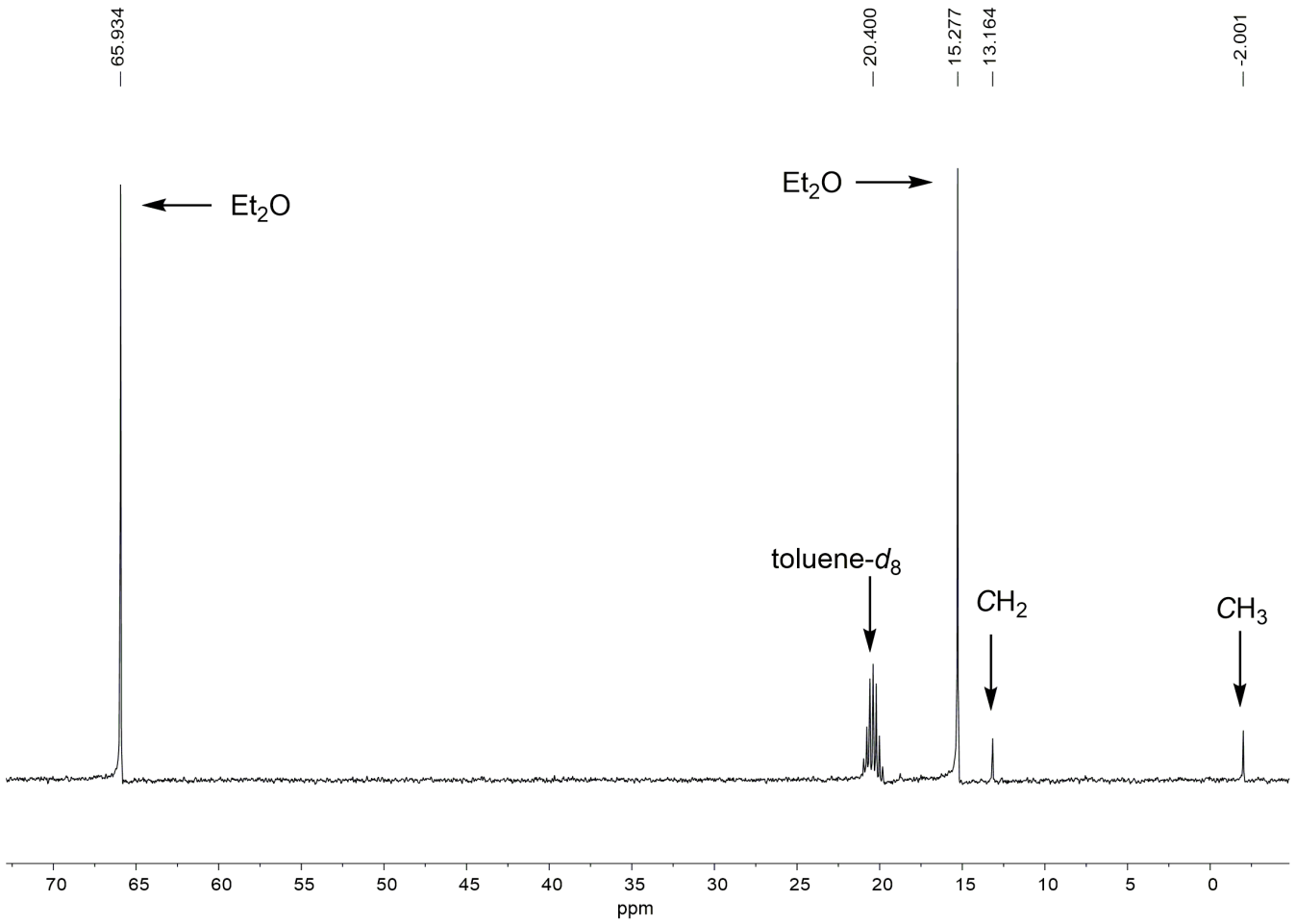

Figure 3.6. $^{13}C\{^{1}H\}$ NMR spectrum of **5** in a benzene/Et_2O solution in toluene-d_8 at 23 °C.

3.2.4. Synthesis and Characterization of Zr[MeC(N^{i}Pr)$_2$]$_3$Et (6)

To a solution of Zr[MeC(N^{i}Pr)$_2$]$_3$Cl (**1**) in Et$_2$O at -40 °C, 1 equiv of EtMgCl (**5**) was added via syringe. The solution was allowed to warm to room temperature and stirred for 16 h. The volatiles were removed, and the crude products extracted with pentane. These steps were followed by filtration and concentration of the solution. After the solution was concentrated, it was cooled to -32 °C to afforded yellow crystals of Zr[MeC(N^{i}Pr)$_2$]$_3$Et (**6**) at 47% yield.

The ^{1}H NMR spectrum of **6** (Figure 3.7) in benzene-d_6 showed a singlet at 1.71 ppm assigned to the –C(*Me*)- on the amidinate groups. The peaks for C*H*Me$_2$ and CH*Me*$_2$ on the isopropyl groups were located at 3.66 and 1.26 ppm, respectively. The peak for CH*Me*$_2$ appeared as a well-defined doublet. The C*H*$_2$ and C*H*$_3$ groups on the ethyl ligand were assigned to the quartet and triplet at 1.06 and 1.85 ppm, respectively. In the ^{13}C{^{1}H} NMR spectrum (Figure 3.8), the quaternary -*C*(Me)- was located at 174.88 ppm, and -*C*(Me) was located at 14.01 ppm. The singlets at 47.83 and 24.49 ppm were assigned to the *C*HMe$_2$ and CH*Me*$_2$ groups, respectively. The peak at 53.85 ppm belongs to the Zr-*C*H$_2$ group on the CH$_2$CH$_3$ ligand, and the peak at 16.11 ppm was assigned to the *C*H$_3$ peak. The $J_{C\text{-}H}$ for the CH$_2$ group on the ethyl ligand was 117 Hz. These peaks were confirmed by DEPT-135 and ^{1}H-gated-decoupled ^{13}C NMR spectroscopies. The structure of **6** was obtained via single-crystal X-ray diffraction. ORTEP, crystallographic data, and selected bonds and angles are given in Figure 3.9 and Tables 3.1-3.2, respectively. The rest of the crystal tables are in Appendix B. The unit cell of **6** contains two slightly different molecules. The average length of the Zr-N bonds in **6** is slightly longer (2.283 Å) than that of **1** (2.226 Å). The dihedral angle

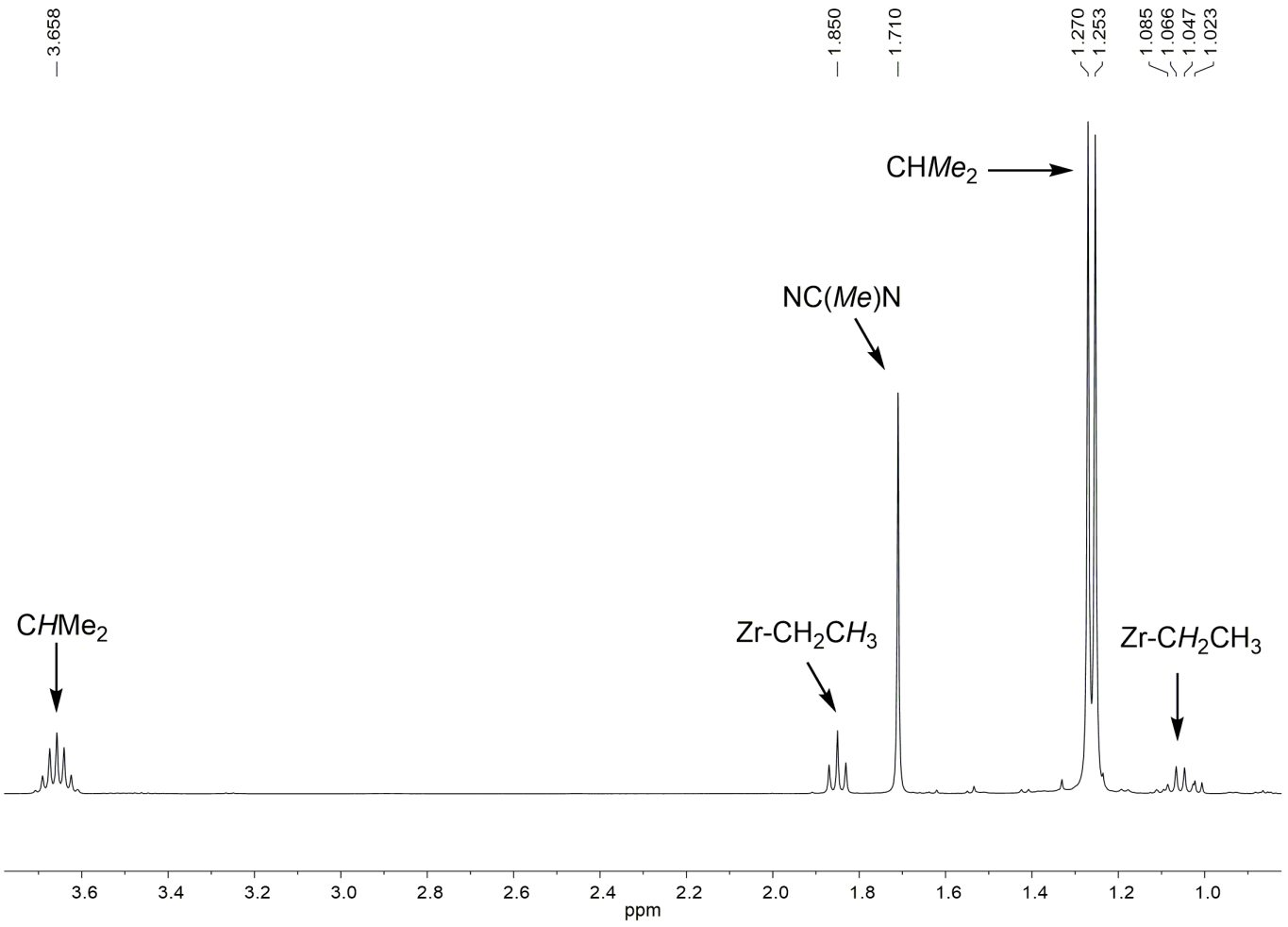

Figure 3.7. ^{1}H NMR spectrum of **6** in benzene-d_6 at 23 °C.

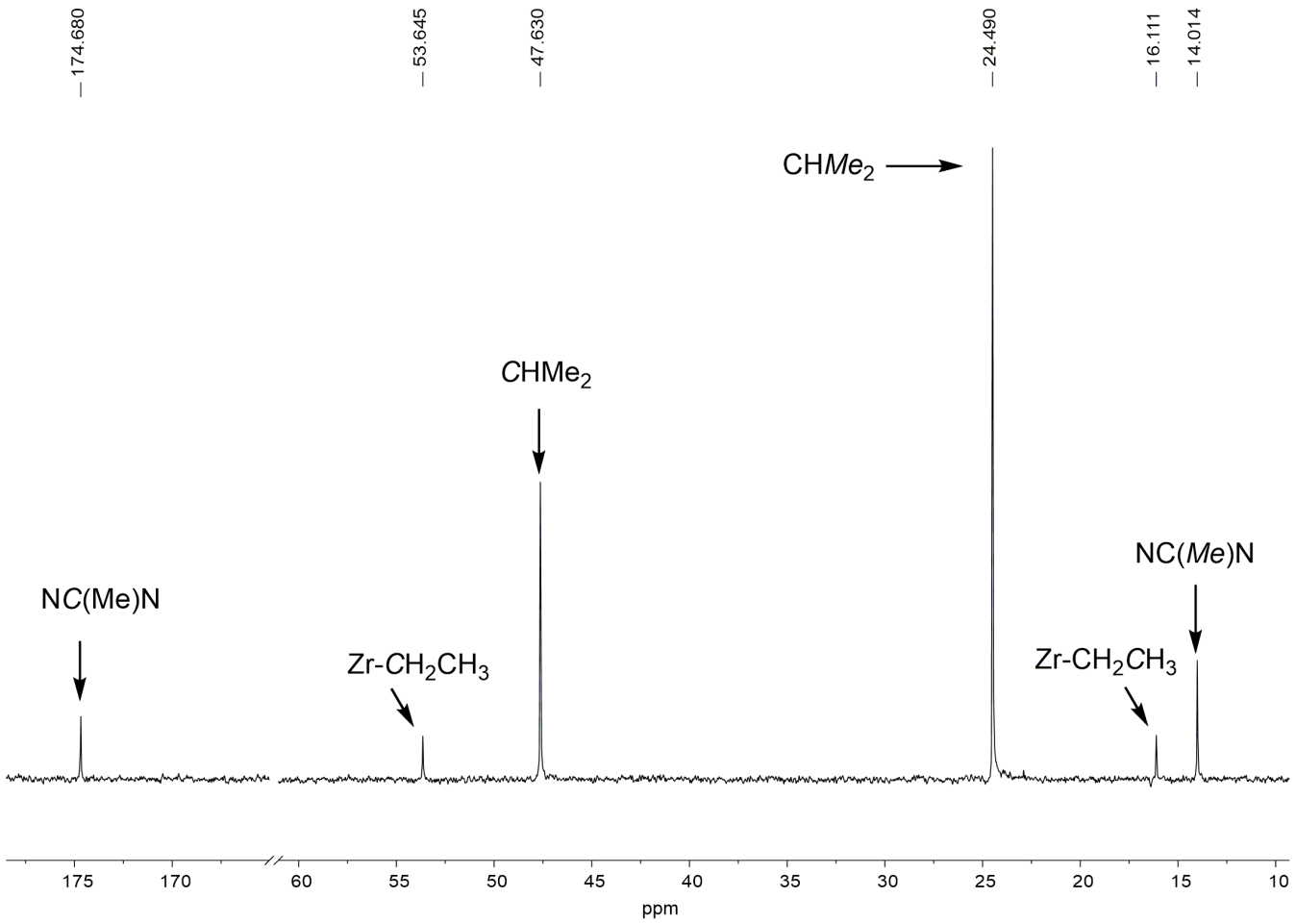

Figure 3.8. $^{13}C\{^{1}H\}$ NMR spectrum of **6** in benzene-d_6 at 23 °C.

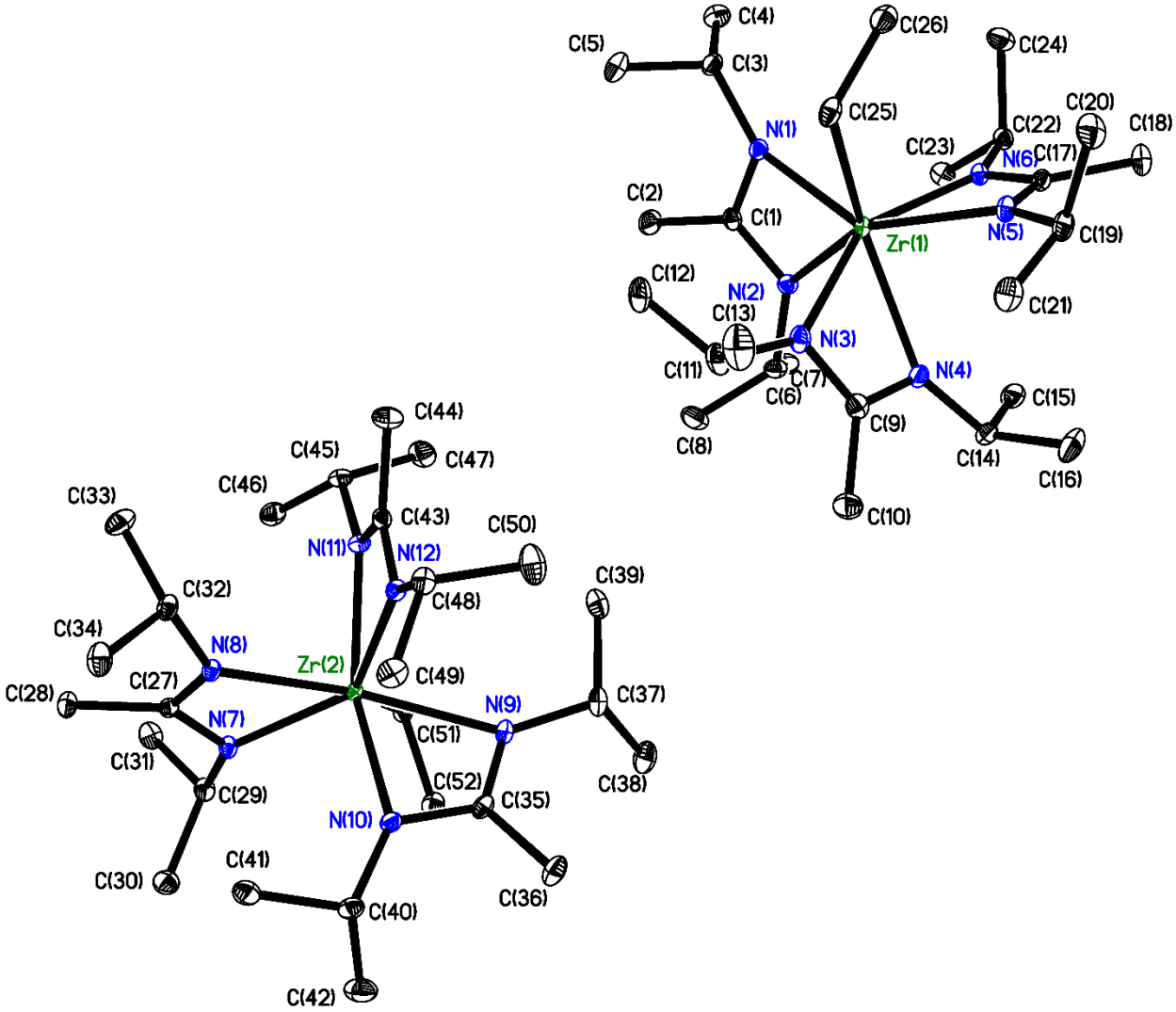

Figure 3.9. ORTEP of **6** at 100(2) K. Thermal ellipsoids are 30% probability level. Hydrogen atoms were removed for clarity.

Table 3.1. Crystal data and structure refinement for **6**

Empirical formula	$C_{26}H_{56}N_6Zr$
Formula weight	549.98
Temperature	100(2) K
Wavelength	0.71073 Å
Crystal System	Monoclinic
Space Group	$P2_1/c$
Unit cell dimensions	a = 21.699(7) Å α = 90°
	b = 15.619(5) Å β = 103.401(4)°
	c = 18.597(6) Å γ= 90°
Volume	6131(3) Å^3
Z	8
Density (calculated)	1.179 g/cm^3
Absorption coefficient	0.381 mm^{-1}
F(000)	2352.0
Crystal size	0.552 × 0.382 × 0.152 mm^3
Theta range for data collection	1.62 to 27.74°
Index ranges	$-28 \le h \le 28$, $-20 \le k \le 20$, $-24 \le l \le 24$
Reflections collected	69813
Independent reflections	14282 [R_{int} = 0.0330]
Completeness to theta = 27.74°	99.0%
Max. and min. transmission	0.746 and 0.658
Refinement method	Full-matrix least-squares on F^2
Absorption correction	Semi-empirical from equivalents
Data / restraints / parameters	14282 / 0 / 627
Goodness-of-fit on F^2	1.046

Table 3.1. Continued

Final *R* indices [$I > 2\sigma(I)$]	$R1 = 0.0273$, $wR2 = 0.0643$
R indices (all data)	$R1 = 0.0332$, $wR2 = 0.0679$
Largest diff. peak and hole	0.51 and -0.44 eÅ^{-3}

[a] $R1 = \Sigma ||F_o| - |F_c|| / \Sigma |F_o|$; $wR2 = [\Sigma w(F_o^2 - F_c^2)^2 / \Sigma w(F_o^2)^2]^{1/2}$;

$w = 1/[\sigma^2(F_o) + (aP)^2 + bP]$; $P = [2Fc^2 + \text{Max}(F_o^2, 0)]/3$

Table 3.2. Selected distances (Å) and angles (°) in **6**

Distances			
Zr(1)-C(25)	2.3207(17)	Zr(2)-C(51)	2.3154(15)
Zr(1)-N(1)	2.2600(13)	Zr(2)-N(7)	2.2552(13)
Zr(1)-N(2)	2.2856(13)	Zr(2)-N(8)	2.2956(12)
Zr(1)-N(3)	2.2281(15)	Zr(2)-N(9)	2.3221(14)
Zr(1)-N(4)	2.3678(14)	Zr(2)-N(10)	2.2422(13)
Zr(1)-N(5)	2.3278(14)	Zr(2)-N(11)	2.2278(13)
Zr(1)-N(6)	2.2265(13)	Zr(2)-N(12)	2.3468(13)
Angles			
N(1)-Zr(1)-C(25)	79.85(5)	N(7)-Zr(2)-C(51)	81.14(5)
N(2)-Zr(1)-C(25)	134.13(5)	N(8)-Zr(2)-C(51)	134.57(5)
N(1)-Zr(1)-N(2)	57.96(5)	N(7)-Zr(2)-N(8)	57.67(5)
N(1)-C(1)-N(2)	111.55(13)	N(7)-C(27)-N(8)	110.85(12)
N(3)-Zr(1)-C(25)	92.90(5)	N(9)-Zr(2)-C(51)	79.39(5)
N(4)-Zr(1)-C(25)	136.88(5)	N(10)-Zr(2)-C(51)	105.78(5)
N(3)-Zr(1)-N(4)	57.72(4)	N(9)-Zr(2)-N(10)	58.31(5)
N(3)-C(9)-N(4)	112.87(13)	N(9)-C(35)-N(10)	113.24(13)
N(5)-Zr(1)-C(25)	78.31(5)	N(11)-Zr(2)-C(51)	90.77(5)
N(6)-Zr(1)-C(25)	103.99(5)	N(12)-Zr(2)-C(51)	134.53(5)
N(5)-Zr(1)-N(6)	58.31(4)	N(11)-Zr(2)-N(12)	58.07(4)
N(5)-C(17)-N(6)	112.99(12)	N(11)-C(43)-N(12)	113.27(12)

between the propellers N(1)–Zr(1)–N(2) and N(3)–Zr(1)–N(4), N(3)–Zr(1)–N(4) and N(5)–Zr(1)–N(5), and N(5)–Zr(1)–N(6) and N(1)–Zr(1)–N(2) are 89.5°, 105.8°, and 90.4°, respectively. For the other molecule, the angles are 90.5°, 106.4°, and 88.6° for N(7)–Zr(2)–N(8) and N(9)–Zr(2)–N(10), N(9)–Zr(2)–N(10) and N(11)–Zr(2)–N(12), and N(11)–Zr(2)–N(12) and N(7)–Zr(2)–N(8). Each of the two molecules shows a distorted propeller structure.

3.2.5. Synthesis and Characterization of Hf[MeC(N^{i}Pr)$_2$]$_3$Et (7)

Complex **7** was prepared by a procedure similar to that used for the synthesis of its Zr analog. Hf[MeC(N^{i}Pr)$_2$]$_3$Cl (**2**) in a Et$_2$O solution at -40 °C was added 1 equiv of **5** via syringe. After warming to room temperature, the solution was stirred for 16 h to give **7**. After removing the volatiles in vacuo, pentane extraction, filtration, and condensing the solution, it was cooled at -32 °C afforded yellow crystals of Hf[MeC(N^{i}Pr)$_2$]$_3$Et (**7**) in 59% yield.

^{1}H NMR spectrum of **7** in benzene-d_6 (Figure 3.10) shows a multiplet at 3.74 ppm and a doublet at 1.25 ppm for C*H*Me$_2$ and CH*Me*$_2$, respectively, on the isopropyl groups. A singlet at 1.69 ppm was assigned to the –C(*Me*)- group on the amidinate groups. The Hf-C*H*$_2$ and C*H*$_3$ groups on the ethyl ligand were assigned to the quartet and triplet at 0.73 and 2.01 ppm, respectively. The ^{13}C{^{1}H} NMR spectrum (Figure 3.11) shows singlets at 47.38 and 24.50 ppm which are assigned to the *C*HMe$_2$ and CH*Me*$_2$ groups, respectively. The quaternary -*C*(Me) atom was located at 173.87 ppm, and -*C*(Me) was located at 14.57 ppm. The peaks at 58.25 and 16.11 ppm is assigned to the

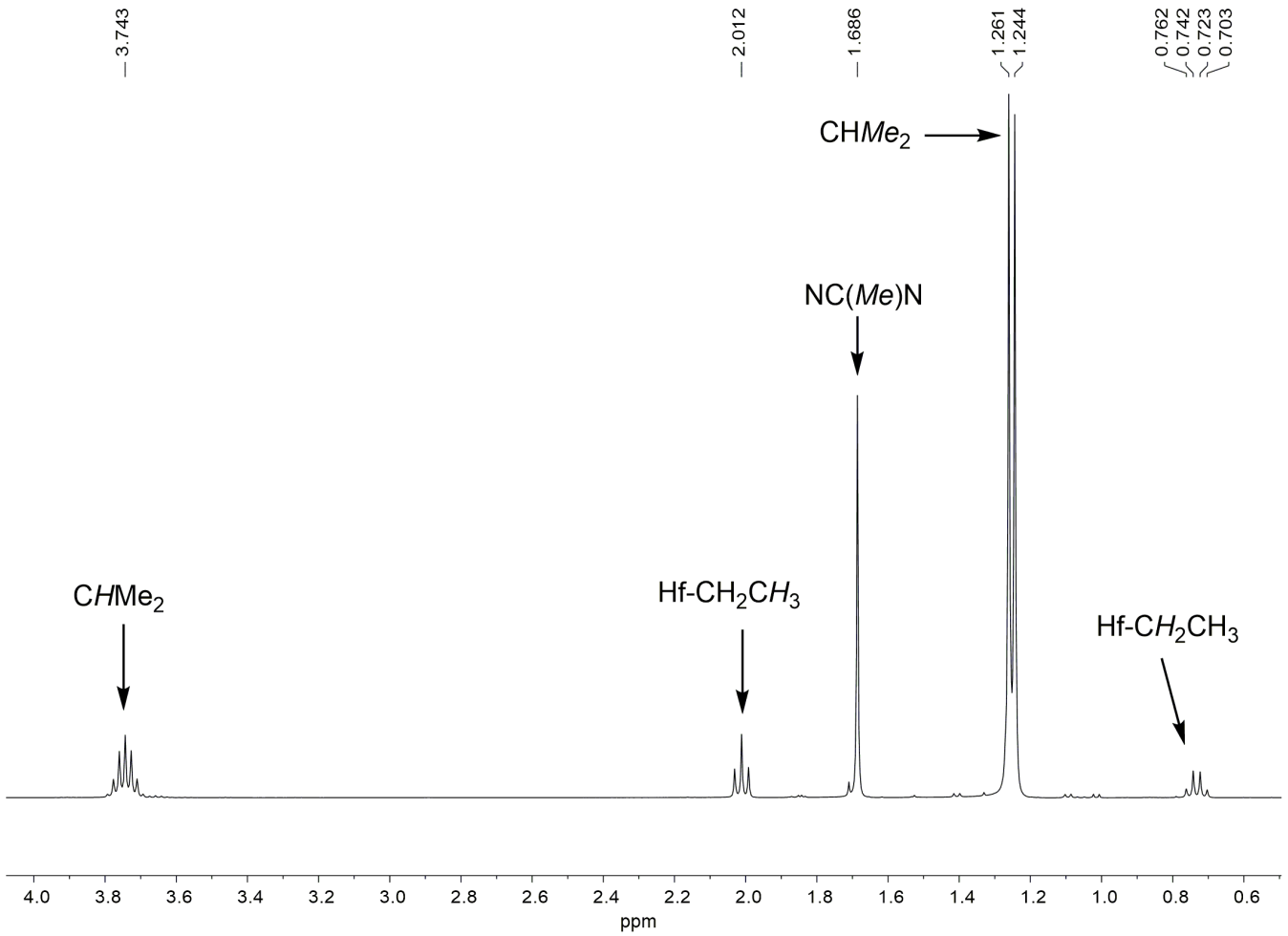

Figure 3.10. ^{1}H NMR spectrum of **7** in benzene-d_6 at 23 °C.

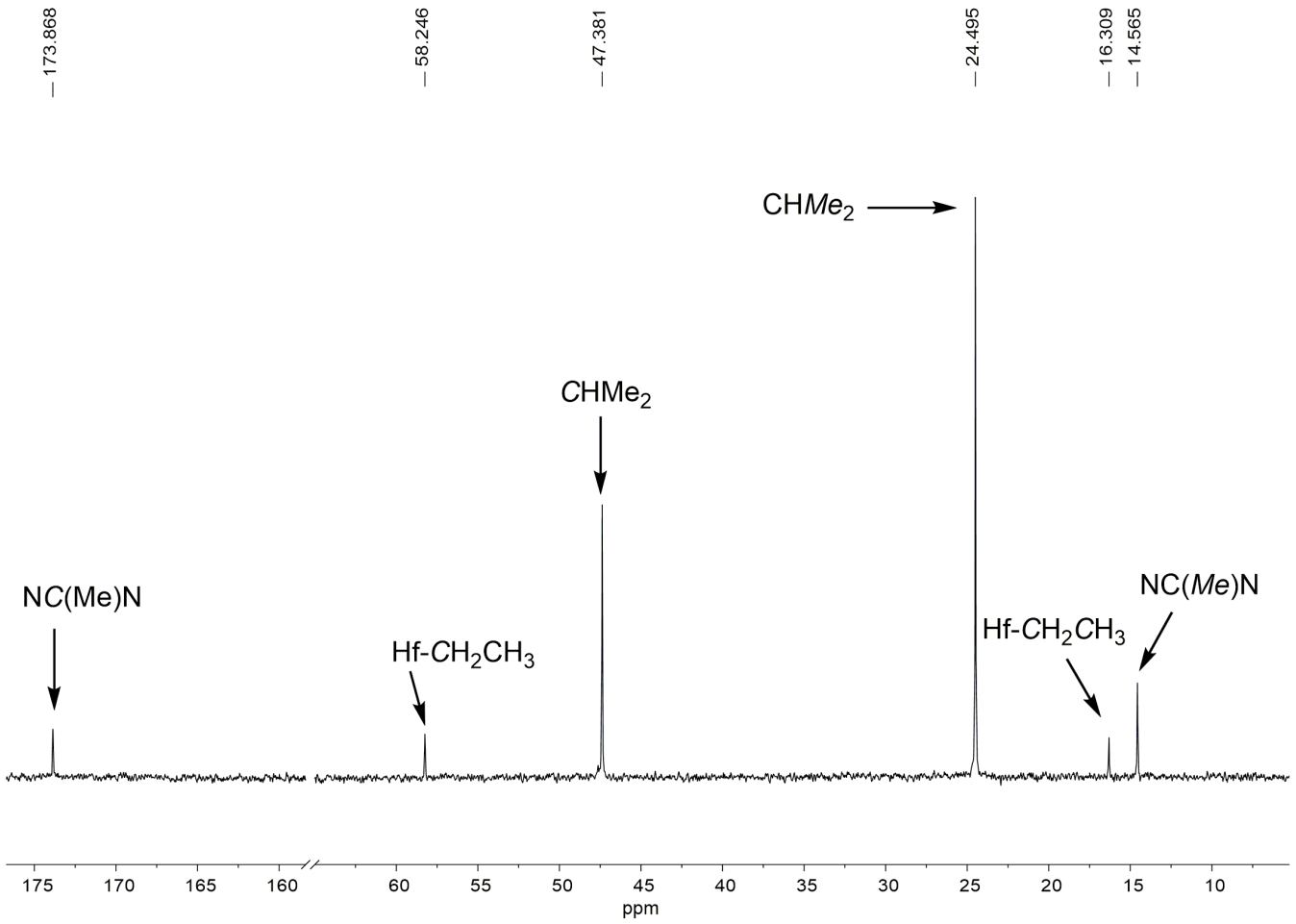

Figure 3.11. $^{13}C\{^{1}H\}$ NMR spectrum of **7** in benzene-d_6 at 23 °C.

Hf-*C*H_2 and *C*H_3 groups on the ethyl ligand, respectively. These peaks were confirmed by DEPT-135 and ^{1}H-gated-decoupled ^{13}C NMR spectroscopies. The $J_{C\text{-}H}$ for the *C*H_2 ethyl ligand was 111 Hz. The chemical shift of the α-C atom of the ethyl ligand in **7** is downfield shifted from the α-C the Zr-*Et* peak in **6** (53.85 ppm). This phenomenon will be discussed in Part 5.

ORTEP, crystallographic data, and selected bonds and angles of **7** are given in Figure 3.12 and Tables 3.3-3.4, respectively. Remaining crystal tables are given in Appendix B. Similar to that of **6**, the unit cell of **7** contains two independent molecules. The dihedral angle between the propellers N(1)–Hf(1)–N(2) and N(3)–Hf(1)–N(4), N(3)-Hf(1)–N(4) and N(5)–Hf(1)–N(5), and N(5)–Hf(1)–N(6) and N(1)–Hf(1)–N(2) are 88.7°, 73.0°, and 89.6°, respectively, for one molecule. For the other molecule, the angles are 90.3°, 89.4°, and 106.1° for N(7)–Hf(2)–N(8) and N(9)–Hf(2)–N(10), N(9)–Hf(2)–N(10) and N(11)–Hf(2)–N(12), and N(11)–Hf(2)–N(12) and N(7)–Hf(2)–N(8). The average length of the Hf-C bonds is 2.296 Å, which is shorter than the average length of the Zr-C bonds in **6** (2.318 Å), but longer than the Hf-C bond in Hf[MeC(N^{i}Pr)$_2$]$_2$Me$_2$ reported by Devi and coworkers.[7]

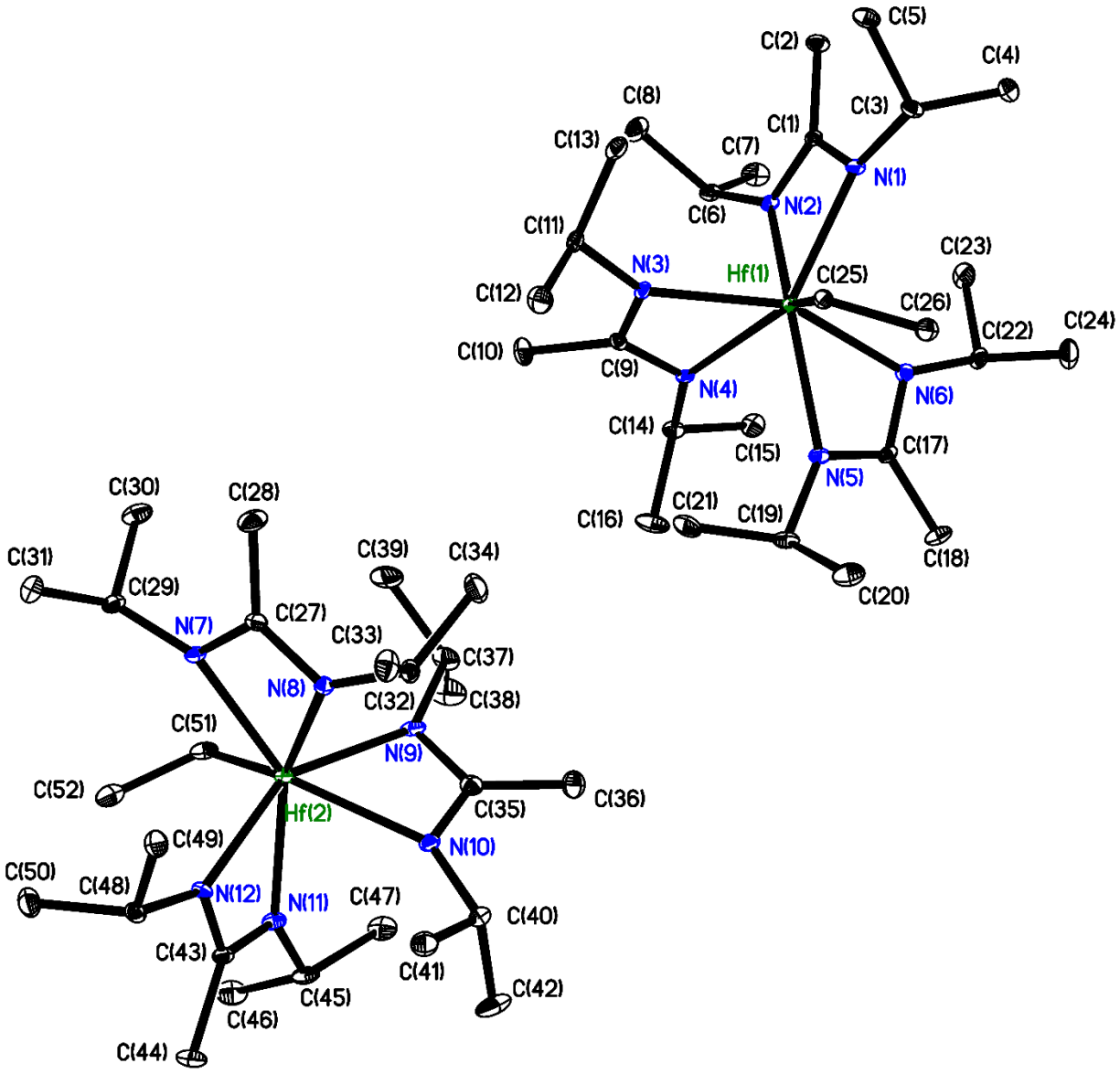

Figure 3.12. ORTEP of **7** at 100(2) K. Thermal ellipsoids are 30% probability level. Hydrogen atoms were removed for clarity.

Table 3.3. Crystal data and structure refinement for **7**

Empirical formula	$C_{26}H_{56}N_6Hf$	
Formula weight	631.25	
Temperature	100(2) K	
Wavelength	0.71073 Å	
Crystal System	Monoclinic	
Space Group	$P2_1/c$	
Unit cell dimensions	a = 21.658(7) Å	α = 90°
	b = 15.566(5) Å	β = 103.681(4)°
	c = 18.594(6) Å	γ = 90°
Volume	6091(3) Å^3	
Z	8	
Density (calculated)	1.377 g/cm^3	
Absorption coefficient	3.448 mm^{-1}	
F(000)	2608.0	
Crystal size	0.404 × 0.381 × 0.32 mm^3	
Theta range for data collection	1.67 to 27.83°	
Index ranges	$-27 \le h \le 27$, $-20 \le k \le 20$, $-24 \le l \le 24$	
Reflections collected	69357	
Independent reflections	14157 [R_{int} = 0.0333]	
Completeness to theta = 27.83°	97.8%	
Max. and min. transmission	0.746 and 0.485	
Refinement method	Full-matrix least-squares on F^2	
Absorption correction	Semi-empirical from equivalents	
Goodness-of-fit on F^2	1.038	
Final R indices [$I > 2\sigma(I)$]	$R1$ = 0.0199, w$R2$ = 0.0467	

Table 3.3. Continued

R indices (all data)	$R1 = 0.0223$, $wR2 = 0.0477$
Largest diff. peak and hole	0.83 and -1.08 eÅ^{-3}

[a] $R1 = \Sigma||F_o| - |F_c|| / \Sigma|F_o|$; $wR2 = [\Sigma\, w(F_o^2 - F_c^2)^2 / \Sigma\, w(F_o^2)^2]^{1/2}$;

$w = 1/[\sigma^2(F_o) + (aP)^2 + bP]$; $P = [2Fc^2 + \mathrm{Max}(F_o^2, 0)]/3$

Table 3.4. Selected distances (Å) and angles (°) in **7**

Distances			
Hf(1)-C(25)	2.295(2)	Hf(2)-C(51)	2.298(2)
Hf(1)-N(1)	2.2379(18)	Hf(2)-N(7)	2.2405(18)
Hf(1)-N(2)	2.2831(17)	Hf(2)-N(8)	2.2795(18)
Hf(1)-N(3)	2.2057(17)	Hf(2)-N(9)	2.2041(19)
Hf(1)-N(4)	2.3305(18)	Hf(2)-N(10)	2.3487(19)
Hf(1)-N(5)	2.3072(18)	Hf(2)-N(11)	2.3105(19)
Hf(1)-N(6)	2.2831(17)	Hf(2)-N(12)	2.2047(17)
Angles			
N(1)-Hf(1)-C(25)	81.50(7)	N(7)-Hf(2)-C(51)	80.42(7)
N(2)-Hf(1)- C(25)	135.50(7)	N(8)-Hf(2)-C(51)	135.01(7)
N(1)-Hf(1)-N(2)	57.93(6)	N(7)-Hf(2)-N(8)	58.12(6)
N(1)-C(1)-N(2)	110.80(17)	N(7)-C(27)-N(8)	111.35(18)
N(3)-Hf(1)-C(25)	91.12(7)	N(9)-Hf(2)-C(51)	93.06(8)
N(4)-Hf(1)-C(25)	134.68(7)	N(10)-Hf(2)-C(51)	136.99(7)
N(3)-Hf(1)-N(4)	58.58(6)	N(9)-Hf(2)-N(10)	58.25(6)
N(3)-C(9)-N(4)	113.36(18)	N(9)-C(35)-N(10)	112.66(19)
N(5)-Hf(1)-C(25)	79.20(7)	N(11)-Hf(2)-C(51)	78.04(7)
N(6)-Hf(1)-C(25)	105.19(7)	N(12)-Hf(2)-C(51)	103.40(7)
N(5)-Hf(1)-N(6)	58.63(6)	N(11)-Hf(2)-N(12)	58.66(6)
N(5)-C(17)-N(6)	113.05(18)	N(11)-C(43)-N(12)	112.76(18)

3.2.6. Studies of the Thermal Decomposition of Zr[MeC(N^{i}Pr)$_2$]$_3$Et (6)

Zr[MeC(N^{i}Pr)$_2$]$_3$Et (**6**) was found to decompose at raised temperatures to give ethane, ethylene, and other unknown species (Scheme 3.3). A ^{1}H spectrum of the decomposition in progress is given in Figure 3.13. ^{1}H and ^{13}C NMR spectra of the mixture of thermal decomposition after the reaction is completed are given in Figure 3.14-3.15. The ratio of ethylene to ethane is ca. 1:6 in the solution of the final reaction mixture.

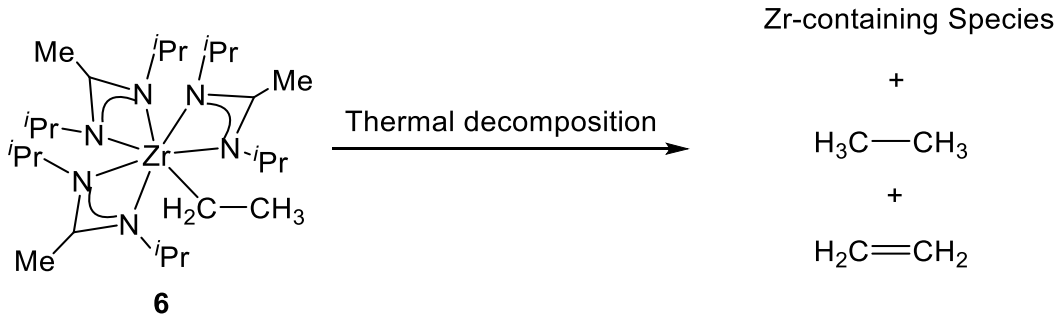

6

Scheme 3.3. Thermal decomposition of **6.**

n-Butane could not be identified in the products, suggesting that it is at least not a major product from the thermolysis. ^{1}H and ^{13}C NMR chemical shifts of *n*-butane in toluene-d_8 have not been reported. The ^{1}H NMR shifts of *n*-butane in $CDCl_3$ are reported to be 0.887 and 1.285 ppm, respectively.[10] No significant peaks were observed around the regions in the mixture of the thermolysis of **6**.

There is more than one Zr-containing product in the reaction mixture. Though several attempts have been made to separate and characterize these products, none was successful. The Zr-containing products could not be characterized either.

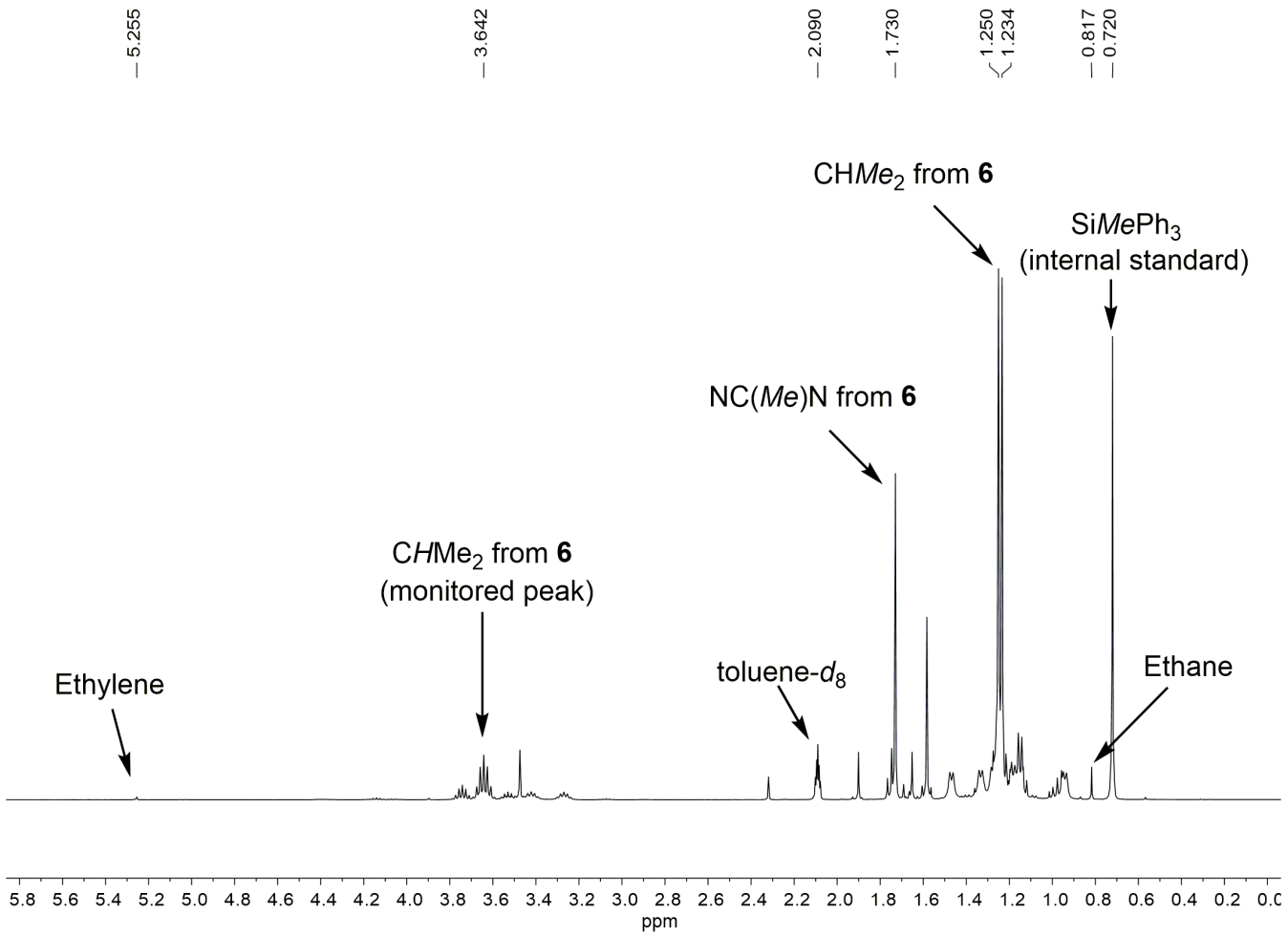

Figure 3.13. ^{1}H NMR spectrum of the reaction mixture in toluene-d_8 after a half of **6** has decomposed.

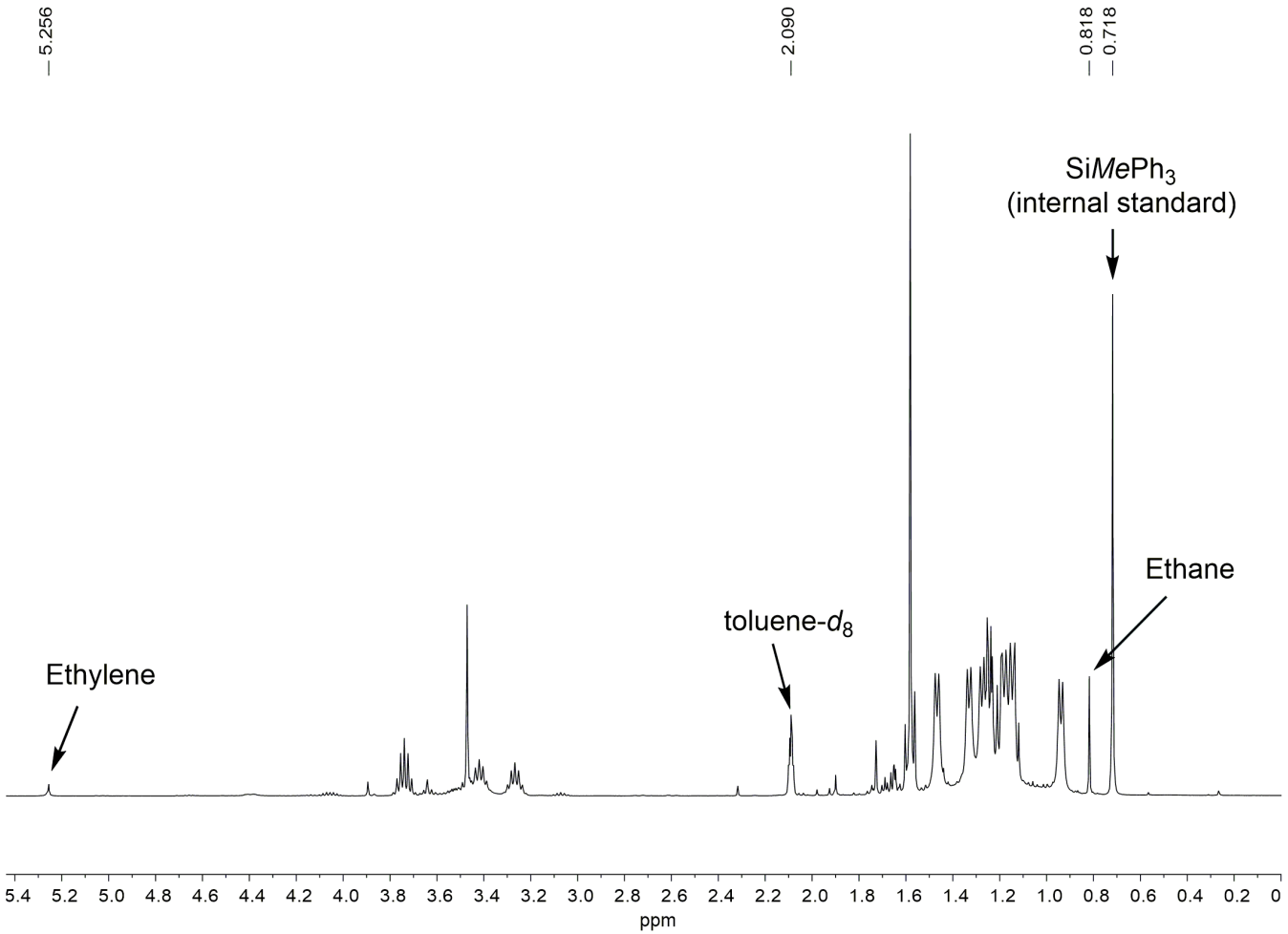

Figure 3.14. ^{1}H NMR spectrum of the reaction mixture in toluene-d_8 after **6** has decomposed.

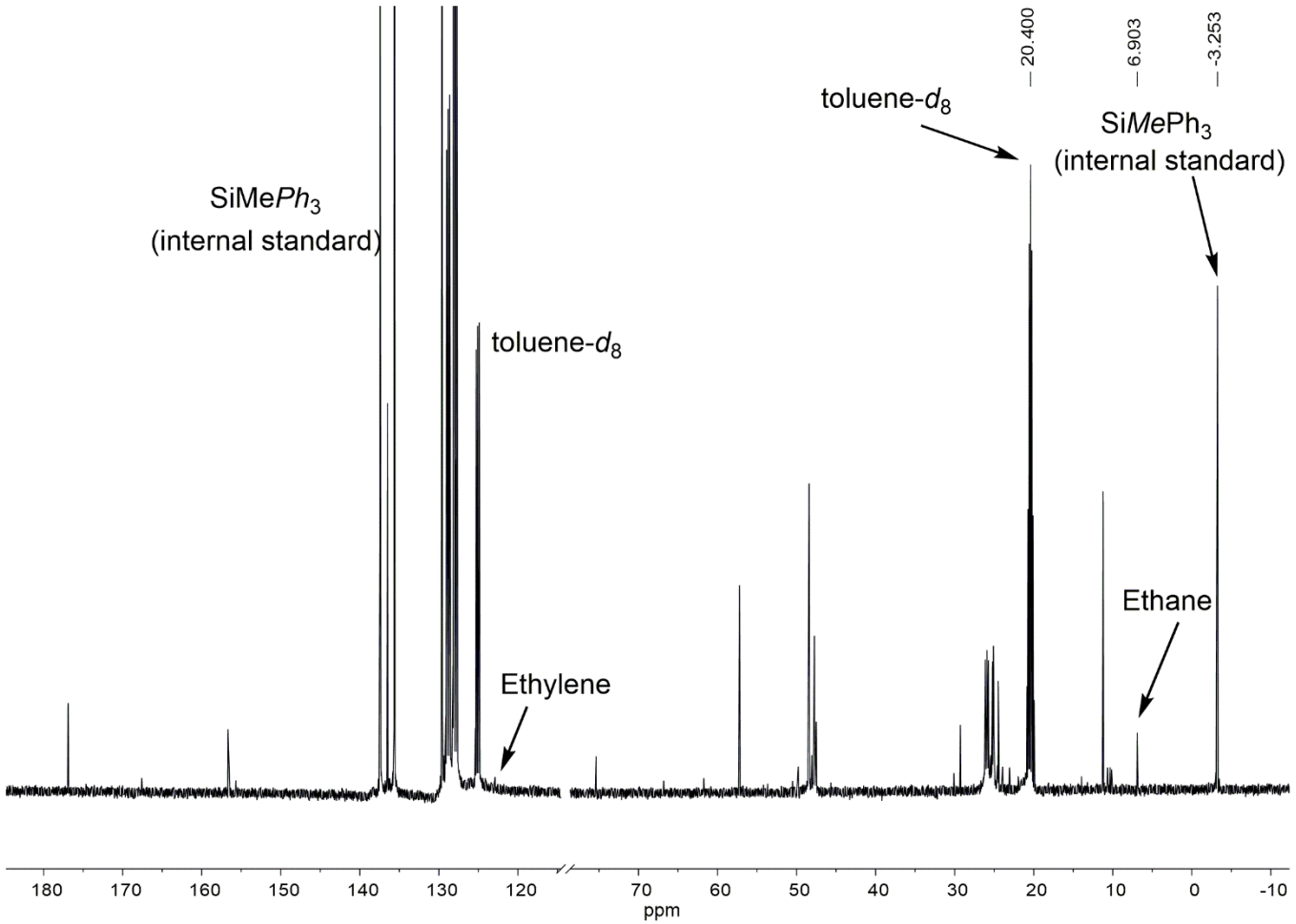

Figure 3.15. ^{13}C NMR spectrum of the reaction mixture in toluene-d_8 after **6** has decomposed.

Thermolysis of **6** in toluene-d_8 was observed to follow first-order kinetics, as the disappearance of concentrations of **6** over time. The decrease in the area of the C*H*Me_2 peak of **6** in the ^{1}H NMR spectra was monitored. The kinetic studies were conducted between 373 and 388 K, and were monitored for several days. $SiMePh_3$ was used as an internal standard. The ln(C/C_0) vs *t* plots (Figure 3.16) give rate constants for the decomposition at different temperatures (Table 3.5). The Eyring plot is given in Figure 3.17. The activation parameters calculated from the Eyring plot for the decomposition are: $\Delta H^{\neq}$ = 29(4) kcal/mol, $\Delta S^{\neq}$ = -5(8) eu, and $\Delta G^{\neq}_{298}$ = 31(6) kcal/mol.

The lack of characterization about the Zr-containing intermediates and products makes the understanding of the mechanistic pathway(s) in the thermal decomposition difficult. The first-order kinetics suggests that the rate-determining step is unimolecular. The presence of ethylene may be formed by a unimolecular, β-hydrogen elimination process (Scheme 3.4), which is consistent with the first-order kinetics of the thermolysis of **6**.

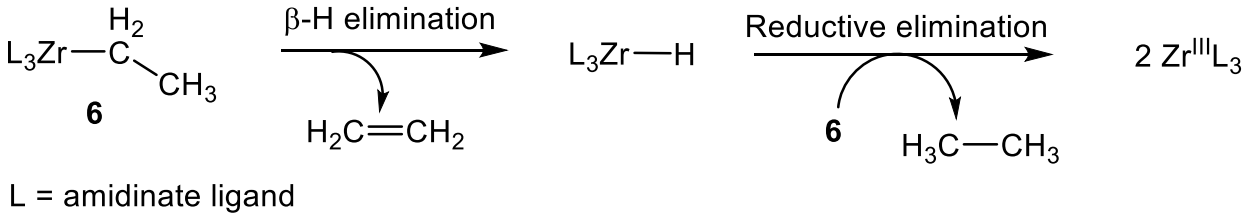

Scheme 3.4. β-hydrogen elimination in **6** releasing ethylene followed by the formation of ethane via reductive elimination between an additional molecule of **6** and $Zr[MeC(N^iPr)_2]_3H$.

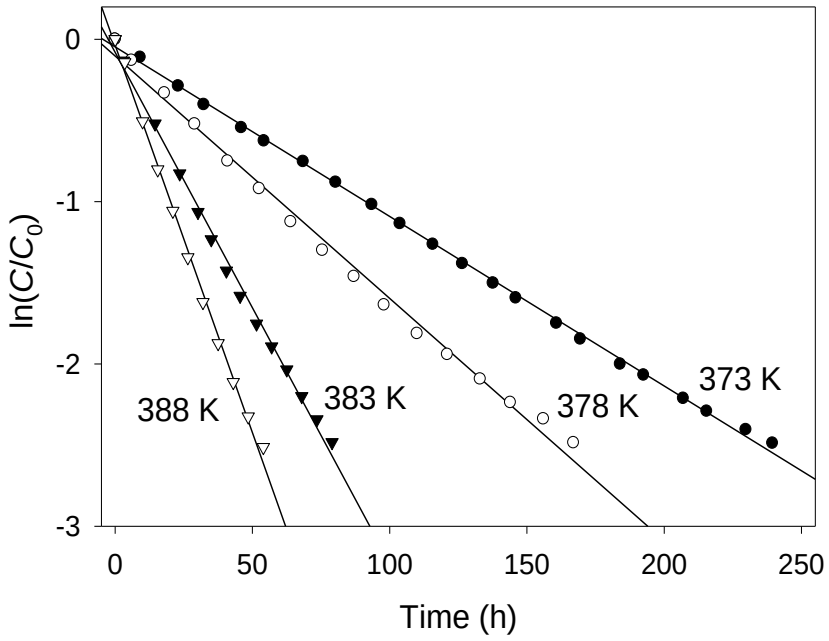

Figure 3.16. Kinetic plots of the thermal decomposition of **6** at 373-388 K.

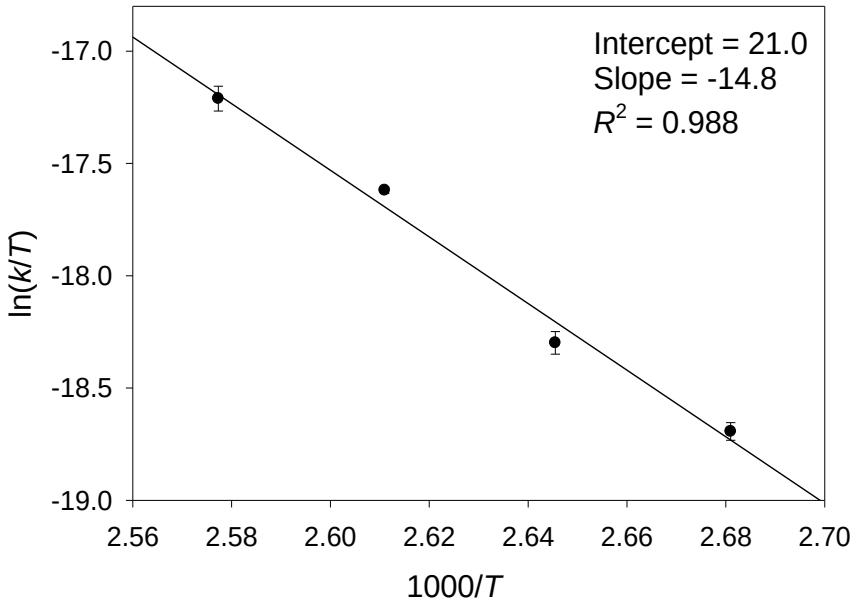

Figure 3.17. Eyring plot of the thermal decomposition of **6**.

Table 3.5. Rate constants for the decomposition of **6**[a]

T (K)	k x10^{-6} (s^{-1})
373(1)	2.84(11)
378(1)	3.99(20)
383(1)	8.54(11)
388(1)	13.0(7)

[a] The total uncertainties $\delta k/k$ were calculated from $\delta k_{ran}/k$ from each column and $\delta k_{sys}/k$ = 0.050. $\delta k_{ran}/k$ = 0.054, $\delta k/k$ = 0.073.

However, heptacoordinate **6** is sterically bulky, making the β-hydrogen elimination process difficult. Ethane may be produced by reductive elimination between the newly generated L_3Zr-H and the ethyl complex **6**. This process, however, would directly involve **6** (Scheme 3.4). In other words, if the unimolecular β-hydrogen elimination operates here (and is observed as the first-order kinetic process), the subsequent reductive elimination would lead to errors in the measured rates and kinetic parameters.

Another possible pathway to generate both ethylene and ethane is hydrogen abstraction between two molecules of **6** in Scheme 3.5. In this pathway, one of the ethyl ligands on one molecule abstracts an H atom from the ethyl ligand of another molecule. This abstraction forms ethylene from one ligand and ethane from the other, yielding one Zr(II), $Zr^{II}L_3$, and one Zr(IV), $Zr^{IV}L_3$, species. However, this pathway, involving two molecules of **6**, is expected to follow second-order kinetics and is thus not likely.

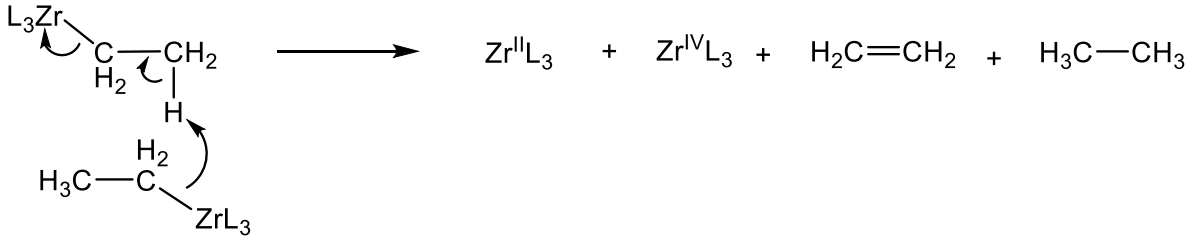

L = amidinate ligand

Scheme 3.5. Proposed hydrogen abstraction to form ethylene and ethane.

3.2.7. Studies of the Reactions between Zr and Hf Heptacoordinate Amidinate Complexes and H_2O

Loading samples for use in a mass spectrometer usually requires exposing the sample to air, even briefly. Thus the process of loading and ionizing the sample can cause side reactions if the compound is sensitive to O_2 or water from air. These complexes degrade within a few seconds when exposed to H_2O. Therefore, the mass spectrometry (MS) process also provides the opportunities to study the reactions of the complexes with O_2 or H_2O and identify the products that may not be isolated.

Since zirconium and hafnium each have several isotopes, compounds containing these elements are easily identified using MS spectrometry. In Part 2, DART-MS was used to characterize and identify **1** and **2**. The compounds **3**, **4**, **6**, and **7** could not be identified in MS due to the presence of the labile alkyl groups. However, the hydroxyl complexes $M[MeC(N^iPr)_2]_3OH$ (M = Zr, **8**; Hf **9**) were identified as products in the MS spectra. These products stemmed from the reactions of the metal complexes with H_2O (Scheme 3.6). Figures 3.18 and 3.19 show the calculated and observed MS spectra of [**8**+H^+] and [**9**+H^+], respectively. These complexes undergo nucleophilic attack by water. This was followed by the release of HCl or HR (R = Me, Et) as well as forming **8** or **9**. Since [**8**+H^+] and [**9**+H^+] were observed in the MS spectra, elimination of H_2O from them would yield $M[MeC(N^iPr)_2]_3^+$ (Scheme 3.6), which were also observed in the MS spectra.

Several attempts have been made to study the reactions of water with **1**, **2**, **3**, **4**, **6**, and **7** on a larger scale in order to isolate **8**, **9**, $M[MeC(N^iPr)_2]_3^+$ and other products, but none was successful. These studies did show that complexes **1**, **2**, **3**, **4**, **6**, and **7** are

sensitive to water. When 1 equiv of water was added to a solution of **6** in benzene-d_6, immediate reaction(s) occurred with the formation of insoluble white solids, ethane, and amidine ^{i}PrNH-C(Me)=N^{i}Pr. Ethane was identified in the ^{1}H NMR spectrum of the mixture. The presence of ^{i}PrNH-C(Me)=N^{i}Pr in the reaction mixture was confirmed by the ^{1}H and ^{13}C NMR spectra of the mixture and a gas chromatography (GC)-MS analysis of the supernatant solution of the mixture.

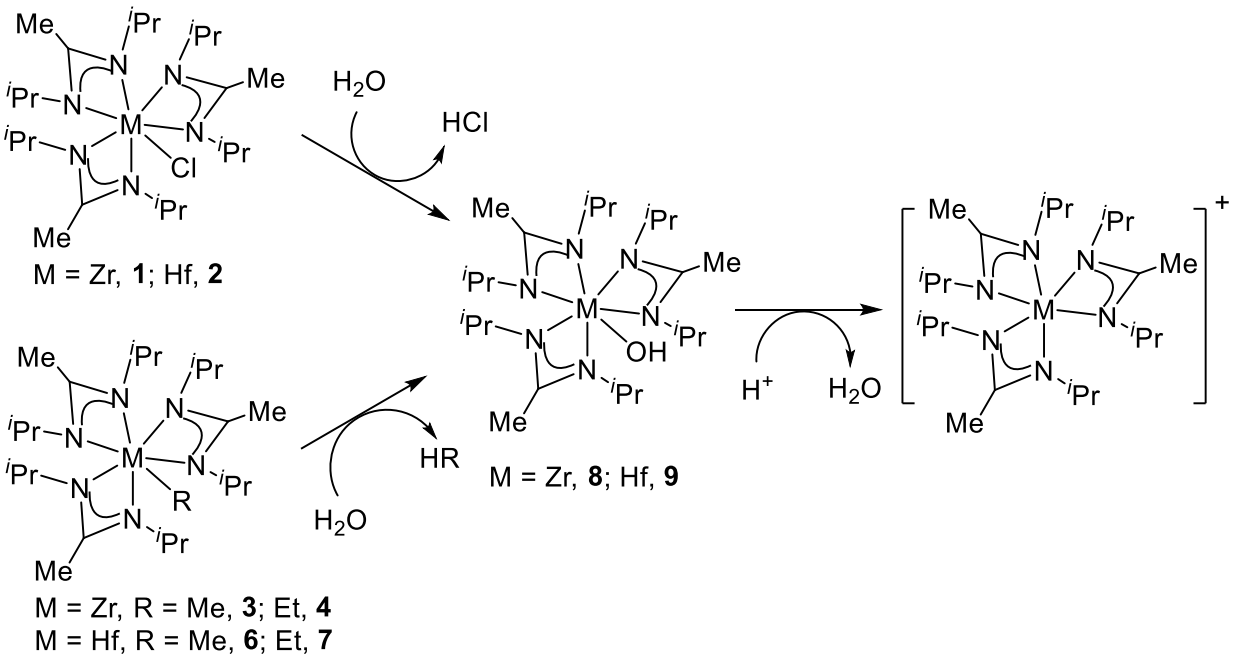

Scheme 3.6. Reactions of Zr and Hf complexes **1**-**4** and **6**-**7** with water yielding hydroxyl products **8**, **9** and M[MeC(N^{i}Pr)$_2$]$_3^+$.

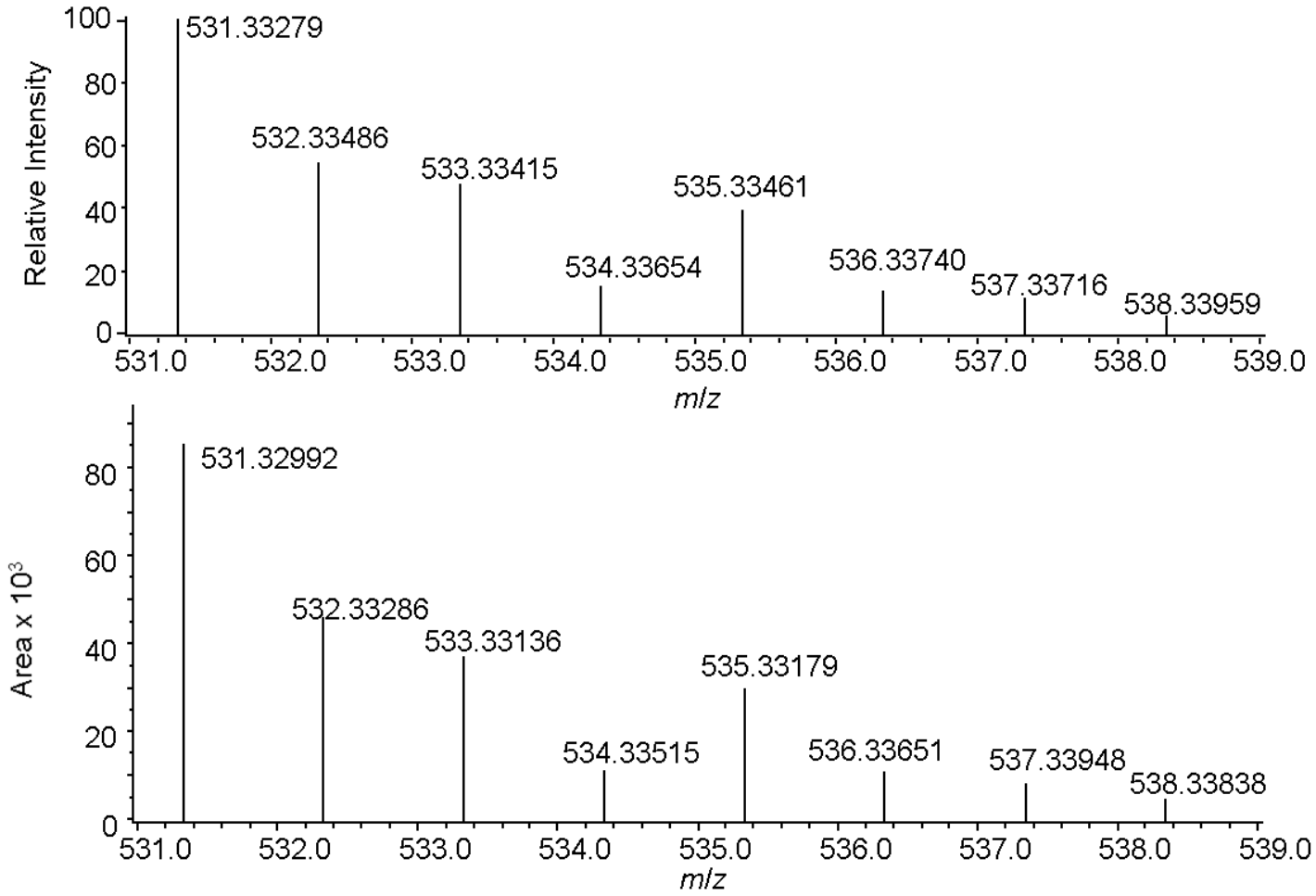

Figure 3.18. (Top) Calculated and (Bottom) Observed MS of [**8**+H^+].

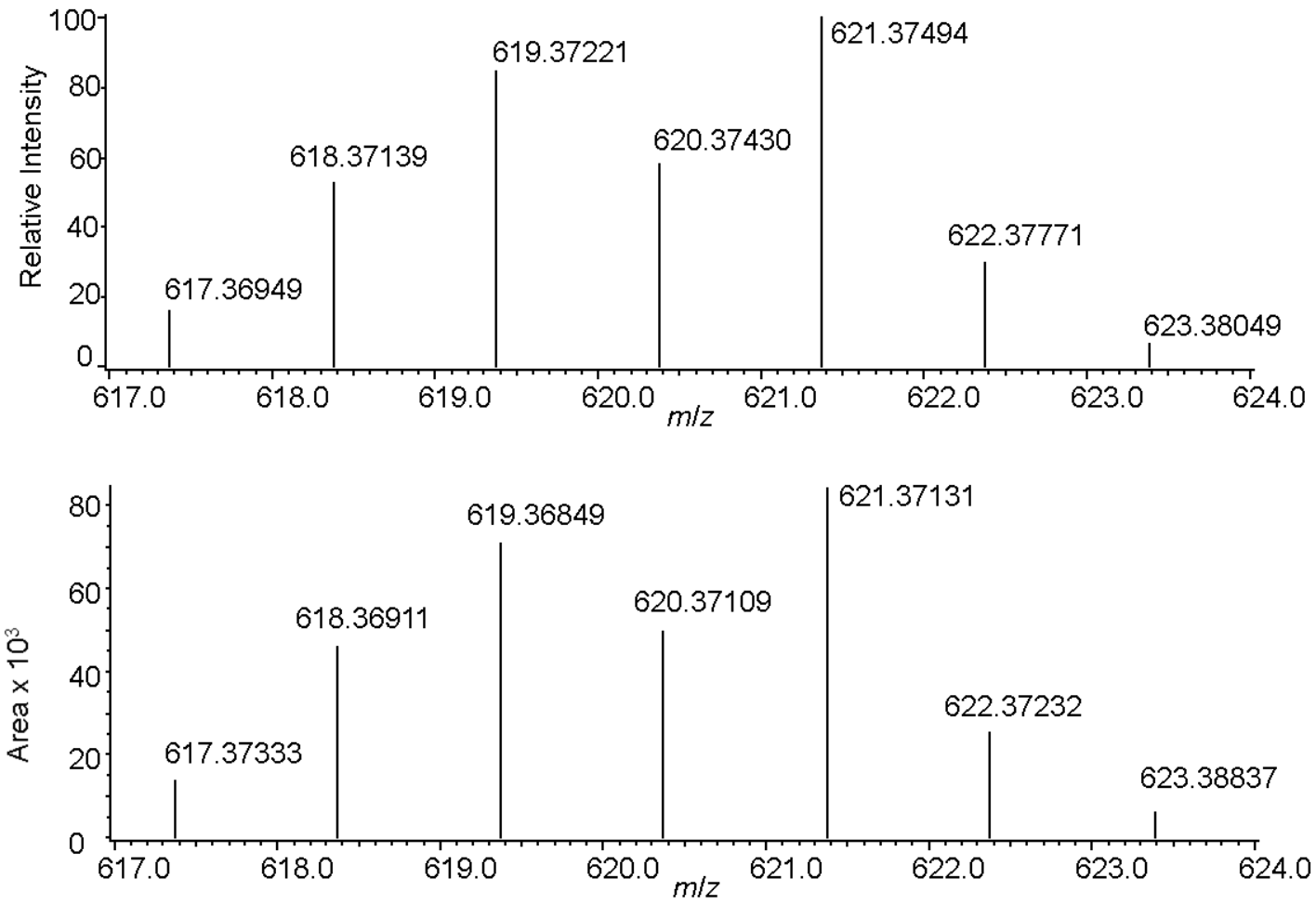

Figure 3.19. (Top) Calculated and (Bottom) Observed MS of [**9**+H^+].

3.3. Concluding Remarks

In this part, syntheses and characterization of several heptacoordinated Group 4 alkyl amidinates were reported. DART-MS studies were done on these alkyl complexes as well as compounds **1** and **2**. These complexes were found to undergo fast reactions with water in air, yielding hydroxyl products M[MeC(N^{i}P)$_2$]$_3$(OH) (M = Zr, **8**; Hf, **9**) that were observed in MS spectra. The decomposition of **6** follows first-order kinetics and the activation, and the activation parameters are: $\Delta H^{\neq}$ = 29(4) kcal/mol, $\Delta S^{\neq}$ = -5(8) eu, and $\Delta G^{\neq}_{298}$ = 31(6) kcal/mol.

3.4. Experimental Section

All manipulations were carried out under a dry nitrogen atmosphere with the use of either a glovebox or standard Schlenk techniques. All glassware was flamed dried under vacuum. Hexanes, THF, and pentane were purified by distillation from potassium benzophenone ketyl. NMR solvents were dried and stored over 5 Å molecular sieves. EtCl was purchased from Eastman and diluted with benzene to 9.7 M before use. The solution was stored in a -32 °C freezer. NMR spectra were recorded on a Bruker Avance 400 MHz or Varian VNMRS-500 spectrometer. Elemental analyses were conducted by Complete Analysis Laboratories, Inc., Parsippany, NJ. Mass spectra were recorded on a JEOL AccuTOF™ DART Mass Spectrometer.

3.4.1. Synthesis of Zr[MeC(N^{i}Pr)$_2$]$_3$Me (3)

Zr[MeC(N^{i}Pr)$_2$]$_3$Me (**3**) was prepared by adding MeLi (0.70 mL, 1.6 M in Et$_2$O, 1.1 mmol) to Zr[MeC(N^{i}Pr)$_2$]$_3$Cl (**1**, 539.1 mg, 0.9795 mmol) at -40 °C in Et$_2$O. The solution

was allowed to stir for 16 h before volatiles were removed. Pentane was used to extract the crude product. After filtration, the volume of the solution was reduced. After cooling in a -32 ° C freezer, white crystals of **3** formed (345.5 mg, 0.6519 mmol, 67% yield based on **1**). Though several attempts were made to use X-ray diffraction to study this compound, the crystals were not suitable for X-ray diffraction. ^{1}H NMR (benzene-d_6, 399.84 MHz, 23 °C): δ 3.54 (m, 6H, C*H*Me$_2$), 1.68 (s, 9H, NC(*Me)*N), 1.28 (d, 36H, CH*Me*$_2$), 0.81 (s, 3H, Zr*Me*); ^{13}C{^{1}H} NMR (benzene-d_6, 100.54 MHz, 23 °C): δ 147.30 (N*C*(Me)N), 49.44 (Zr*Me,* J_{C-H} = 117 Hz), 48.01 (*C*HMe$_2$), 24.51 (CH*Me*$_2$), 12.50 (NC(*Me*)N). ^{1}H and ^{13}C{^{1}H} NMR assignments were confirmed by HSQC (Figure A3) and ^{1}H-gated-decoupled ^{13}C NMR experiments (Figure A4). Anal. Calcd: C, 56.66; H, 10.27; N, 15.86. Found: C, 56.50; H, 10.42; N, 15.77.

3.4.2. Synthesis of Hf[MeC(N^{i}Pr)$_2$]$_3$Me (4)

The synthesis of Hf[MeC(N^{i}Pr)$_2$]$_3$Me (**4**) was accomplished by adding Hf[MeC(N^{i}Pr)$_2$]$_3$Cl (**2**, 193.9 mg, 0.3041 mmol) to Et$_2$O and cooling the solution to -40 °C. MeLi (0.20 mL, 1.6 M in Et$_2$O, 0.32 mmol) was added to the solution via syringe and stirred for 16 h. The volatiles are then removed. Pentane was added to the residue and the solution filtered to another flask. The solution containing crude product is reduced and put into a -32 °C freezer to afford clear crystals of **4** (94.1 mg, 0.1524 mmol, 50% yield based on **2**). The crystals were not suitable for X-ray diffraction. ^{1}H NMR (benzene-d_6, 399.84 MHz, 23 °C): δ 3.64 (m, 6H, C*H*Me$_2$), 1.65 (s, 9H, NC(*Me)*N), 1.27 (d, 36H, CH*Me*$_2$), 0.52 (s, 3H, Hf*Me*); ^{13}C{^{1}H} NMR (benzene-d_6, 100.54 MHz, 23 °C): δ 173.43 (N*C*(Me)N), 54.71 (Hf*Me,* J_{C-H} = 111 Hz), 47.75 (*C*HMe$_2$), 24.50 (CH*Me*$_2$), 13.14

(NC(*Me*)N). ^{1}H and $^{13}C\{^{1}H\}$ NMR assignments were confirmed by HSQC (Figure A5) and ^{1}H-gated-decoupled ^{13}C NMR (Figure A6) experiments. Anal. Calcd: C, 48.65; H, 8.82; N, 13.62. Found: C, 48.48; H, 8.69; N, 13.83.

3.4.3. Synthesis of EtMgCl (5)

To make EtCl easier to handle, 45 g of benzene at 0 °C was added to a 100 g of EtCl and the solution was kept at 0 °C. EtMgCl (**5**) was prepared using a modified procedure for synthesis of EtMgBr reagents.[8] A Schlenk flask was charged with Mg turnings (1.231 g, 0.05065 mol), and a single crystal of I_2 (~1 mg). Et_2O (~100 mL) was added and the solution was stirred at room temperature for 16 h. The Mg solution was then cooled to -50 °C. EtCl (4.5 mL EtCl in C_6H_6, ~0.044 mol EtCl) was diluted in Et_2O (~10 mL) and also cooled to -50 °C. The EtCl was added to the Mg turnings dropwise. The reaction was slowly heated to 35 °C and allowed to stir overnight. The turbid solution was then allowed to cool to room temperature. The excess Mg turnings were removed via filtration. A small portion (~10 mL) of the solution was removed in vacuo to remove any unreacted EtCl. The concentration of EtMgCl (0.68 M) was determined via titration with a standard HCl solution. ^{1}H NMR (toluene-d_8, 399.84 MHz, 32 °C): δ 1.62 (t, 3H, $MgCH_2C\mathit{H}_3$), -0.11 (m, 2H, $MgC\mathit{H}_2CH_3$); $^{13}C\{^{1}H\}$ NMR (toluene-d_8, 100.54 MHz, 32 °C): δ 13.16 ($MgCH_2CH_3$), 2.00 ($MgCH_2CH_3$). The position of the CH_2 peak in the $^{13}C\{^{1}H\}$ NMR spectrum was confirmed by DEPT-135 NMR spectroscopy (Figure A7).

3.4.4. Synthesis of Zr[MeC(N^{i}Pr)$_2$]$_3$Et (6)

Zr[MeC(N^{i}Pr)$_2$]$_3$Cl (**1**, 346.8 mg, 0.6356 mmol) was dissolved in Et_2O and cooled to -30 °C. EtMgCl (1.0 mL, 0.68 M in Et_2O/C_6H_6, 0.68 mmol) was added via syringe. The solution was allowed to warm to room temperature over 3 h and stirred for 16 h. Volatiles were removed in vacuo, and pentane was used to extract the crude product. The solution was condensed and placed in a -32 °C freezer to afford yellow crystals of Zr[MeC(N^{i}Pr)$_2$]$_3$Et (**6**, 161.0 mg, 0.2960 mmol, 47% yield based on **1**). ^{1}H NMR (benzene-d_6, 399.84 MHz, 23 °C): δ 3.66 (m, 6H, C*H*Me$_2$), 1.85 (t, 3H, ZrCH$_2$C*H*$_3$), 1.71 (s, 9H, NC(*Me)*N), 1.26 (d, 36H, CH*Me*$_2$), 1.06 (m, 2H, ZrC*H*$_2$CH$_3$); ^{13}C{^{1}H} NMR (benzene-d_6, 100.54 MHz, 23 °C): δ 174.68 (N*C*(Me)N), 53.65 (Zr*C*H$_2$CH$_3$, J_{C-H} = 117 Hz), 47.63 (*C*HMe$_2$), 24.49 (CH*Me*$_2$), 16.11 (ZrCH$_2$*C*H$_3$), 14.01 (NC(*Me*)N); ^{1}H NMR (toluene-d_8, 399.84 MHz, 23 °C): δ 3.64 (m, 6H, C*H*Me$_2$), 1.740 (t, 3H, ZrCH$_2$C*H*$_3$), 1.73 (s, 9H, NC(*Me)*N), 1.237 (d, 36H, CH*Me*$_2$), 0.96 (m, 2H, ZrC*H*$_2$CH$_3$); ^{13}C{^{1}H} NMR (toluene-d_8, 100.54 MHz, 23 °C): δ 174.67 (N*C*(Me)N), 53.76 (Zr*C*H$_2$CH$_3$), 47.68 (*C*HMe$_2$), 24.490 (CH*Me*$_2$), 16.06 (ZrCH$_2$*C*H$_3$), 13.96 (NC(*Me*)N). ^{1}H and ^{13}C{^{1}H} NMR assignments were confirmed by HSQC (Figure A8), DEPT-135 (Figure A9), and ^{1}H-gated-decoupled ^{13}C NMR (Figure A10) experiments. Anal. Calcd: C, 57.40; H, 10.38; N, 15.45. Found: C, 57.24; H, 10.19; N, 15.28.

3.4.5. Synthesis of Hf[MeC(N^{i}Pr)$_2$]$_3$Et (7)

EtMgCl (0.80 mL, 0.6796 M in Et_2O/C_6H_6, 0.54 mmol) was added via syringe to a solution of Hf[MeC(N^{i}Pr)$_2$]$_3$Cl (**2**, 333.1 mg, 0.5224 mmol) in Et_2O at -30 °C. The solution was allowed to warm to room temperature and stir overnight. Volatiles were removed in

vacuo. Pentane was used to extract the crude product. After filtration, the volume of the solution was reduced, and the flask was placed in a -32 °C freezer to afford pale yellow crystals of Hf[MeC(N^{i}Pr)$_2$]$_3$Et (**7**, 196.5 mg, 0.3113 mmol, 59% yield based on **2**). ^{1}H NMR (benzene-d_6, 399.84 MHz, 23 °C): δ 3.74 (m, 6H, C*H*Me$_2$), 2.01 (t, 3H, HfCH$_2$C*H$_3$*), 1.69 (s, 9H, NC(*Me)*N), 1.25 (d, 36H, CH*Me*$_2$), 0.73 (m, 2H, HfC*H*$_2$CH$_3$); ^{13}C{^{1}H} NMR (benzene-d_6, 100.54 MHz, 23 °C) δ 173.87 (N*C*(Me)N), 58.25 (Hf*C*H$_2$CH$_3$, $J_{C\text{-}H}$ = 117 Hz), 47.38 (*C*HMe$_2$), 24.50 (CH*Me*$_2$), 16.31 (HfCH$_2$*C*H$_3$), 14.57 (NC(*Me*)N); ^{1}H NMR (toluene-d_8, 399.84 MHz, 23 °C): δ 3.72 (m, 6H, C*H*Me$_2$), 1.91 (t, 3H, HfCH$_2$C*H$_3$*), 1.70 (s, 9H, NC(*Me)*N), 1.23 (d, 36H, CH*Me*$_2$), 0.64 (m, 2H, HfC*H*$_2$CH$_3$); ^{13}C{^{1}H} NMR (toluene-d_8, 100.54 MHz, 23 °C): δ 173.83 (N*C*(Me)N), 58.23 (Hf*C*H$_2$CH$_3$), 47.40 (*C*HMe$_2$), 24.49 (CH*Me*$_2$), 16.302 (HfCH$_2$*C*H$_3$), 14.49 (NC(*Me*)N). ^{1}H and ^{13}C{^{1}H} NMR assignments were confirmed by HSQC (Figure A11), DEPT-135 (Figure A12), and ^{1}H-gated-decoupled ^{13}C NMR (Figure A13) experiments. ^{1}H and ^{13}C{^{1}H} NMR assignments were confirmed by HSQC, DEPT-135, and ^{1}H-gated-decoupled ^{13}C NMR experiments. Anal. Calcd: C, 49.47; H, 8.94; N, 13.31. Found: C, 49.00; H, 8.60; N, 15.28.

3.4.6. Kinetic Studies of the Thermal Decomposition of Zr[MeC(N^{i}Pr)$_2$]$_3$Et (6)

For the thermodynamic studies, the rate constants were obtained from two separate experiments at each temperature, and their averages are listed in Table 3.5. The maximum random uncertainty in the rate constants was combined with the estimated systematic uncertainty of ca. 5%. The total uncertainties in the equilibrium constants were used in the ln(*k*/T) vs. 1000/*T* plot in Figure 3.17 and the error

propagation calculations. The estimated uncertainty in the temperature measurements for an NMR probe was 1 K. The activation enthalpy ($\Delta H^{\neq}$) and entropy ($\Delta S^{\neq}$) changes were calculated from an unweighted nonlinear least-squares procedure in the SigmaPlot Scientific Graph System. The uncertainties in $\Delta H°$ and $\Delta S°$ were computed from error propagation formulas which were derived from $R\ln(kh/k_bT) = -\Delta H^{\neq}/T + \Delta S^{\neq}$.[11] The uncertainties in $\Delta H^{\neq}$ and $\Delta S^{\neq}$ were computed from the error propagation formulas derived by Girolami and coworkers from the Eyring.[12]

For a typical kinetic run, $Zr[MeC(N^iPr)_2]_3Et$ (**6**, 20 mg, 0.0368 mmol) and an internal standard $SiMePh_3$ (10 mg) were dissolved in toluene-d_8 in a J. R. Young's NMR tube. The tube was then suspended in a pre-heated oil bath set to the given temperature. The temperature of the oil bath was held constant until the experiment was completed. After heating for a given amount of time, the NMR tube was placed in an ice bath, and the ^1H NMR spectra was taken at room temperature. After the spectrum was taken, the NMR tube was placed back into the oil bath to continue decomposing.

Caution: (1) Only the bottom portion of the tubes containing the solution should be submerged in the hot oil bath. The top portion containing the head space should be kept in air; (2) For kinetic experiments conducted at 110 °C or above, a small fan may be utilized to keep the top portion of the NMR tube cooled; (3) Tests should be performed behind a safety shield, especially for those done at 110 °C or above.

3.4.7. Determination of the X-ray Crystal Structures of 6 and 7

The X-ray structures of **6** and **7** were determined on a Bruker ASX Smart 1000 X-ray diffractometer equipped with a CCD area detector and a graphite-monochromated Mo source (*K*α radiation, 0.71073 Å) and fitted with an upgraded Nicolet LT-2 low temperature device. A suitable crystal was chosen from a batch and was coated paratone oil (Exxon). The crystal was mounted onto the diffractometer using a fiber loop under a stream of nitrogen at 100(2) K. The structure was solved by direct methods, and all non-hydrogen atoms were refined anisotropically using Olex2 software. SADABS was used for the empirical absorption corrections. Global refinements for the unit cells and data reduction were performed using the Saint program (Version 6.02). Calculations of atom positions and dihedral angles were done using SHELXTL (Version 5.1) proprietary software package and Olex2.[13,14]

3.4.8. Mass Spectrometry Studies of 3, 4, 6, and 7

Mass spectra were recorded on a JEOL AccuTOF™ DART Mass Spectrometer. The closed end of a capillary tube was inserted into either solid powders or a solution (in pentane) of the samples. The tube was then placed into a heated stream of He (200 °C) in the spectrometer. The spectra were referenced to a polyethylene glycol (PEG) standard.

References

1. Zucchini, U.; Albizzat, E.; Giannini, U. *J. Organomet. Chem.* **1971**, *26*, 357.

2. Pfennig, V.; Seppelt, K. *Science* **1996**, *271*, 626.

3. a) Stanciu, C.; Jones, M. E.; Fanwick, P. E.; Abu-Omar, M. M. *J. Am. Chem. Soc.* **2007**, *129*, 12400. (b) Tilley, T. D. *Organometallics*, **1985**, *4*, 1452. (c) Blackburn, T. F.; Labinger, J. A.; Schwartz, J. *Tetrahedron Lett.* **1975**, *16*, 3041. (d) Lubben, T. V.; Wolczanski, P. T. *J. Am. Chem. Soc.* **1987**, *109*, 424. (e) Wang, R.; Folting, K.; Huffman, J. C.; Chamberlain, L. R.; Rothwell, I. P. *Inorg. Chim. Acta* **1986**, *120*,81. (f) Gibson, V. C.; Redshaw, C.; Walker, G. L. P.; Howard, J. A. K.; Hoy, V. J.; Cole, J. M.; Kuzmina, L. G.; De Silva, D. S. *Dalton Trans.* **1999**, 161. (g) Schaverien, C. J.; Orpen, A. G. *Inorg. Chem.* **1991**, *30*, 4968. (h) Liu, X.; Cui, D. *Dalton Trans.* **2008**, 3747. (i) Van Asselt, A.; Trimmer, M. S.; Henling, L. M.; Bercaw, J. E. *J. Am. Chem. Soc.* **1988**, *110*, 8254. (j) Brindley, P. B.; Hodgson, J.C. *J. Organomet. Chem.* **1974**, *65*, 57. (k) Boro, B. J.; Lansing, R.; Goldberg, K. I.; Kemp, R. A. *Inorg. Chem. Comm.* **2011**, *14*, 531. (l) Lu, F.; Zarkesh, R. A.; Heyduk, A. F. *Eur. J. Inorg. Chem.* **2012**, *3*, 467. (m) Chisholm, M. H.; Hammond, C. E.; Huffman, J. C. *Chem. Comm.* **1987**, 1423. (n) Wang, R.-T.; Zhang, X.-H.; Chen, S.-J.; Yu, X.-H.; Wang, C.-S.; Beach, D. B.; Wu, Y.-D.; Xue, Z.-L. *J. Am. Chem. Soc.* **2005**, *127*, 5204. (o) Chen, S.-J.; Zhang, X.-H.; Yu, X.; Qiu, H.; Yap, G. P. A.; Guzei, I. A.; Lin, Z.; Wu, Y. D.; Xue, Z.-L. *J. Am. Chem. Soc.* **2007**, *129*, 14408. (p) Chen, S.-J.; Zhang, J.; Yu, X.; Bu, X.; Chen, X.-T.; Xue, Z.-L. *Inorg. Chem.* **2010**, *49*, 4017. (q) Morton, L. A.; Miao, M.; Callaway, T. M.; Chen, T.; Chen, S.-J.; Tuinman, A. A.; Yu, X.-H.; Lu, Z.; Xue, Z.-L. *Chem.*

Comm. **2013**, *49*, 9555. (r) Chen, T.-N.; Zhang, X.-H.; Wang, C.-S.; Chen, S.-J.; Wu, Z.-Z.; Li, L.- T.; Sorasaenee, K. R.; Diminnie, J. B.; Pan, H.-J.; Guzei, I. A.; Rheingold, A. L.; Wu, Y.-D.; Xue, Z.-L. *Organometallics* **2005**, *24*, 1214. (s) Qiu, H.; Chen, S.-J.; Wang, C.-S.; Wu, Y.-D.; Guzei, I. A.; Chen, X.-T.; Xue, Z.-L. *Inorg. Chem.* **2009**, *48*, 3073. (t) Yu, X.; Chen, X.-T.; Xue, Z.-L. *Organometallics* **2009**, *28*, 6642. (u) Chen, S.-J.; Yap, G. P. A.; Xue, Z.-L. *Sci. China: Chem.* **2009**, *52*, 1583. (v) Chen, S.-J.; Zhang, X.-H.; Lin, Z.; Wu, Y.-D.; Xue, Z.-L. *Sci. China: Chem.* **2009**, *52*, 1723. (w) Chen, S.-J.; Xue, Z.-L. *Organometallics* **2010**, *29*, 5579. (x) Sharma, B.; Callaway, T. M.; Lamb, A. C.; Steren, C. A.; Chen, S.-J.; Xue, Z.-L. *Inorg. Chem.* **2013**, *52*, 11409.

4. (a) Lamb, A. C.; Lu, Z.; Xue, Z.-L. *Chem. Comm.* **2014**, *50*,10517. (b) Lamb, A. C.; Wang, Z.; Cook, T. M.; Sharma, B.; Chen, S.-J.; Lu, Z.; Steren, C. A.; Lin, Z.; Xue, Z.-L. *Polyhedron* **2016**, *103*, 2.

5. (a) Campbell, S. A. *Science and Engineering of Microelectronic Fabrication,* ed. Sedra, A. S., Oxford University Press, 2nd Ed., 2001. (b) Panda, D.; Tseng, T.–Y. *Thin Solid Films* **2013***, 531,* 1. (c) Hitchman, M. L.; Jenson, K. F. in *Chemical Vapor Deposition: Principles and Applications*. eds. Hitchman, M. L.; Jenson, K. F., Academic Press, 1993, 1. (d) Jenson, K. F. in *Chemical Vapor Deposition: Principles and Applications*. eds. Hitchman, M. L.; Jenson, K. F., Academic Press, 1993, 31. (d) Pierson, H. O. in *Handbook of Chemical Vapor Deposition: Principles, Technology, and Applications.* eds. Bunshah, R. F.; McGuire, G. E.; Rossnagel, S. M., Noyes Publications, 1992. (f) Powell, C. F.; Oxley, J. H.; Blocher, J. M. *Vapor Deposition*, The Electrochemical Society, New York, 1966.

(g) Wallace, R.; Wilk, G. D. *MRS Bull*. **2002**, *27*, 192. (h) Jones, A. C.; Hitchman, M. L. *Chemical Vapour Deposition: Precursors, Processes and Applications*, Royal Society of Chemistry, 2009, 1. (i) Ritala, M.; Niinisö, J. in *Chemical Vapour Deposition: Precursors, Processes and Applications.* eds. Jones A. C.; Hitchman, M. L., Royal Society of Chemistry, 2009, 158. (j) Malik, M. A.; O'Brien, P. in *Chemical Vapour Deposition: Precursors, Processes and Applications.* eds. Jones, A. C.; Hitchman, M. L., Royal Society of Chemistry, 2009, 207. (k) Jones, A. C.; Aspinall, H. C.; Chalker, P. R. in *Chemical Vapour Deposition: Precursors, Processes and Applications.* eds. Jones, A. C.; Hitchman, M. L., Royal Society of Chemistry, 2009, 357. (l) Devi, A. *Coord. Chem. Rev.* **2013**, *257,* 3332.

6. (a) Smith, R. C.; Ma, T.; Hoilien, N.; Tsung, L. Y.; Bevan, M. J.; Colombo, L.; Roberts, J.; Campbell, S. A.; Gladfelter, W. L. *Adv. Mater. Opt. Electr.* **2000**, *10*, 105. (b) Wallace, R.; Wilk, G. D. *Crit. Rev. Solid State Mater. Sci.* **2003**, *28*, 231. (c) Wilk, G. D.; Wallace, R. M.; Anthony, J. M. *J. Appl. Phys.* **2001**, *89*, 5243. (d) Arghavani, R.; Miner, G.; Agustin, M. *Semicond. Internal.* **2007**, *30*, 32. (e) Jones, A. C.; Aspinall, H. C.; Chalker, P. R.; Potter, R. J.; Kukli, K.; Rahtu, A.; Ritala, M.; Leskelae, M. *J. Mater. Chem.* **2004**, *14*, 3101. (f) Walawalkar, M. G.; Kottanthrayil, A.; Rao, R. *Syn. React. Inorg. Met.* **2009**, *39*, 331. (g) Degraeve, R.; Cartier, E.; Kauerauf, T.; Carter, R.; Pantisano, L.; Kerber, A.; Groeseneken. G. *MRS Bull.* **2002**, *27*, 222.

7. Xu, K.; Milanov, A. P.; Winter, M.; Barreca, D.; Gasparotto, A.; Becker, H.-W.; Devi, A. *Eur. J. Inorg. Chem.* **2010**, 1679.

8. Glöckner, A.; Bauer, H.; Maekawa, M.; Bannenberg, T.; Daniliuc, C. G.; Jones, P.

G.; Sun, Y.; Sitzmann, H.; Tamm, M.; Walter, M. D. *Dalton Trans.* **2012**, *41*, 6614.

9. Gizbar, H.; Vestfrid, Y.; Chusid, O.; Gofer, Y.; Gottlieb, H. E.; Marks, V.; Aurbach, D. *Organometallics* **2004**, *23,* 3826.

10. Altona, C.; Ippel, J. H.; Hoekzema, A. J. A. W.; Erkelens, C.; Groesbeek, M.; Donders, L. A. *Magnetic Resonance in Chemistry*, **1989**, *27*, 564.

11. Green, M. L. H.; Wong, L. L.; Sella, A. *Organometallics* **1992**, *11*, 2660.

12. Morse, P. M.; Spencer, M. D.; Wilson, S. R.; Girolami, G. S. *Organometallics* **1994**, *13*, 1646.

13. (a) Sheldrick, G. M. SADABS, *A Program for Empirical Absorption Correction of Area Detector Data*; Bruker-AXS, Madison, Wisconsin, USA. 2002. (b) Sheldrick, G. M. SHELXL-97, *A Program for the Refinement of Crystal Structures*, University of Göttingen, Göttingen, Germany, 1997.

14. Dolomanov, O. V.; Bourhis, L. J.; Gildea, R. J; Howard, J. A. K.; Puschmann, H. *J. Appl. Cryst.* **2009**, *42*, 339.

Part 4

Studies of the Reactions between Tungsten Alkylidyne Complexes and Water

A section of this part pertaining to the reaction of H_2O with $W(\equiv CSiMe_3)$-$(CH_2SiMe_3)_3$ was published in the following paper:

Laurel A. Morton, Maozhong Miao, Tabitha M. Cook (née Callaway), Tianniu Chen, Shu-Jian Chen, Albert A. Tuinman, Xianghua Yu, Zheng Lu and Zi-Ling Xue. "Reactions of d^0 Tungsten Alkylidyne Complexes with O_2 or H_2O. Formation of an Oxo Siloxy Complex through Unusual Silyl Migrations." *Chem. Comm*. **2013**, *49*, 9555.

Abstract

Reaction of $W(\equiv CSiMe_3)(Me_3SiCH_2)_3$ (**11**) with water in THF at 23 °C gave the trimer $[(\mu\text{-}O)W(CH_2SiMe_3)_2(=O)(THF)]_3$ (**12**). The crystal and molecular structure of **13** has been determined. Reaction of $W(\equiv C^tBu)(O^tBu)_3$ (**10**) with H_2O gave $W(CH_2{}^tBu)(O^tBu)_3(=O)$ (**13**) in solution. DART-MS was used to identify several other products in the reaction of **10** with H_2O in air. W-containing complexes products observed by DART-MS include the following: unreacted **10**, **13**, $W(\equiv C^tBu)(O^tBu)(=O)$ (**14**), $W(\equiv C^tBu)(O^tBu)_2(OH)$ (**15**), $W(=CH^tBu)(OC^tBu)_2(=O)$ (**16**), $W(CH_2{}^tBu)(OC^tBu)(=O)_2$ (**17**), and $W(CH_2{}^tBu)(O^tBu)(=O)_2$ (**18**).

4.1. Introduction

Alkylidyne complexes, or high-valent, early transition metal complexes containing the M≡C bonds, are typically reactive with water. Schrock, Lippard and coworkers have studied the reaction of the alkyl alkylidyne W(≡C^{t}Bu)(CH$_2$^{t}Bu)$_3$ with H$_2$O. In the presence of excess water, the reaction gives CMe$_4$ and O[W(=O)(CH$_2$^{t}Bu)$_3$]$_2$ (Scheme 4.1).[1] They have also studied the reaction of the alkoxy alkylidyne W(≡C^{t}Bu)(O^{t}Bu)$_3$ (**10**) with excess H$_2$O, giving an insoluble product.[2] When 1 equiv of NEt$_4$OH was added to H$_2$O, the reaction with **10** gives [NEt$_4$][WO$_3$(CH$_2$^{t}Bu)] (Scheme 4.1).[2] In the reaction, all alkoxide ligands are removed and the alkylidyne ligand ≡C^{t}Bu is converted to an alkyl ligand in [NEt$_4$][WO$_3$(CH$_2$^{t}Bu)]. This product was found to be thermally stable and did not decompose further in water at pH 7. Levy and coworkers studied the organic products formed when an excess of water was added to **10**.[3] The organic products, after the reaction was completed, included HO^{t}Bu, CMe$_4$, and ^{t}Bu-C≡C-^{t}Bu.

Our group has studied the reactions of W alkylidyne complexes with water. The reaction of W(≡CSiMe$_3$)(CH$_2$^{t}Bu)$_3$ with H$_2$O or D$_2$O in THF yielded the trimer W$_3$O$_3$(μ=O)$_3$(CH$_2$^{t}Bu)$_6$ as either a THF or D$_2$O adduct, comprising two neopentyl ligands per W atom (Scheme 4.2).[4] The intermediate W$_2$(=O)$_2$(μ-O)(CD$_2$SiMe$_3$)$_2$(CH$_2$^{t}Bu)$_4$ was observed in the reaction of W(≡CSiMe$_3$)(CH$_2$^{t}Bu)$_3$ with D$_2$O in THF. The trimer is then formed following the elimination of the –CD$_2$SiMe$_3$ ligands by D$_2$O.

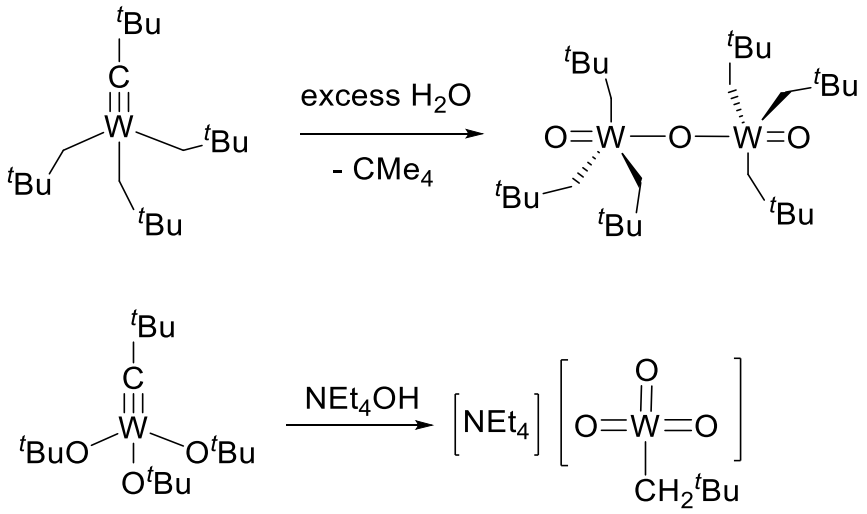

Scheme 4.1. Reactions of W alkylidyne complexes with H_2O.[1,2]

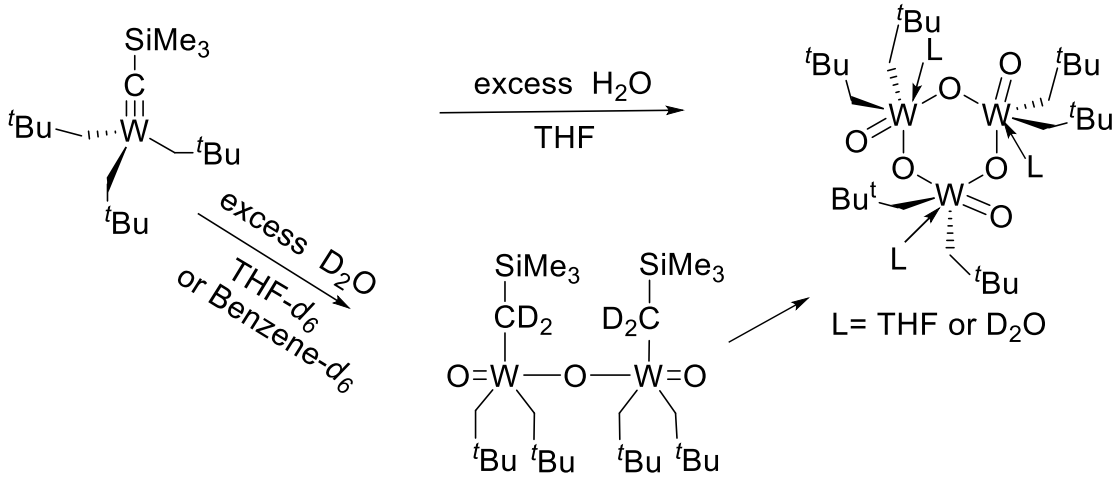

Scheme 4.2. Reactions of $W(\equiv CSiMe_3)(CH_2{}^tBu)_3$ with H_2O and D_2O.[4]

Our group has also studied the reaction of $W(\equiv CSiMe_3)(CH_2SiMe_3)_3$ (**11**) with H_2O at -78 °C. At this temperature, the complex $W(=O)(OSiMe_3)(CH_2SiMe_3)_3$ was formed, indicating the migration of the oxophilic $SiMe_3$ to a W=O ligand. Since this species was found to be unstable, another equiv of **11** was added to $W(=O)(OSiMe_3)(CH_2SiMe_3)_3$ to cap and stabilize it for characterization (Scheme 4.3).[5,6] Recently, Grekov and coworkers have used the reactions of $W(=O)(Cl)(CH_2SiMe_3)_3$, an analog of $W(=O)(OSiMe_3)(CH_2SiMe_3)_3$, with the hydroxyl groups on silica to generate surface-grafted $W(=O)(CH_2SiMe_3)_3(OSi\equiv)$ and $W(=O)_2(CH_2SiMe_3)_2(OSi\equiv)_2$ through the elimination of HCl and $SiMe_4$.[7] Both species lead to tungsten oxo catalysts for propene metathesis.

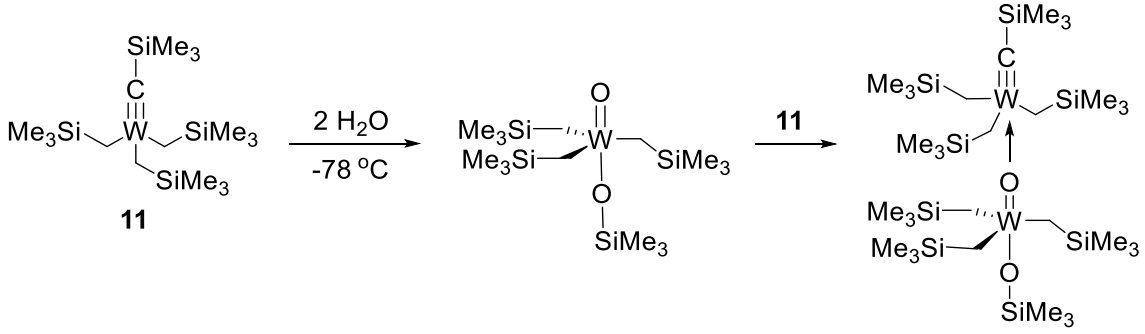

Scheme 4.3. Reaction of **11** with water at -78 °C.

Herein, we report the studies of the reaction between $W(\equiv CSiMe_3)(CH_2SiMe_3)_3$ (**11**) and water at room temperature, yielding the trimer $[(\mu\text{-}O)W(CH_2SiMe_3)_2(=O)\text{-}(THF)]_3$ (**12**). Also, the reactions of $W(\equiv C^tBu)(O^tBu)_3$ (**10**) with H_2O have been studied

via NMR spectroscopy and DART-MS. While only one product was identified by both NMR and MS, several more species were identified via MS alone.

4.2. Results and Discussion

4.2.1. Reaction between W(≡CSiMe$_3$)(Me$_3$SiCH$_2$)$_3$ (11) in THF and H$_2$O at 23 °C to Give the Trimer [(μ-O)W(CH$_2$SiMe$_3$)$_2$(=O)(THF)]$_3$ (12)

A solution of water in THF was added to W(≡CSiMe$_3$)(CH$_2$SiMe$_3$)$_3$ (**11**) at 23 °C and the mixture was stirred overnight. Once the volatiles were removed, the product was recrystallized in hexanes at -32 °C, yielding white crystals of W$_3$O$_3$(μ=O)$_3$(CH$_2$SiMe$_3$)$_6$(THF)$_3$ (**12**) (Scheme 4.4).[6] These crystals had to be kept cold, because the trimer was found to be unstable at room temperature and would decompose to a green solid in less than 2 h. The NMR spectra were taken immediately after the crystals were dissolved in benzene-d_6. In the ^{1}H NMR spectrum at 23 °C (Figure 4.1), the triplets assigned to the THF ligand were found at 3.57 and 1.40 ppm.

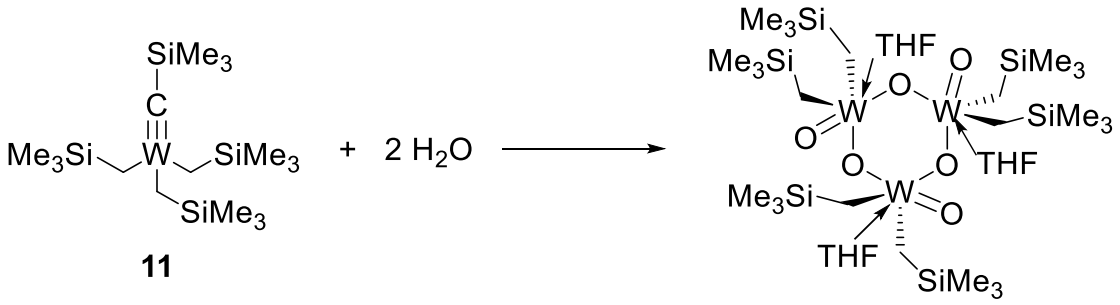

11 **12**

Scheme 4.4. Reaction of **11** with water at room temperature.[6]

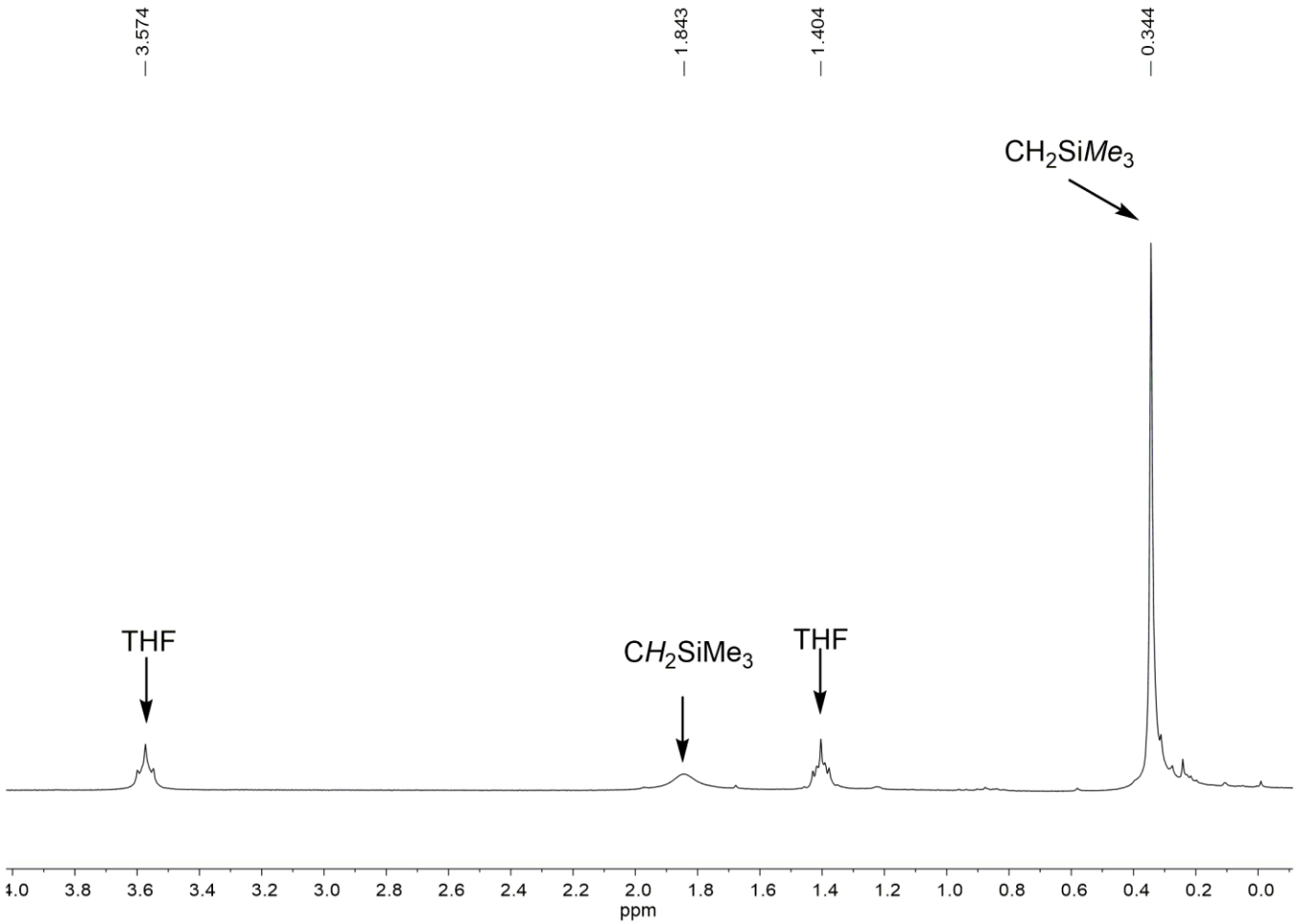

Figure 4.1. ^{1}H NMR spectrum of **12** in benzene-d_6 at 23 °C.

A broad peak at 1.85 ppm was assigned to the C*H*$_2$SiMe$_3$ groups. The CH$_2$Si*Me*$_3$ singlet was found at 0.35 ppm. ^{13}C{^{1}H} NMR spectrum of **12** in benzene-*d*$_6$ (Figure 4.2) shows that the *C*H$_2$SiMe$_3$ and CH$_2$Si*Me*$_3$ peaks are singlets at 70.0 and 1.73 ppm, respectively. The THF peaks were found to be at 68.0 and 25.8 ppm.

The ORTEP, crystallographic data, and selected bond lengths and angles in **12** are given in Figure 4.3 and Tables 4.1 and 4.2, respectively. The W centers, bridging oxo ligands, and bound THF form a plane. The CH$_2$SiMe$_3$ ligands are in axial positions. Each W center has a slightly distorted octahedral geometry. One oxo ligand bonds to the W via a W=O double bond. The other is a W←O dative bond. The dative bond W←O has a bond length of 2.239(2) Å, and the W=O bond has a shorter length of 1.758(3) Å. The W-THF bond length is 2.363(3) Å. The THF is nearly perpendicular to the datively bound O atom [88.97(15)°] as well as the terminal O ligand [88.97(15)°]. These are all similar to the bond lengths and angles of the analogous compound W$_3$O$_3$(μ=O)$_3$(CH$_2$*t*Bu)$_6$(THF)$_3$.[4] A comparison between structural features of W$_3$O$_3$(μ=O)$_3$(CH$_2$*t*Bu)$_6$(THF)$_3$ and **12** is given in Table 4.2.

4.2.2. NMR-scale Reaction of W(≡C^{t}Bu)(O^{t}Bu)$_3$ (10) with H$_2$O in Benzene-d$_6$

The reaction of **10** with H$_2$O was monitored by ^{1}H and ^{13}C{^{1}H} NMR spectroscopy. Addition of 2 equiv of H$_2$O in THF to **10** in benzene-*d*$_6$ was found to give the products HO*t*Bu and W(CH$_2$*t*Bu)(O*t*Bu)$_3$(=O) (**13**). The HO*t*Bu was observed as a singlet in ^{1}H NMR spectrum (Figure 4.4) at 1.11 ppm and two singlets at 68.08 and 31.38 ppm in the ^{13}C{^{1}H} NMR spectrum (Figure 4.5).

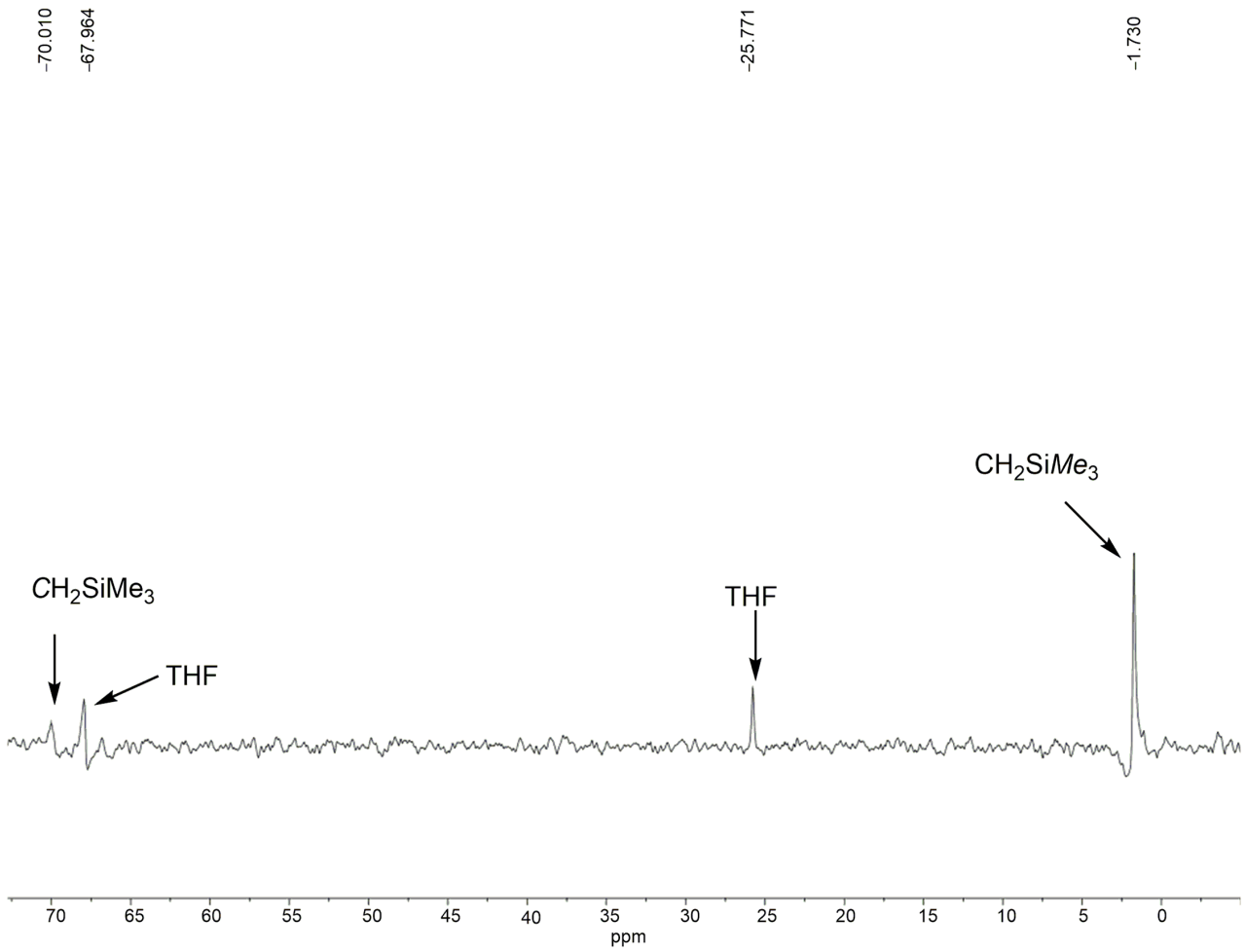

Figure 4.2. $^{13}C\{^{1}H\}$ NMR spectrum of **12** in benzene-d_6 at 23 °C.

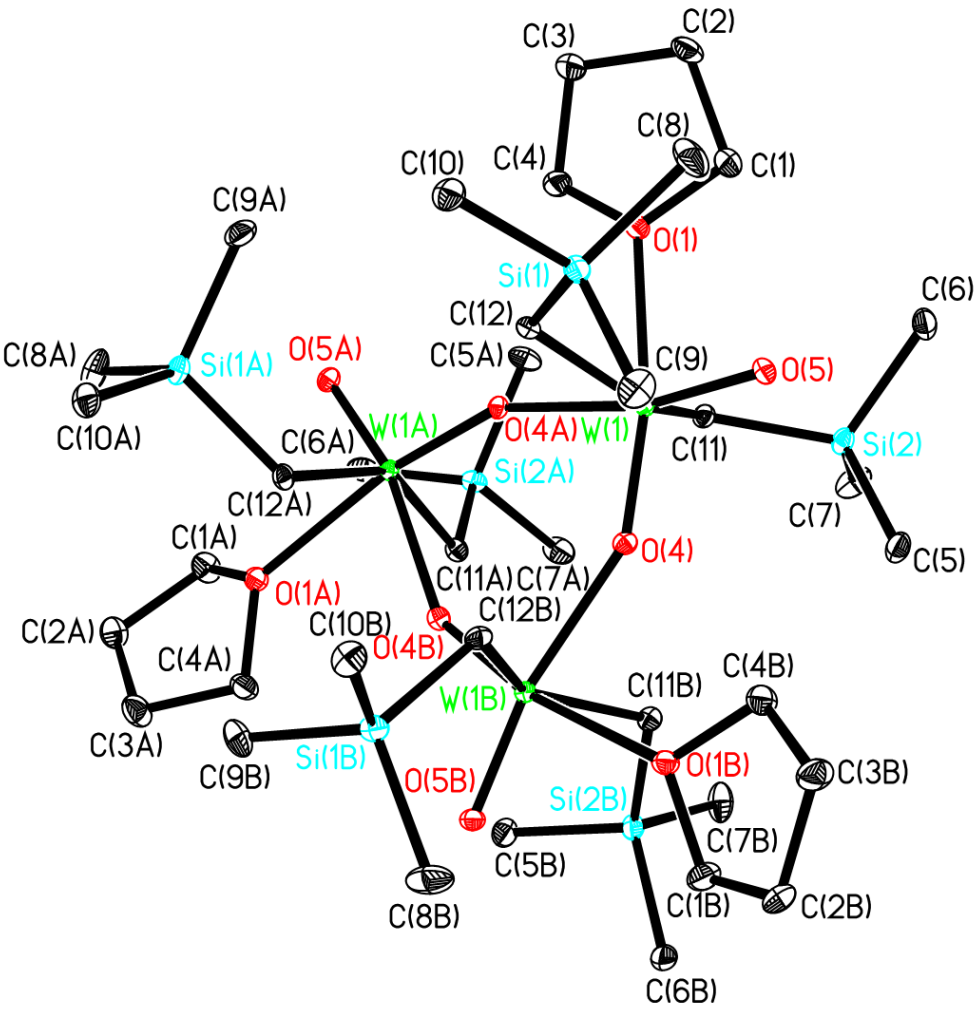

Figure 4.3. ORTEP of **12** was at 173(2) K. Thermal ellipsoids are 30% probability level. Hydrogen atoms were removed for clarity.

Table 4.1. Crystal data and structure refinement for **12**

Empirical formula	$C_{36}H_{90}O_9Si_6W_3$
Formula weight	1387.17
Temperature	173(2) K
Wavelength	0.71073 Å
Crystal System	Cubic
Space Group	*I*-43*d*
Unit cell dimensions	*a* = 28.065(3) Å α = 90°
	b = 28.065(3) Å β = 90°
	c = 28.065(3) Å γ = 90°
Volume	22105(4) Å^3
Z	16
Density (calculated)	1.667 g/cm^3
Absorption coefficient	6.400 mm^{-1}
F(000)	10944.0
Crystal size	0.15 × 0.09 × 0.07 mm^3
Theta range for data collection	1.78 to 28.61°
Index ranges	-37 ≤ *h* ≤ 32, -36 ≤ *k* ≤ 37, -31 ≤ *l* ≤ 36
Reflections collected	67995
Independent reflections	4603 [R_{int} = 0.1358]
Completeness to theta = 28.61°	98.0%
Max. and min. transmission	0.6629 and 0.4469
Refinement method	Full-matrix least-squares on F^2
Absorption correction	Semi-empirical from equivalents
Data / restraints / parameters	4603 / 0 / 169
Goodness-of-fit on F^2	0.999

Table 4.1. Continued

Final *R* indices [$I > 2\sigma(I)$]	$R1 = 0.0218$, $wR2 = 0.0480$
R indices (all data)	$R1 = 0.0256$, $wR2 = 0.0490$
Largest diff. peak and hole	1.17 and -0.62 eÅ^{-3}

[a] $R1 = \Sigma \, ||F_o| - |F_c|| \, / \, \Sigma \, |F_o|$; $wR2 = [\Sigma \, w(F_o^2 - F_c^2)^2 \, / \, \Sigma \, w(F_o^2)^2]^{1/2}$;

$w = 1/[\sigma^2(F_o) + (aP)^2 + bP]$; $P = [2Fc^2 + \text{Max}(F_o^2, 0)]/3$

Table 4.2. Comparison of bond lengths (Å) and angles (°) between **12** and $W_3O_3(\mu{=}O)_3(CH_2{}^tBu)_6(THF)_3$[4]

Compound No./Name	**$W_3O_3(\mu{=}O)_3(CH_2{}^tBu)_6(THF)_3$**	**12**
	Bond lengths (Å)	
W=O_T	1.709(4)	1.711(3)
W=O_B	1.773(4)	1.758(3)
W←O_B	2.214(4)	2.239(2)
W-C	2.186*	2.163*
	Bond angles (°)	
W-O_B-W	149.7(2)	150.90(15)
C-W-C	145.9(2)	146.83(14)
O_T=W-C	98.6(2)	98.38(13)
O_{THF}-W←O_B	90.2(2)	88.97(15)
O_{THF}-W=O_T	86.45(18)	86.28(11)

* Average; a) O_T = terminal oxygen atom; b) O_B = bridging oxygen atom; b) O_{THF} = oxygen atom on THF.

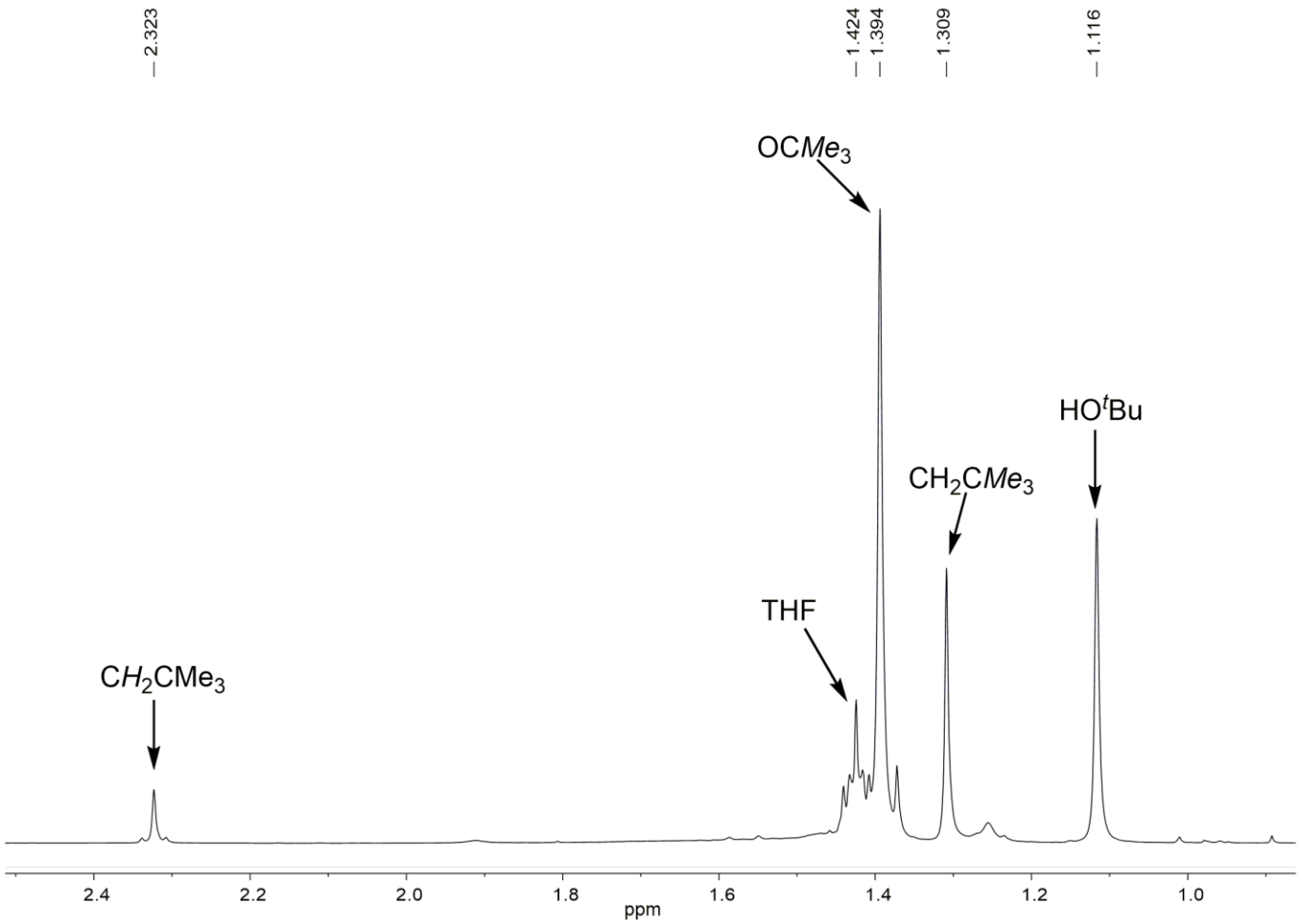

Figure 4.4. ^{1}H NMR spectrum of **13** and HO^{t}Bu in THF and benzene-d_6 at 23 °C.

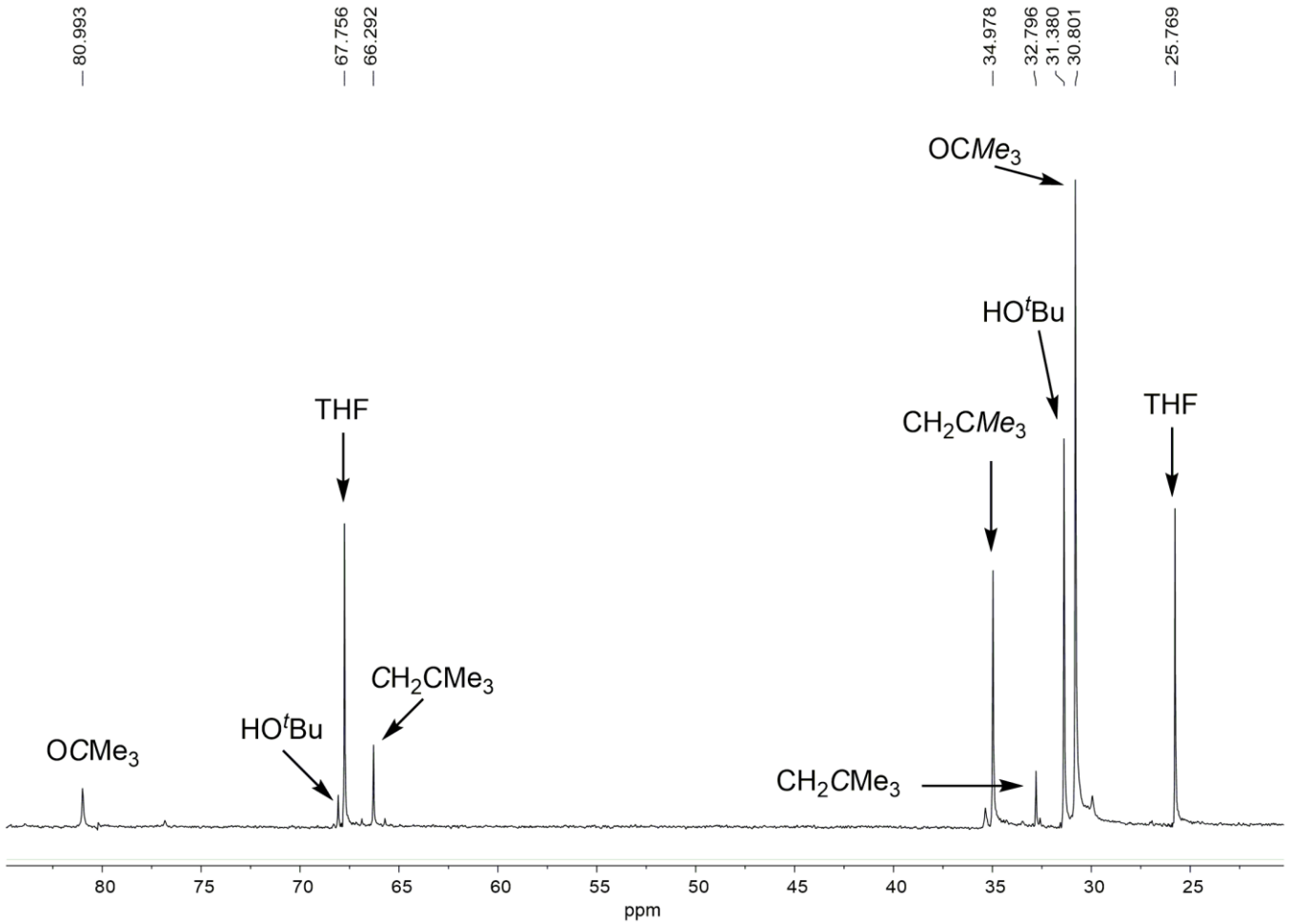

Figure 4.5. $^{13}C\{^{1}H\}$ NMR spectrum of **13** and HO^{t}Bu in THF and benzene-d_6 at 23 °C.

The two singlets at 1.39 and 1.31 ppm in the ^{1}H NMR spectrum correspond to new OC*Me*$_3$ and CH$_2$C*Me*$_3$ methyl groups in **13**, respectively. The singlet at 2.32 ppm in the ^{1}H NMR spectrum corresponds to the C*H*$_2$ moiety. There are small satellites on either side of the C*H*$_2$ peak at 2.32 ppm in the ^{1}H NMR spectra. There were also two satellites on either side of the *C*H$_2$ peak at 66.29 ppm the ^{13}C{^{1}H} NMR spectrum. Since the spin (*I*) of the ^{183}W isotope (natural abundance = 14.3%) is ½, it couples to the ^{1}H and ^{13}C atoms, giving the observation of these satellite peaks ($J_{W\text{-}H}$ = 12.3 Hz; $J_{W\text{-}C}$ = 117.0 Hz). The OC*Me*$_3$ group in **13** is at 30.80 ppm in the ^{13}C{^{1}H} NMR spectrum. The peak for the tertiary carbon atom O*C*Me$_3$ was assigned to the singlet at 80.99 ppm. The CH$_2$*C*Me$_3$ and CH$_2$C*Me*$_3$ peaks were found at 32.80 and 34.98 ppm, respectively.

4.2.3. DART-TOF MS Analysis of W(≡C^{t}Bu)(O^{t}Bu)$_3$ (10)

Loading samples for use in a mass spectrometer usually requires the sample to be exposed to air. The DART ion source uses energetic He atoms to ionize water in air. For compounds stable to air, this process attaches a H^+ cation to the compound enabling it to be separated via a mass-to-charge ratio from other ions and then detected. The process of loading and ionizing the sample can cause reactions if the compound is sensitive to O_2 or water from air. However, this MS technique also gives the opportunities to identify products that may not be isolated in a typical experiment of the reaction in solution. Since tungsten has several isotopes with different abundances (Table 4.3), tungsten-containing compounds have a distinctive pattern in the DART-MS spectrum. A few crystals of **10** were crushed into powders and collected on the end of a small capillary tube. These crystals were passed through a heated (200 °C) He stream.

Since the DART ionizes H_2O in air providing the H^+ ions needed to protonate complexes for analysis, some of the sample of **10** reacts with H_2O before the ions reach the detector.

The following W-containing complexes were observed in MS and their spectra, plus a H^+ ion, are given in Figures 4.6-4.11: unreacted **10** ([**10**+H^+] *m*/*z* = 473.23, Figure 4.6), **13** ([**13**+H^+] *m*/*z* = 491.24, Figure 4.7), W(≡C^{t}Bu)(O^{t}Bu)(=O) (**14**, [**14**+H^+] *m*/*z* = 343.09, Figure 4.8), W(≡C^{t}Bu)(O^{t}Bu)$_2$(OH) (**15**, [**15**+H^+] *m*/*z* = 417.16, Figure 4.9), W(=CH^{t}Bu)(O^{t}Bu)$_2$(=O) (**16**, [**16**+H^+] *m*/*z* = 417.16, Figure 4.9), W(CH$_2$^{t}Bu)(O^{t}Bu)(=O)$_2$ (**17**, [**17**+H^+] *m*/*z* = 361.10, Figure 4.10), and W(CH$_2$^{t}Bu)(O^{t}Bu)(=O)$_2$ (**18**, [**18**+H^+] *m*/*z* = 305.04, Figure 4.11). Compounds **15** and **16** have the same mass to charge ratio (*m*/*z*), and they cannot be distinguished from one another by MS alone.

Both W(≡C^{t}Bu)(CH$_2$^{t}Bu)$_3$ and it β-Si analog W(≡CSiMe$_3$)(CH$_2$SiMe$_3$)$_3$ have three alkyl ligands. These complexes may react differently to water than their alkoxyl analog **10**. For example, when W(≡C^{t}Bu)(CH$_2$^{t}Bu)$_3$ reacts with water, the H^+ ion in H_2O is transferred to the alkylidyne C atom first to make a W alkylidene product. Subsequent reactions with water and the loss of CMe$_4$ yield the W dimer W$_2$O$_2$(μ-O)(CH$_2$^{t}Bu)$_4$ -(CH$_2$^{t}Bu)$_2$ (Scheme 4.5).[1]

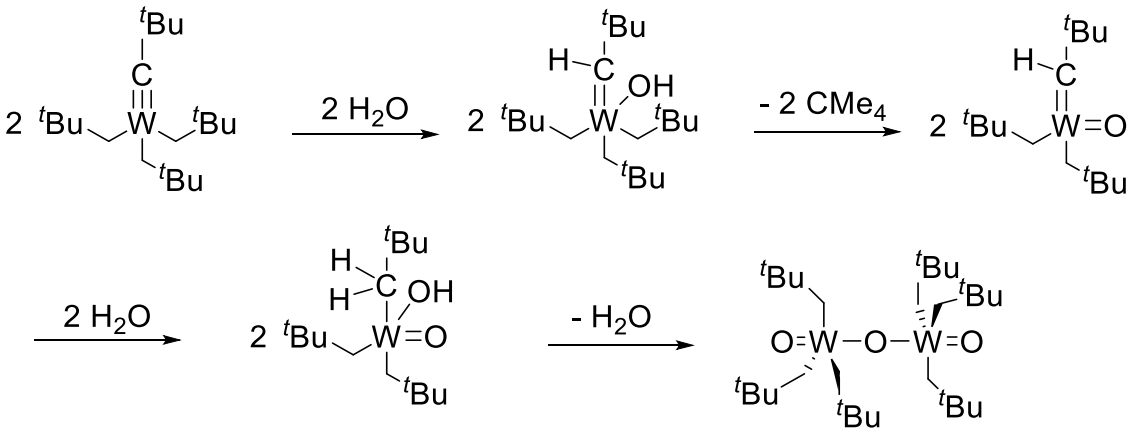

Scheme 4.5. Pathway of the reaction of W(≡C^{t}Bu)(CH$_2$^{t}Bu)$_3$ with H$_2$O.[1]

Table 4.3. Stable isotopes of tungsten

Isotope	Accurate Mass	% Natural Abundance
^{180}W	179.946701(5)	0.12 (1)
^{182}W	181.948202(3)	26.50(16)
^{183}W	182.950220 (3)	14.31 (4)
^{184}W	183.950925(3)	30.64 (2)
^{186}W	185.954357 (4)	28.43 (19)

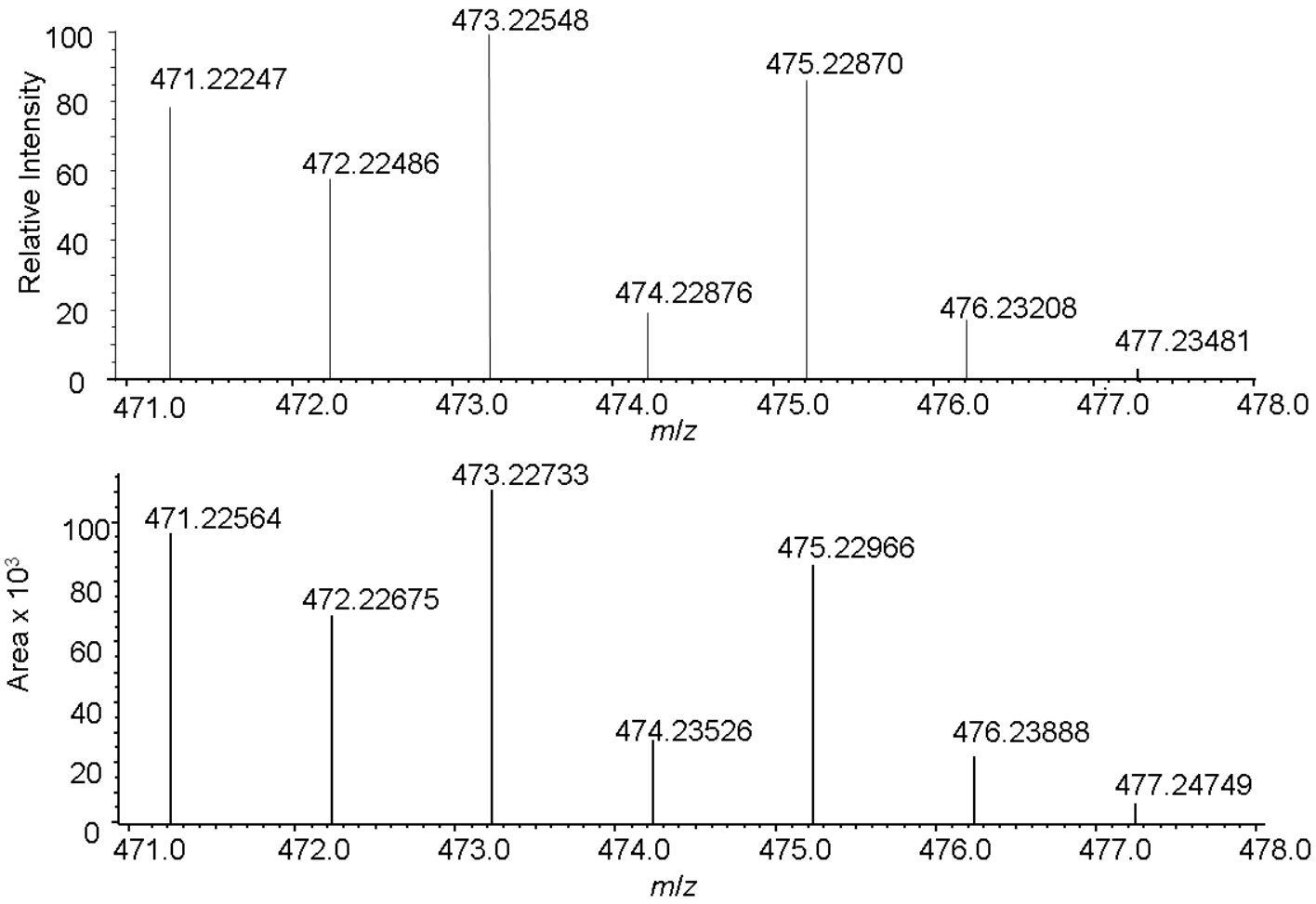

Figure 4.6. (Top) Calculated and (Bottom) Observed MS for [**10**+H^+].

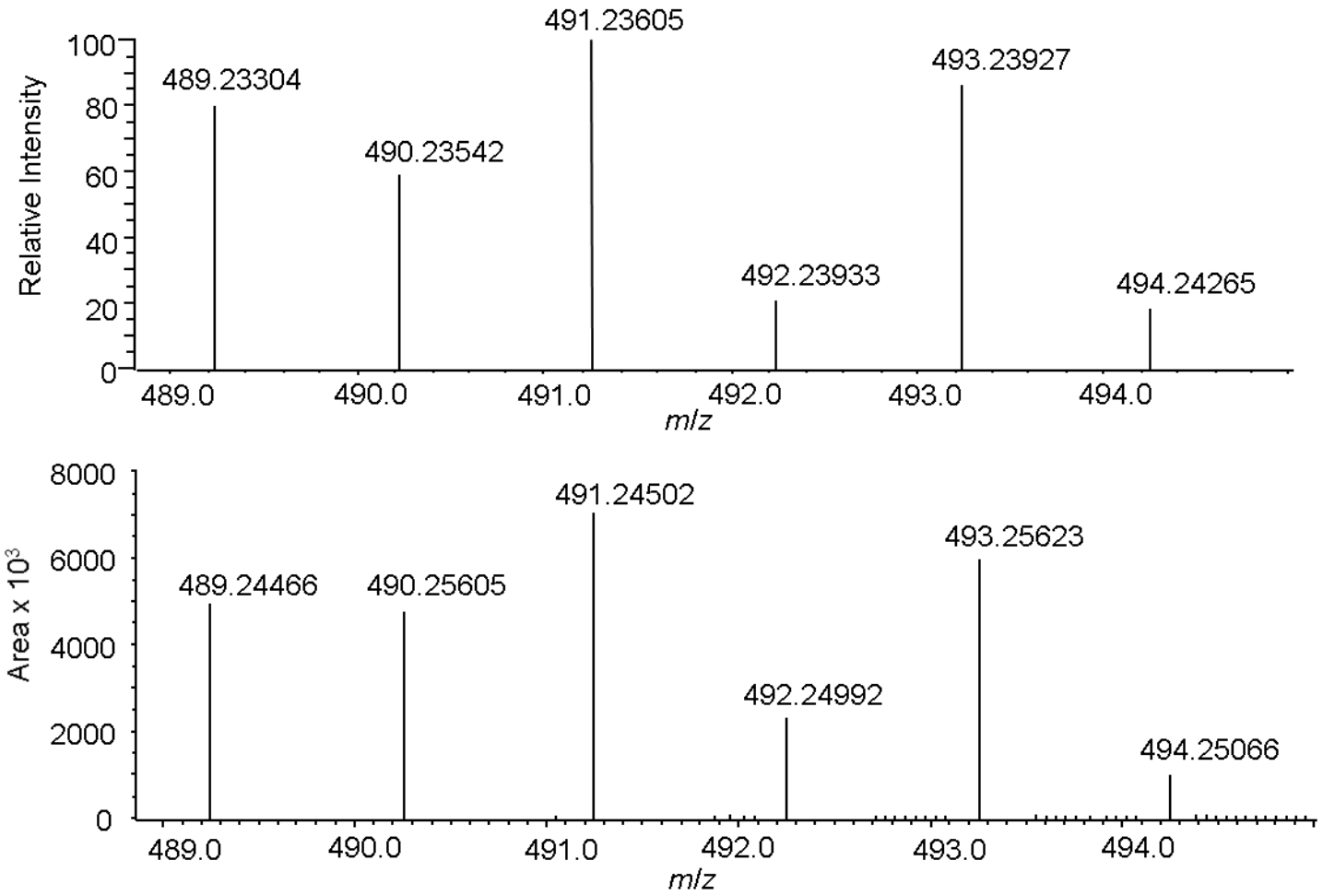

Figure 4.7. (Top) Calculated and (Bottom) Observed MS for [**13**+H^+].

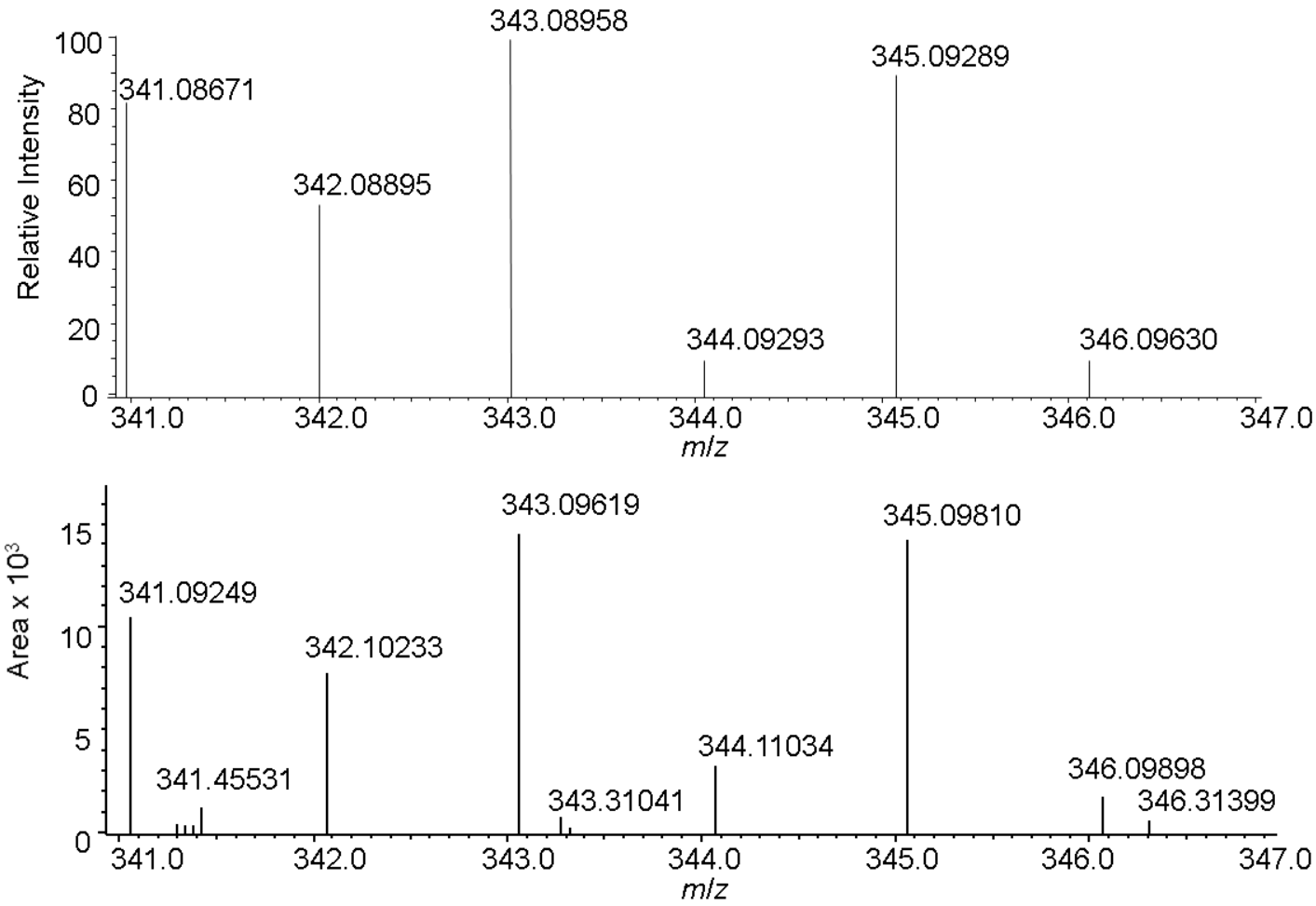

Figure 4.8. (Top) Calculated and (Bottom) Observed MS for [**14**+H^+].

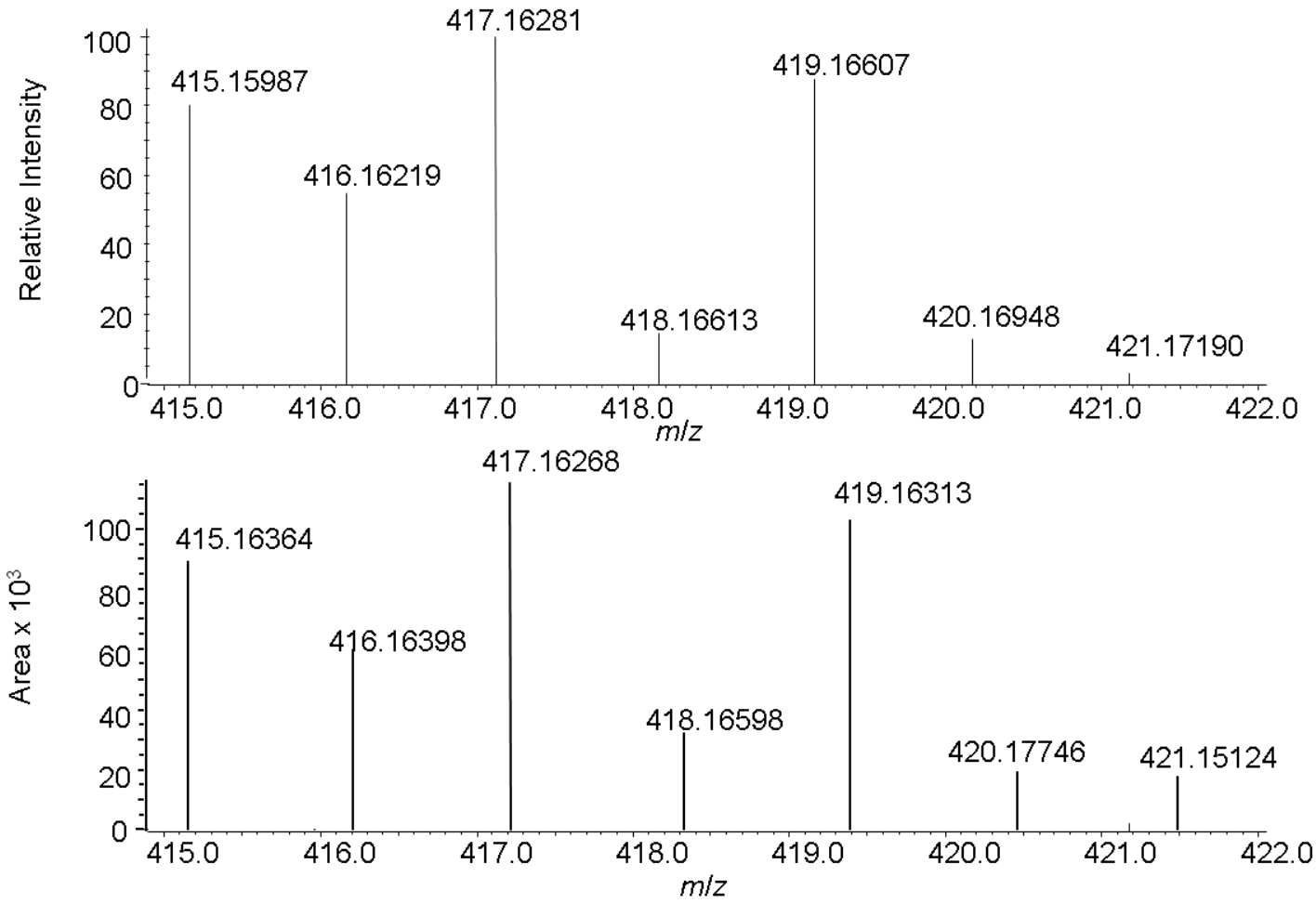

Figure 4.9. (Top) Calculated and (Bottom) Observed MS for [**15**+H^+] and/or [**16**+H^+].

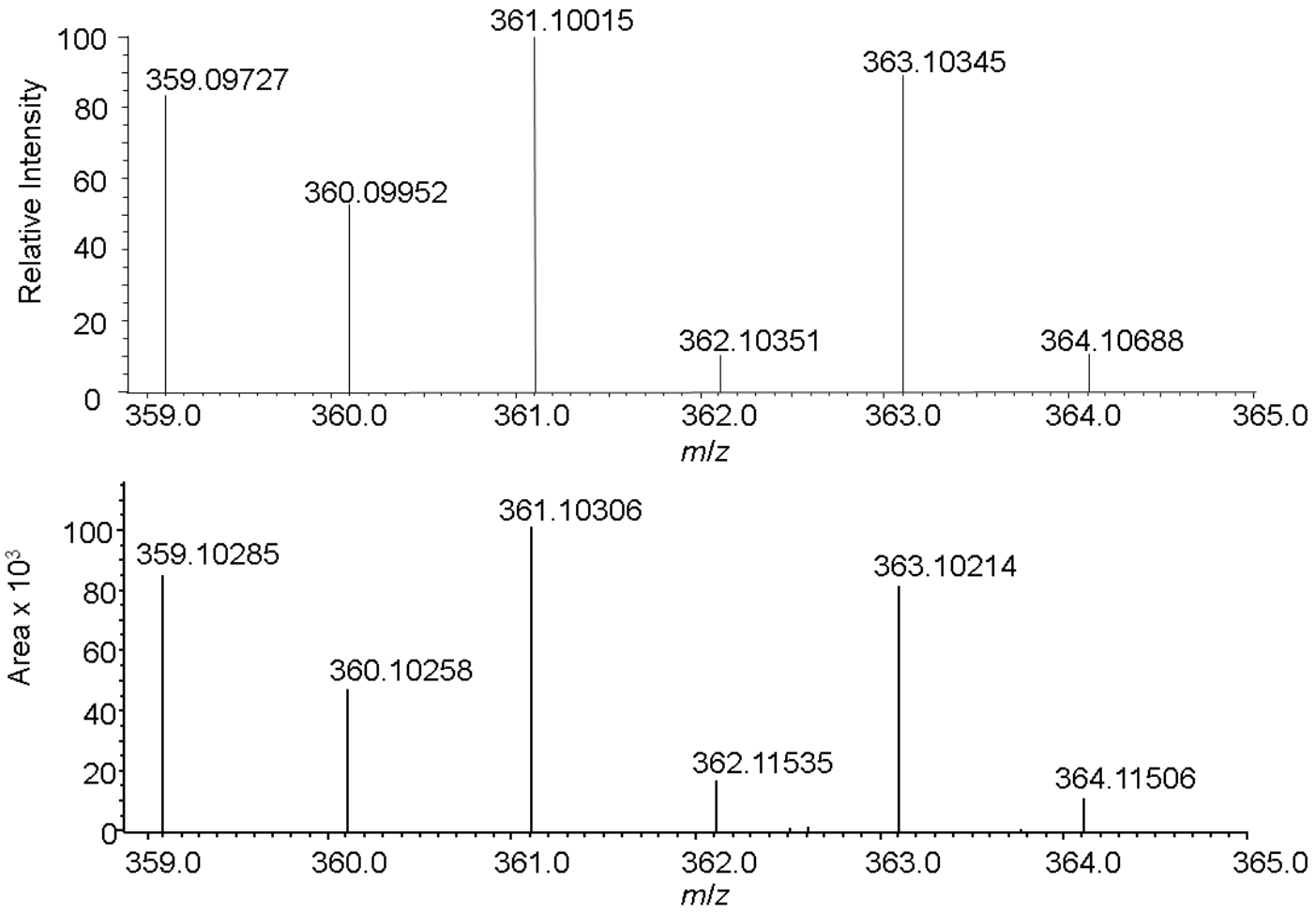

Figure 4.10. (Top) Calculated and (Bottom) Observed MS for [**17**+H^+].

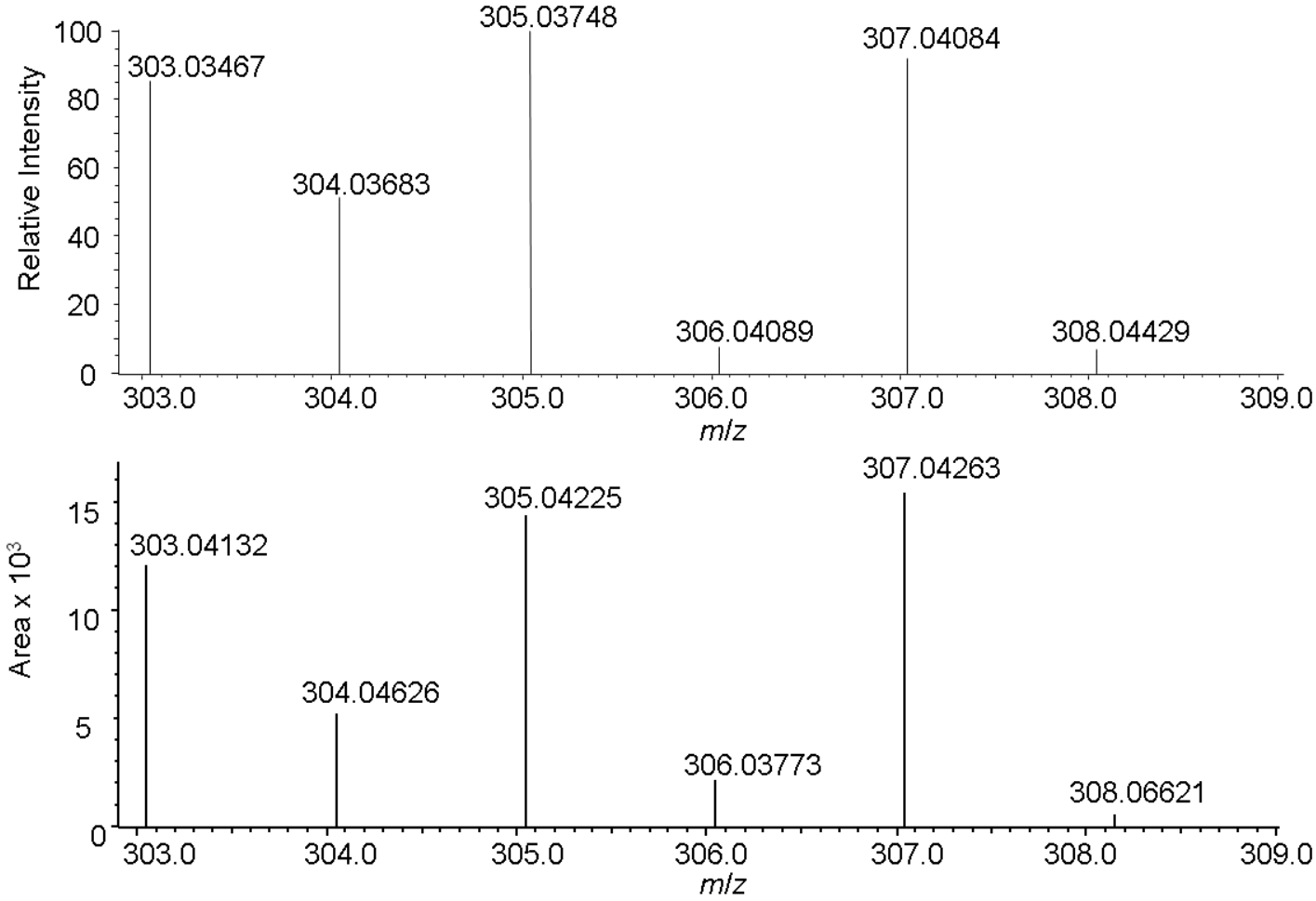

Figure 4.11. (Top) Calculated and (Bottom) Observed MS for [**18**+H^+]

Compound **10** contains α-O atoms with two lone pairs of electrons. The presence of these electrons may play a key role in the reaction pathway. Schwartz and coworkers have studied the reactions of $Zr(CH_2{}^tBu)_4$ and $Zr(O{}^tBu)_4$ with surface Al-OH groups.[8] The rate-determining step is the H^+ transfer from Al-OH to the O atoms in $Zr(O{}^tBu)_4$. The reactions of $Zr(O{}^tBu)_4$ with the surface OH groups are much faster than those of its alkyl analog $Zr(CH_2{}^tBu)_4$. Schwartz and coworkers attributed the results to the presence of the lone electron pairs on the O atoms of the $O{}^tBu$ ligands in $Zr(O{}^tBu)_4$, providing kinetically favorable sites for the proton transfer. $HO{}^tBu$ is a by-product in these reactions.

The proposed pathways for the reaction of **10** with H_2O in air at 200 °C are given in Scheme 4.6, and this scheme includes all species observed in the MS spectrum. The presence of the α-O atoms may encourage the elimination of the $O{}^tBu$ ligand before adding to the alkylidyne carbon atom. First, an $-O{}^tBu$ ligand is removed by water, making complex **15** containing a –OH ligand and removing $HO{}^tBu$. Then, the proton (H^+) on the hydroxy ligand can either eliminate another $-O{}^tBu$ ligand to form complex **14** (Path A) or add to the alkylidyne C atom to form the alkylidene complex **16** (Path B). **16** can also be made by the addition of $HO{}^tBu$ to **14**. In this process, H^+ ion in $HO{}^tBu$ also adds across the alkylidyne C atom in **14**. Another $HO{}^tBu$ molecule can add to the W=C bond in **16** to form alkyl compound **13** (Path C). Two more water molecules can react with **13** to form **18**, removing the three $-O{}^tBu$ ligands from **13**. One of the H_2O molecules eliminates 2 $-O{}^tBu$ ligands to form 2 equiv of $HO{}^tBu$ and an oxo (W=O) ligand. The other H_2O molecule removes the last $-O{}^tBu$ ligand to form one more equiv of $HO{}^tBu$ and a hydroxy ligand in **18**. Path D shows how H_2O may react with **16**. In this

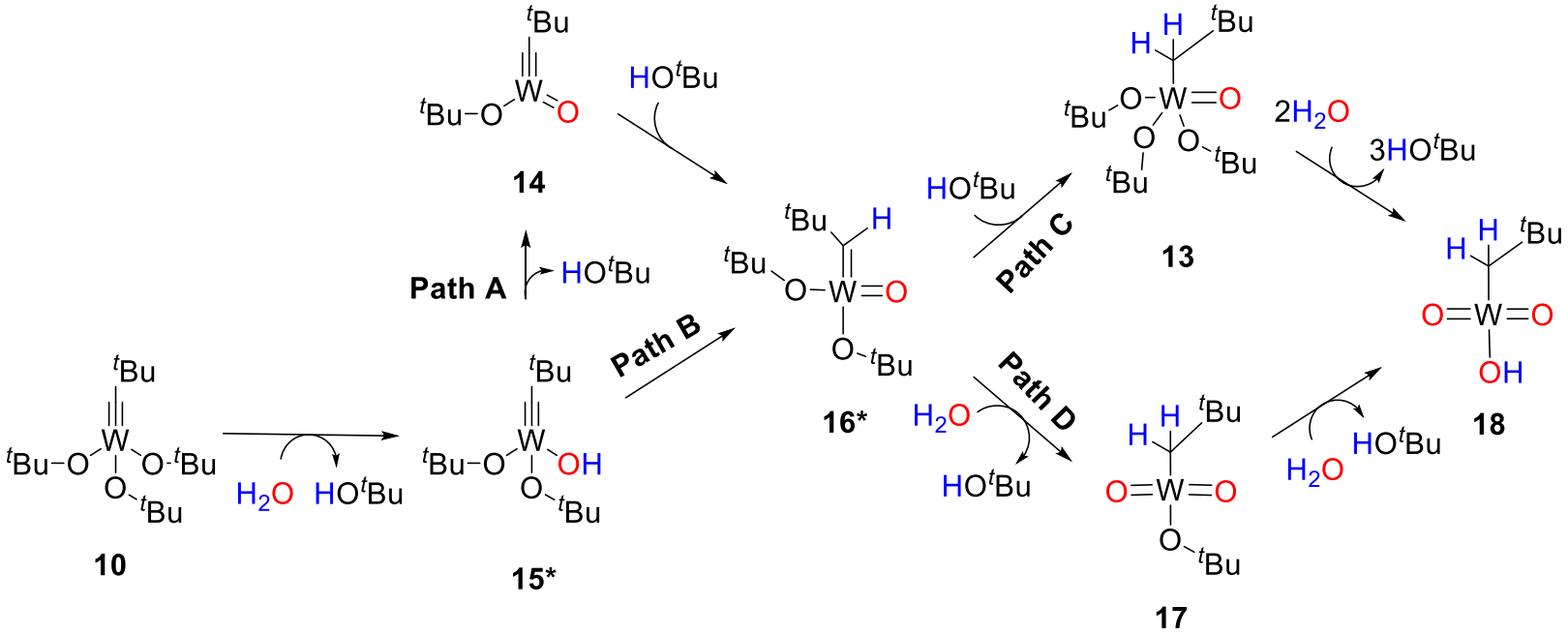

Scheme 4.6. Proposed pathways for the hydrolysis of **10** at 200 °C in air. Compounds with the same *m*/*z* are denoted by *.

reaction, one H^+ ion in H_2O adds to the alkylidene C atom and the other H^+ ion eliminates an -O^{t}Bu ligand to form the dioxo complex **17**. Lastly, one more H_2O molecule reacts with **17**, eliminating the last -O^{t}Bu ligand and forming the hydroxyl complex **18**. Though the pathways are proposed in Scheme 4.6, we cannot exclude the likelihood that other pathways may operate here. DFT calculations may be done in order to better model the reactions.

4.3. Concluding Remarks

The reaction of W(≡CSiMe$_3$)(Me$_3$SiCH$_2$)$_3$ (**11**) with water at room temperature was found to give the trimer $W_3O_3(\mu{=}O)_3(CH_2SiMe_3)_6(THF)_3$ (**12**) with the elimination of two ligands in **11**. The NMR-scale reaction of W(≡C^{t}Bu)(O^{t}Bu)$_3$ (**10**) with H_2O gives HO^{t}Bu and W(CH$_2$^{t}Bu$_3$)(O^{t}Bu)$_3$(=O) (**13**). In the reaction of water in air with **10** at 200 °C via the DART-MS process, several other W-containing species have been identified.

4.4. Experimental Section

All manipulations were performed under a dry nitrogen atmosphere with the use of either a dry box or standard Schlenk techniques. W(≡C^{t}Bu)(O^{t}Bu)$_3$ (**10**) was prepared via the literature procedure.[9] W(≡CSiMe$_3$)(CH$_2$SiMe$_3$)$_3$ (**11**) was synthesized using a procedure similar to that for the preparation of W(≡C^{t}Bu)(CH$_2$^{t}Bu)$_3$ using $WCl_3(OMe)_3$ and ClMgCH$_2$SiMe$_3$.[10] THF and hexanes were purified by distillation from potassium/benzophenone ketyl and stored under N_2. *t*-Butyl alcohol was dried over CaH_2 and distilled. Benzene-d_6 was dried over activated molecular sieves and stored under N_2. Deionized H_2O was put in a conical solvent storage flask, degassed via three

freeze/pump/thaw cycles, and stored under N_2. NMR spectra were recorded on a Bruker AC-250, Bruker Avance 400 MHz, or Varian VNMRS-500 spectrometer. Elemental analyses were conducted by Complete Analysis Laboratories, Inc., Parsippany, NJ. Mass spectra were recorded on a JEOL AccuTOF™ DART Mass Spectrometer.

4.4.1. Preparation of [(μ-O)W(CH$_2$SiMe$_3$)$_2$(=O)(THF)]$_3$ (12) via the Reaction of W(≡CSiMe$_3$)(CH$_2$SiMe$_3$)$_3$ (11) with H$_2$O at Room Temperature

W(≡CSiMe$_3$)(CH$_2$SiMe$_3$)$_3$ (**11**, 508.5 mg, 0.958 mmol) was dissolved in 10 mL of THF at 23 °C. Two equiv of H_2O (34.5 uL) were added to the solution via a syringe. The orange solution turned light brown after the addition. The mixture was stirred overnight at room temperature. After the volatiles were then removed in vacuo, the remaining solid was then dissolved in 1 mL of hexanes. The reaction flask was placed at -32 °C which afforded yielded white crystals of [(μ-O)W(CH$_2$SiMe$_3$)$_2$(=O)(THF)]$_3$ (**12**, 113.5 mg, 0.0818 mmol, 25.6% yield). ^{1}H NMR (benzene-d_6, 250.1 MHz): δ 3.57 (t, 2H, THF), 1.85 (broad s, 2H, C*H*$_2$SiMe$_3$), 1.40 (m, 2H, THF), 0.35 (s, 9H, CH$_2$Si*Me*$_3$); ^{13}C{^{1}H} NMR (benzene-d_6, 62.9 MHz): δ 70.0 (*C*H$_2$SiMe$_3$), 68.0 (THF), 25.8 (THF), 1.73 (CH$_2$Si*Me*$_3$).

4.4.2. Reaction of W(≡C^{t}Bu)(O^{t}Bu)$_3$ (10) with H$_2$O in Benzene-d$_6$

W(≡C^{t}Bu)(O^{t}Bu)$_3$ (**10**, 57.7 mg, 0.122 mmol) was added to benzene-d_6 in a J. R. Youngs NMR tube. The NMR tube was cooled to 2 °C and a conical storage solvent flask containing the H_2O/THF solution were cooled to 0 °C. The H_2O/THF solution was added (32 μL of H_2O /THF, 0.266 mmol of H_2O) via syringe. The amber solution turned a dark brown. The reaction was monitored via NMR spectroscopy. After ca 12 h, the

formation of W($CH_2{}^tBu$)(O^tBu)$_3$(=O) (**13**) was completed. Of the W-containing species that were observed in MS, only **13** was observed via NMR spectroscopy. The solution was characterized by NMR. When volatiles and benzene-d_6 were removed, **13** began to decompose. Repeated attempts were made to isolate and purify **13**. In each case only decomposition of **13** was observed. ^{1}H NMR (benzene-d_6, 400.00 MHz): δ 2.32 (s, 2H, CH_2CMe$_3$), 1.39 (s, 27 H, OCMe_3), 1.31 (m, 9H, CH_2CMe_3); ^{13}C{^{1}H} NMR (benzene-d_6, 100.58 MHz) δ 80.99 (OCMe$_3$), 66.292 (CH$_2$CMe$_3$), 34.98 (CH_2CMe_3), 32.80 (CH_2CMe$_3$), 30.80 (OCMe_3). The CH$_2$ assignment was confirmed via a DEPT-135 NMR spectroscopy (Figure A14).

4.4.3. DART-TOF MS Analysis of the Reactions between W(≡C^{t}Bu)(O ^{t}Bu)$_3$ (10) and Water in Air

Mass spectra were recorded on a JEOL AccuTOF™ DART Mass Spectrometer. The closed end of a capillary tube was inserted into the crystalline powders of **10**. Once a few crystals were gathered, the tube was placed into a heated stream of He (200 °C) in the spectrometer. The spectra were referenced to a polyethylene glycol (PEG) standard.

References

1. Feinstein-Jaffe, I.; Gibson, D.; Lippard, S. J.; Schrock, R. R.; Spool, A. *J. Am. Chem. Soc*. **1984**, *106*: 6305.
2. (a) Feinstein-Jaffe, I.; Pedersen, S. J.; Schrock, R. R. *J. Am. Chem. Soc*. **1983**, *105*, 7176. (b) Feinstein-Jaffe, I.; Dewan, J. C.; Schrock, R. R. *Organometallics* **1985**, *4*, 1189.
3. Levy, O.; Musa, S.; Bino, A. *Dalton Trans.* **2013**, *42*, 12248.
4. Dougan, B. A. and Xue, Z.-L. *Sci. China Chem*. **2011**, *54*, 1903.
5. Morton, L. A., Ph. D. dissertation, The University of Tennessee, Knoxville, 2005.
6. Morton, L. A.; Miao, M.; Callaway, T. M.; Chen, T. Chen, S.-J.; Tuinman, A. A.; Yu, X.; Lu, Z.; Xue, Z.-L. *Chem. Comm.* **2013**, *49*, 9555.
7. Grekov, D.; Bouhoute, Y.; Szeto, K. C.; Merle, N.; De Mallmann, A.; Lefebvre, F.; Lucas, C.; Del Rosal, I.; Maron, L.; Gauvin, R. M.; Delevoye, L.; Taoufik, M. *Organometallics* **2016**, *35*, 2188.
8. Miller, J. B.; Bernasek, S. L; Schwartz, J. *J. Am. Chem. Soc.* **1995**, *117*, 4037.
9. Mark L. Listemann, M. L.; Schrock. R. R. *Organometallics* **1985**, *4*, 74.
10. Schrock, R. R.; Sancho, J.; Pederson, S. F. *Inorg. Synth.* **1989**, *26*, 45.

Part 5

Trends in NMR Chemical Shifts of d^0 Transition Metal Compounds

Tables for this part listing NMR chemical shifts are placed in Appendix C.

Abstract

NMR chemical shifts of d^0 transition metal compounds show the following trends: (1) For single-bonded ligands such as M-H, M-CR_3 and M-SiR_3, ^{1}H, ^{13}C and ^{29}Si shifts of the α atoms in the complexes of both first- and third-row transition metals are typically *downfield shifted* from those of the second-row analogs with a “V-shape” (Trend 1). (2) For multiple-bonded ligands including those with d-p π bonds, such as M=CHR, M≡CR, M=O and M–F, ^{13}C, ^{17}O and ^{19}F NMR chemical shifts of the α atoms in the complexes of d^0 third-row transition metals are typically *upfield shifted* from those of the second-row analogs (Trend 2). NMR shifts of lanthanum(III) complexes help interpret Trend 1 in Group 3 congeners. Scandide (d-block) and lanthanide (f-block) contractions and relativistic effects are believed to contribute to the NMR shifts, leading to the observed trends. Comparisons are made with NMR of d^n complexes and organic compounds.

5.1. Introduction

5.1.1. Interpretation of NMR Shifts

Interpretation and calculations of NMR chemical shifts have been active areas of research and these studies have been reviewed.[1-5] A summary of the earlier studies for general readers is presented. The readers are encouraged to consult the original publications to get a better and more comprehensive understanding.

For the nucleus of the atom *N* in a molecule placed inside in a magnetic field, its electronic shielding is usually described by Eq. 5.1.[6]

$$\sigma = \sigma^{d} + \sigma^{p} + \sigma^{SOC} \qquad \text{(Eq. 5.1)}$$

where σ^{d}, σ^{p} and σ^{SOC} are the diamagnetic, paramagnetic and spin-orbital coupling terms, respectively.

The first two terms in Eq. 5.1, σ^{d} and σ^{p}, are what Ramsey developed to evaluate the field created by the electrons in the molecule inside the magnetic field.[6-8] The diamagnetic σ^{d} term describes the screening of paired electrons in the electronic ground state in the molecule. The external magnetic field causes the electrons to precess about the axis of the field, generating a spherical current and thus its own small magnetic field. The small magnetic field opposes the external magnetic field, leading to the shielding of the nucleus of the atom X.[9]

The paramagnetic term σ^p reflects the screening as a result of the mixing of the electronic ground state with excited states under the magnetic field, leading to non-spherical, local electron circulations, with induced current densities $\boldsymbol{J}^p$. If the X-Z bonding orbital $\sigma_{X\text{-}Z}$ is involved in the mixing, the induced current densities $\boldsymbol{J}^p$ are primarily around the nuclei X and Z. The paramagnetic term σ^p is so named as it could also be understood qualitatively in terms of the formation of two unpaired electrons as a result of the mixing between the filled MOs and empty excited states. The orbitals involved in the mixing are mainly frontier MOs, such as the highest occupied MOs (HOMOs) and lowest unoccupied MOs (LUMOs), and other near-frontier orbitals. The unpaired electrons precess about the axis of the external magnetic field, generating the non-spherical, local electron circulations and their own small magnetic fields. The precession is essentially through the motion of the unpaired electrons in their respective orbitals (orbital angular momenta). As discussed below, the nature of the frontier and near-frontier MOs and thus the atoms on which the unpaired electrons reside are critical to the impact of σ^p. The paramagnetic contribution is typically much larger than the diamagnetic effect, and, other than ^{1}H, it is the main source for variation in chemical shifts in nuclei.[9] This is discussed below.

The induced current density $\boldsymbol{J}^p$ on the atom X makes another contribution to the shielding of the nucleus *N*, whether or not the orbitals of the N-X bond are involved in the mixing. The effect, described by the term σ^{SOC}, is spin-orbital coupling (SOC). SOC here is primarily the effect of the unpaired electron, centered on X (induced current density or the sum of the small magnetic fields by the orbital motion and spin of the

electron), on the nucleus of the neighboring atom N (Figure 5.1). Since the term σ^{SOC} includes the effects of the unpaired electron spins, it has been described in analogy to nuclear spin-spin coupling (with coupling constant *J*) in, e.g., ^{1}H-^{19}F.[2,10-12] As in the nuclear spin-spin coupling, the effect of σ^{SOC} depends on the Fermi-contact interaction and the s electron density on the atom N in Figure 5.1, as only s orbitals have non-zero values at the site of the nucleus. Studies thus far have shown that the SOC effect on NMR shielding typically becomes important when a heavy element such as iodine or a post-lanthanide element such as Hg, Pt or Au is present in the compounds. This is a result of relativistic effects of the heavy element.[2,5,10-14]

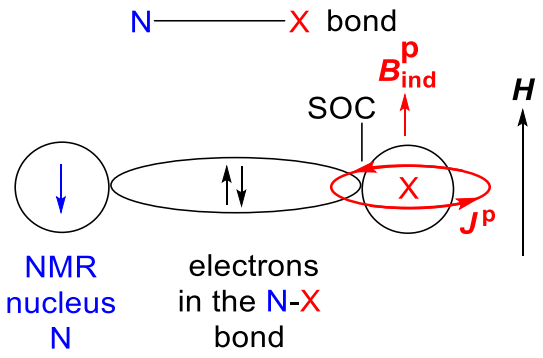

Figure 5.1. Schematic representation of the spin-orbital coupling (SOC) effect by the induced current density $\boldsymbol{J}^{p}$ on the atom X on the nucleus spin of the atom *N*. The arrows represent magnetic dipole moments of the nucleus on the atom *N* and electrons.[11]

In an atom of a heavy element such as I and Au, the velocities of its electrons are close to the speed of light if they approach the nucleus.[15-17] Einstein's theory of relativity

indicates that the negative electrons at such high velocities have higher masses, increasing their electromagnetic attraction with the positive nucleus and leading to the contraction of the inner atomic orbitals in comparison to non-relativistic analogs. The relativistic effects on NMR shielding are in general two-fold: (1) Change of the atomic structure - Including the relativistic effect which gives more accurate diamagnetic σ^d and paramagnetic σ^p terms; (2) SOC, giving additional shielding of the neighboring nuclei, as shown in Figure 5.1. For lighter atoms, the relativistic effects are small and may be ignored in the consideration of the NMR shielding. Relativistic effects contribute to ca. 10% of the lanthanide contraction, which is discussed below.[18]

The mixing of ground and excited states is through the orbital angular moment operators. Since the 1s orbital is spherical, the orbital angular momentum of an unpaired electron in the s orbital is zero. More precisely, there is no mixing between an s orbital and another orbital.[19] For a C-H bond, both the σ_{CH} and σ^*_{CH} are formed using the 1s orbital of the H atom. Thus, the σ_{CH} bond must mix with empty orbitals at higher energies such as 2p orbitals of the H atom (as the 2s orbital does not mix well either). However, these empty orbitals are very high in energy, leading to little mixing with the ground state.

Thus, the paramagnetic contributions to chemical shifts in ^{1}H NMR are typically not significant.[19] The diamagnetic term σ^d, describing the screening of paired electrons in the electronic ground state around the H atom, is the principal contribution in ^{1}H NMR shifts. A consequence of little σ^p contributions in ^{1}H NMR spectra is that the range of typical ^{1}H chemical shifts (0-10 ppm) is smaller than the ranges in, e.g., ^{13}C and ^{17}O

NMR spectra. In other words, the induced, non-spherical, local electron circulations around the H atoms in a molecule are very small.

5.1.2. Early Studies of NMR Chemical Shifts in Transition Metal Compounds

For NMR chemical shifts in transition metal compounds, Buckingham and Stephens developed a theory in 1964 to explain upfield hydride (negative in reference to $SiMe_4$) shifts of O_h, d^n complexes such as $HCo(CN)_5$.[20] They indicated that the distortion of the partly-filled d orbitals by the magnetic field is the main contributor to the chemical shift and noted the difficulties in comparing the theory with experimental data. Braterman and coworkers reported in 1973 their studies of ^{13}C NMR shifts of the CO ligands in d^6 Mo and W carbonyls $M(CO)_6$ and their phosphine and phosphite derivatives $M(CO)_{6-n}(PR_3)_n$ (n = 1, 2), noting downfield shifts with increases in π-back bonding to the CO ligands.[21] Kreiter and Formacek in 1972[22] and Bodner and coworkers in 1973[23] noted large downfield ^{13}C shifts of the carbene C atoms in d^n Fischer carbene complexes such as $(OC)_5M(=CMeX)$ (M = Cr, W; X = OMe, NH_2). Bodner found that decreasing π-donor ability of the substituent leads to an additional downfield shift.[23] Evans and Norton in 1974 summarized calculations of NMR shifts of carbon atoms bound to transition metals.[8] Citing conclusions of Lauterbur and King in their 1965 work,[24] Evans and Norton indicated that there was no convincing explanation of NMR chemical shifts using the appropriate shielding theory at the time.[8] Buchner and Schenk in 1982 published their calculations of ^{13}C NMR shifts of the CO ligands.[25] The theoretical studies and calculations of NMR parameters from 1953, when Ramsey introduced his theories, to the early 1980s were reviewed by Pyykkö.[1,6]

Ziegler and coworkers pioneered the calculations of NMR chemical shifts based on gauge-including atomic orbitals (GIAOs) and density functional theory (DFT).[26,27] They reported in 1996 the use of the approaches on d^n metal hydrides such as $HM(CO)_5$ (M = Mn, Tc, Re), $H_2Fe(CO)_4$, and $HCo(CO)_4$,[28] and found a good agreement between the calculated and experimental ^1H chemical shifts. Contributions to the ^1H chemical shifts in the d^n metal hydrides have been analyzed in detail. The σ^p term in Eq. 5.1 is written as the sum of the two paramagnetic contributions according to Eq. 5.2 (without the inclusion of σ^{SOC})

$$\sigma = \sigma^d + \sigma^p = \sigma^d + (1/3\ \sigma_{\parallel}^p + 2/3\ \sigma_{\perp}^p) \qquad \text{(Eq. 5.2)}$$

where $\sigma_{\parallel}^p$ and $\sigma_{\perp}^p$ refer to the paramagnetic shielding terms when the external magnetic field $\boldsymbol{B_0}$ is parallel and perpendicular, respectively, to the M-H bond in the molecules (Figure 5.2).

The analyses by Ziegler and coworkers show that the major contribution to the upfield shifts of the d^n metal hydrides is mainly $\sigma_{\perp}^p$ which is a result of coupling of the occupied π orbitals (HOMO, filled d orbitals that back-donate electrons to CO) and the empty (virtual) σ^* antibonding orbital (between the metal d orbitals and CO). In other words, the presence of the d electrons on the metal atoms, through the mixing of their orbitals with an empty MO, generates the induced current density shown in Figure 5.2 ($\perp$ orientation) that shields the hydride ligands.

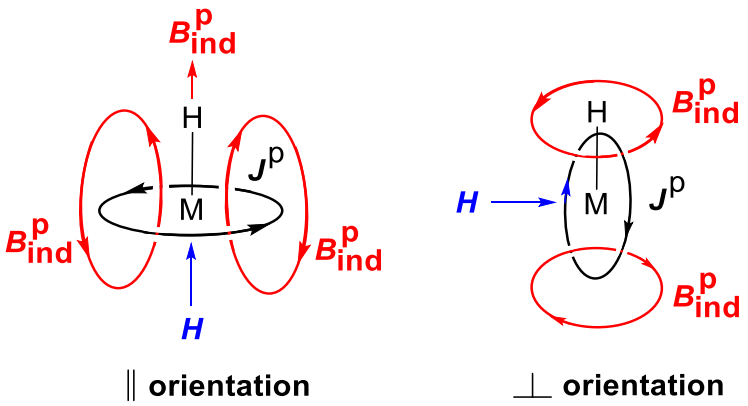

Figure 5.2. Schematic representations of the external magnetic field ***H***, induced current $\boldsymbol{J^p}$, induced magnetic fields $\boldsymbol{B^P_{ind}}$, and the positions of the hydride atom in the || and $\perp$ orientations.[28]

In contrast, the paramagnetic $\sigma_{\parallel}^{p}$ term reduces the shielding on the hydride atom (Figure 5.2, || orientation), but its contribution, in comparison to that of $\sigma_{\perp}^{p}$, is smaller in the d^n metal hydrides. In addition, the calculations show that the diamagnetic terms σ^d vary little among the metal hydrides and, when referenced to the σ^d for $SiMe_4$, contribute to downfield shifts. The studies of Ziegler and coworkers support the Buckingham-Stephens model in their 1964 paper[20] that the paramagnetic contributions from the adjacent metal atoms lead to the upfield chemical shifts of the d^n metal hydrides.

Ziegler and coworkers also reported in 1996 the calculations of ^{13}C chemical shifts in metal carbonyl complexes such as d^6 $M(CO)_6$ (M = Cr, Mo, W) using the GIAO-DFT approach.[29,30] Their studies show that the back-bonding from the occupied π_{MC}

orbitals (HOMOs) to the antibonding π^*_{CO} orbitals on the CO ligands reduces electron density on the metal atoms, leading to downfield shifts. In addition, σ_{CO} bonds (between the CO ligands and M) increases the electron density on the metal center, leading to the shielding of the C atoms in $M(CO)_6$ through the coupling between the σ_{MC} orbitals and the π^*_{CO} orbitals. Relativistic effects in $W(CO)_6$ lead to the stabilization of its $\sigma_{M\text{-}C}$ orbitals, thus reducing the σ_{MC}-π^*_{CO} coupling. Kaupp, Malkin, Malkina and Salahub reported in 1996 a method based on DFT and the quasirelativistic effective-core potentials (ECP-DFT) and used the method to calculate ^{13}C chemical shifts of d^6 $M(CO)_6$ (M = Cr, Mo, W).[31] The calculated chemical shift tensors match those from solid-state NMR experiments obtained by Oldfield et al.,[32] and the studies show that the paramagnetic contributions to the chemical shifts are a result of the coupling between the filled MO orbitals, such as σ_{MC}, π_{CO} and the occupied d_π orbitals, and the essentially empty π^*_{CO} orbitals. The shielding increase from $Cr(CO)_6$ to $W(CO)_6$ is attributed to the increase energy gap between filled bonding and empty antibonding orbitals, especially between $1e_g$ and $2e_g^*$ orbitals of M-C σ bonds, thus reducing the paramagnetic contributions. Relativistic effects are found important for the difference between $Mo(CO)_6$ and $W(CO)_6$.

Kaupp, Malkin, Malkina and Salahub also reported in 1995 the use of the ECP-DFT method to study relativistic effects on ^{17}O NMR chemical shifts of d^0 transition-metal oxides such as MO_4^{2-} (M = Cr, Mo, W), MO_4^- (M = Mn, Tc, Re) and MO_4 (M = Ru, Os).[31] The calculated and experimental data match well. Relativistic effects increase the

HOMO-LUMO gaps and an increase of the negative charge on the O atoms, perhaps leading to the upfield change of the experimental chemical shifts down a group.

Jolibois and coworkers reported in 2008 DFT calculations of ^{1}H and ^{13}C NMR chemical shifts in d^n transition metal hydrides, including $Ru(L)(H)(dppm)_2$ [L = H, Cl; dppm = 1,2-bis(diphenylphosphino)methane], $[Ru(H)(H_2O)(dppm)_2]^+$, $Ru(H)_2(dppm)(PPh_3)$, $[Fe(H(H_2)(dmpe)_2]^+$ [dmpe = 1,2-bis(dimethylphosphino)ethane] and $[H_3Ru(\eta^6\text{-benzene})_4(CO)]^+$.[33] More recently Hrobárik, Hrobáriková, Repiský, Kaupp and coworkers have used state-of-the-art relativistic four-component DFT-GIAO-based calculations of ^{1}H chemical shifts in several classes of d^n metal hydrides and demonstrated significant spin-orbital coupling (SOC)-induced heavy atom effects on the hydride shifts, especially for the second- and third-row transition metal complexes, on top of paramagnetic contributions from the Buckingham-Stephens model.[34] These calculations gave a much better fit between the experimental and calculated chemical shifts. The calculations reproduced the experimental observations that, in partially filled d^n metal hydrides, such as $HM(CO)(PH_3)_3$ (M = Co, Rh, Ir) and $HMCl(PH_3)_2$ (M = Ni, Pd, Pt), chemical shifts of 4d complexes are typically downfield shifted from those of 3d and 5d congeners (so-called "Λ-shape behavior"). Furthermore, the calculations of chemical shifts in d^{10} hydrides HMPh (M = Zn, Cd, Hg) fit well the experimental data, showing that the shifts are downfield from that of $SiMe_4$. They attributed the downfield shift to the occupied σ orbitals that dominate the deshielding SOC contributions to the hydride shifts in the d^{10} hydrides HMPh (M = Zn, Cd, Hg).[34] Greif, Hrobárik, Autschbach, Kaupp and coworkers recently conducted a relativistic quantum-chemical analysis of the influence of *trans* ligands X in $HPtX(PMe_3)_2$ ($X = BH_2$, CH_3, CN, Cl, NO_2, NO_3) on

hydride shifts.[14] Bagno and Saielli also reported a relativistic DFT study of the NMR properties of Rh and Ir methane and methyl hydride complexes and found that relativistic effects are mostly responsible for the large shielding of the ^{1}H and ^{13}C resonances of the methane moiety.[35]

Halbert, Copéret, Raynaud and Eisenstein have recently used computational models $Et_2Ta(=CHMe)[OSi(OH)_3]$, $Et(PhN=)M(=CHMe)[OSi(OH)_3]$ (M = Mo, W), (pyrrolyl)(PhN=)Mo(=CHMe)[$OSi(OH)_3$], and $EtRe(=CHMe)(\equiv CMe)[OSi(OH)_3]$ for surface-grafted d^0 alkylidene complexes ($(^tBuCH_2)_2Ta(=CH^tBu)$(O-silica), ($(^tBuCH_2)(ArN=)M(=CH^tBu)$(O-silica) (M = Mo, W; Ar = 2,6-^{i}Pr$_2$-C_6H_3), (pyrrolyl)(ArN=)Mo(=CH^{t}Bu)(O-silica), and (^{t}BuCH$_2$)Re(=CH^{t}Bu)(≡C^{t}Bu)(O-silica), respectively, to study the downfield shifts and anisotropy of carbene C atoms obtained from solid-state NMR spectroscopy.[36] Their studies show that, for the M=C bonds, the gaps between filled bonding orbitals, σ_{MC} and π_{MC}, and empty antibonding orbitals, π^*_{MC} and σ^*_{MC}, respectively, are small, leading to the larger paramagnetic coupling between the bonding and antibonding orbitals and larger deshielding of the C atoms. For Mo complexes, the energies of the empty 4d orbitals are lower than those of the 5d orbitals in W complexes. As a result, the energy gap between the σ_{MC} and π^*_{MC} orbitals is smaller in the Mo complexes, making Mo=^{13}C further downfield shifted than W=^{13}C.

It should be pointed out that relativistic effects on, e.g., ^{1}H NMR chemical shifts in HX (X = F, Cl, Br, I) [37-39] and RHgH (R = Me, Et, CH_2=CH, Ph, C_6F_5)[40] as well as ^{13}C shifts in CH_3X and third-row metal hexacarbonyls and XHgMe (X = CN, Cl, CH_3, H, SiH_3),[40-42] have been studied, demonstrating the impact of the spin-orbital coupling

(SOC) in heavy atoms on the shielding of neighboring light nuclei (Heavy-Atom effect on the Light-Atom shielding or HALA). Studies in the areas have been reviewed by, e.g., Kaupp,[2,3] Autschbach,[4,5] and Ziegler.[5]

We have surveyed the published NMR chemical shifts of d^0 transition metal complexes with single and double M-ligand bonds and found that the chemical shifts follow two trends. Our studies are reported.

5.2. Results and Discussion

We have found that NMR chemical shifts of d^0 transition metal complexes show the following two trends:

(1) For single-bonded ligands such as M-H, M-CR_3 and M-SiR_3, ^{1}H, ^{13}C and ^{29}Si shifts of the α atoms in the complexes of both first- and third-row transition metals are typically *downfield shifted* from those of the second-row analogs with a “V-shape” (Trend 1). Examples of chemical shifts following Trend 1 are given in Figure 5.3.

(2) For multiple-bonded ligands including those with d-p π bonds, such as M=CHR, M≡CR, M=O and M–F, ^{13}C, ^{17}O and ^{19}F shifts of the α atoms in the complexes of d^0 third-row transition metals are typically *upfield shifted* from those of the second-row analogs (Trend 2).

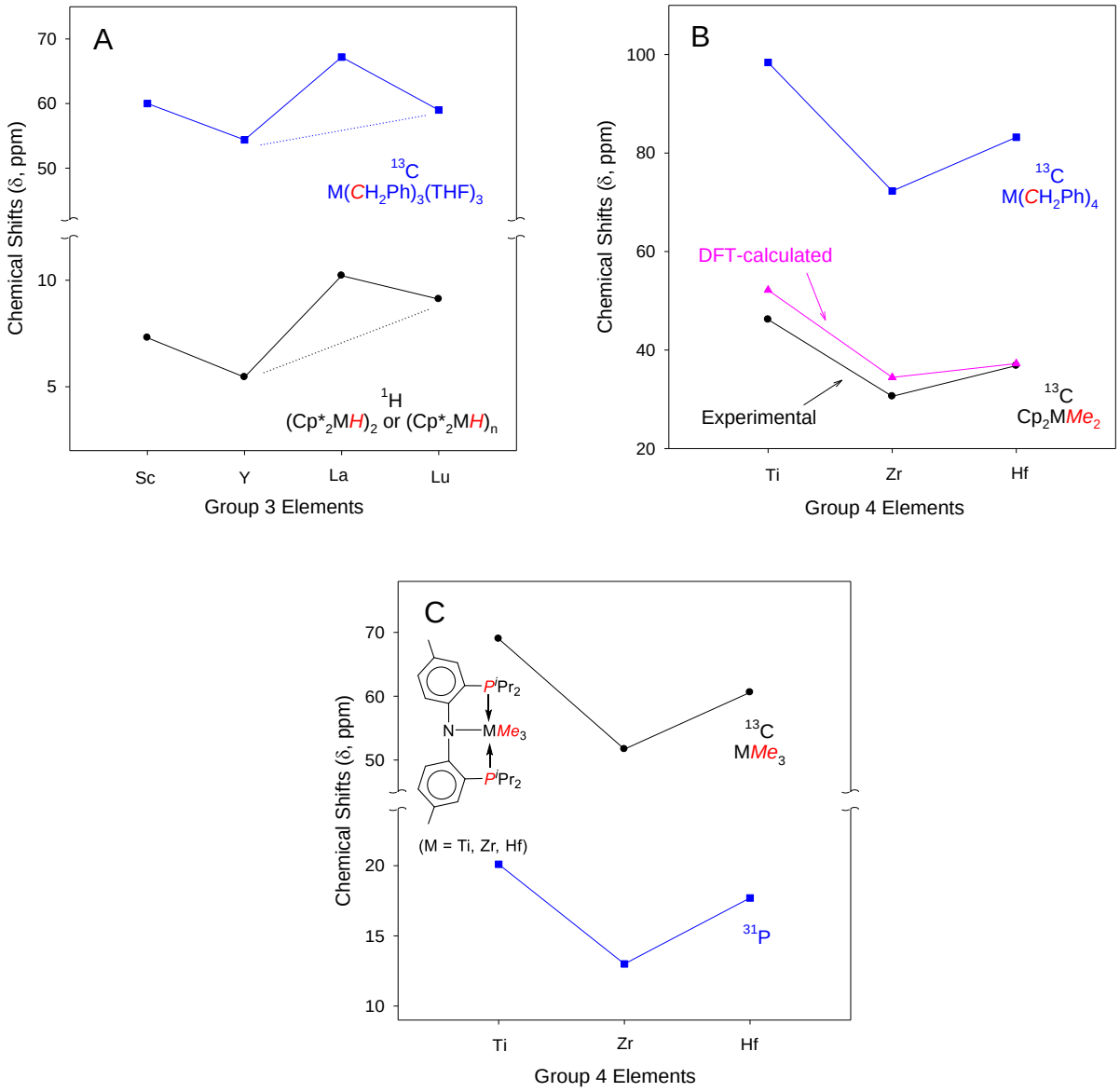

Figure 5.3. Examples of chemical shifts following Trend 1: (A) ^{1}H and ^{13}C shifts of Group 3 hydrides and alkyls. The dotted lines represent the "V shape" when the shifts of La complexes are not included. It is interesting to note that the "V-shape" for the d^0 transition metal triads here is opposite of the "Λ-shape" for d^n complexes.[34] (B) ^{13}C shifts of Group 4 alkyls, including DFT-calculated shifts (Table C14). (C) ^{13}C and ^{31}P shifts of Group 4 complexes.

Reported chemical shifts following Trends 1 and 2 are listed in Tables C1-C7 and C10-C13, respectively. There are a small number of exceptions to these trends indicated in blue color in the tables. ^{31}P shifts of phosphine ligands in Groups 3-4 complexes mostly follow Trend 1 (Table C8), while those in Groups 5-6 complexes (Table C9) do not. Reported chemical shifts following Trends 1 and 2 are listed in Tables C1-C7 and C10-C13, respectively. There are a small number of exceptions to these trends indicated in blue color in the tables. ^{31}P shifts of phosphine ligands in Groups 3-4 complexes mostly follow Trend 1 (Table C8), while those in Groups 5-6 complexes (Table C9) do not. Relatively few congeners of first-row transition metals, nearly all of which are Sc^{III} and Ti^{IV} hydrides and alkyls, have been reported. d^n complexes, such as Fischer carbenes, usually do not follow the trends.

It should be pointed out that the ^{17}O NMR of metal oxides (Table C11) and surface-grafted alkylidenes have been studied by Kaupp[31] and Figgis[43] and by Halbert[36] and coworkers, respectively. The current work provides comprehensive lists of the shifts. The earlier theoretical studies are discussed in the context of other d^0 complexes.

These complexes have different ligands, structures and chemical shifts. Each set of congeners is unique and perhaps deserves detailed studies. However, the large collection here has allowed us to analyze the trends at a qualitative level and find common, principal features leading to the trends. While the primary purpose of this part is to point out the trends, attempts are made below to provide a qualitative understanding of the trends.

5.2.1. NMR Chemical Shifts of Hydride Ligands in d^0 Transition Metal Complexes

^{1}H chemical shifts of Sc-Y-La-Lu, Ti-Zr-Hf, Nb-Ta, Mo-W compounds in Tables C1-C2 show that 4d complexes are the most shielded. Lanthanum is in a unique position in the periodic table with no counterpart in other groups.[44] Among shifts of Sc^{III}-Y^{III}-La^{III}-Lu^{III} hydrides in Table C1 and alkyls in Table C3, La^{III} analogs are usually the most downfield (or least shielded), while the Y^{III} analogs are the most upfield (or most shielded). Four questions about the shifts and our thoughts are given below:

(1) *Why are resonances of the d^0 hydrides downfield from H atoms of the C-H bonds in, e.g., $SiMe_4$?*

The mixing of ground and excited states is through the orbital angular moment operators. Since the 1s orbital of an H atom is spherical, the orbital angular momentum of an unpaired electron in the s orbital is zero. More precisely, there is no mixing between an s orbital and another orbital.[19] For a C-H bond, both σ_{CH} and σ^*_{CH} are formed using the 1s orbital of the H atom. Thus the σ_{CH} bond must mix with empty orbitals at higher energies such as 2p orbitals of the H atom (as the 2s orbital does not mix well either). However, these empty orbitals are very high in energies, leading to little mixing with the ground state. Thus, the paramagnetic contributions to ^{1}H resonances of the organic compounds are typically not significant.[19] The diamagnetic term σ^d, describing the screening of paired electrons in the electronic ground state around the H atom, is the principal contribution in ^{1}H NMR. Thus, the range of typical ^{1}H shifts (0-10 ppm) is smaller than those in, e.g., ^{13}C and ^{17}O NMR spectra. In other words, the

induced, non-spherical, local electron circulations around the H atoms in organic molecules are very small.

For an M-H bond in a d^0 complex, the HOMO is typically σ_{MH} between the H 1s orbital and a d orbital.[45,46] Other empty d orbitals are not far above σ_{MH}. These d orbitals can mix with HOMO, leading to *larger* paramagnetic contributions around the M and H atoms, making the M-*H* resonances downfield from those of C-*H*. The shifts of some complexes, such as $Cp^*_2HfH_2$, are >10 ppm from that of $SiMe_4$.

(2) *Why are resonances of d^0 and d^n hydrides down- and upfield, respectively, from that of $SiMe_4$?*

In d^n hydrides, the mixing primarily involves the filled d-p π orbitals, not σ_{MH} (Figure 5.4). As a result, the induced current densities centered on the M and C atoms (of the CO ligands), contributing to the downfield shift of the CO ligands in ^{13}C NMR. σ_{MH} is affected by the induced current densities centered on the M and C atoms, as explained by Ziegler and coworkers[28] (Figures 5.2 and 5.4), giving the upfield shifts to the negative ppm region. In contrast, d^0 complexes do not have valence d electrons. Empty d orbitals likely mix with σ_{MH}, as discussed above, leading to the downfield shifts of the hydrides.

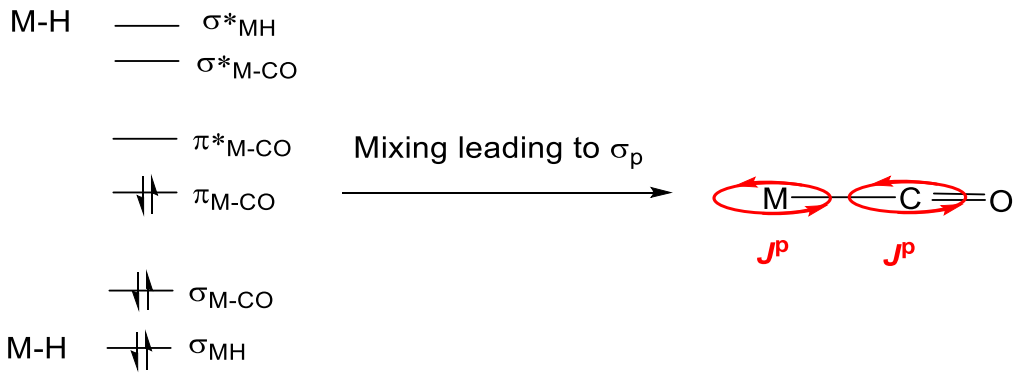

Figure 5.4. Frontier orbitals in d^n hydride carbonyl complexes and schematic representation of the mixing, leading to the induced current densities $\boldsymbol{J}^{\mathbf{p}}$ centered on the M and C atom of the CO ligands.[28] See Figure 5.2 for additional explanation.

(3) *Why are La^{III} hydrides the least shielded among Group 3 tetrads? Why are the hydrides in Sc and Lu complexes less shielded than the Y congeners?*

In $[Cp^*_2M(\mu\text{-}H)]_2$ (M = Y, La, Lu) and $(Cp^*_2ScH)_n$[47] (Figure 5.3A), La-H (10.21 ppm) and Y-H (5.45 ppm) are the most downfield and upfield, respectively, with Sc-H at 7.3 and Lu-H at 9.27/9.11 ppm. The electronic configurations of these d^0 cations are:

(a) Sc^{III}, [Ar] (or $1s^22s^22p^63s^23p^6$)

(b) Y^{III}, [Kr] (or $[Ar]3d^{10}4s^24p^6$)

(c) La^{III}, $[Kr]4d^{10}5s^25p^6$

(d) Lu^{III}, $[Kr]4d^{10}5s^25p^64f^{14}$

with the following features: (i) There is no d electron in Sc^{III}. (ii) Y^{III} is the first transition metal ion after 3d orbitals are filled. (iii) La^{III} is the first transition metal ion after 4d orbitals, the second d set, are filled. In other words, a difference between Y^{III} and La^{III} is that La^{III} uses the 5d vs 4d orbitals for Y^{III}. (iv) Lu^{III} is the first metal ion after 4f orbitals are filled. Both La^{III} and Lu^{III} use the 5d set as valance orbitals.

Scandide and lanthanide contractions have been used to describe anomalous properties of post-scandide (Ga-Br) and post-lanthanide elements (third-row transition metals, Tl, Pb and Bi).[17,34,48-51] As Huheeys indicated,[48] the effect of the contractions is the "most notable after the first filling of the new type of orbitals because the comparison is with a lighter congener that does not have these orbitals. All of the heavier congeners will have the same effect from similar subshells with higher principal quantum numbers and so the properties should once again vary smoothly (until a new type of orbital is filled)."[48]

Scandide and lanthanide contractions may explain the trend of the NMR shifts of Group 3 elements in Figure 5.3A. The decrease in shifts from the Sc^{III} to Y^{III} congeners is probably the result of scandide contraction when 3d orbitals are first filled at Y^{III}. Afterwards, when the 4d orbitals are filled in La^{III} congeners, the increase in shifts is perhaps a normal property. When 4f orbitals in Lu^{III} are then first filled, the NMR shifts make a turn to decrease. In other words, the "parallel" decreases in Figure 5.3A may be the results of scandide and lanthanide contractions.

Understanding of the trend using the σ^d, σ^p and σ^{SOC} terms requires theoretical studies and quantum calculations. The following are offered to start the discussion. σ^d is assumed to be similar among the hydrides. Larger SOC and relativistic effect in Y^{III} may

contribute to more shielding in Y-H than Sc-H. Relativistic effect makes valence d and f orbitals expanded and destabilized. This is known as the indirect relativistic orbital expansion[15] and discussed mostly for post-lanthanide elements.[15] If it operates for post-scandide elements, albeit at a smaller degree, the expanded 4d orbitals in Y^{III} may make energy gaps among 4d orbitals relatively large. σ_{YH} may have contributions from one of 4d orbitals, and other empty LUMO 4d orbitals in the Y^{III} ion are further apart, making mixing more difficult and generating smaller induced current densities than in its Sc-H analog. Sc^{III} ion does not have a significant relativistic effect. As a result, the energy gaps among its 3d orbitals are perhaps small, making mixings easier.

Why is the La-H shift downfield from both Y-H and Lu-H shifts? In the La^{III} ion, its 4d orbitals are filled. This is the second time d orbitals are filled. Thus, the empty, valence 5d orbitals do not experience significant indirect relativistic orbital expansion. In other words, its 5d orbitals return to “normal” sizes and energy gaps, although their energies are higher than either 3d or 4d orbitals. The 5d orbitals in La^{III} are perhaps closer in energy (with smaller energy gaps) than 4d orbitals in Y^{III} (Figure 5.5), increasing mixings in the La^{III}-H complex and generating larger induced current densities.

The upfield shift (with more shielding) of Lu-H from La-H is probably in part due to the combination of SOC and a larger relativistic effect in Lu^{III} than in La^{III}. Larger SOC in Lu^{III} leads to additional shielding of the neighboring ^{1}H nucleus (Figure 5.6).[2,3,5,11] The 5d orbitals in Lu^{III} are more expanded, as a result of the indirect relativistic effect after its 4f orbitals are filled. The expansion may lead to perhaps larger energy gaps among the 5d orbitals in Lu^{III} than in La^{III},[15,48] making mixings more difficult in Lu^{III} than in La^{III}. Both

SOC and the indirect relativistic effect lead to the upfield shift. However, this upfield shift of Lu-H from La-H is smaller than the downfield shift of the La-H from Y-H, thus making Lu-H to be downfield from Y-H, giving the “V-shape” for the shifts of Sc-Y-Lu hydrides (Figure 5.3A, dotted lines not counting La-H). The same factors may lead to Trend 1 for hydrides of the Ti-Zr-Hf triad (Figure 5.3B) and Zr-Hf, Nb-Ta and Mo-W pairs.

As noted earlier, the “V-shape” for the d^0 Sc-Y-Lu hydrides here (Figures 5.3) is opposite of the “Λ-shape” for d^n hydrides $HM(CO)(PH_3)_3$ (M = Co, Rh, Ir) and $HMCl(PH_3)_2$ (M = Ni, Pd, Pt), demonstrating that whether there are valence d electrons in the complexes play a critical role in their NMR properties.[34]

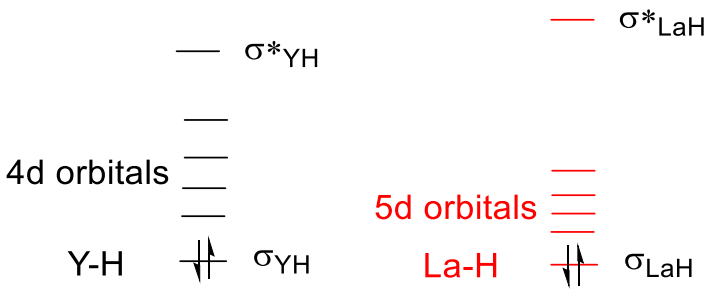

Figure 5.5. Schematic energy gaps between σ_{MH} and d orbitals and among the d orbitals in Y-H and La-H complexes.

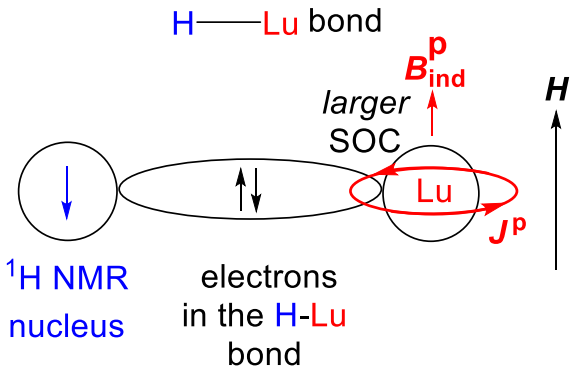

Figure 5.6. Schematic representation of SOC effect by the induced current densities $\boldsymbol{J}^{\mathbf{p}}$ on the Lu^{III} ion on the neighboring ^{1}H nucleus spin. The arrows represent magnetic dipole moments of the ^{1}H nucleus and electrons. The induced current densities on the H atom are not shown.[11]

5.2.2. NMR Chemical Shifts of Alkyl and Silyl Ligands in d^0 Transition Metal Complexes

A tetraad of Sc-Y-La-Lu alkyl complexes, $M(CH_2Ph)_3(THF)_3$, show a trend similar to that of the hydrides (Figure 5.3A). Perhaps similar factors discussed earlier contribute to the trend. The Ti-C, Zr-C and Hf-C shifts are typically in a "V-shape" (Figure 5.3B). For Groups 5 and 6 complexes, Ta-C and W-C bonds are in general downfield shifted from those of Nb-C (Table C5) and Mo-C bonds (Table C6). We could only find ^{13}C NMR for one pair of Tc and Re alkyl complexes, $MeM(=N\text{-}2,6\text{-}^iPr_2\text{-}C_6H_3)_3$ (Table C6). Their ^{13}C shifts do not follow Trend 1.

^{13}C shifts are over a larger range (ca. 0-400 ppm) than the ^{1}H NMR range (ca. 10 ppm), for both organic and organometallic compounds, as a result of greater

participation of C 2p orbitals, with non-zero orbital momenta, in the mixings. The empty orbitals they mix with are not necessarily high in energy.[19] Thus, there are larger paramagnetic contributions in ^{13}C NMR (Figure 5.7). In d^0 alkyl complexes, the mixings generate induced current densities $\boldsymbol{J^p}$ centered on the M and C atom of the α-C atom of the alkyl ligands, leading to a large downfield of the ^{13}C shift.

As shown in Table C7, except for $Cp^*_2M(SiPh_3)Cl$ (M = Zr, Hf), Hf-^{29}Si shifts are in general downfield from Zr-^{29}Si shifts. For the M-Si σ bond, reasons similar to those given for the Y-^{13}C/Zr-^{13}C and Lu-^{13}C/Hf-^{13}C shifts could be given for the difference here.

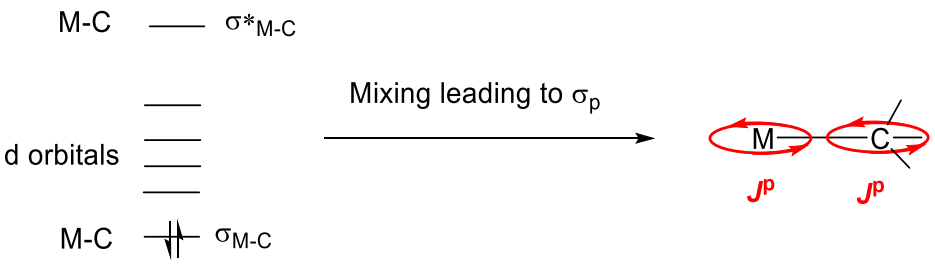

Figure 5.7. Schematic representation of the mixings involving $\sigma_{M\text{-}C}$, leading to induced current densities $\boldsymbol{J^p}$ centered on the M and α-C atom of alkyl ligands.

5.2.3. NMR Chemical Shifts of Phosphine Ligands in d^0 Transition Metal Complexes

Although the dative M←PR_3 bonds are single, σ-bond in nature, there are small and different degrees of π-back bonding from the metal ions to $\sigma_{P\text{-}C}$* orbitals.[52] Both the

dative σ- and π-back bonds are among valence orbitals. The dative σ-bonds are involved in the mixings similar to those of the M-C bonds in Figure 5.7, making the ^{31}P shifts to follow Trend 1. For example, ^{31}P shifts of the bisphosphine complex (PNP)MMe_3 [M = Ti, Zr, Hf; PNP^- = N(2-^{i}Pr$_2$P-4-methylphenyl)$_2$] show a "V" shape (Figure 5.4C).[53-55] The weak π-back bonds may participate in mixings similar to π bonds of other ligands, such as oxo ligands discussed below. Perhaps when complexes form relatively strong π back bonds, the ^{31}P shifts are less likely to follow Trend 1. However, it is not clear why ^{31}P shifts of Groups 3 and 4 follow Trend 1, while those of Groups 5 and 6 do not. It should be pointed out that there are relatively few d^0 phosphine complexes that we could find in the literature, especially Groups 5 and 6 complexes. The small number of data in Table C10 is small. Thus, caution should be excised in the discussions here.

5.2.4. NMR Chemical Shifts of Alkylidene and Alkylidyne Ligands in d^0 Transition Metal Complexes

For d^0 complexes with M=CHR and M≡CR bonds (Table C8), NMR shifts of the α-C atoms in third-row transition metals are typically *upfield* from those of the second-row congeners (Trend 2). The frontier and near-frontier bonding orbitals σ_{MC} and π_{MC} and empty antibonding orbitals σ^*_{MC} and π^*_{MC} are significantly involved in mixings. The operator of the mixings, the angular moment operator, couples σ_{MC} with π^*_{MC} and π_{MC} with σ^*_{MC}.[36]

There are two questions regarding the M=CHR shifts: (1) *Why are the M=^{13}C shifts typically more downfield shifts from those of olefins (^{13}C=^{13}C)?* This is because of the smaller energy gaps between σ_{MC} and π^*_{MC} and between π_{MC} and σ^*_{MC} in M=C complexes than the gaps between σ_{CC} and π^*_{CC} and between π_{CC} and σ^*_{CC} orbitals in olefins, as recent work by Halbert, Copéret, Raynaud and Eisenstein shows.[36] (2) *Why are the M=^{13}C shifts of the third-row transition metals (Hf=^{13}C, Ta=^{13}C and W=^{13}C) typically more upfield shifted from those of second-row transition metal congeners (Zr=^{13}C, Nb=^{13}C and Mo=^{13}C)?* Halbert and coworkers indicate that, since the energies of 4d orbitals are lower than those of 5d orbitals, the energy gap between, e.g., σ_{MC}, which is localized on the C atom, and π^*_{MC} localized on the M atom is smaller for the 4d Mo complex than for the 5d W complex, leading to smaller mixings and more upfield shift of the latter.

The alkylidyne complexes are expected to have even *smaller* energy gaps between σ_{MC} and π^*_{MC} orbitals and between π_{MC} and σ^*_{MC}, leading to larger mixings in M≡C bonds. The M≡^{13}C shifts are thus in general further downfield than the M=^{13}C shifts. As in the M=^{13}C shifts, smaller mixings in the third-row complexes lead to more upfield shifts of W≡^{13}C than Mo≡^{13}C.

5.2.5. NMR Chemical Shifts of Oxo and Fluoride Ligands in d^0 Transition Metal Complexes

^{17}O NMR of d^0 complexes with M=O bonds has been studied by Kaupp [31] and Figgis [43] and coworkers. The mixings leading to the paramagnetic term probably involve

d-p π electrons on the O atoms (Figure 5.8). As in the alkylidenes, W=^{17}O, Re=^{17}O and Os=^{17}O shifts of the 5d complexes are more upfield (Table 11), as the energy gaps between d-p π orbitals and antibonding orbitals are larger, leading to smaller mixings.

In the M-F complexes (Tables 12-13), lone pair electrons from d-p π orbitals mix with the empty d orbitals on the metals. Thus M-^{19}F shifts are expected to follow Trend 2 as M=^{13}C and M=^{17}O shifts.

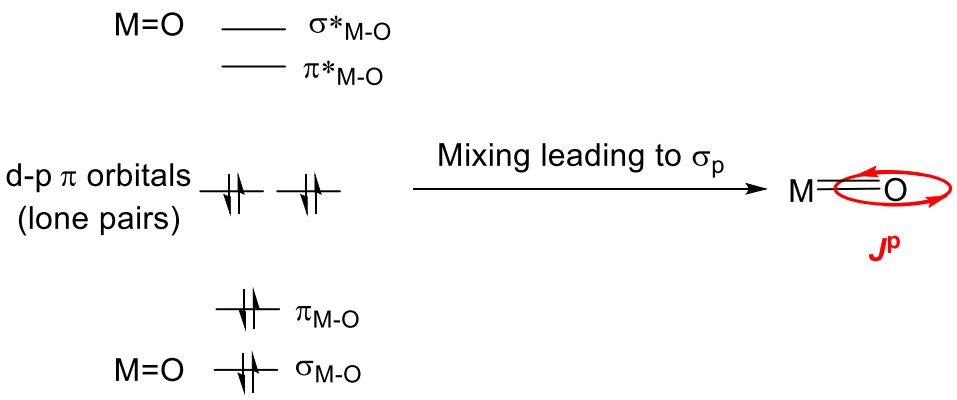

Figure 5.8. Frontier orbitals in d^0 oxo complexes and schematic representation of the mixings using d-p π electrons (from the lone pairs on the O atom).

5.3. Concluding Remarks

Paramagnetic contributions from mixing the d orbitals in the d^0 single-bonded complexes play a critical role in the trends discussed here. NMR shifts of lanthanum, a unique element in the periodic table (and Group 3), provide additional parameters in Trend 1. For M-H, M-C and M-Si complexes (with no lone pairs from the nuclei of the

observed atoms), HOMOs are the σ bonding orbitals that mix with empty d orbitals. For M=C, M≡C, M=O and M-F complexes with either π or d-p π bonds, the mixings involve the σ and π bonding orbitals and π^* and σ^* orbitals. Since many chemical properties of the second- and third-row congeners such as Zr and Hf are similar, as a result of the lanthanide contraction, the NMR chemical shifts are perhaps a rare property to distinguish compounds of the otherwise nearly identical congeners.

References

1. Pyykkö, P. *Angew. Chem. Int. Ed.* **2004**, *43*, 4412.
2. Kaupp, M. In *Theor. Comput. Chem.*; ed. Peter, S.; Elsevier: 2004; Vol. 14, p 552.
3. Kaupp, M. In *Calculation of NMR and EPR Parameters*; Wiley-VCH, 2004, p. 293.
4. Autschbach, J. In *Science and Technology of Atomic, Molecular, Condensed Matter & Biological Systems*; ed. Rubén, H. C., Elsevier: 2013; Vol. 3, p. 69.
5. Autschbach, J.; Ziegler, T. In *Encyclopedia of Nuclear Magnetic Resonance*; eds. Grant, D. M.; Harris R. K., Wiley, 2007; Vol. 9, p 306.
6. Pyykkö, P. *Theor. Chem. Acc.* **2002**, *103*, 214.
7. Drago, R. S. *Physical Methods in Inorganic Chemistry*; Saunders, 1977.
8. Evans, J.; Norton, J. R. *Inorg. Chem.* **1974**, *13*, 3042.
9. Carbajo, R. J.; Neira, J. L. In *Spectroscopic Parameters in Nuclear Magnetic Resonance*; Springer, 2013, p. 31.
10. Nomura, Y.; Takeuchi, Y.; Nakagawa, N. *Tetrahedron Letters* **1969**, *10*, 639.
11. Kaupp, M.; Malkina, O. L.; Malkin, V. G.; Pyykkö, P. *Chem. Eur. J.* **1998**, *4*, 118.
12. Vícha, J.; Straka, M.; Munzarová, M. L.; Marek, R. *J. Chem. Theory. Comput.* **2014**, *10*, 1489.
13. (a) Pawlak, T.; Munzarová, M. L.; Pazderski, L.; Marek, R. *J. Chem. Theory. Comput.* **2011**, *7*, 3909. (b) Pyykkö, P. *Annu. Rev. Phys. Chem.* **2012**, *63*, 45.
14. Greif, A. H.; Hrobárik, P.; Hrobáriková, V.; Arbuznikov, A. V.; Autschbach, J.; Kaupp, M. *Inorg. Chem.* **2015**, *54*, 7199.

15. Kaltsoyannis, N. *J. Chem. Soc. Dalton Trans.* **1997**, 1.

16. McKelvey, D. R. *J. Chem. Educ.* **1983**, *60*, 112.

17. Wiberg, N.; Hollerman, A. F.; Wiberg, E. *Inorganic Chemistry*; 1st Ed.; Academic Press, 2001.

18. Pyykkö, P. *Chem. Rev.* **1988**, *88*, 563.

19. Drago, R. S. In *Physical Methods in Inorganic Chemistry*; Saunders, 1977, p 288.

20. Buckingham, A. D.; Stephens, P. J. *J. Chem. Soc.* **1964**, 2747.

21. Braterman, P. S.; Milne, D. W.; Randall, E. W.; Rosenberg, E. *J. Chem. Soc. Dalton Trans.* **1973**, 1027.

22. Kreiter, C. G.; Formáček, V. *Angew. Chem. Int. Ed.* **1972**, *11*, 141.

23. Bodner, G. M.; Kahl, S. B.; Bork, K.; Storhoff, B. N.; Wuller, J. E.; Todd, L. J. *Inorg. Chem.* **1973**, *12*, 1071.

24. Lauterbur, P. C.; King, R. B. *J. Am. Chem. Soc.* **1965**, *87*, 3266.

25. Buchner, W.; Schenk, W. A. *J. Magn. Res.* **1982**, *48*, 148.

26. Schreckenbach, G.; Ziegler, T. *J. Phys. Chem.* **1995**, *99*, 606.

27. Skachkov, D.; Krykunov, M.; Ziegler, T. *Can. J. Chem.* **2011**, *89*, 1150.

28. Ruiz-Morales, Y.; Schreckenbach, G.; Ziegler, T. *Organometallics* **1996**, *15*, 3920.

29. Schrock, R. R.; Fellmann, J. D. *J. Am. Chem. Soc.* **1978**, *100*, 3359.

30. Ehlers, A. W.; Ruiz-Morales, Y.; Baerends, E. J.; Ziegler, T. *Inorg. Chem.* **1997**, *36*, 5031.

31. Kaupp, M.; Malkin, V. G.; Malkina, O. L.; Salahub, D. R. *J. Am. Chem. Soc.* **1995**, *117*, 1851.

32. Oldfield, E.; Keniry, M. A.; Shinoda, S.; Schramm, S.; Brown, T. L.; Gutowsky, H. S. *J. Chem. Soc. Chem. Comm.* **1985**, 791.

33. Del Rosal, I.; Maron, L.; Poteau, R.; Jolibois, F. *Dalton Trans.* **2008**, 3959.

34. Hrobárik, P.; Hrobáriková, V.; Meier, F.; Repiský, M.; Komorovský, S.; Kaupp, M. *J. Phys. Chem. A* **2011**, *115*, 5654.

35. Bagno, A.; Saielli, G. *Phys. Chem. Chem. Phys.* **2011**, *13*, 4285.

36. Halbert, S.; Copéret, C.; Raynaud, C.; Eisenstein, O. *J. Am. Chem. Soc.* **2016**, *138*, 2261.

37. Pyykkö, P.; Görling, A.; Rösch, N. *Mol. Phys.* **1987**, *61*, 195.

38. Morishima, I.; Endo, K.; Yonezawa, T. *J. Chem. Phys.* **1973**, *59*, 3356

39. Malkin, V. G.; Malkina, O. L.; Salahub, D. R. *Chem. Phys. Lett.* **1996**, *261*, 335.

40. Kaupp, M.; Malkina, O. L. *J. Chem. Phys.* **1998**, *108*, 3648.

41. Vaara, J.; Malkina, O. L.; Stoll, H.; Malkin, V. G; Kaupp, M. *J. Chem. Phys.* **2001**, *114*, 61.

42. Wolff, S. K.; Ziegler, T. *J. Chem. Phys.* **1998**, *103*, 895.

43. Figgis, B. N.; Kidd, R. G.; Nyholm, R. S. *Proc. R. Soc. A* **1962**, *269*, 469.

44. Jensen, W. B. *J. Chem. Edu.* **1982**, *59*, 634.

45. Green, J. C. *Chem. Soc. Rev.* **1998**, *27*, 263.

46. Lauher, J. W.; Hoffmann, R. *J. Am. Chem. Soc.* **1976**, *98*, 1729.

47. The structure of the Sc hydride has not been reported. The differences in their structures are not considered here.

48. Huheey, J. E.; Huheey, C. L. *J. Chem. Educ.* **1972**, *49*, 227.

49. Greenwood, N. N.; Earnshaw, A. *Chemistry of the Elements*; 2nd Ed. Butterworth-Heinemann, 1997.

50. Cotton, S. *Lanthanide and Actinide Chemistry*, Wiley, 2006.

51. Pfenning, B. W. *Principles of Inorganic Chemistry*, Wiley, 2015.

52. Spessard, G. O.; Miessler, G. L. *Organometallic Chemistry*; 3rd Ed.; Oxford University Press, 2016.

53. Bailey, B. C.; Huffman, J. C.; Mindiola, D. J.; Weng, W.; Ozerov, O. V. *Organometallics* **2005**, *24*, 1390.

54. Weng, W.; Yang, L.; Foxman, B. M.; Ozerov, O. V. *Organometallics* **2004**, *23*, 4700.

55. Brammell, C. M.; Pelton, E. J.; Chen, C.-H.; Yakovenko, A. A.; Weng, W.; Foxman, B. M.; Ozerov, O. V. *J. Organomet. Chem.* **2011**, *696*, 4132.

Part 6

Concluding Remarks and Future Studies

This dissertation covered three areas of chemistry: (1) Synthesis, characterization, and reactions of heptacoordinated Group 4 complexes; (2) Reactions of W alkylidyne complexes with water; (3) Overview of two NMR trends observed in d^0 transition metal complexes.

In Part 2, the heptacoordinate amidinate chloride complexes M[MeC(N^{i}Pr)$_2$]$_3$Cl (M = Zr, **1**; Hf, **2**) have been synthesized via salt metathesis reactions between MCl_4 and Li[MeC(N^{i}Pr)$_2$]. These complexes have been characterized via by ^{1}H and ^{13}C{^{1}H} NMR spectroscopies, single-crystal X-ray diffraction, elemental analysis, and MS. The crystals of **1** and **2** contained both Δ and Λ enantiomers. The enantiomers of **1** and **2** undergo fast exchanges in solution. These exchanges have been studied using variable-temperature NMR (VT-NMR) spectroscopy. This study has yielded the activation parameters $\Delta H^{\neq}$, $\Delta S^{\neq}$, and $\Delta G^{\neq}$ for both **1** and **2**. Compounds **1** and **2** are good candidates to be precursors for a variety of different trisamidinate complexes including alkyl complexes.

In Part 3, the methyl complexes M[MeC(N^{i}Pr)$_2$]$_3$Me (M = Zr, **3**; Hf, **4**) have been prepared via the reactions of **1** or **2** with MeLi. The ethyl complexes M[MeC(N^{i}Pr)$_2$]$_3$Et (M = Zr, **6**; Hf, **7**) have been prepared via salt metathesis of **1** or **2** with EtMgCl (**5**). These complexes have been characterized by elemental analysis and ^{1}H and ^{13}C{^{1}H} NMR spectroscopies. **6** and **7** have been also characterized by single-crystal X-ray diffraction. The alkyl ligands were found to be too labile for characterization of **3**, **4**, **6**, and **7** via MS. Using MS, compounds **9** and **10** were identified as products of the reactions of H_2O with these complexes as well as with **1** and **2**. The thermal decomposition of **6** was also studied. The thermolysis has been found to follow first-

order kinetics with activation parameters $\Delta H^{\neq}$ = 29(4) kcal/mol, $\Delta S^{\neq}$ = -5(8) eu, and $\Delta G^{\neq}_{298}$ = 31(6) kcal/mol.

In Part 4, the reactions of W alkylidyne complexes with water have been explored. In the reaction of W(≡CSiMe$_3$)(CH$_2$SiMe$_3$)$_3$ (**11**) with H$_2$O at room temperature, the trimer [(μ-O)W(CH$_2$SiMe$_3$)$_2$(=O)(THF)]$_3$ (**12**) has been isolated as a crystalline product at -32 °C and its structure has been determined by single-crystal X-ray diffraction. Reactions of water with a second alkylidyne complex, W(≡C^{t}Bu)(O^{t}Bu)$_3$ (**10**), have also been studied. Only the product, W(CH$_2$^{t}Bu)(O^{t}Bu)$_3$(=O) (**13**), was formed in the NMR reactions. Using DART-TOF-MS, products of the reaction of **10** with H$_2$O from air were identified. These complexes included: unreacted **10**, **13**, W(≡C^{t}Bu)(O^{t}Bu)(=O) (**14**), W(≡C^{t}Bu)(O^{t}Bu)$_2$(OH) (**15**), W(=CH^{t}Bu)(O^{t}Bu)$_2$(=O) (**16**), W(CH$_2$^{t}Bu)(O^{t}Bu)(=O)$_2$ (**17**), and W(CH$_2$^{t}Bu)(O^{t}Bu)(=O)$_2$ (**18**).

Part 5 presented two trends found in the NMR spectra of d^0 transition metal complexes. Since many chemical properties of second- and third-row analogous complexes are similar because of the lanthanide contraction, the chemical shifts found in the α atoms connected to the metals in their NMR spectra may be a distinguishing feature. Complexes containing single-bonded ligands as M-H, M-CR$_3$ and M-SiR$_3$ were found to follow Trend 1, which was described as the *downfield shift* of the ^{1}H, ^{13}C and ^{29}Si shifts of the α atoms second-row analogs of both first- and third-row transition metal complexes. Shifts of lanthanum complexes provide additional parameters in Trend 1. Trend 2 was observed for complexes containing M=C, M≡CR, M=O and M–F. Trend 2 was described as the *upfield shift of* third-row transition metals from those of the

second-row analogs observed in ^{13}C, ^{17}O and ^{19}F NMR. For the as M-H, M-CR_3 and M-SiR_3 complexes in Trend 1, the frontier, σ bonding orbitals mix with empty d orbitals. In Trend 2, M=C, M≡C, M=O and M-F complexes contain either π or d-p π bonds. In these complexes, mixing involves the σ and π bonding orbitals and π^* and σ^* orbitals.

Future work on heptacoordinate Group 4 amidinate complexes, especially the alkyl complexes, will focus on their reactions with O_2 and water and their application to CVD and ALD processes. Hexacoordinate Group 4 amidinate amide complexes M[MeC(N^iPr)$_2$]$_2$(NR_2)$_2$ (R = Me, Et) have been shown to be reactive to O_2 and water.[1] Thus, it would be intriguing to see the reactivities of heptacoordinate amidinate amide complexes such as M[MeC(N^iPr)$_2$]$_3$(NMe_2) (M = Zr, Hf) which have not been reported. The reactions of these heptacoordinate complexes with O_2 and water may be probed. The deposition of these complexes via CVD and/or ALD processes may also be studied. Since these complexes have three amidinate ligands, they are expected to be more stable than their hexacoordinate analogs such as M[MeC(N^iPr)$_2$]$_2$(NR_2)$_2$ (R = Me, Et). The reactions of these complexes with water are very fast, forming unknown white solid(s) immediately. This property makes these complexes ideal for ALD of MO_2 films, which requires fast reactions of the precursors with the surface hydroxyl groups on the substrate. Though **1** and **2** react with H_2O, HCl is a product, perhaps making **1** and **2** less desirable precursors. HCl is corrosive and may leave chlorine in the newly formed thin films. In comparison, the alkyl complexes **3**, **4**, **6**, and **7** may be more suitable as precursors for the ALD of the MO_2 films, as they do not have a Cl^- ligand. In addition, the amide complexes M[MeC(N^iPr)$_2$]$_3$(NMe_2) (M = Zr, Hf) proposed above may also be used. It would be interesting to study the composition of the metal oxide thin films to see

if there are any C or N impurities in the films. Theoretical studies on the pathways of these systems would be interesting since these complexes have a high coordination number.

Future work for the W alkylidyne project would be to analyze other alkylidynes, such as $W(\equiv CSiMe_3)(CH_2SiMe_3)_3$ and $W(\equiv C^tBu)(CH_2{}^tBu)_3$, via MS to identify more W-containing products from the reactions of these complexes with H_2O from air.

References

1. (a) Lamb, A. C.; Lu, Z.; Xue, Z.-L. *Chem. Comm.* **2014**, *50*, 10517. (b) Lamb, A. C.; Wang, Z.; Cook, T. M.; Sharma, B.; Chen, S.-J.; Lu, Z.; Steren, C. A.; Lin, Z.; Xue, Z.-L. *Polyhedron* **2016**, *103*, 2.

Appendices

Appendix A

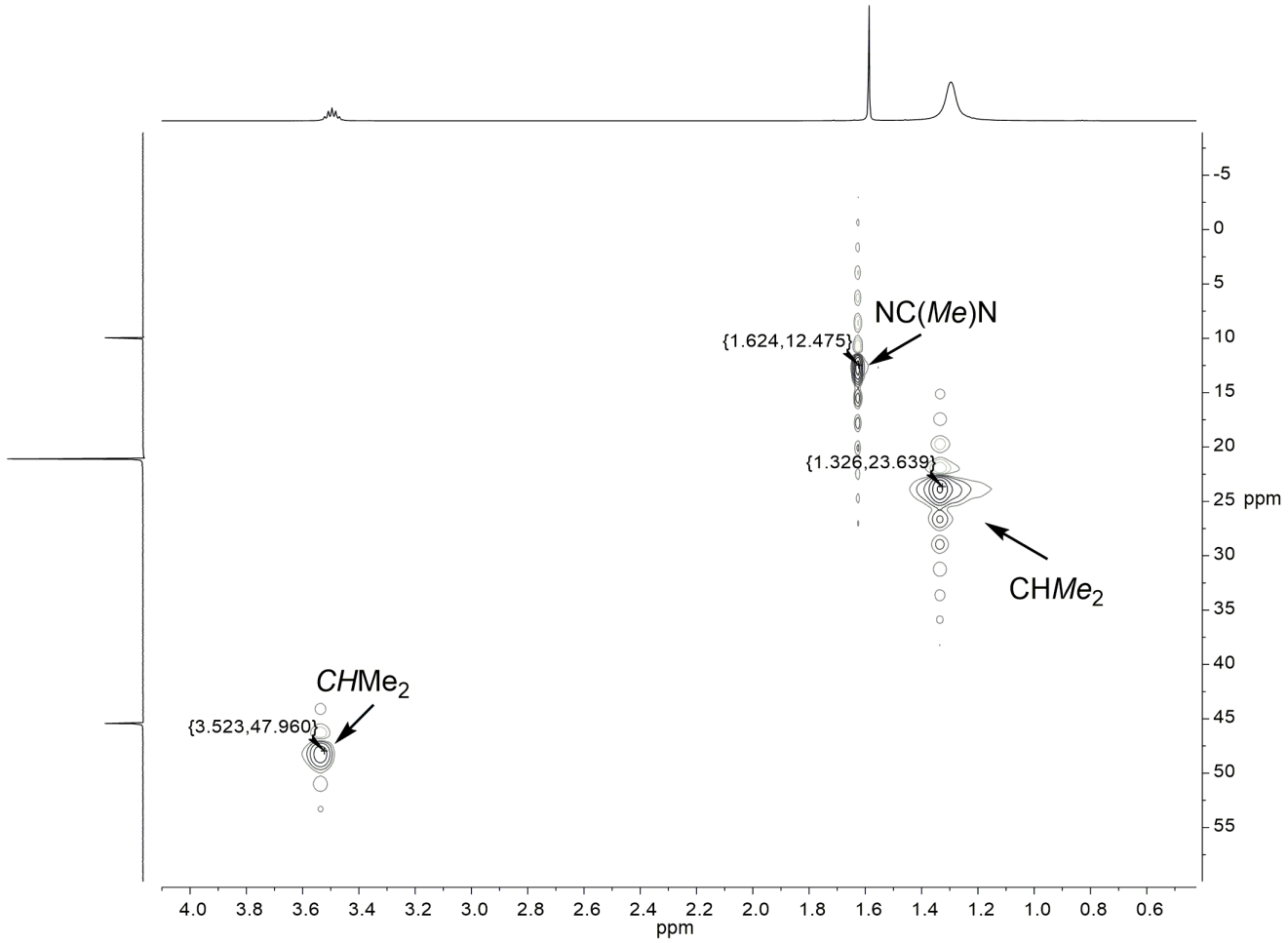

Figure A1. HSQC NMR spectrum of **1** in benzene-d_6 at 23 °C.

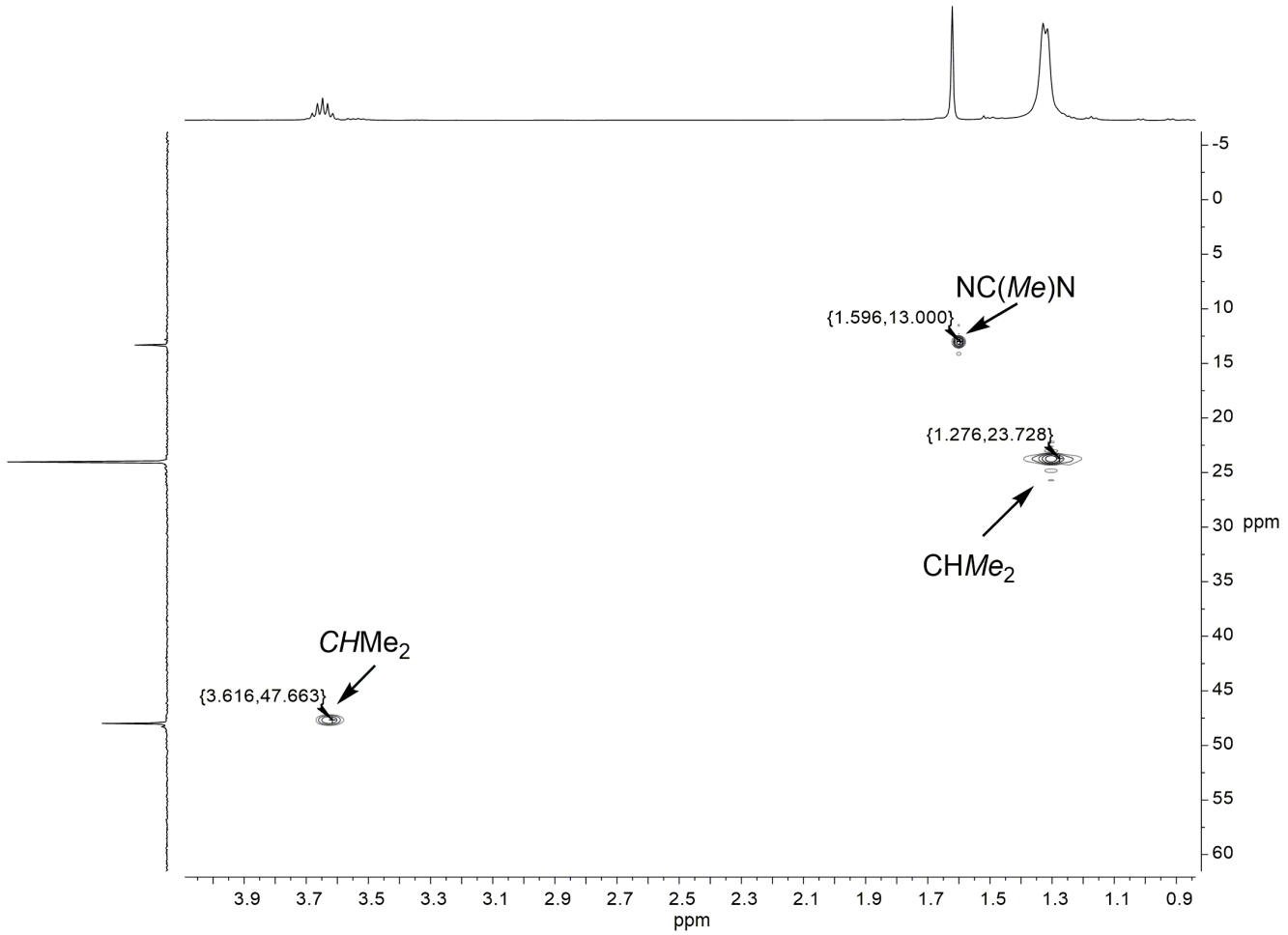

Figure A2. HSQC NMR spectrum of **2** in benzene-d_6 at 23 °C.

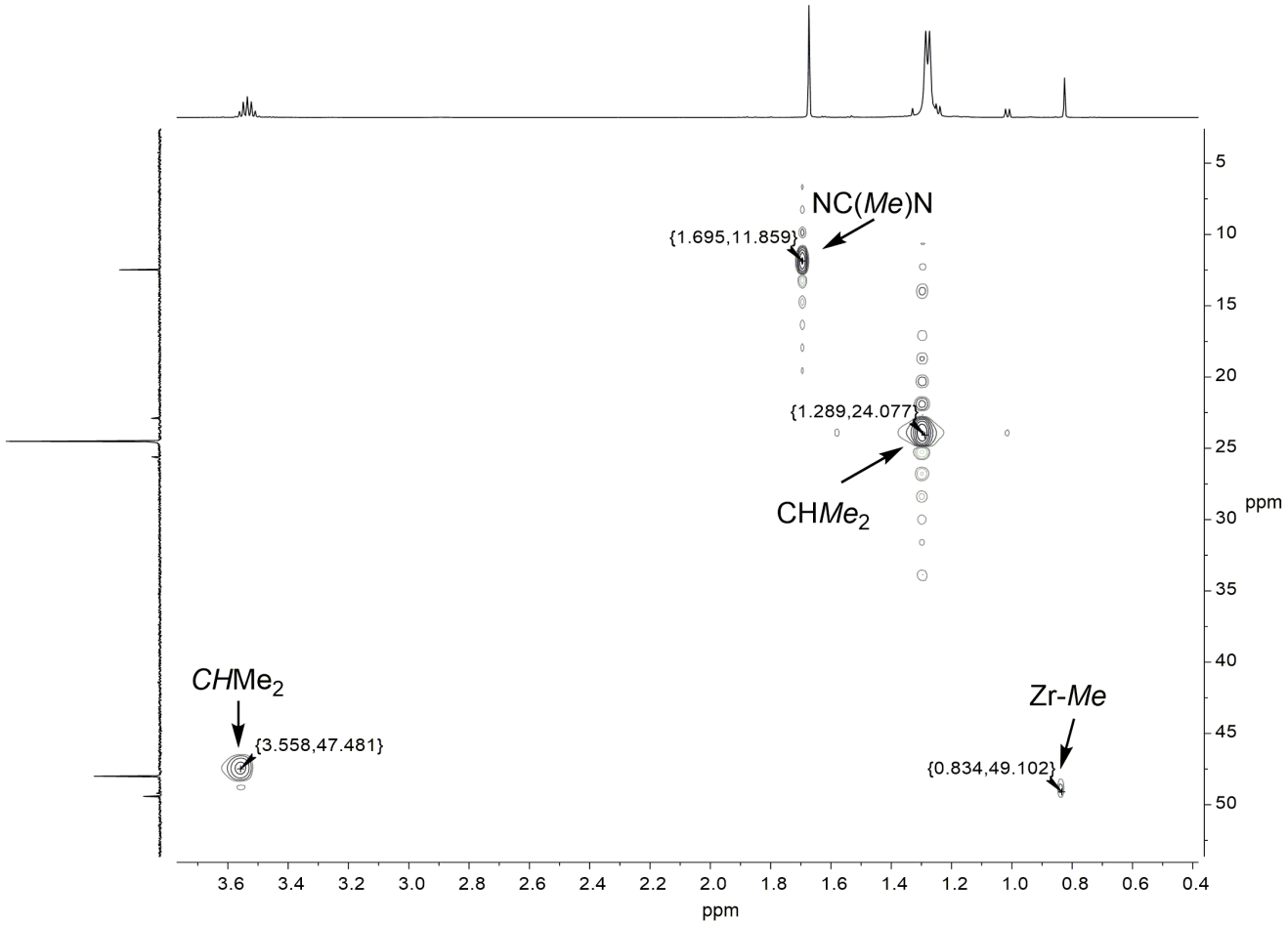

Figure A3. HSQC NMR spectrum of **3** in benzene-d_6 at 23 °C.

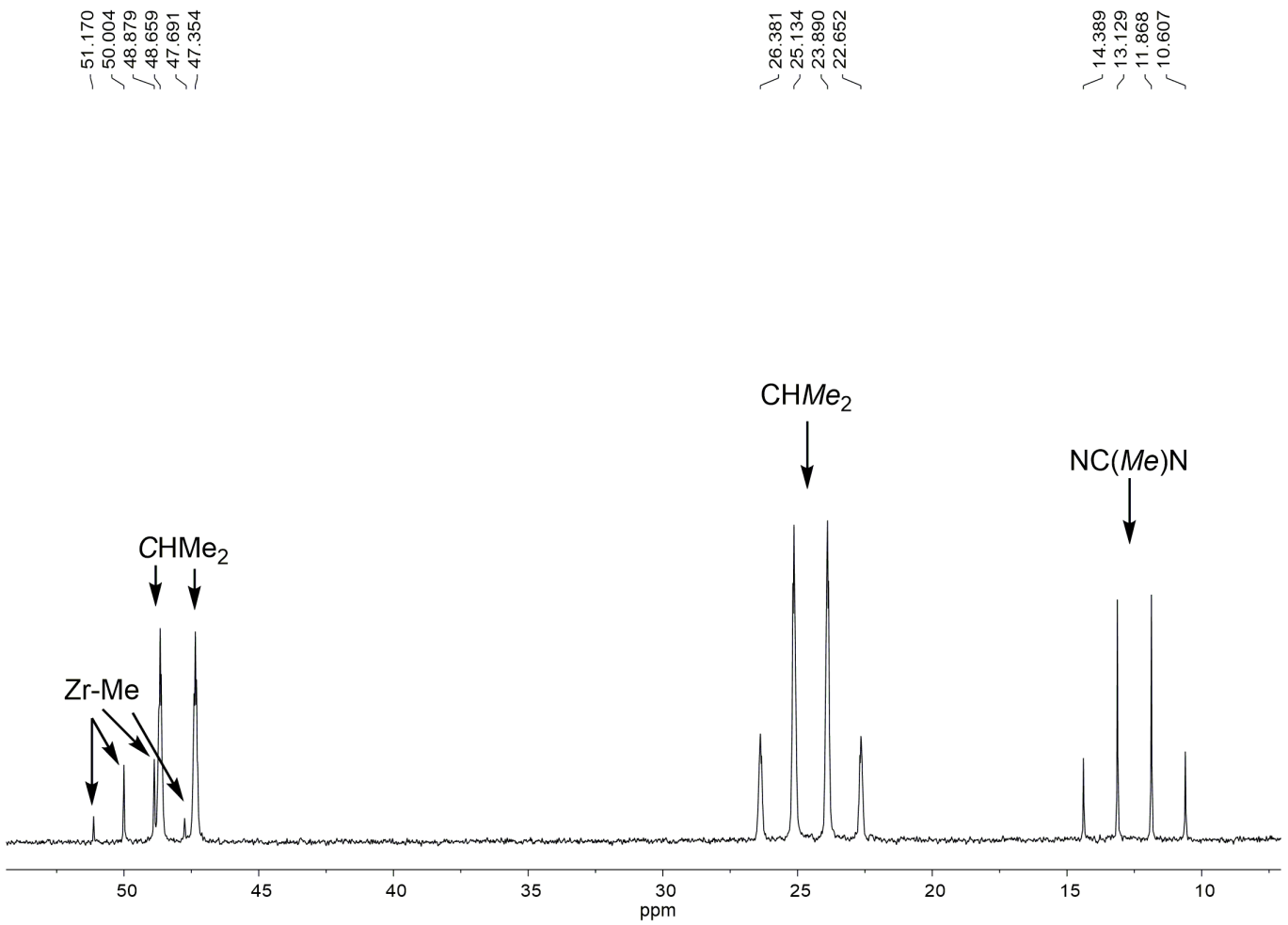

Figure A4. ^{1}H-gated-decoupled ^{13}C NMR spectrum of **3** in benzene-d_6 at 23 °C.

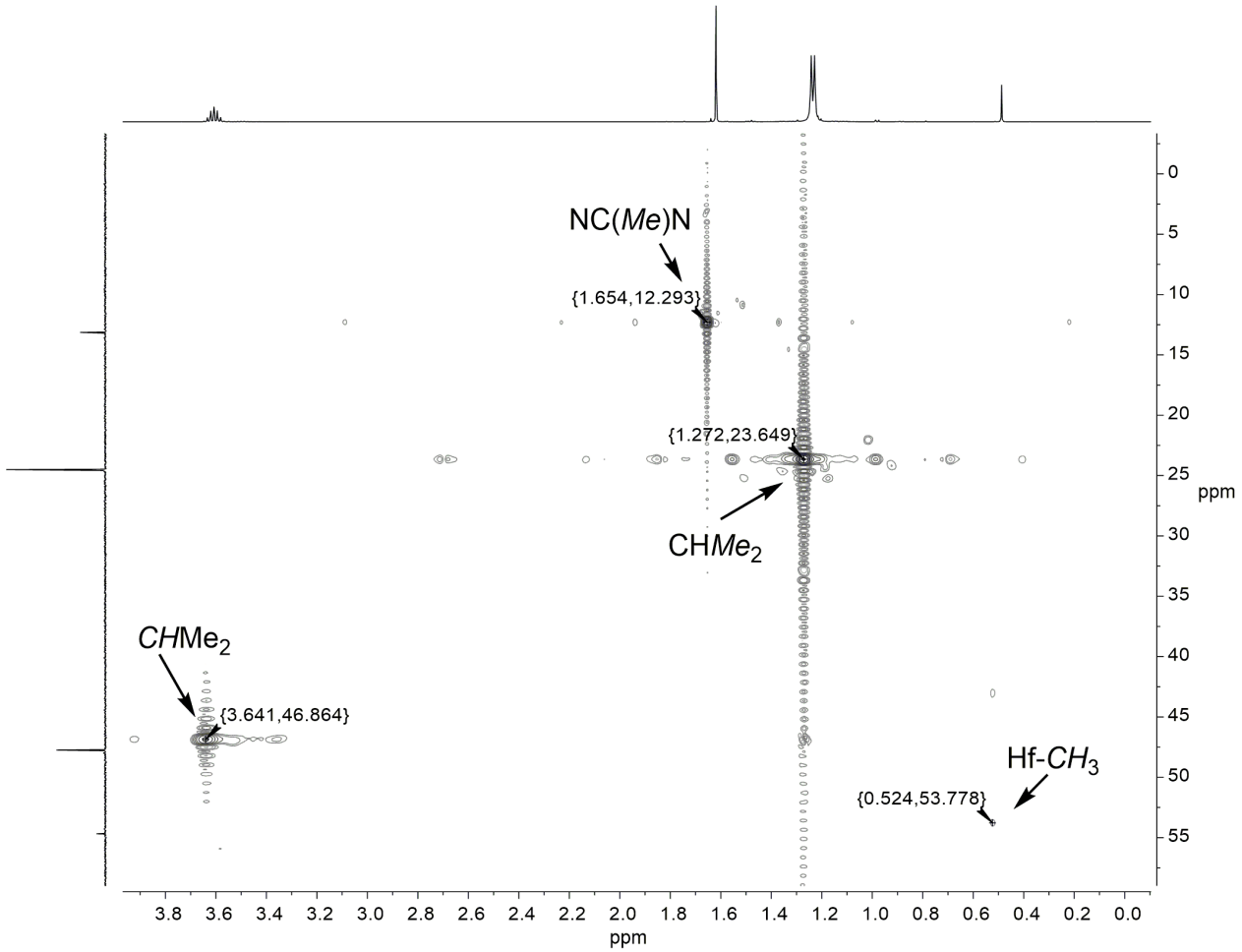

Figure A5. HSQC NMR spectrum of **4** in benzene-d_6 at 23 °C.

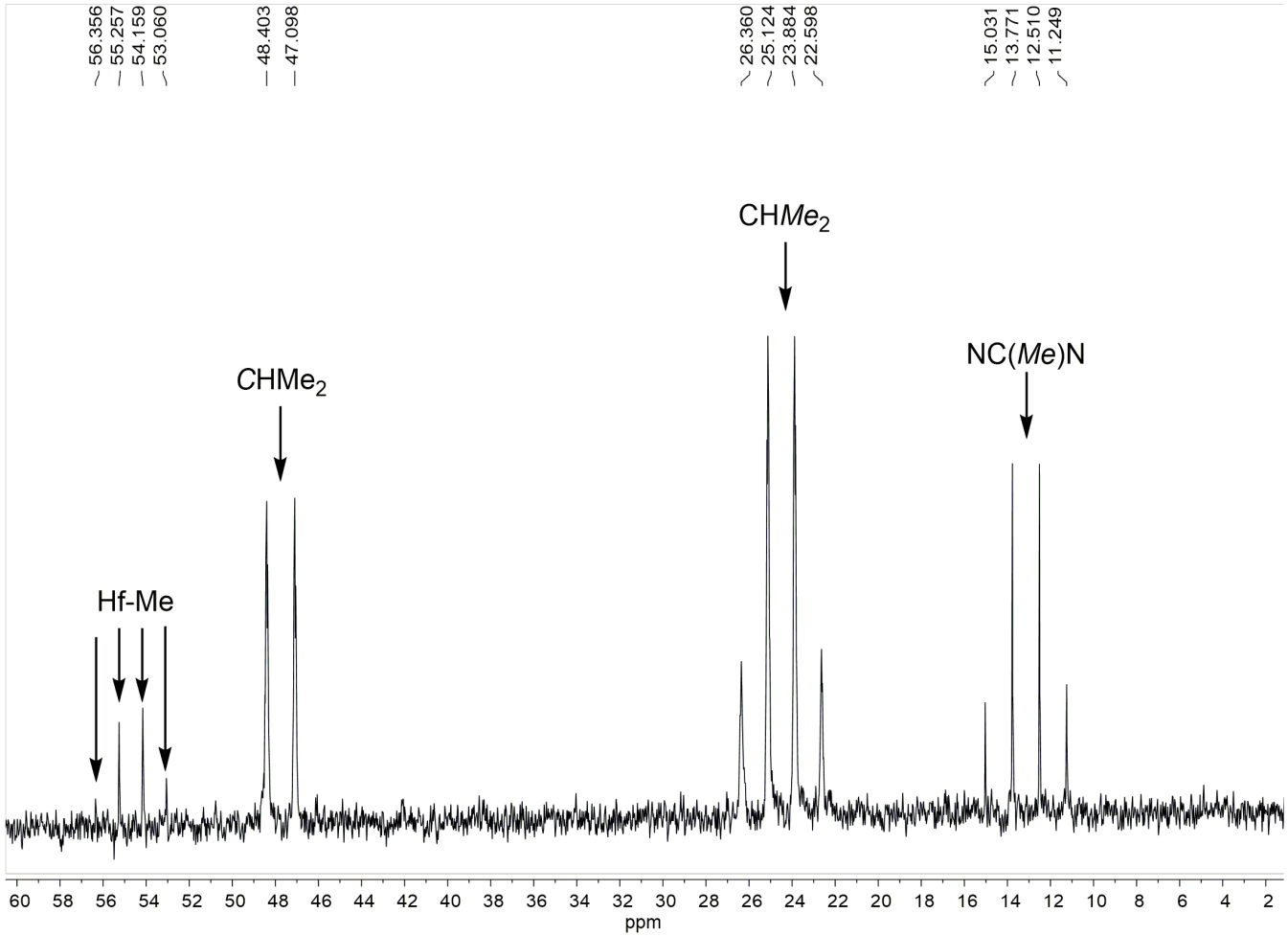

Figure A6. ^{1}H-gated-decoupled ^{13}C NMR spectrum of **4** in benzene-d_6 at 23 °C.

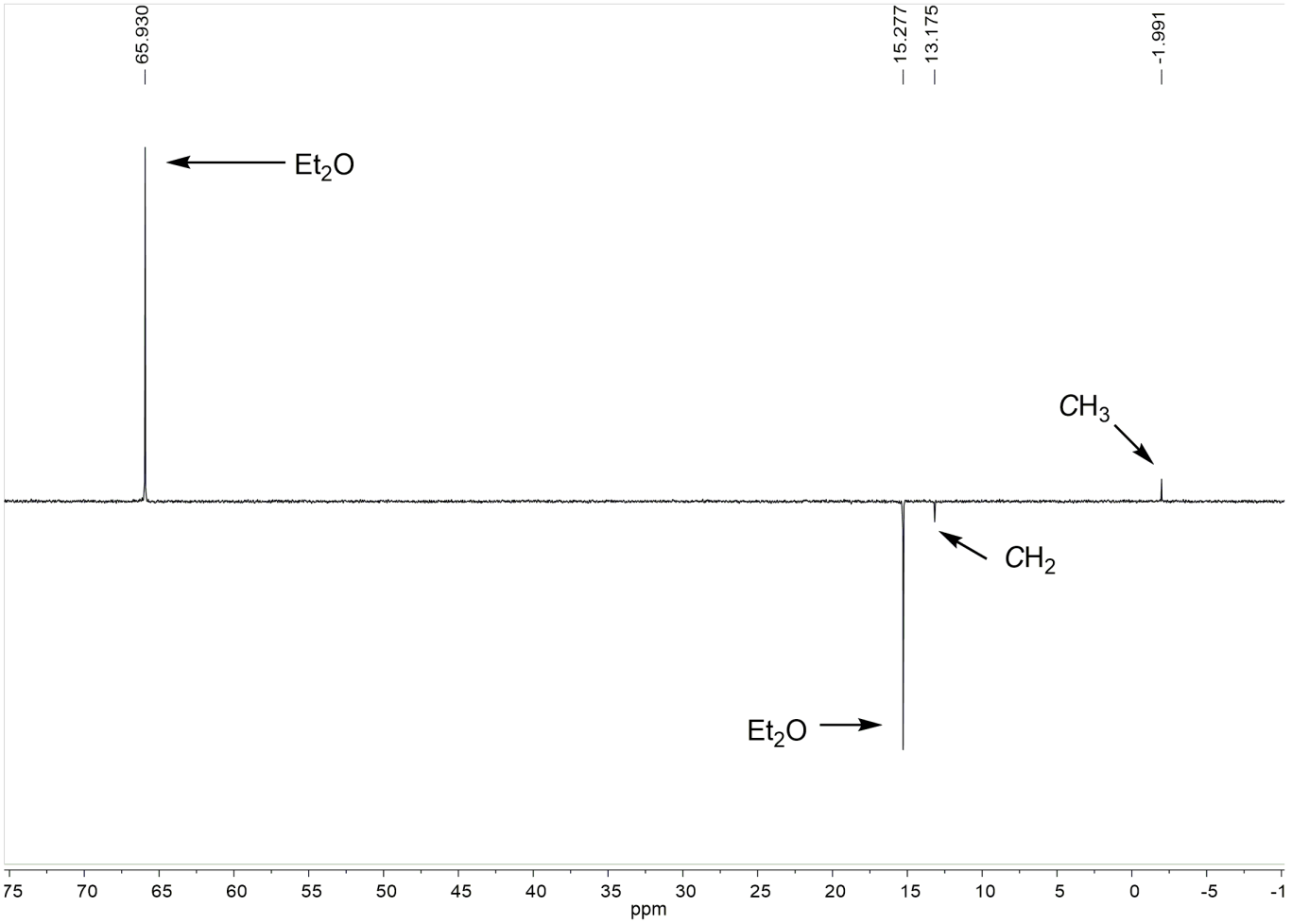

Figure A7. DEPT-135 NMR spectrum of **5** in a benzene/Et_2O solution in toluene-d_8 at 23 °C.

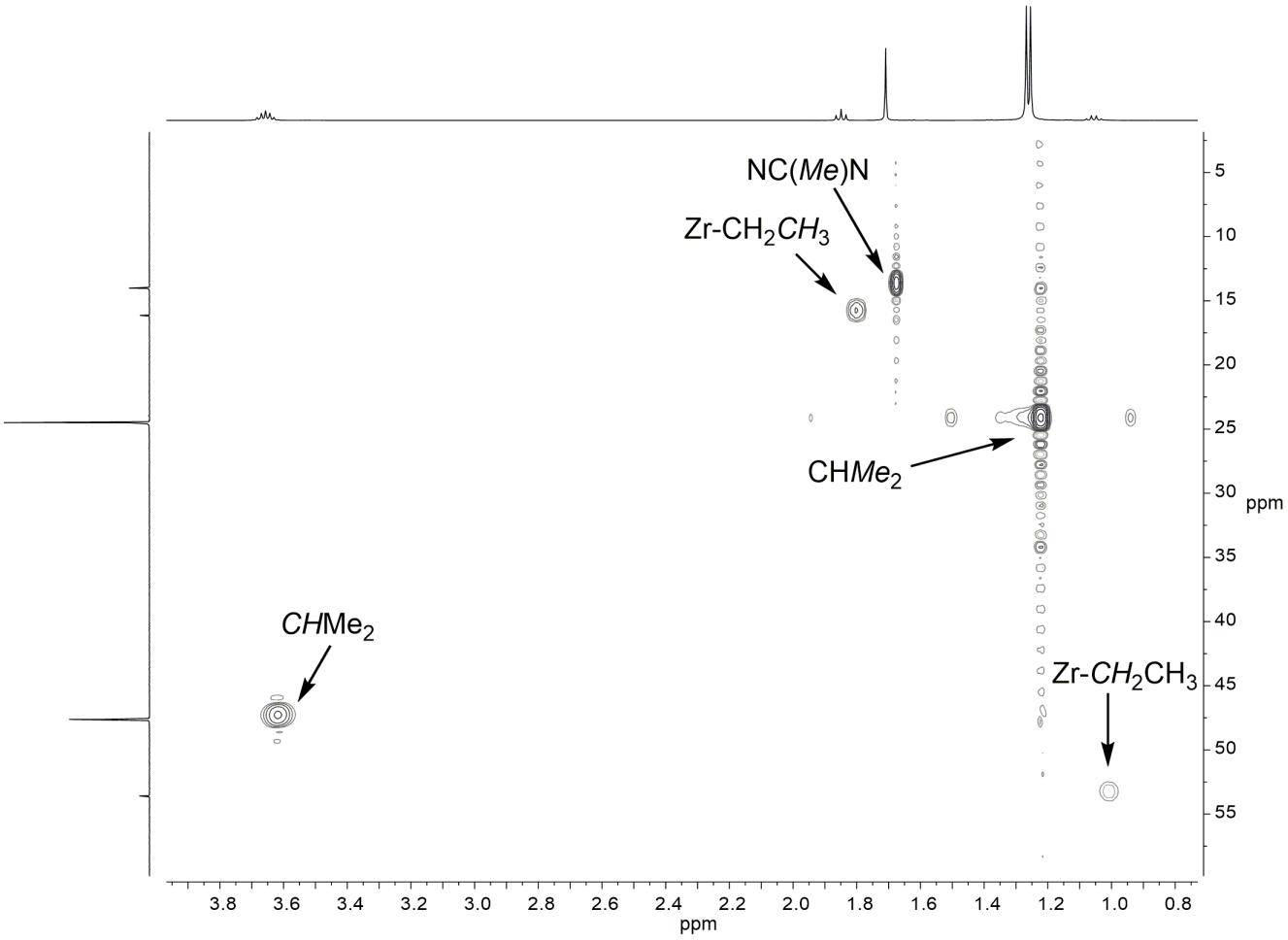

Figure A8. HSQC NMR spectrum of **6** in a benzene-d_6 at 23 °C.

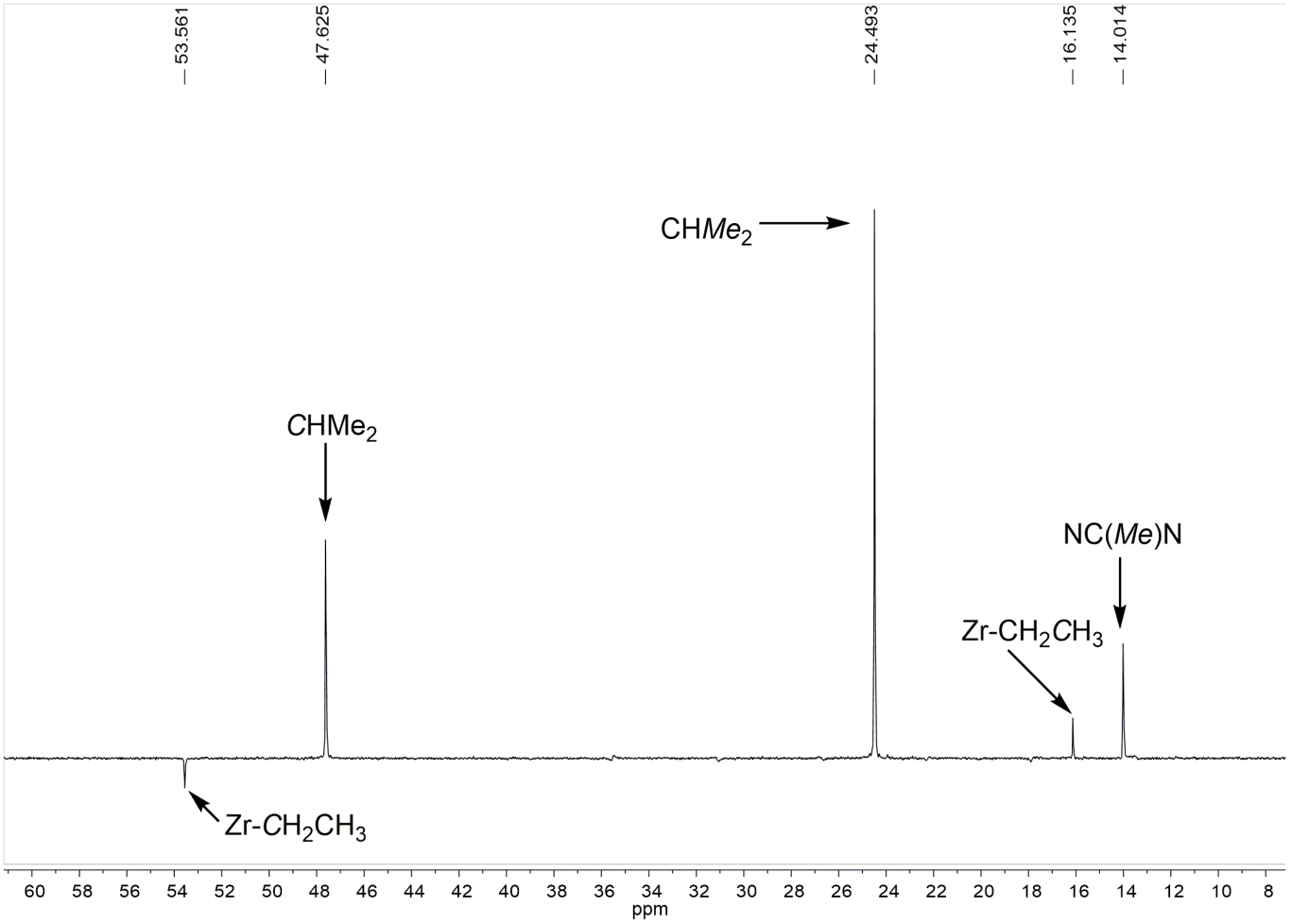

Figure A9. DEPT-135 NMR spectrum of **6** in a benzene-d_6 at 23 °C.

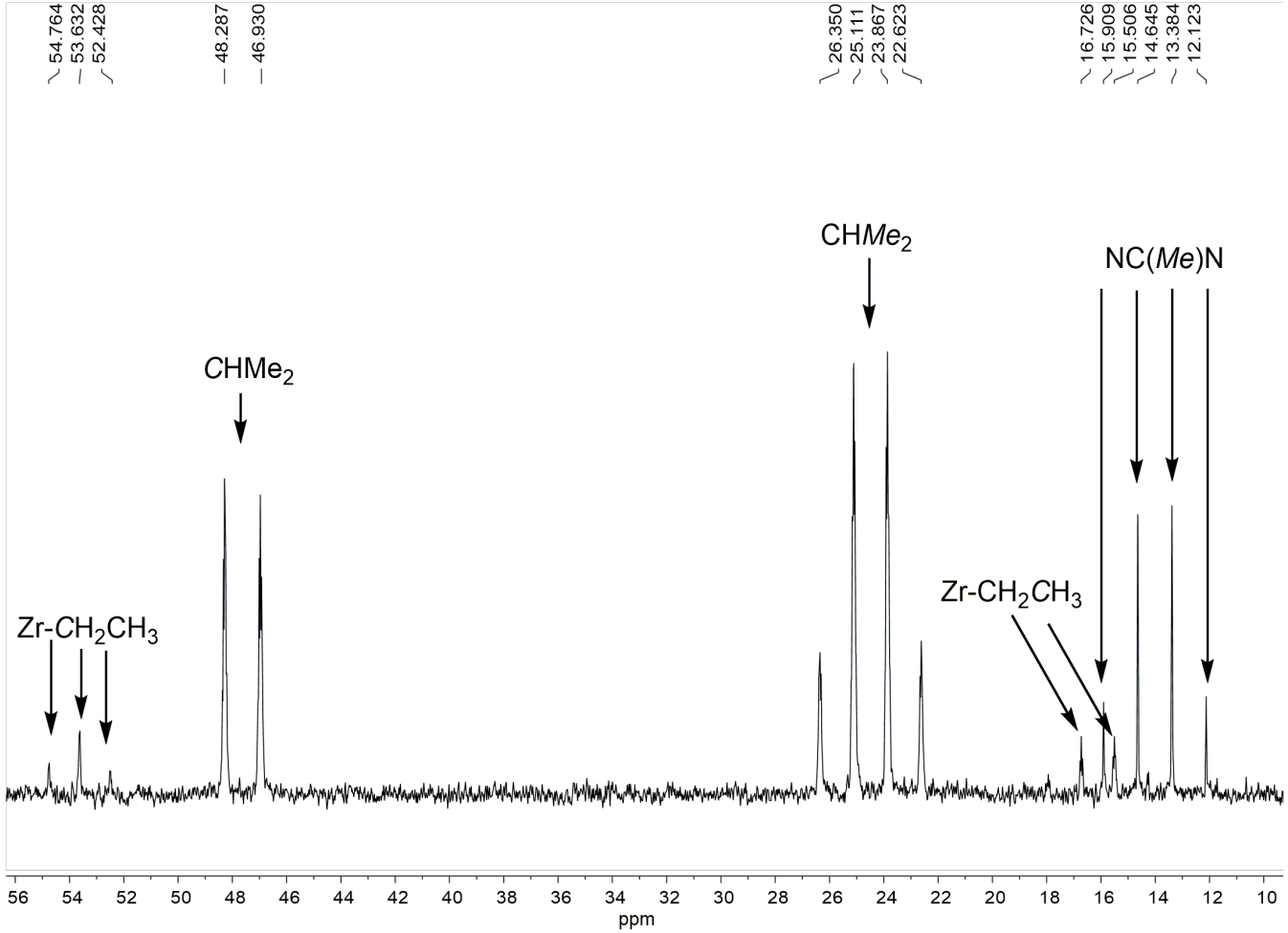

Figure A10. ^{1}H-gated-decoupled ^{13}C NMR spectrum of **6** in a benzene-d_6 at 23 °C.

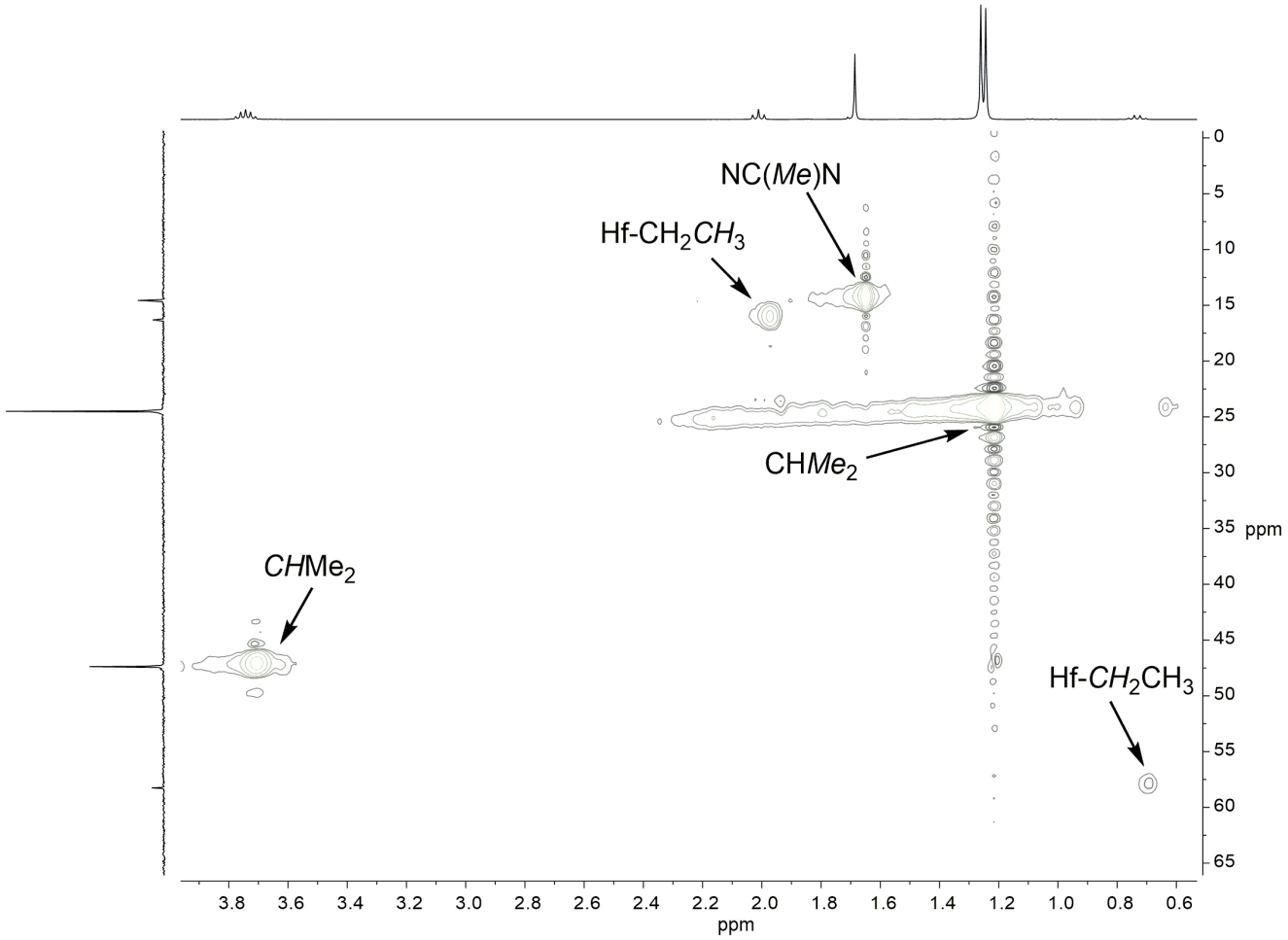

Figure A11. HSQC NMR spectrum of **7** in a benzene-d_6 at 23 °C.

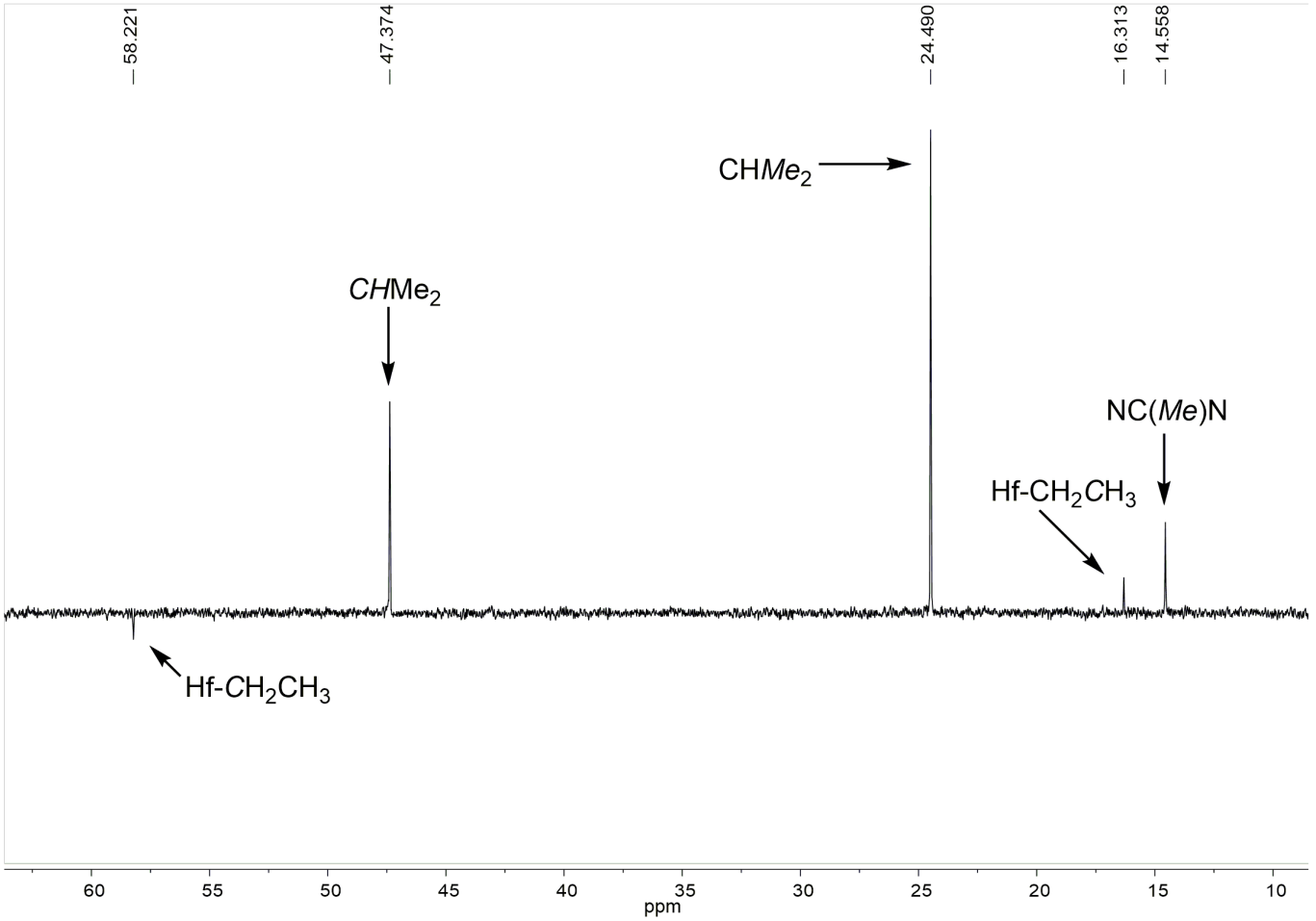

Figure A12. DEPT-135 NMR spectrum of **7** in a benzene-d_6 at 23 °C.

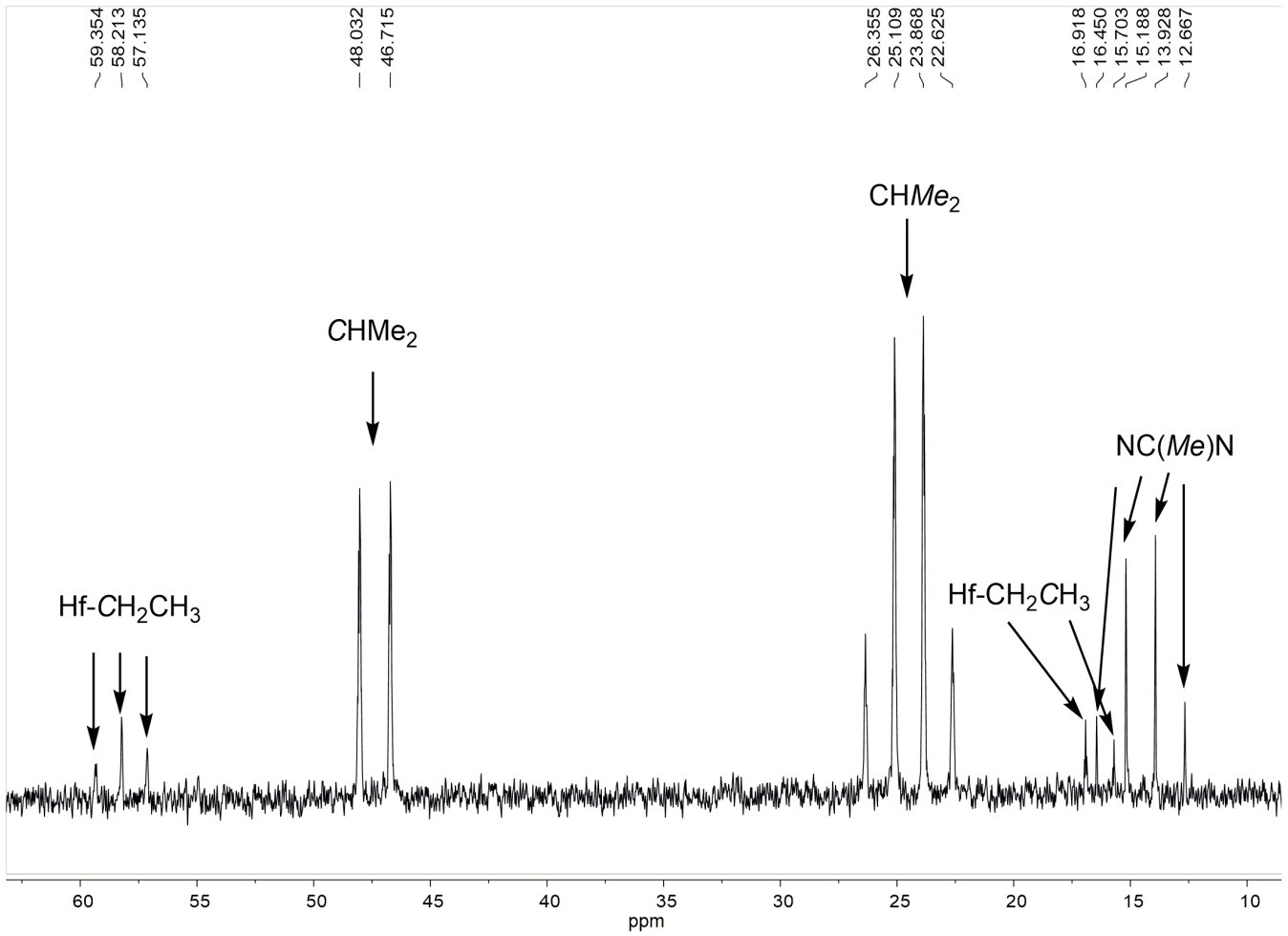

Figure A13. ^{1}H-gated-decoupled ^{13}C NMR spectrum of **7** in a benzene-d_6 at 23 °C.

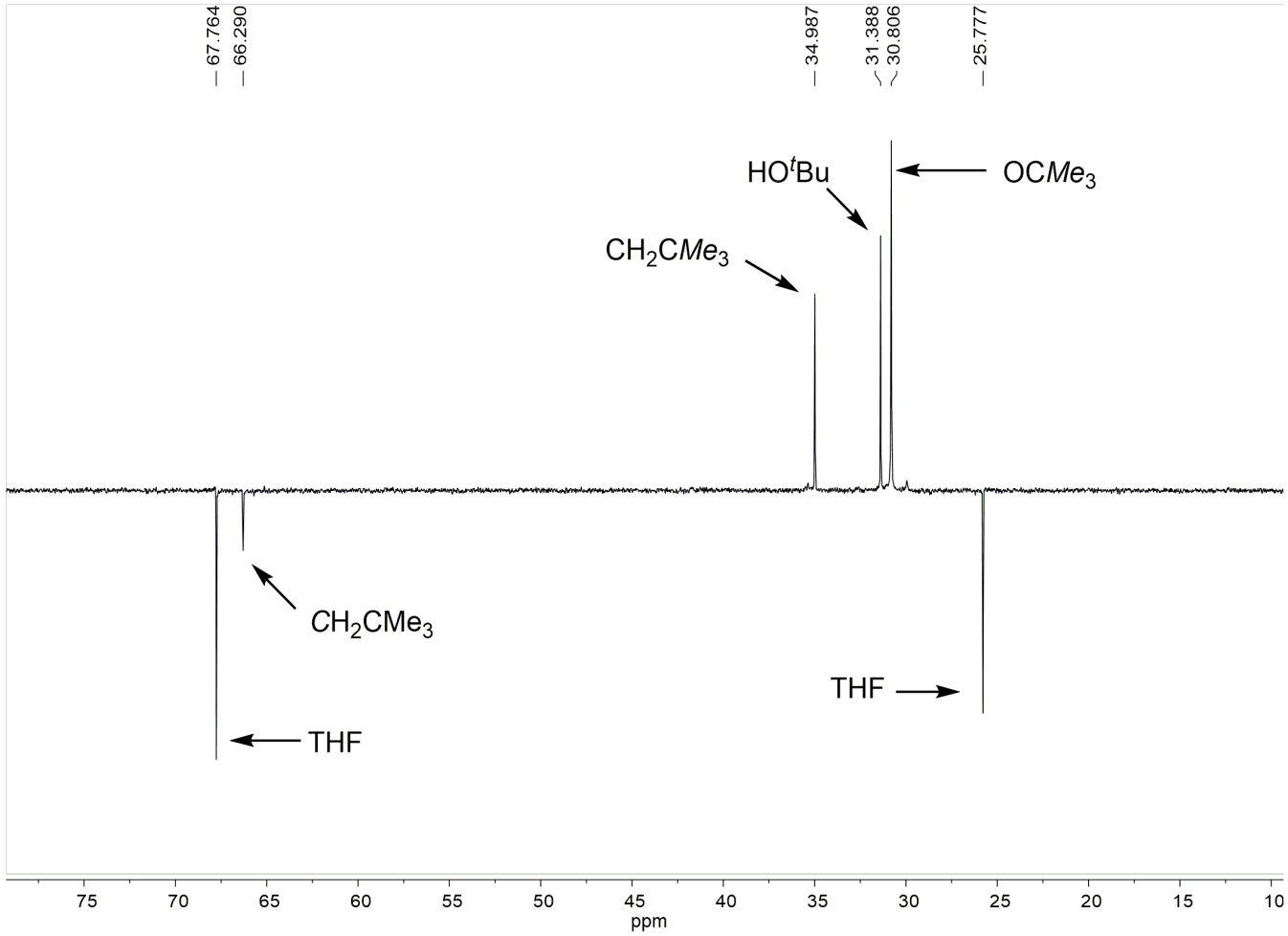

Figure A14. DEPT-135 NMR spectrum of reaction mixture of **13** in THF and benzene-d_6 at 23 °C.

Appendix B

Table B1. Atomic coordinates ($\times 10^4$) and equivalent isotropic displacement parameters ($Å^2 \times 10^3$) for **1**. U(eq) is defined as one third of the trace of the orthogonalized U^{ij}

	x	y	z	U(eq)
Zr(1)	5195.4(2)	2402.8(2)	7437.1(2)	13.32(5)
Cl(1)	5840.8(4)	935.1(2)	7362.0(2)	21.81(9)
N(1)	4311.6(13)	1989.1(8)	8513.6(8)	17.6(3)
N(2)	3171.7(13)	2833.3(8)	7736.9(8)	18.6(3)
N(3)	4369.4(14)	2219.1(8)	6236.3(8)	18.7(3)
N(4)	5147.8(13)	3432.5(8)	6542.4(8)	18.8(3)
N(5)	7281.0(12)	2648.4(8)	7425.6(8)	17.1(3)
N(6)	6177.2(13)	3375.0(8)	8248.6(8)	17.5(3)
C(1)	3198.3(15)	2380(1)	8380.5(9)	17.5(3)
C(2)	2110.1(17)	2315.2(12)	8922.1(10)	26.6(4)
C(3)	4575.6(16)	1473.6(10)	9202.2(10)	21.2(3)
C(4)	4037.8(19)	615.1(11)	9079.2(12)	32.1(4)
C(5)	6023.2(17)	1451.8(11)	9398.3(10)	25.5(4)
C(6)	2010.3(15)	3295.3(10)	7488.7(10)	19.8(3)
C(7)	2026.7(18)	4140.1(11)	7865.3(11)	27.4(4)
C(8)	1841.3(17)	3374.8(11)	6600.6(10)	25.0(4)
C(9)	4679.7(15)	2959.5(10)	5971.8(9)	18.6(3)
C(10)	4466.8(17)	3198.8(11)	5123.9(10)	25.2(4)
C(11)	3720.1(18)	1605.3(10)	5734.9(10)	26.5(4)
C(12)	4681(2)	1050.0(13)	5357.1(12)	39.0(5)
C(13)	2802(2)	1117.2(12)	6213.9(13)	37.5(5)
C(14)	5717.5(18)	4244(1)	6472.3(11)	24.9(4)
C(15)	4732.9(19)	4890.4(10)	6218.6(11)	27.5(4)
C(16)	6913.4(19)	4274.1(12)	6006.8(13)	34.8(4)
C(17)	7319.7(15)	3224.0(9)	7978.7(9)	16.9(3)
C(18)	8537.2(17)	3661.1(12)	8247.7(11)	27.2(4)
C(19)	6046.3(17)	3967.3(10)	8883.8(10)	21.1(3)
C(20)	5850(2)	4829.2(10)	8566.9(11)	30.6(4)
C(21)	4954.4(19)	3736.3(11)	9390.1(10)	28.3(4)

Table B1. Continued

	x	y	z	U(eq)
C(22)	8431.2(16)	2367.1(10)	7057.5(10)	21.6(3)
C(23)	9131.2(17)	1715.8(11)	7555.6(11)	28.0(4)
C(24)	8064.5(18)	2043.4(12)	6237.5(11)	28.3(4)

Table B2. Bond lengths (Å) in **1**

Zr(1)-Cl(1)	2.5125(5)	N(6)-C(17)	1.328(2)
Zr(1)-N(1)	2.2141(14)	N(6)-C(19)	1.472(2)
Zr(1)-N(2)	2.3154(14)	C(1)-C(2)	1.511(2)
Zr(1)-N(3)	2.2015(14)	C(3)-C(4)	1.530(2)
Zr(1)-N(4)	2.2814(13)	C(3)-C(5)	1.530(2)
Zr(1)-N(5)	2.2172(13)	C(6)-C(7)	1.532(2)
Zr(1)-N(6)	2.3175(13)	C(6)-C(8)	1.524(2)
N(1)-C(1)	1.337(2)	C(9)-C(10)	1.506(2)
N(1)-C(3)	1.464(2)	C(11)-C(12)	1.528(3)
N(2)-C(1)	1.328(2)	C(11)-C(13)	1.526(3)
N(2)-C(6)	1.473(2)	C(14)-C(15)	1.525(2)
N(3)-C(9)	1.346(2)	C(14)-C(16)	1.521(3)
N(3)-C(11)	1.466(2)	C(17)-C(18)	1.509(2)
N(4)-C(9)	1.320(2)	C(19)-C(20)	1.528(2)
N(4)-C(14)	1.470(2)	C(19)-C(21)	1.520(2)
N(5)-C(17)	1.337(2)	C(22)-C(23)	1.528(2)
N(5)-C(22)	1.464(2)	C(22)-C(24)	1.528(2)

Table B3. Bond angles (°) in **1**

N(1)-Zr(1)-Cl(1)	82.71(4)	C(17)-N(5)-Zr(1)	96.44(10)
N(1)-Zr(1)-N(2)	58.64(5)	C(17)-N(5)-C(22)	122.43(13)
N(1)-Zr(1)-N(4)	142.37(5)	C(22)-N(5)-Zr(1)	141.07(11)
N(1)-Zr(1)-N(5)	121.39(5)	C(17)-N(6)-Zr(1)	92.19(9)
N(1)-Zr(1)-N(6)	84.60(5)	C(17)-N(6)-C(19)	120.29(14)
N(2)-Zr(1)-Cl(1)	123.82(4)	C(19)-N(6)-Zr(1)	147.37(11)
N(2)-Zr(1)-N(6)	91.97(5)	N(1)-C(1)-C(2)	122.67(14)
N(3)-Zr(1)-Cl(1)	84.96(4)	N(2)-C(1)-N(1)	112.78(14)
N(3)-Zr(1)-N(1)	125.00(5)	N(2)-C(1)-C(2)	124.54(15)
N(3)-Zr(1)-N(2)	86.28(5)	N(1)-C(3)-C(4)	111.95(14)
N(3)-Zr(1)-N(4)	58.96(5)	N(1)-C(3)-C(5)	109.11(13)
N(3)-Zr(1)-N(5)	110.42(5)	C(4)-C(3)-C(5)	111.02(15)
N(3)-Zr(1)-N(6)	142.10(5)	N(2)-C(6)-C(7)	110.99(14)
N(4)-Zr(1)-Cl(1)	132.45(4)	N(2)-C(6)-C(8)	112.15(13)
N(4)-Zr(1)-N(2)	86.37(5)	C(8)-C(6)-C(7)	109.80(14)
N(4)-Zr(1)-N(6)	83.14(5)	N(3)-C(9)-C(10)	122.35(15)
N(5)-Zr(1)-Cl(1)	84.72(3)	N(4)-C(9)-N(3)	111.82(14)
N(5)-Zr(1)-N(2)	148.95(5)	N(4)-C(9)-C(10)	125.81(15)
N(5)-Zr(1)-N(4)	80.90(5)	N(3)-C(11)-C(12)	111.49(16)
N(5)-Zr(1)-N(6)	58.57(5)	N(3)-C(11)-C(13)	109.44(15)
N(6)-Zr(1)-Cl(1)	125.68(4)	C(13)-C(11)-C(12)	111.18(17)
C(1)-N(1)-Zr(1)	96.39(10)	N(4)-C(14)-C(15)	112.78(15)
C(1)-N(1)-C(3)	122.47(14)	N(4)-C(14)-C(16)	114.91(15)
C(3)-N(1)-Zr(1)	141.12(11)	C(16)-C(14)-C(15)	112.92(15)
C(1)-N(2)-Zr(1)	92.08(10)	N(5)-C(17)-C(18)	122.90(14)
C(1)-N(2)-C(6)	120.37(13)	N(6)-C(17)-N(5)	112.79(14)
C(6)-N(2)-Zr(1)	147.29(10)	N(6)-C(17)-C(18)	124.30(14)
C(9)-N(3)-Zr(1)	95.75(10)	N(6)-C(19)-C(20)	111.66(14)
C(9)-N(3)-C(11)	122.66(14)	N(6)-C(19)-C(21)	111.10(13)
C(11)-N(3)-Zr(1)	141.56(11)	C(21)-C(19)-C(20)	110.16(15)
C(9)-N(4)-Zr(1)	92.90(10)	N(5)-C(22)-C(23)	111.12(14)
C(9)-N(4)-C(14)	127.59(14)	N(5)-C(22)-C(24)	109.67(14)
C(14)-N(4)-Zr(1)	137.41(11)	C(24)-C(22)-C(23)	110.69(14)

Table B4. Anisotropic displacement parameters ($Å^2 \times 10^3$) for **1**. The anisotropic displacement factor exponent takes the form: $-2\pi^2[h^2a^{*2}U^{11} + 2hka^*b^*U^{12} + \ldots]$

	U^{11}	U^{22}	U^{33}	U^{23}	U^{13}	U^{12}
Zr(1)	14.12(8)	11.30(7)	14.59(7)	0.23(5)	1.15(5)	0.36(5)
Cl(1)	27.7(2)	13.27(16)	24.2(2)	-0.63(14)	-0.49(15)	3.43(14)
N(1)	19.6(7)	15.9(6)	17.3(6)	2.8(5)	1.0(5)	0.3(5)
N(2)	17.8(6)	19.3(6)	18.8(7)	1.8(5)	2.3(5)	1.6(5)
N(3)	24.0(7)	15.8(6)	16.1(6)	-1.3(5)	-0.5(5)	2.1(5)
N(4)	21.8(7)	14.7(6)	20.0(7)	3.6(5)	0.7(5)	-0.2(5)
N(5)	14.5(6)	17.0(6)	20.0(6)	-2.4(5)	2.3(5)	1.7(5)
N(6)	21.5(7)	15.0(6)	16.2(6)	-2.1(5)	3.6(5)	-1.6(5)
C(1)	18.0(7)	18.7(7)	15.8(7)	-0.7(6)	2.5(6)	-2.5(6)
C(2)	18.9(8)	39.6(10)	21.8(8)	6.7(7)	4.4(6)	-0.5(7)
C(3)	25.5(8)	20.4(8)	17.6(8)	5.0(6)	0.1(6)	-2.6(6)
C(4)	35.7(10)	24.5(9)	35.3(10)	12.8(8)	-4.8(8)	-7.9(8)
C(5)	27.0(9)	25.5(8)	23.1(9)	4.4(7)	-6.1(7)	0.0(7)
C(6)	16.1(7)	21.0(8)	22.3(8)	1.2(6)	2.5(6)	3.3(6)
C(7)	26.3(9)	24.1(9)	31.7(10)	-2.1(7)	0.0(7)	7.8(7)
C(8)	22.0(8)	29.9(9)	22.9(9)	3.8(7)	-1.0(7)	6.8(7)
C(9)	16.3(7)	21.3(8)	18.5(8)	2.6(6)	4.0(6)	5.4(6)
C(10)	27.9(9)	30.1(9)	17.7(8)	4.3(7)	2.1(7)	3.0(7)
C(11)	35(1)	19.3(8)	23.5(9)	-2.7(7)	-10.9(7)	1.8(7)
C(12)	58.6(14)	30.1(10)	26.8(10)	-10.9(8)	-10.3(9)	14.6(9)
C(13)	38.3(11)	24.7(9)	47.6(12)	2.8(9)	-13.3(9)	-9.9(8)
C(14)	29.7(9)	18.2(8)	26.8(9)	5.1(7)	0.3(7)	-3.1(7)
C(15)	35.7(10)	17.3(8)	29.7(9)	5.3(7)	3.1(8)	2.6(7)
C(16)	28.9(10)	29.8(10)	46.0(12)	10.7(9)	5.2(9)	-5.2(8)
C(17)	19.6(7)	15.0(7)	16.0(7)	3.1(6)	-0.5(6)	-0.8(6)
C(18)	20.3(8)	30.4(9)	30.8(10)	-8.0(7)	-0.1(7)	-4.1(7)
C(19)	26.4(8)	19.3(8)	17.9(8)	-4.0(6)	2.5(6)	-2.2(6)
C(20)	47.6(12)	15.8(8)	29.7(10)	-4.0(7)	13.2(8)	0.2(8)
C(21)	38.7(10)	24.7(9)	22.8(9)	-6.7(7)	11.4(8)	-5.0(8)
C(22)	17.0(7)	22.4(8)	25.9(8)	-0.6(7)	5.0(6)	3.6(6)
C(23)	21.6(8)	26.5(9)	35.6(10)	-4.1(8)	-2.6(7)	7.3(7)

Table B4. Continued

	U^{11}	U^{22}	U^{33}	U^{23}	U^{13}	U^{12}
C(24)	30.0(9)	31.2(10)	24.5(9)	-2.9(7)	7.5(7)	7.3(8)

Table B5. Atomic coordinates ($\times 10^4$) and equivalent isotropic displacement parameters ($Å^2 \times 10^3$) for **2**. U(eq) is defined as one third of the trace of the orthogonalized U^{ij}

	x	y	z	U(eq)
Hf(1)	5186.6(2)	7590.2(2)	7433.8(2)	14.55(9)
Cl(1)	5827.5(17)	9052.6(9)	7359.7(10)	20.9(3)
N(1)	4394(7)	7785(4)	6241(3)	20.5(13)
N(2)	5158(6)	6576(3)	6542(3)	17.7(12)
N(3)	7260(6)	7353(3)	7423(4)	17.7(12)
N(4)	6154(6)	6626(4)	8248(3)	17.1(12)
N(5)	4312(6)	8006(4)	8508(3)	16.5(12)
N(6)	3173(6)	7167(4)	7727(4)	18.9(12)
C(1)	4679(7)	7037(4)	5967(4)	18.2(14)
C(2)	4461(8)	6791(5)	5124(4)	23.1(16)
C(3)	3719(9)	8393(5)	5739(5)	27.3(18)
C(4)	4672(11)	8950(6)	5351(5)	42(2)
C(5)	2808(9)	8883(5)	6217(6)	37(2)
C(6)	5732(8)	5757(5)	6466(4)	23.3(16)
C(7)	4745(8)	5110(4)	6219(5)	26.2(17)
C(8)	6918(9)	5723(6)	6003(6)	34(2)
C(9)	7302(7)	6780(5)	7977(4)	18.1(14)
C(10)	8518(8)	6337(5)	8242(5)	28.0(17)
C(11)	8421(7)	7638(5)	7055(4)	21.6(15)
C(12)	8063(9)	7957(6)	6234(5)	30.6(19)
C(13)	9116(7)	8283(5)	7556(5)	27.0(17)
C(14)	6024(8)	6037(4)	8888(4)	21.4(15)
C(15)	4933(9)	6269(5)	9388(4)	28.6(18)
C(16)	5811(10)	5171(5)	8564(5)	31.9(19)
C(17)	3199(7)	7623(5)	8376(4)	18.5(14)
C(18)	2104(8)	7689(6)	8920(5)	27.9(17)
C(19)	4582(8)	8526(4)	9196(4)	20.7(15)
C(20)	4041(9)	9393(5)	9070(5)	32.0(19)
C(21)	6012(8)	8549(5)	9385(5)	25.8(17)

Table B5. Continued

	x	y	z	U(eq)
C(22)	2012(7)	6714(4)	7478(5)	20.0(14)
C(23)	2008(8)	5864(5)	7861(5)	26.9(17)
C(24)	1839(8)	6633(5)	6593(4)	24.2(16)

Table B6. Bond lengths (Å) in **2**

Hf(1)-Cl(1)	2.5014(16)	N(6)-C(17)	1.339(9)
Hf(1)-N(1)	2.183(6)	N(6)-C(22)	1.466(9)
Hf(1)-N(2)	2.259(5)	C(1)-C(2)	1.502(9)
Hf(1)-N(3)	2.199(6)	C(3)-C(4)	1.529(12)
Hf(1)-N(4)	2.306(6)	C(3)-C(5)	1.518(12)
Hf(1)-N(5)	2.202(6)	C(6)-C(7)	1.526(11)
Hf(1)-N(6)	2.293(6)	C(6)-C(8)	1.505(12)
N(1)-C(1)	1.354(9)	C(9)-C(10)	1.511(11)
N(1)-C(3)	1.472(9)	C(11)-C(12)	1.526(11)
N(2)-C(1)	1.319(9)	C(11)-C(13)	1.522(11)
N(2)-C(6)	1.482(9)	C(14)-C(15)	1.508(11)
N(3)-C(9)	1.335(9)	C(14)-C(16)	1.540(11)
N(3)-C(11)	1.470(9)	C(17)-C(18)	1.514(10)
N(4)-C(9)	1.331(10)	C(19)-C(20)	1.545(11)
N(4)-C(14)	1.472(9)	C(19)-C(21)	1.510(11)
N(5)-C(17)	1.330(9)	C(22)-C(23)	1.543(10)
N(5)-C(19)	1.469(9)	C(22)-C(24)	1.519(11)

Table B7. Bond angles (°) in **2**

N(1)-Hf(1)-Cl(1)	84.30(16)	C(17)-N(5)-Hf(1)	96.2(4)
N(1)-Hf(1)-N(2)	59.2(2)	C(17)-N(5)-C(19)	122.7(6)
N(1)-Hf(1)-N(3)	110.0(2)	C(19)-N(5)-Hf(1)	141.1(5)
N(1)-Hf(1)-N(4)	142.8(2)	C(17)-N(6)-Hf(1)	91.9(4)
N(1)-Hf(1)-N(5)	125.5(2)	C(17)-N(6)-C(22)	120.4(6)
N(1)-Hf(1)-N(6)	86.7(2)	C(22)-N(6)-Hf(1)	147.5(5)
N(2)-Hf(1)-Cl(1)	132.08(16)	N(1)-C(1)-C(2)	123.4(7)
N(2)-Hf(1)-N(4)	83.6(2)	N(1)-C(1)-N(2)	110.3(6)
N(2)-Hf(1)-N(6)	86.8(2)	N(2)-C(1)-C(2)	126.3(7)
N(3)-Hf(1)-Cl(1)	84.52(15)	N(1)-C(3)-C(4)	111.0(7)
N(3)-Hf(1)-N(2)	80.8(2)	N(1)-C(3)-C(5)	109.9(7)
N(3)-Hf(1)-N(4)	58.9(2)	C(4)-C(3)-C(5)	110.8(8)
N(3)-Hf(1)-N(5)	120.9(2)	N(2)-C(6)-C(7)	112.8(6)
N(3)-Hf(1)-N(6)	149.4(2)	N(2)-C(6)-C(8)	115.3(7)
N(4)-Hf(1)-Cl(1)	125.58(17)	C(7)-C(6)-C(8)	112.9(7)
N(5)-Hf(1)-Cl(1)	82.36(16)	N(3)-C(9)-C(10)	123.3(7)
N(5)-Hf(1)-N(2)	143.2(2)	N(3)-C(9)-N(4)	112.6(6)
N(4)-Hf(1)-N(5)	84.1(2)	N(4)-C(9)-C(10)	124.1(7)
N(5)-Hf(1)-N(6)	59.2(2)	N(3)-C(11)-C(12)	109.6(6)
N(6)-Hf(1)-Cl(1)	123.58(15)	N(3)-C(11)-C(13)	111.2(6)
N(6)-Hf(1)-N(4)	92.1(2)	C(13)-C(11)-C(12)	111.3(7)
C(1)-N(1)-Hf(1)	96.3(4)	N(4)-C(14)-C(15)	111.0(6)
C(1)-N(1)-C(3)	121.5(6)	N(4)-C(14)-C(16)	111.0(6)
C(3)-N(1)-Hf(1)	142.2(5)	C(15)-C(14)-C(16)	109.8(7)
C(1)-N(2)-Hf(1)	93.9(4)	N(5)-C(17)-N(6)	112.6(6)
C(1)-N(2)-C(6)	126.6(6)	N(5)-C(17)-C(18)	122.9(6)
C(6)-N(2)-Hf(1)	137.7(5)	N(6)-C(17)-C(18)	124.5(7)
C(9)-N(3)-Hf(1)	96.6(4)	N(5)-C(19)-C(20)	111.9(6)
C(9)-N(3)-C(11)	122.1(6)	N(5)-C(19)-C(21)	109.3(6)
C(11)-N(3)-Hf(1)	141.3(5)	C(21)-C(19)-C(20)	110.9(7)
C(9)-N(4)-Hf(1)	91.9(4)	N(6)-C(22)-C(23)	111.0(6)
C(9)-N(4)-C(14)	120.3(6)	N(6)-C(22)-C(24)	112.7(6)
C(14)-N(4)-Hf(1)	147.7(5)	C(24)-C(22)-C(23)	109.9(6)

Table B8. Anisotropic displacement parameters ($Å^2 \times 10^3$) for **2**. The anisotropic displacement factor exponent takes the form: $-2\pi^2[h^2a^{*2}U^{11} + 2hka^*b^*U^{12} + \ldots]$

	U^{11}	U^{22}	U^{33}	U^{23}	U^{13}	U^{12}
Hf(1)	15.03(13)	10.87(13)	17.85(15)	-0.14(10)	1.81(9)	-0.17(14)
Cl(1)	27.1(10)	10.6(7)	25.0(8)	0.4(6)	-0.2(7)	-3.1(6)
N(1)	31(4)	13(3)	17(3)	-2(2)	-5(2)	-3(2)
N(2)	24(3)	13(3)	16(3)	-3(2)	0(2)	3(2)
N(3)	22(3)	10(3)	21(3)	2(2)	4(2)	-3(2)
N(4)	25(3)	14(3)	12(3)	4(2)	6(2)	7(2)
N(5)	20(3)	12(3)	18(3)	-2(2)	2(2)	1(2)
N(6)	21(3)	13(3)	23(3)	-4(2)	5(2)	2(2)
C(1)	20(4)	23(4)	11(3)	-6(2)	-3(3)	-9(3)
C(2)	27(4)	32(4)	11(3)	-5(3)	2(3)	-6(3)
C(3)	40(5)	17(4)	24(4)	1(3)	-13(3)	2(3)
C(4)	70(7)	29(5)	25(4)	10(3)	-11(4)	-18(5)
C(5)	41(5)	22(4)	46(5)	-6(4)	-15(4)	11(4)
C(6)	34(4)	19(4)	16(3)	-4(3)	-1(3)	5(3)
C(7)	34(5)	17(4)	28(4)	-5(3)	1(3)	1(3)
C(8)	28(5)	26(5)	48(5)	-10(4)	5(4)	6(4)
C(9)	21(4)	18(4)	16(3)	-4(3)	0(3)	1(3)
C(10)	22(4)	33(5)	29(4)	7(3)	1(3)	2(3)
C(11)	16(3)	18(4)	31(4)	-1(3)	7(3)	-4(3)
C(12)	33(5)	35(5)	24(4)	6(3)	9(3)	-11(4)
C(13)	17(4)	26(4)	38(4)	4(3)	-1(3)	-6(3)
C(14)	33(4)	17(4)	14(3)	3(3)	4(3)	1(3)
C(15)	42(5)	24(4)	20(4)	5(3)	8(3)	4(4)
C(16)	51(6)	16(4)	30(4)	4(3)	12(4)	2(4)
C(17)	20(3)	20(4)	15(3)	1(3)	2(2)	3(3)
C(18)	24(4)	38(5)	22(4)	-5(3)	4(3)	-2(3)
C(19)	24(4)	18(4)	20(3)	-3(3)	1(3)	2(3)
C(20)	32(5)	23(4)	41(5)	-11(3)	-4(4)	6(3)
C(21)	28(4)	24(4)	24(4)	-7(3)	-7(3)	1(3)
C(22)	16(4)	17(3)	28(4)	0(3)	4(3)	-3(3)
C(23)	29(4)	21(4)	31(4)	0(3)	3(3)	-8(3)

Table B8. Continued

	U^{11}	U^{22}	U^{33}	U^{23}	U^{13}	U^{12}
C(24)	20(4)	28(4)	24(4)	-1(3)	-2(3)	-5(3)

Table B9. Atomic coordinates ($\times 10^4$) and equivalent isotropic displacement parameters ($Å^2 \times 10^3$) for **6**. U(eq) is defined as one third of the trace of the orthogonalized U^{ij}

	x	y	z	U(eq)
Zr(1)	8651.2(2)	2107.1(2)	3392.0(2)	13.62(4)
N(1)	7673.5(5)	1558.8(8)	2945.8(7)	16.0(2)
N(2)	7928.1(6)	1986.4(8)	4105.6(7)	16.5(2)
N(3)	8622.8(6)	3517.8(8)	3559.4(7)	20.3(3)
N(4)	9214.6(6)	2780.3(8)	4489.1(7)	17.8(2)
N(5)	9701.0(6)	1927.0(8)	3323.5(7)	17.7(2)
N(6)	9156.9(5)	869.5(8)	3682.0(7)	15.6(2)
C(1)	7458.3(7)	1779.5(9)	3538.8(8)	16.5(3)
C(2)	6764.5(7)	1821.8(12)	3550.8(9)	26.3(3)
C(3)	7274.7(7)	1270.7(10)	2236.8(8)	20.2(3)
C(4)	6985.4(8)	385.1(11)	2281.6(10)	27.8(4)
C(5)	6777.6(8)	1917.3(12)	1840.5(9)	29.2(4)
C(6)	7857.7(7)	2317.6(10)	4823.2(8)	19.1(3)
C(7)	7640.3(8)	1630.9(11)	5300.2(9)	25.6(3)
C(8)	7470.7(8)	3142.3(11)	4787(1)	29.2(4)
C(9)	9004.0(7)	3539.8(9)	4247.4(9)	20.0(3)
C(10)	9161.9(8)	4360.7(10)	4684.8(10)	29.9(4)
C(11)	8298.7(8)	4288.3(10)	3208.6(10)	26.7(4)
C(12)	7650.3(8)	4035.9(11)	2747.6(10)	31.2(4)
C(13)	8682.7(9)	4740.6(12)	2730.0(12)	41.8(5)
C(14)	9649.2(7)	2645.1(10)	5211.4(9)	21.2(3)
C(15)	9566.8(8)	1743.3(10)	5483.9(9)	26.4(3)
C(16)	10341.6(8)	2785.8(14)	5179.9(10)	35.7(4)
C(17)	9717.9(7)	1135.8(9)	3568.9(8)	17.2(3)
C(18)	10303.6(7)	580.7(11)	3739.1(10)	25.6(3)
C(19)	10255.7(7)	2370.5(10)	3183.1(9)	22.0(3)
C(20)	10407.5(8)	2095.1(12)	2454.7(10)	30.8(4)
C(21)	10149.9(8)	3334.6(11)	3181.4(10)	28.3(4)
C(22)	9061.6(7)	-15.0(9)	3892.4(8)	18.2(3)

Table B9. Continued

	x	y	z	U(eq)
C(23)	8527.9(7)	-54.1(10)	4297.3(9)	22.0(3)
C(24)	8910.7(8)	-595.9(11)	3213.9(10)	28.0(4)
C(25)	8575.3(7)	2246.5(10)	2132.1(9)	22.4(3)
C(26)	8749.0(8)	1431.0(12)	1755.7(9)	28.9(4)
Zr(2)	6250.7(2)	7297.5(2)	4667.2(2)	11.21(4)
N(7)	5389.2(6)	7983.5(8)	4861.4(7)	15.3(2)
N(8)	5605.5(5)	8109.9(8)	3770.3(6)	14.8(2)
N(9)	7293.6(6)	7000.4(8)	5258.3(7)	16.7(2)
N(10)	6935.9(6)	8340.0(8)	5139.2(7)	16.4(2)
N(11)	5954.2(6)	6180.7(8)	3922.3(7)	15.7(2)
N(12)	6708.7(5)	7009.0(8)	3667.1(7)	15.1(2)
C(27)	5176.5(6)	8247.0(9)	4161.6(8)	14.6(3)
C(28)	4531.8(7)	8641.4(10)	3864.8(8)	20.3(3)
C(29)	5027.3(7)	8024.7(10)	5435.9(8)	18.7(3)
C(30)	5024.6(8)	8922.5(11)	5765.2(9)	25.7(3)
C(31)	4362.7(7)	7633.2(10)	5230.4(9)	23.7(3)
C(32)	5501.9(7)	8215(1)	2967.1(8)	18.5(3)
C(33)	4945.8(8)	7698.9(12)	2515.7(9)	28.2(4)
C(34)	5480.8(8)	9153.5(11)	2717.3(9)	26.9(3)
C(35)	7437.7(7)	7818.0(9)	5360.8(8)	16.7(3)
C(36)	8101.0(7)	8140.2(11)	5683.0(9)	25.9(3)
C(37)	7766.6(7)	6316.7(10)	5442.9(9)	21.7(3)
C(38)	7958.1(8)	6135.5(12)	6275.6(9)	30.6(4)
C(39)	7509.1(8)	5503.8(10)	5032.2(10)	28.4(4)
C(40)	6995.2(7)	9268.5(9)	5250.3(8)	19.5(3)
C(41)	6451.0(8)	9716.1(10)	4724.4(10)	28.6(4)
C(42)	6999.8(9)	9507.4(11)	6048.5(9)	32.2(4)
C(43)	6334.9(7)	6349.1(9)	3460.5(8)	16.2(3)
C(44)	6308.1(8)	5830.8(11)	2765.2(9)	25.9(3)
C(45)	5493.5(7)	5480.4(9)	3781.3(8)	18.7(3)
C(46)	4911.8(7)	5728.9(10)	4057.2(9)	23.9(3)
C(47)	5779.0(8)	4648.3(10)	4144(1)	27.7(4)

Table B9. Continued

	x	y	z	U(eq)
C(48)	7162.4(7)	7308.7(10)	3250.2(8)	19.5(3)
C(49)	7298.4(8)	8253.3(10)	3408.1(9)	24.6(3)
C(50)	7778.8(8)	6794.7(13)	3436.5(11)	34.0(4)
C(51)	6101.5(7)	6514.8(9)	5670.5(8)	16.4(3)
C(52)	6401.4(7)	6936.1(11)	6419.3(8)	22.2(3)

Table B10. Bond lengths (Å) in **6**

Zr(1)-N(1)	2.2600(13)	Zr(2)-N(7)	2.2552(13)
Zr(1)-N(2)	2.2856(13)	Zr(2)-N(8)	2.2956(12)
Zr(1)-N(3)	2.2281(15)	Zr(2)-N(9)	2.3221(14)
Zr(1)-N(4)	2.3678(14)	Zr(2)-N(10)	2.2422(13)
Zr(1)-N(5)	2.3278(14)	Zr(2)-N(11)	2.2278(13)
Zr(1)-N(6)	2.2265(13)	Zr(2)-N(12)	2.3468(13)
Zr(1)-C(25)	2.3207(17)	Zr(2)-C(51)	2.3154(15)
N(1)-C(1)	1.3385(19)	N(7)-C(27)	1.3407(18)
N(1)-C(3)	1.4699(19)	N(7)-C(29)	1.4666(18)
N(2)-C(1)	1.3253(19)	N(8)-C(27)	1.3251(18)
N(2)-C(6)	1.4719(19)	N(8)-C(32)	1.4673(18)
N(3)-C(9)	1.353(2)	N(9)-C(35)	1.3181(19)
N(3)-C(11)	1.4683(19)	N(9)-C(37)	1.4657(18)
N(4)-C(9)	1.3127(19)	N(10)-C(35)	1.3461(19)
N(4)-C(14)	1.4667(19)	N(10)-C(40)	1.4664(19)
N(5)-C(17)	1.315(2)	N(11)-C(43)	1.3484(19)
N(5)-C(19)	1.4637(19)	N(11)-C(45)	1.4639(18)
N(6)-C(17)	1.3481(19)	N(12)-C(43)	1.3128(19)
N(6)-C(22)	1.4635(18)	N(12)-C(48)	1.4639(18)
C(1)-C(2)	1.512(2)	C(27)-C(28)	1.511(2)
C(3)-C(4)	1.529(2)	C(29)-C(30)	1.531(2)
C(3)-C(5)	1.536(2)	C(29)-C(31)	1.531(2)
C(6)-C(7)	1.534(2)	C(32)-C(33)	1.530(2)
C(6)-C(8)	1.531(2)	C(32)-C(34)	1.535(2)
C(9)-C(10)	1.515(2)	C(35)-C(36)	1.511(2)
C(11)-C(12)	1.520(2)	C(37)-C(38)	1.534(2)
C(11)-C(13)	1.526(2)	C(37)-C(39)	1.520(2)
C(14)-C(15)	1.522(2)	C(40)-C(41)	1.518(2)
C(14)-C(16)	1.533(2)	C(40)-C(42)	1.528(2)
C(17)-C(18)	1.510(2)	C(43)-C(44)	1.515(2)
C(19)-C(20)	1.528(2)	C(45)-C(46)	1.519(2)
C(19)-C(21)	1.523(2)	C(45)-C(47)	1.528(2)
C(22)-C(23)	1.522(2)	C(48)-C(49)	1.520(2)

Table B10. Continued

C(22)-C(24)	1.527(2)	C(48)-C(50)	1.529(2)
C(25)-C(26)	1.542(2)	C(51)-C(52)	1.541(2)

Table B11. Bond angles (°) in **6**

N(1)-Zr(1)-N(2)	57.96(5)	N(7)-Zr(2)-N(8)	57.67(4)
N(1)-Zr(1)-N(4)	137.56(4)	N(7)-Zr(2)-N(9)	140.56(5)
N(1)-Zr(1)-N(5)	141.39(5)	N(7)-Zr(2)-N(12)	137.50(4)
N(1)-Zr(1)-C(25)	79.85(5)	N(7)-Zr(2)-C(51)	81.14(5)
N(2)-Zr(1)-N(4)	79.82(5)	N(8)-Zr(2)-N(9)	144.87(4)
N(2)-Zr(1)-N(5)	146.51(4)	N(8)-Zr(2)-N(12)	80.17(5)
N(2)-Zr(1)-C(25)	134.13(5)	N(8)-Zr(2)-C(51)	134.57(5)
N(3)-Zr(1)-N(1)	111.84(5)	N(9)-Zr(2)-N(12)	77.96(5)
N(3)-Zr(1)-N(2)	87.45(5)	N(10)-Zr(2)-N(7)	95.25(5)
N(3)-Zr(1)-N(4)	57.72(4)	N(10)-Zr(2)-N(8)	96.92(5)
N(3)-Zr(1)-N(5)	100.74(5)	N(10)-Zr(2)-N(9)	58.31(5)
N(3)-Zr(1)-C(25)	92.90(5)	N(10)-Zr(2)-N(12)	94.90(5)
N(5)-Zr(1)-N(4)	77.55(5)	N(10)-Zr(2)-C(51)	105.78(5)
N(6)-Zr(1)-N(1)	97.36(5)	N(11)-Zr(2)-N(7)	109.93(5)
N(6)-Zr(1)-N(2)	98.85(5)	N(11)-Zr(2)-N(8)	86.64(5)
N(6)-Zr(1)-N(3)	148.51(5)	N(11)-Zr(2)-N(9)	104.31(5)
N(6)-Zr(1)-N(4)	92.85(5)	N(11)-Zr(2)-N(10)	151.86(4)
N(6)-Zr(1)-N(5)	58.31(4)	N(11)-Zr(2)-N(12)	58.07(4)
N(6)-Zr(1)-C(25)	103.99(5)	N(11)-Zr(2)-C(51)	90.77(5)
C(25)-Zr(1)-N(4)	136.88(5)	C(51)-Zr(2)-N(9)	79.39(5)
C(25)-Zr(1)-N(5)	78.31(5)	C(51)-Zr(2)-N(12)	134.53(5)
C(1)-N(1)-Zr(1)	94.41(9)	C(27)-N(7)-Zr(2)	95.86(9)
C(1)-N(1)-C(3)	124.94(12)	C(27)-N(7)-C(29)	124.86(12)
C(3)-N(1)-Zr(1)	138.83(9)	C(29)-N(7)-Zr(2)	137.83(9)
C(1)-N(2)-Zr(1)	93.63(9)	C(27)-N(8)-Zr(2)	94.47(9)
C(1)-N(2)-C(6)	125.77(13)	C(27)-N(8)-C(32)	125.42(12)
C(6)-N(2)-Zr(1)	136.63(9)	C(32)-N(8)-Zr(2)	136.49(9)
C(9)-N(3)-Zr(1)	97.27(9)	C(35)-N(9)-Zr(2)	92.71(9)
C(9)-N(3)-C(11)	121.61(13)	C(35)-N(9)-C(37)	122.84(13)
C(11)N(3)-Zr(1)	140.75(11)	C(37)-N(9)-Zr(2)	144.02(10)
C(9)-N(4)-Zr(1)	92.12(10)	C(35)-N(10)-Zr(2)	95.51(9)
C(9)-N(4)-C(14)	122.86(13)	C(35)-N(10)-C(40)	121.17(12)
C(14)-N(4)-Zr(1)	145.01(10)	C(40)-N(10)-Zr(2)	143.31(10)

Table B11. Continued

C(17)-N(5)-Zr(1)	92.49(9)	C(43)-N(11)-Zr(2)	96.43(9)
C(17)-N(5)-C(19)	123.28(13)	C(43)-N(11)-C(45)	121.70(12)
C(19)-N(5)-Zr(1)	143.91(10)	C(45)-N(11)-Zr(2)	141.56(9)
C(17)-N(6)-Zr(1)	96.11(9)	C(43)-N(12)-Zr(2)	92.08(9)
C(17)-N(6)-C(22)	121.44(12)	C(43)-N(12)-C(48)	122.81(12)
C(22)-N(6)-Zr(1)	142.38(9)	C(48)-N(12)-Zr(2)	144.95(10)
N(1)-C(1)-C(2)	124.19(13)	N(7)-C(27)-C(28)	124.12(13)
N(2)-C(1)-N(1)	111.55(13)	N(8)-C(27)-N(7)	110.85(12)
N(2)-C(1)-C(2)	124.22(14)	N(8)-C(27)-C(28)	125.03(13)
N(1)-C(3)-C(4)	113.06(13)	N(7)-C(29)-C(30)	112.59(12)
N(1)-C(3)-C(5)	115.54(13)	N(7)-C(29)-C(31)	115.66(13)
C(4)-C(3)-C(5)	111.68(13)	C(30)-C(29)-C(31)	112.02(13)
N(2)-C(6)-C(7)	112.90(12)	N(8)-C(32)-C(33)	114.51(12)
N(2)-C(6)-C(8)	115.28(13)	N(8)-C(32)-C(34)	113.68(13)
C(8)-C(6)-C(7)	112.01(13)	C(33)-C(32)-C(34)	111.88(13)
N(3)-C(9)-C(10)	122.81(14)	N(9)-C(35)-N(10)	113.24(13)
N(4)-C(9)-N(3)	112.87(13)	N(9)-C(35)-C(36)	123.52(13)
N(4)-C(9)-C(10)	124.31(15)	N(10)-C(35)-C(36)	123.23(13)
N(3)-C(11)-C(12)	108.88(13)	N(9)-C(37)-C(38)	112.46(13)
N(3)-C(11)-C(13)	111.62(14)	N(9)-C(37)-C(39)	109.58(12)
C(12)-C(11)-C(13)	110.49(16)	C(39)-C(37)-C(38)	109.59(14)
N(4)-C(14)-C(15)	109.76(12)	N(10)-C(40)-C(41)	109.57(12)
N(4)-C(14)-C(16)	111.86(13)	N(10)-C(40)-C(42)	111.04(13)
C(15)-C(14)-C(16)	109.72(14)	C(41)-C(40)-C(42)	110.02(14)
N(5)-C(17)-N(6)	112.99(12)	N(11)-C(43)-C(44)	122.10(13)
N(5)-C(17)-C(18)	124.52(14)	N(12)-C(43)-N(11)	113.27(12)
N(6)-C(17)-C(18)	122.45(13)	N(12)-C(43)-C(44)	124.61(13)
N(5)-C(19)-C(20)	112.34(14)	N(11)-C(45)-C(46)	109.57(12)
N(5)-C(19)-C(21)	109.78(12)	N(11)-C(45)-C(47)	111.49(12)
C(21)-C(19)-C(20)	109.86(13)	C(46)-C(45)-C(47)	110.61(13)
N(6)-C(22)-C(23)	109.94(12)	N(12)-C(48)-C(49)	109.41(12)
N(6)-C(22)-C(24)	110.89(13)	N(12)-C(48)-C(50)	111.86(13)

Table B11. Continued

C(23)-C(22)-C(24)	110.06(13)	C(49)-C(48)-C(50)	110.20(14)
C(26)-C(25)-Zr(1)	114.41(10)	C(52)-C(51)-Zr(2)	113.20(10)

Table B12. Anisotropic displacement parameters ($Å^2 \times 10^3$) for **6**. The anisotropic displacement factor exponent takes the form: $-2\pi^2[h^2a^{*2}U^{11} + 2hka^*b^*U^{12} + \ldots]$

	U^{11}	U^{22}	U^{33}	U^{23}	U^{13}	U^{12}
Zr(1)	10.89(7)	14.99(7)	14.65(7)	2.68(5)	2.28(5)	1.06(5)
N(1)	12.5(6)	20.2(6)	15.5(6)	0.0(5)	3.5(5)	0.1(5)
N(2)	15.9(6)	17.5(6)	16.9(6)	-1.5(5)	5.0(5)	-0.8(5)
N(3)	16.4(6)	17.2(6)	26.3(7)	5.4(5)	2.8(5)	0.4(5)
N(4)	14.3(6)	18.9(6)	19.2(6)	0.1(5)	1.7(5)	-0.8(5)
N(5)	12.5(6)	22.2(6)	18.5(6)	4.7(5)	4.0(5)	0.7(5)
N(6)	14.3(6)	16.1(6)	16.2(6)	2.3(5)	3.3(5)	2.1(4)
C(1)	15.2(7)	13.9(6)	20.6(7)	2.6(5)	4.4(6)	1.2(5)
C(2)	16.0(7)	39.2(9)	24.6(8)	-4.1(7)	6.4(6)	-0.8(7)
C(3)	15.0(7)	28.0(8)	16.8(7)	-1.5(6)	1.8(6)	-0.4(6)
C(4)	27.1(9)	27.1(8)	27.4(9)	-5.8(7)	2.8(7)	-3.1(7)
C(5)	22.4(8)	36.3(9)	24.5(8)	5.4(7)	-3.3(7)	0.6(7)
C(6)	18.8(7)	21.7(7)	18.0(7)	-4.6(6)	6.4(6)	-3.4(6)
C(7)	30.7(9)	29.1(8)	19.1(8)	-3.8(6)	10.0(7)	-6.7(7)
C(8)	30.9(9)	24.8(8)	34.1(9)	-8.4(7)	12.1(7)	0.8(7)
C(9)	16.6(7)	19.0(7)	25.8(8)	0.6(6)	7.7(6)	-2.2(6)
C(10)	30.8(9)	20.7(8)	37.1(10)	-5.4(7)	5.8(7)	-3.7(7)
C(11)	27.5(9)	16.9(7)	35.7(9)	7.8(7)	7.1(7)	5.3(6)
C(12)	26.2(9)	27.6(9)	37.3(10)	11.5(7)	2.5(7)	8.4(7)
C(13)	37.6(11)	30.8(10)	58.7(13)	24.2(9)	14.8(10)	2.8(8)
C(14)	17.9(7)	25.6(8)	18.6(7)	-2.5(6)	0.8(6)	-0.3(6)
C(15)	28.3(9)	26.2(8)	21.0(8)	0.8(6)	-2.2(6)	3.7(7)
C(16)	18.5(8)	57.1(12)	28.4(9)	2.6(8)	-0.6(7)	-4.6(8)
C(17)	14.9(7)	22.5(7)	13.4(7)	0.4(5)	1.6(5)	3.1(5)
C(18)	17.0(7)	28.9(8)	31.6(9)	7.2(7)	6.6(6)	6.3(6)
C(19)	13.0(7)	29.5(8)	23.6(8)	7.0(6)	4.6(6)	-0.8(6)
C(20)	25.3(9)	39.9(10)	31.6(9)	6.7(8)	15.5(7)	0.0(7)
C(21)	20.9(8)	30.7(9)	35.0(9)	6.2(7)	9.7(7)	-6.4(7)
C(22)	18.8(7)	15.2(7)	20.0(7)	1.8(6)	3.6(6)	2.5(5)

Table B12. Continue

	U^{11}	U^{22}	U^{33}	U^{23}	U^{13}	U^{12}
C(23)	25.7(8)	17.5(7)	23.7(8)	2.2(6)	7.9(6)	-1.4(6)
C(24)	30.0(9)	24.2(8)	31.7(9)	-8.2(7)	11.3(7)	-2.6(7)
C(25)	16.0(7)	31.9(9)	18.7(7)	7.7(6)	2.9(6)	-0.1(6)
C(26)	21.9(8)	46.2(10)	19.0(8)	-0.6(7)	5.9(6)	-0.6(7)
Zr(2)	10.66(7)	12.65(7)	9.91(7)	0.23(5)	1.58(5)	-0.56(4)
N(7)	13.2(6)	19.5(6)	13.8(6)	2.4(5)	4.3(5)	2.8(4)
N(8)	14.8(6)	17.0(6)	11.9(6)	2.7(4)	2.1(4)	1.3(4)
N(9)	13.2(6)	19.6(6)	16.5(6)	4.2(5)	1.8(5)	2.2(5)
N(10)	15.8(6)	15.5(6)	16.5(6)	-0.4(5)	1.0(5)	-2.3(5)
N(11)	17.3(6)	15.3(6)	14.3(6)	-1.6(5)	3.3(5)	-2.9(5)
N(12)	12.7(6)	18.7(6)	14.4(6)	0.4(5)	4.1(5)	0.1(4)
C(27)	13.3(6)	12.8(6)	17.0(7)	-0.3(5)	1.9(5)	-1.1(5)
C(28)	16.3(7)	25.3(8)	18.7(7)	3.3(6)	2.9(6)	4.6(6)
C(29)	18.1(7)	25.3(8)	14.4(7)	1.4(6)	7.2(6)	4.5(6)
C(30)	26.0(8)	30.3(9)	22.4(8)	-5.5(7)	8.6(6)	2.1(7)
C(31)	21.9(8)	25.8(8)	26.9(8)	3.6(6)	12.7(6)	1.7(6)
C(32)	17.8(7)	25.0(8)	12.3(7)	4.4(6)	3.0(5)	3.2(6)
C(33)	28.6(9)	39.2(10)	14.9(7)	-2.6(7)	1.0(6)	-3.0(7)
C(34)	28.6(9)	30.1(9)	22.2(8)	12.1(7)	6.1(7)	5.1(7)
C(35)	13.7(7)	23.7(7)	12.1(7)	2.5(5)	1.9(5)	-2.5(5)
C(36)	15.6(7)	30.6(9)	28.1(9)	4.3(7)	-1.6(6)	-4.6(6)
C(37)	15.7(7)	24.8(8)	24.6(8)	7.9(6)	4.4(6)	4.9(6)
C(38)	28.1(9)	33.8(9)	26.2(9)	11.7(7)	-1.1(7)	5.7(7)
C(39)	27.5(9)	23.8(8)	33.4(9)	4.0(7)	6.2(7)	9.3(7)
C(40)	20.1(7)	17.1(7)	20.3(7)	-1.7(6)	3.0(6)	-5.8(6)
C(41)	33.7(9)	14.7(7)	33.0(9)	-0.9(6)	-0.9(7)	-1.1(6)
C(42)	43.2(11)	28.4(9)	24.4(9)	-7.9(7)	6.5(8)	-1.8(8)
C(43)	18.6(7)	16.5(7)	13.0(7)	1.6(5)	2.5(5)	4.5(5)
C(44)	32.7(9)	26.5(8)	20.7(8)	-6.7(6)	10.6(7)	-3.4(7)
C(45)	22.2(7)	16.4(7)	16.7(7)	-3.4(5)	2.8(6)	-4.8(6)
C(46)	20.9(8)	25.1(8)	25.6(8)	-2.7(6)	5.0(6)	-6.0(6)
C(47)	31.3(9)	17.4(7)	35.0(9)	1.0(7)	8.6(7)	-3.5(6)

Table B12. Continued

	U^{11}	U^{22}	U^{33}	U^{23}	U^{13}	U^{12}
C(48)	18.4(7)	24.7(8)	17.3(7)	3.6(6)	7.7(6)	1.0(6)
C(49)	23.8(8)	27.6(8)	24.0(8)	2.2(6)	8.9(6)	-6.7(6)
C(50)	23.3(9)	40.8(10)	43.0(11)	12.5(8)	18.1(8)	8.3(7)
C(51)	17.0(7)	17.3(7)	14.8(7)	1.3(5)	3.5(5)	0.8(5)
C(52)	21.9(8)	30.0(8)	15.0(7)	0.9(6)	5.1(6)	2.5(6)

Table B13. Atomic coordinates ($\times 10^4$) and equivalent isotropic displacement parameters ($Å^2 \times 10^3$) for **7**. U(eq) is defined as one third of the trace of the orthogonalized U^{ij}

	x	y	z	U(eq)
Hf(1)	3751.7(2)	7290.3(2)	5334.9(2)	8.38(3)
N(1)	4615.4(8)	7962.1(11)	5152.3(9)	11.5(3)
N(2)	4394.5(8)	8094.1(11)	6237.0(9)	10.9(3)
N(3)	4048.0(8)	6178.7(11)	6071.4(9)	11.4(3)
N(4)	3293.4(8)	7011.0(11)	6325.4(9)	10.7(3)
N(5)	2708.5(8)	6999.9(11)	4753.2(10)	12.6(3)
N(6)	3076.8(8)	8335.9(11)	4866.3(9)	12.0(3)
C(1)	4823.2(9)	8238.0(12)	5849.0(11)	11.0(4)
C(2)	5464.1(10)	8654.7(14)	6144.1(12)	17.0(4)
C(3)	4975.1(10)	8008.4(14)	4579.4(11)	14.1(4)
C(4)	4965.1(11)	8902.2(15)	4239.3(13)	20.5(5)
C(5)	5647.9(10)	7634.5(14)	4788.6(13)	18.4(4)
C(6)	4496.6(10)	8202.5(14)	7040.5(11)	14.2(4)
C(7)	4513.8(12)	9141.7(15)	7289.5(13)	23.0(5)
C(8)	5060.0(12)	7694.0(16)	7494.8(13)	23.2(5)
C(9)	3665.9(9)	6349.3(13)	6531.9(11)	11.4(4)
C(10)	3693.1(12)	5827.3(15)	7225.8(12)	21.2(5)
C(11)	4508.5(10)	5478.2(13)	6211.6(12)	14.5(4)
C(12)	4221.7(12)	4644.9(14)	5845.4(14)	23.0(5)
C(13)	5094.1(10)	5730.3(15)	5942.2(13)	19.4(5)
C(14)	2841.4(10)	7314.2(14)	6741.9(12)	14.8(4)
C(15)	2704.5(11)	8258.6(15)	6580.9(13)	20.9(5)
C(16)	2222.4(11)	6799.9(17)	6560.1(15)	28.1(6)
C(17)	2569.2(10)	7818.2(13)	4643.3(11)	12.2(4)
C(18)	1906.7(10)	8145.0(15)	4320.7(13)	20.9(5)
C(19)	2234.3(10)	6318.8(14)	4565.6(12)	17.3(4)
C(20)	2044.8(12)	6138.1(16)	3733.1(13)	24.7(5)
C(21)	2488.4(11)	5499.2(15)	4976.8(14)	23.4(5)
C(22)	3021.1(10)	9267.0(13)	4750.4(12)	15.7(4)

Table B13. Continued

	x	y	z	U(eq)
C(23)	3576.8(12)	9713.8(14)	5267.4(14)	22.9(5)
C(24)	3000.2(13)	9504.6(16)	3951.1(13)	27.0(5)
C(25)	3883.8(10)	6517.1(13)	4331.2(11)	12.8(4)
C(26)	3589.4(11)	6942.4(15)	3576.9(12)	17.8(4)
Hf(2)	1346.3(2)	2111.9(2)	6609.5(2)	10.93(3)
N(7)	2320.5(8)	1570.3(11)	7053.0(9)	12.4(3)
N(8)	2064.2(8)	1995.5(11)	5894.5(10)	12.7(3)
N(9)	1377.3(8)	3512.5(11)	6447.2(10)	15.3(4)
N(10)	784.0(8)	2773.8(11)	5514.6(10)	13.7(4)
N(11)	298.7(8)	1942.2(12)	6664.7(10)	14.2(4)
N(12)	846.0(8)	880.4(11)	6322.0(9)	11.6(3)
C(27)	2534.6(9)	1774.6(13)	6456.6(12)	13.0(4)
C(28)	3228.1(10)	1786.2(18)	6438.6(13)	24.9(5)
C(29)	2717.3(10)	1275.9(14)	7760.5(12)	16.1(4)
C(30)	3218.3(11)	1918.3(16)	8161.3(14)	25.0(5)
C(31)	3007.4(11)	386.6(15)	7716.8(13)	23.2(5)
C(32)	2132.6(11)	2316.3(13)	5176.2(12)	15.6(4)
C(33)	2347.6(12)	1624.6(15)	4701.4(13)	22.1(5)
C(34)	2524.4(12)	3139.7(15)	5209.4(14)	25.6(5)
C(35)	997(1)	3535.6(14)	5754.6(13)	16.7(4)
C(36)	837.6(12)	4356.2(15)	5314.9(15)	25.8(5)
C(37)	1706.5(11)	4282.4(14)	6794.3(14)	22.1(5)
C(38)	1325.2(13)	4740.3(18)	7273.3(18)	36.9(7)
C(39)	2355.6(11)	4028.9(16)	7259.8(15)	27.7(5)
C(40)	349.7(10)	2636.5(14)	4791.5(12)	16.9(4)
C(41)	430.6(12)	1729.2(15)	4520.0(13)	22.7(5)
C(42)	-346.4(12)	2782.6(19)	4813.5(15)	31.7(6)
C(43)	282.5(10)	1147.4(14)	6430.1(11)	13.4(4)
C(44)	-303.8(10)	585.7(15)	6264.7(14)	21.3(5)
C(45)	-256.2(10)	2390.8(15)	6804.5(13)	18.1(4)
C(46)	-407.5(12)	2115.5(17)	7537.1(14)	26.2(5)
C(47)	-150.9(11)	3352.8(15)	6804.9(14)	23.5(5)

Table B13. Continued

	x	y	z	U(eq)
C(48)	943(1)	-7.2(13)	6117.4(12)	14.2(4)
C(49)	1474.0(11)	-51.3(14)	5710.9(12)	17.5(4)
C(50)	1096.5(12)	-583.4(15)	6799.9(13)	23.7(5)
C(51)	1412.3(10)	2243.4(15)	7856.2(12)	18.1(4)
C(52)	1238.8(11)	1430.7(17)	8239.9(13)	23.7(5)

Table B14. Bond lengths (Å) in **7**

Hf(1)-N(1)	2.2379(18)	Hf(2)-N(7)	2.2405(18)
Hf(1)-N(2)	2.2831(17)	Hf(2)-N(8)	2.2795(18)
Hf(1)-N(3)	2.2057(17)	Hf(2)-N(9)	2.2041(19)
Hf(1)-N(4)	2.3305(18)	Hf(2)-N(10)	2.3487(19)
Hf(1)-N(5)	2.3072(18)	Hf(2)-N(11)	2.3105(19)
Hf(1)-N(6)	2.2231(17)	Hf(2)-N(12)	2.2047(17)
Hf(1)-C(25)	2.295(2)	Hf(2)-C(51)	2.298(2)
N(1)-C(1)	1.338(3)	N(7)-C(27)	1.338(3)
N(1)-C(3)	1.463(3)	N(7)-C(29)	1.464(3)
N(2)-C(1)	1.323(3)	N(8)-C(27)	1.321(3)
N(2)-C(6)	1.467(3)	N(8)-C(32)	1.466(3)
N(3)-C(9)	1.350(3)	N(9)-C(35)	1.355(3)
N(3)-C(11)	1.459(2)	N(9)-C(37)	1.464(3)
N(4)-C(9)	1.309(3)	N(10)-C(35)	1.312(3)
N(4)-C(14)	1.463(3)	N(10)-C(40)	1.463(3)
N(5)-C(17)	1.314(3)	N(11)-C(43)	1.310(3)
N(5)-C(19)	1.460(3)	N(11)-C(45)	1.465(3)
N(6)-C(17)	1.347(3)	N(12)-C(43)	1.349(3)
N(6)-C(22)	1.466(3)	N(12)-C(48)	1.461(3)
C(1)-C(2)	1.513(3)	C(27)-C(28)	1.510(3)
C(3)-C(4)	1.526(3)	C(29)-C(30)	1.533(3)
C(3)-C(5)	1.531(3)	C(29)-C(31)	1.530(3)
C(6)-C(7)	1.531(3)	C(32)-C(33)	1.533(3)
C(6)-C(8)	1.530(3)	C(32)-C(34)	1.530(3)
C(9)-C(10)	1.514(3)	C(35)-C(36)	1.512(3)
C(11)-C(12)	1.527(3)	C(37)-C(38)	1.527(3)
C(11)-C(13)	1.521(3)	C(39)-C(37)	1.518(3)
C(14)-C(15)	1.516(3)	C(40)-C(41)	1.524(3)
C(14)-C(16)	1.529(3)	C(40)-C(42)	1.535(3)
C(17)-C(18)	1.507(3)	C(43)-C(44)	1.512(3)
C(19)-C(20)	1.531(3)	C(45)-C(46)	1.535(3)
C(19)-C(21)	1.522(3)	C(45)-C(47)	1.515(3)
C(22)-C(23)	1.520(3)	C(48)-C(49)	1.520(3)

Table B14. Continued

C(22)-C(24)	1.522(3)	C(48)-C(50)	1.525(3)
C(25)-C(26)	1.546(3)	C(52)-C(51)	1.542(3)

Table B15. Bond Angles (°) in **7**

N(1)-Hf(1)-N(2)	57.93(6)	N(7)-Hf(2)-N(8)	58.12(6)
N(1)-Hf(1)-N(4)	137.28(6)	N(7)-Hf(2)-N(10)	137.24(6)
N(1)-Hf(1)-N(5)	141.39(6)	N(7)-Hf(2)-N(11)	142.17(7)
N(1)-Hf(1)-C(25)	81.50(7)	N(7)-Hf(2)-C(51)	80.42(7)
N(2)-Hf(1)-N(4)	79.71(6)	N(8)-Hf(2)-N(10)	79.32(7)
N(2)-Hf(1)-N(5)	144.21(6)	N(8)-Hf(2)-N(11)	146.03(6)
N(2)-Hf(1)-C(25)	135.50(7)	N(8)-Hf(2)-C(51)	135.01(7)
N(3)-Hf(1)-N(1)	109.26(6)	N(9)-Hf(2)-N(7)	111.47(6)
N(3)-Hf(1)-N(2)	86.36(7)	N(9)-Hf(2)-N(8)	87.23(6)
N(3)-Hf(1)-N(4)	58.58(6)	N(9)-Hf(2)-N(10)	58.25(6)
N(3)-Hf(1)-N(5)	104.25(6)	N(9)-Hf(2)-N(11)	100.44(6)
N(3)-Hf(1)-N(6)	152.30(6)	N(9)-Hf(2)-N(12)	148.87(6)
N(3)-Hf(1)-C(25)	91.12(7)	N(9)-Hf(2)-C(51)	93.06(8)
N(5)-Hf(1)-N(4)	77.35(6)	N(11)-Hf(2)-N(10)	77.02(6)
N(6)-Hf(1)-N(1)	95.40(7)	N(12)-Hf(2)-N(7)	97.36(7)
N(6)-Hf(1)-N(2)	96.72(6)	N(12)-Hf(2)-N(8)	98.82(6)
N(6)-Hf(1)-N(4)	94.75(6)	N(12)-Hf(2)-N(10)	92.69(6)
N(6)-Hf(1)-N(5)	58.63(6)	N(12)-Hf(2)-N(11)	58.66(6)
N(6)-Hf(1)-C(25)	105.19(7)	N(12)-Hf(2)-C(51)	103.40(7)
C(25)-Hf(1)-N(4)	134.68(7)	C(51)-Hf(2)-N(10)	136.99(7)
C(25)-Hf(1)-N(5)	79.20(7)	C(51)-Hf(2)-N(11)	78.04(7)
C(1)-N(1)-Hf(1)	96.02(12)	C(27)-N(7)-Hf(2)	94.95(13)
C(1)-N(1)-C(3)	125.04(17)	C(27)-N(7)-C(29)	125.04(17)
C(3)-N(1)-Hf(1)	137.89(13)	C(29)-N(7)-Hf(2)	138.59(13)
C(1)-N(2)-Hf(1)	94.41(12)	C(27)-N(8)-Hf(2)	93.68(13)
C(1)-N(2)-C(6)	125.43(17)	C(27)-N(8)-C(32)	125.76(18)
C(6)-N(2)-Hf(1)	136.87(13)	C(32)-N(8)-Hf(2)	137.24(13)
C(9)-N(3)-Hf(1)	96.17(12)	C(35)-N(9)-Hf(2)	97.17(13)
C(9)-N(3)-C(11)	121.96(17)	C(35)-N(9)-C(37)	121.36(19)
C(11)-N(3)-Hf(1)	141.57(14)	C(37)-N(9)-Hf(2)	140.97(15)
C(9)-N(4)-Hf(1)	91.74(12)	C(35)-N(10)-Hf(2)	91.90(13)
C(9)-N(4)-C(14)	122.82(18)	C(35)-N(10)-C(40)	122.87(18)
C(14)-N(4)-Hf(1)	145.26(13)	C(40)-N(10)-Hf(2)	145.23(14)

Table B15. Continued

C(17)-N(5)-Hf(1)	92.66(12)	C(43)-N(11)-Hf(2)	92.43(13)
C(17)-N(5)-C(19)	122.97(18)	C(43)-N(11)-C(45)	123.42(18)
C(19)-N(5)-Hf(1)	144.09(14)	C(45)-N(11)-Hf(2)	143.96(14)
C(17)-N(6)-Hf(1)	95.50(12)	C(43)-N(12)-Hf(2)	96.09(13)
C(17)-N(6)-C(22)	120.89(17)	C(43)-N(12)-C(48)	121.41(17)
C(22)-N(6)-Hf(1)	143.61(14)	C(48)-N(12)-Hf(2)	142.42(13)
N(1)-C(1)-C(2)	123.96(18)	N(7)-C(27)-C(28)	124.25(19)
N(2)-C(1)-N(1)	110.80(17)	N(8)-C(27)-N(7)	111.35(18)
N(2)-C(1)-C(2)	125.24(18)	N(8)-C(27)-C(28)	124.36(19)
N(1)-C(3)-C(4)	112.88(17)	N(7)-C(29)-C(30)	115.48(19)
N(1)-C(3)-C(5)	115.79(18)	N(7)-C(29)-C(31)	113.36(18)
C(4)-C(3)-C(5)	111.79(18)	C(31)-C(29)-C(30)	111.33(19)
N(2)-C(6)-C(7)	113.87(18)	N(8)-C(32)-C(33)	113.29(17)
N(2)-C(6)-C(8)	114.27(17)	N(8)-C(32)-C(34)	115.03(19)
C(8)-C(6)-C(7)	111.58(18)	C(34)-C(32)-C(33)	111.75(19)
N(3)-C(9)-C(10)	121.91(18)	N(9)-C(35)-C(36)	123.1(2)
N(4)-C(9)-N(3)	113.36(18)	N(10)-C(35)-N(9)	112.66(19)
N(4)-C(9)-C(10)	124.71(19)	N(10)-C(35)-C(36)	124.3(2)
N(3)-C(11)-C(12)	111.50(18)	N(9)-C(37)-C(38)	111.4(2)
N(3)-C(11)-C(13)	109.66(17)	N(9)-C(37)-C(39)	109.10(18)
C(13)-C(11)-C(12)	110.81(19)	C(39)-C(37)-C(38)	110.1(2)
N(4)-C(14)-C(15)	109.43(17)	N(10)-C(40)-C(41)	109.91(17)
N(4)-C(14)-C(16)	112.06(18)	N(10)-C(40)-C(42)	112.08(19)
C(15)-C(14)-C(16)	110.11(19)	C(41)-C(40)-C(42)	109.7(2)
N(5)-C(17)-N(6)	113.05(18)	N(11)-C(43)-N(12)	112.76(18)
N(5)-C(17)-C(18)	123.45(19)	N(11)-C(43)-C(44)	124.68(19)
N(6)-C(17)-C(18)	123.48(19)	N(12)-C(43)-C(44)	122.51(19)
N(5)-C(19)-C(20)	112.35(19)	N(11)-C(45)-C(46)	112.36(19)
N(5)-C(19)-C(21)	109.77(18)	N(11)-C(45)-C(47)	109.97(18)
C(21)-C(19)-C(20)	109.42(19)	C(47)-C(45)-C(46)	109.83(19)
N(6)-C(22)-C(23)	109.52(17)	N(12)-C(48)-C(49)	110.15(17)
N(6)-C(22)-C(24)	111.48(18)	N(12)-C(48)-C(50)	110.85(18)

Table B15. Continued

C(23)-C(22)-C(24)	110.0(2)	C(49)-C(48)-C(50)	110.22(18)
C(26)-C(25)-Hf(1)	114.17(14)	C(52)-C(51)-Hf(2)	115.47(15)

Table B16. Anisotropic displacement parameters ($Å^2 \times 10^3$) for **7**. The anisotropic displacement factor exponent takes the form: $-2\pi^2[h^2a^{*2}U^{11} + 2hka^*b^*U^{12} + \ldots]$

	U^{11}	U^{22}	U^{33}	U^{23}	U^{13}	U^{12}
Hf(1)	7.41(4)	9.41(4)	8.10(4)	-0.20(3)	1.36(3)	0.40(3)
N(1)	8.9(8)	14.3(8)	11.3(8)	-1.7(6)	2.5(6)	-1.9(6)
N(2)	9.6(8)	12.4(8)	10.2(8)	-2.4(6)	1.0(6)	-0.6(6)
N(3)	10.0(8)	10.7(8)	12.9(8)	2.0(6)	1.7(6)	3.7(6)
N(4)	5.9(8)	13.6(8)	12.9(8)	0.6(6)	2.7(6)	1.0(6)
N(5)	9.9(8)	14.0(8)	13.0(8)	-3.2(7)	1.2(7)	-2.8(6)
N(6)	10.3(8)	9.9(8)	15.4(8)	-0.3(6)	2.2(7)	1.8(6)
C(1)	8.7(9)	10.0(9)	13.7(9)	0.6(7)	1.5(7)	1.2(7)
C(2)	13.1(10)	21.7(11)	15.8(10)	-3.3(8)	2.6(8)	-5.4(8)
C(3)	12.2(10)	19.2(10)	11.9(10)	-2.7(8)	4.8(8)	-4.3(8)
C(4)	20.1(11)	24.2(12)	18.6(11)	5.2(9)	7.3(9)	-0.4(9)
C(5)	14.9(11)	20.1(11)	23.1(11)	-3.7(9)	10.3(9)	-0.8(8)
C(6)	11.6(10)	20.1(11)	10.3(9)	-4.8(8)	1.1(8)	-2.8(8)
C(7)	24.0(12)	25.6(12)	19.5(11)	-11.8(9)	5.7(9)	-4.1(10)
C(8)	22.2(12)	34.8(14)	10.5(10)	1.2(9)	-0.4(9)	3.2(10)
C(9)	12.5(10)	11.3(9)	10.0(9)	-1.0(7)	1.7(7)	-4.3(7)
C(10)	29.6(13)	19.9(11)	16.7(11)	4.7(9)	10.6(10)	2.3(9)
C(11)	15.7(10)	10.7(9)	16(1)	2.9(8)	1.7(8)	4.7(8)
C(12)	24.6(12)	13.3(10)	31.7(13)	-0.2(9)	7.9(10)	3.1(9)
C(13)	15.5(11)	19.6(11)	22.2(11)	4.5(9)	2.6(9)	7.1(8)
C(14)	12.6(10)	19.7(11)	13.3(10)	-4.0(8)	5.7(8)	-1.0(8)
C(15)	20.4(11)	23.3(12)	20.7(11)	-2.1(9)	8.5(9)	5.5(9)
C(16)	16.6(12)	34.5(14)	38.4(15)	-11.3(11)	16.6(11)	-7.6(10)
C(17)	9.4(9)	19.5(10)	7.5(9)	-0.5(7)	1.4(7)	2.6(8)
C(18)	10.7(10)	25.1(12)	24.1(12)	-3.1(9)	-1.2(9)	4.7(9)
C(19)	11.8(10)	19.4(11)	20.0(11)	-6.9(9)	2.3(8)	-5.0(8)
C(20)	21.3(12)	27.2(12)	22.4(12)	-10.8(10)	-1.2(9)	-5.3(10)
C(21)	22.1(12)	17.4(11)	30.8(13)	-3.8(9)	6.7(10)	-9.0(9)
C(22)	15.9(10)	11.7(10)	18.5(11)	2.9(8)	2.1(8)	5.0(8)

Table B16. Continued

	U^{11}	U^{22}	U^{33}	U^{23}	U^{13}	U^{12}
C(23)	28.6(13)	9.6(10)	27.3(12)	1.0(9)	0.2(10)	-1.0(9)
C(24)	35.0(14)	23.0(12)	21.6(12)	8.5(10)	4.1(10)	0.8(10)
C(25)	12.3(10)	14.1(10)	12.5(10)	0.6(8)	3.6(8)	0.2(8)
C(26)	17.6(11)	24.3(11)	11.4(10)	-0.9(8)	3.4(8)	-2.2(9)
Hf(2)	7.70(4)	11.82(4)	13.09(5)	-2.67(3)	2.09(3)	-1.06(3)
N(7)	8.5(8)	15.3(8)	13.3(8)	-0.5(7)	2.2(6)	-0.6(6)
N(8)	10.7(8)	13.3(8)	14.3(8)	2.0(7)	3.7(7)	0.2(6)
N(9)	7.6(8)	13.5(9)	23.2(9)	-6.8(7)	0.1(7)	0.3(6)
N(10)	9.6(8)	13.6(8)	16.7(9)	-0.2(7)	0.7(7)	0.9(6)
N(11)	9.8(8)	18.2(9)	15.2(9)	-4.2(7)	4.0(7)	1.0(7)
N(12)	10.7(8)	10.4(8)	14.2(8)	-2.4(6)	4.0(7)	-3.0(6)
C(27)	10.5(9)	11.6(9)	17.5(10)	-2.2(8)	4.0(8)	-1.1(7)
C(28)	11.5(11)	42.0(15)	22.5(12)	5.7(11)	6.9(9)	3.7(10)
C(29)	11.2(10)	22.9(11)	13.1(10)	0.7(8)	1.0(8)	-0.1(8)
C(30)	16.0(11)	30.4(13)	24.4(12)	-5.5(10)	-3.8(9)	-0.9(10)
C(31)	21.9(12)	22.3(12)	23.4(12)	5.7(9)	1.6(10)	4.3(9)
C(32)	15.4(10)	16.1(10)	16.7(10)	5.2(8)	6.6(8)	2.8(8)
C(33)	26.5(12)	24.0(12)	18.7(11)	4.4(9)	11.3(9)	6.9(10)
C(34)	27.6(13)	19.8(12)	31.8(13)	8.5(10)	12.1(11)	-0.2(10)
C(35)	11.7(10)	15.3(10)	24.4(11)	0.0(9)	6.7(8)	1.7(8)
C(36)	25.9(13)	15.4(11)	34.9(14)	5.3(10)	4.7(11)	3.6(9)
C(37)	22.8(12)	12.4(10)	30.9(13)	-7.4(9)	6.2(10)	-3.7(9)
C(38)	32.5(15)	25.3(13)	55.3(19)	-23.3(13)	15.0(13)	-4.3(11)
C(39)	21.4(12)	22.7(12)	36.6(14)	-13.3(11)	1.8(11)	-7.3(10)
C(40)	12.7(10)	18.9(11)	17.2(11)	2.1(8)	-0.3(8)	0.4(8)
C(41)	24.7(12)	20.6(11)	19.3(11)	-3.0(9)	-1.7(9)	-5.2(9)
C(42)	12.5(12)	52.2(18)	26.7(13)	-2.9(12)	-2.5(10)	3.5(11)
C(43)	10.3(9)	18.5(10)	10.8(9)	-0.1(8)	1.3(8)	-2.7(8)
C(44)	11.9(10)	23.3(12)	28.7(12)	-7.4(10)	5.1(9)	-5.9(9)
C(45)	8.5(10)	25.1(12)	21.1(11)	-5.9(9)	4.2(8)	1.1(8)
C(46)	18.8(12)	35.9(14)	28.1(13)	-6.1(10)	14(1)	0.6(10)
C(47)	16.7(11)	24.3(12)	31.9(13)	-6.9(10)	10.5(10)	5.7(9)

Table B16. Continued

	U^{11}	U^{22}	U^{33}	U^{23}	U^{13}	U^{12}
C(48)	14.9(10)	10.8(9)	16.8(10)	-1.1(8)	3.4(8)	-2.4(8)
C(49)	21.5(11)	13.5(10)	18.3(11)	-1.4(8)	6.6(9)	1.9(8)
C(50)	26.4(12)	19.4(11)	27.3(13)	6.9(9)	10.6(10)	1.5(9)
C(51)	10.5(10)	25.4(12)	18.4(11)	-7.7(9)	3.0(8)	-0.6(8)
C(52)	16.0(11)	40.0(14)	15.3(11)	0.9(10)	4.1(9)	1.2(10)

Table B17. Atomic coordinates ($\times 10^4$) and equivalent isotropic displacement parameters ($Å^2 \times 10^3$) for **12**. U(eq) is defined as one third of the trace of the orthogonalized U^{ij}

	x	y	z	U(eq)
W(1)	10125.43(5)	4424.60(5)	9461.56(5)	13.26(4)
O(1)	9627.8(10)	4318.5(9)	8790.7(10)	20.9(6)
C(1)	9534.1(17)	3865.7(15)	8572.3(16)	29.9(10)
C(2)	9309.0(16)	3977.3(15)	8089.7(16)	30.7(10)
C(4)	9217.2(16)	4608.2(16)	8664.5(15)	28.6(9)
C(3)	9115.4(18)	4487.2(16)	8153.5(16)	34.4(11)
Si(2)	9616.6(4)	3418.2(4)	9958.5(4)	19.8(2)
Si(1)	10869.3(4)	4788.9(4)	8547.6(4)	19.8(2)
C(7)	9116.1(15)	3261.1(18)	10377.5(17)	35.7(11)
C(5)	10190.7(15)	3318.1(15)	10282.5(16)	28.7(10)
C(6)	9597.2(15)	2999.2(14)	9441.8(17)	29.7(10)
C(10)	10963.0(16)	5299.2(15)	8135.5(15)	27.7(9)
C(9)	11422.0(15)	4665.1(17)	8898.2(16)	30.6(10)
C(8)	10734.0(19)	4255.7(16)	8175.4(18)	40.0(13)
C(11)	9526.4(14)	4052.8(13)	9776.7(14)	18.2(8)
C(12)	10361.6(14)	4946.8(13)	8948.3(13)	17.8(8)
O(4)	10430.1(9)	4609.2(9)	9977.0(9)	16.1(6)
O(5)	10434.6(9)	3939.5(9)	9259.3(9)	17.9(5)

Table B18. Bond lengths (Å) in **12**

W(1)-O(5)	1.711(3)	C(4)-C(3)	1.501(6)
W(1)-O(4)	1.758(3)	Si(2)-C(6)	1.868(4)
W(1)-C(12)	2.159(4)	Si(2)-C(11)	1.870(4)
W(1)-C(11)	2.167(4)	Si(2)-C(5)	1.871(4)
W(1)-O(4)[1]	2.239(2)	Si(2)-C(7)	1.884(5)
W(1)-O(1)	2.363(3)	Si(1)-C(10)	1.859(4)
O(1)-C(1)	1.435(5)	Si(1)-C(8)	1.864(4)
O(1)-C(4)	1.454(5)	Si(1)-C(12)	1.869(4)
C(1)-C(2)	1.527(6)	Si(1)-C(9)	1.869(4)
C(2)-C(3)	1.541(6)	O(4)-W(1)[2]	2.239(2)

[1]1/2+Y,3/2-Z,2-X; [2]2-Z,-1/2+X,3/2-Y

Table B19. Bond angles (°) in **12**

O(5)-W(1)-O(4)	105.11(13)	C(1)-C(2)-C(3)	103.5(3)
O(5)-W(1)-C(12)	99.39(13)	O(1)-C(4)-C(3)	104.9(3)
O(4)-W(1)-C(12)	101.52(13)	C(4)-C(3)-C(2)	104.7(3)
O(5)-W(1)-C(11)	98.38(13)	C(6)-Si(2)-C(11)	112.57(19)
O(4)-W(1)-C(11)	100.56(13)	C(6)-Si(2)-C(5)	107.93(19)
C(12)-W(1)-C(11)	146.83(14)	C(11)-Si(2)-C(5)	113.09(18)
O(5)-W(1)-O(4)[1]	165.93(11)	C(6)-Si(2)-C(7)	108.4(2)
O(4)-W(1)-O(4)[1]	88.97(15)	C(11)-Si(2)-C(7)	107.0(2)
C(12)-W(1)-O(4)[1]	77.30(11)	C(5)-Si(2)-C(7)	107.7(2)
C(11)-W(1)-O(4)[1]	78.68(12)	C(10)-Si(1)-C(8)	107.4(2)
O(5)-W(1)-O(1)	86.28(11)	C(10)-Si(1)-C(12)	107.43(18)
O(4)-W(1)-O(1)	168.51(11)	C(8)-Si(1)-C(12)	111.9(2)
C(12)-W(1)-O(1)	74.65(12)	C(10)-Si(1)-C(9)	110.7(2)
C(11)-W(1)-O(1)	78.81(12)	C(8)-Si(1)-C(9)	108.3(2)
O(4)[1]-W(1)-O(1)	79.65(9)	C(12)-Si(1)-C(9)	111.10(18)
C(1)-O(1)-C(4)	104.2(3)	Si(2)-C(11)-W(1)	117.71(19)
C(1)-O(1)-W(1)	124.1(2)	Si(1)-C(12)-W(1)	118.33(19)
C(4)-O(1)-W(1)	126.3(2)	W(1)-O(4)-W(1)[2]	150.90(15)
O(1)-C(1)-C(2)	105.8(3)		

[1]1/2+Y,3/2-Z,2-X; [2]2-Z,-1/2+X,3/2-Y

Table B20. Anisotropic displacement parameters ($Å^2 \times 10^3$) for **12**. The anisotropic displacement factor exponent takes the form: $-2\pi^2 [h^2 a^{*2} U^{11} + 2hka^*b^*U^{12} + \ldots]$

	U^{11}	U^{22}	U^{33}	U^{23}	U^{13}	U^{12}
W(1)	14.12(7)	12.76(7)	12.91(7)	-0.09(6)	0.43(6)	-0.21(6)
O(1)	22.8(14)	19.8(14)	20.2(13)	-4.1(11)	-2.7(12)	3.8(11)
C(1)	36(3)	22(2)	31(2)	-4.1(18)	-7(2)	-2.1(19)
C(2)	34(2)	31(2)	28(2)	-11.3(19)	-6.6(19)	-4.4(19)
C(4)	30(2)	29(2)	26(2)	-3.7(19)	-8.4(19)	7.2(19)
C(3)	43(3)	31(2)	29(2)	-6(2)	-12(2)	4(2)
Si(2)	17.5(5)	16.8(5)	25.2(6)	5.3(4)	-1.8(4)	-1.8(4)
Si(1)	23.8(5)	18.4(5)	17.1(5)	0.1(4)	5.0(4)	-1.9(5)
C(7)	23(2)	48(3)	36(2)	18(2)	0(2)	-7(2)
C(5)	26(2)	21(2)	39(2)	5.3(18)	-11.0(19)	0.2(18)
C(6)	26(2)	20(2)	43(3)	-5(2)	-10(2)	2.3(17)
C(10)	31(2)	28(2)	24(2)	5.1(18)	3.4(18)	-5.3(19)
C(9)	21(2)	39(3)	32(2)	6(2)	9.5(18)	4.2(19)
C(8)	59(3)	29(2)	31(3)	-10(2)	20(2)	-6(2)
C(11)	19.9(19)	16.8(18)	17.8(18)	2.7(15)	-0.6(15)	-1.6(15)
C(12)	22.1(18)	16.6(18)	14.7(17)	-2.5(14)	-1.7(15)	-0.4(16)
O(4)	16.5(13)	18.6(12)	13.4(12)	1.3(11)	2.3(10)	0.2(11)
O(5)	19.5(13)	15.3(13)	19.0(13)	-2.3(11)	2.9(11)	-0.7(11)

Appendix C

Table C1. ^{1}H NMR chemical shifts of hydride ligands in d^0 Group 3 complexes following Trend 1[a]

Complexes	M = Sc	Y	La	Lu	Refs
[Cp*$_2$M(μ-*H*)]$_2$[b]		5.45 (methylcyclohexane-d_{14})	10.21	9.27, 9.11 (cyclohexane-d_{12})	1,2
[Cp*$_2$Sc*H*]$_n$ (toluene-d_8, -95 °C)	7.3				3
Cp*$_2$Sc*H*(THF)	4.8				3
Cp*$_2$Lu(*H*)$_2$MCp$_2$* (cyclohexane-d_{12})		8.01	8.67	9.27	4,5
Cp*$_2$M(*H*)$_2$LaCp$_2$* (cyclohexane-d_{12})		6.79		8.67	5
Cp*$_2$M(μ-*H*)(μ-η^1:η^5-CH$_2$C$_5$Me$_4$)MCp*		3.77	2.23	6.77 (cyclohexane-d_{12})	6-8
Cp*$_2$M(μ-*H*)(μ-η^1:η^5-CH$_2$C$_5$Me$_4$)LaCp*		6.64		8.19	5
[(C$_5$Me$_4$H)$_2$M(μ-*H*)]$_2$ (cyclohexane-d_{12})		3.82			9
[Cp$_2$M*H*(THF)]$_2$		2.02		4.69	10
[(C$_5$H$_4$Me)$_2$M*H*(THF)]$_2$		2.31		4.99	10
[(CH$_2$)$_3$(C$_5$H$_4$)$_2$M*H*(THF)]$_2$ (THF-d_8)		2.16		4.02	11
[O(CH$_2$CH$_2$C$_5$H$_4$)$_2$M*H*]$_2$ (THF-d_8)		2.57		4.5	12
[(MeOCH$_2$CH$_2$C$_5$H$_4$)$_2$M*H*]$_2$		1.85		6.86	13
Cp$_2$M(THF)*H*$_4$Re(PMe$_2$Ph)$_3$		-7.9		-7.36	14
{(^{t}BuC$_5$H$_4$)$_2$M(μ-*H*)}$_2$		3.09		5.91	15
(^{t}BuC$_5$H$_4$)$_2$M(μ-*H*)(μ-Cl)M(C$_5$H$_4$^{t}Bu)		2.95		5.56	15
[(η^5:η^1-C$_5$Me$_4$SiMe$_2$NCMe$_3$)M(μ-*H*)(THF)]$_2$		5.50 (toluene-d_8, 50 °C)		9.9	16,17
(MeOCH$_2$CH$_2$C$_9$H$_6$)$_2$M(μ-*H*)$_2$BH$_2$		-0.6		-0.2	18
[M(Me$_3$TACD)*H*$_2$]$_3$ (Me$_3$TACDH = 1,4,7-trimethyl-1,4,7,10-tetraazacyclododecane)		6.37		9.81	19

Table C1. Continued

Complexes	M = Sc	Y	La	Lu	Refs
$(C_5Me_4SiMe_3)M(\mu\text{-}H)(OC_6H_2\text{-}{}^tBu_2\text{-}2,6\text{-}Me\text{-}4)]_2$		5.71		9.64	20
$(Tp^{Me2}MH_2)_n$		8.22		12.9	21
$[(C_5Me_4SiMe_3)M(\mu\text{-}H)_2]_4(THF)_n$	3.91 (n = 0)	4.32 (n = 1)		9.46 (n = 1)	22
$[(C_5Me_4SiMe_3)M]_4(\mu\text{-}NH_2)_7(\mu_4\text{-}H)$		3.1		4.81	23
$[(Tp^{iPr2})MH_2]_3$		7.62		11.27	24
$[(NCN)MH_2]_2(THF)_3$ [NCN = $PhC(NC_6H_3{}^iPr_2\text{-}2,6)_2$] (THF-$d_8$)		6.34		8.72	25
[(NCN)MH(THF)]$_2$(PhCH-CHPh) [NCN = $PhC(NC_6H_3{}^iPr_2\text{-}2,6)_2$] (THF-$d_8$)		5.92		9.14	25
[(1,7-Me_2TACD)M*H*]$_4$ (1,7-Me_2TACD)H_2 = 1,7-dimethyl-1,4,7,10-tetraazacyclododecane) (THF-d_8)		5.39	8.56		26
$(Tp^{tBu,Me})M[(\mu\text{-}H)AlMe_3]_2$		5.05 (toluene-d_8)		7.82 (benzene-d_6)	27
$(Tp^{tBu,Me})M[(\mu\text{-}NC_6H_3Me_2\text{-}2,6)(\mu\text{-}H)AlMe_2]$		6.57 (benzene-d_6)		8.67 (toluene-d_8)	27
$Cp_2M(\mu\text{-}H)(\mu\text{-}\eta^1\text{:}\eta^5\text{-}C_5H_4)Ru(dmpe)$		-16.19		-15.04	28
$(OC_6H_3{}^tBu_2\text{-}2,6)M(\mu\text{-}H)(\mu\text{-}\eta^1\text{:}\eta^5\text{-}C_5H_4)\{\kappa\,{}^3C,P,P'\text{-}CH_2(Me)P(CH_2)_2PMe_2\}Ru]_2$		-13.38		-12.17	28

Table C1. Continued

Complexes	M = Sc	Y	La	Lu	Refs
$(OC_6H_3{}^tBu_2\text{-}2,6)M(\mu\text{-}H)(\mu\text{-}\eta^1\text{:}\eta^5\text{-}C_5H_4)\{\kappa^3C,P,P'\text{-}CH_2(Me)P(CH_2)_2PMe_2\}Ru]_2$		-13.38		-12.17	28
$({}^tBuC_5H_4)_2M(\mu\text{-}H)(\mu\text{-}Me)M(C_5H_4{}^tBu)_2$ (also alkyl)		3		5.65	15
$(Ap^*M)_3(\mu_2\text{-}H)_3(\mu_3\text{-}H)_2(CH_2SiMe_3)(THF)_2$ (toluene-d_8)		5.66, 6.94-7.30	9.08, 12.25, 12.37		29
$[(PNP)MH_2]_3$ [PNP^- = N(2-^{i}Pr$_2$P-4-methylphenyl)$_2$]		6.08		9.70	30
$[(PNP)_3M_3H_5](BPh_4)$ (C_6D_5Cl)		5.53 (2H), 6.52 (3H)		8.43 (2H), 11.85 (3H)	30
$[(PNP)_2M_2H_3(THF)_2](BPh_4)$ (THF-d_8)		5.72		8.45	30

[a] Referenced to $SiMe_4$ at 0.00 ppm.

[b] The dimeric and polymeric structures of Cp^*_2MH here are proposed in the original papers. The dimeric structure of $(Cp^*_2YH)_2$ is based on the observation of a triplet as a result of ^{89}Y-^1H coupling.[2] In the case of $(Cp^*_2LuH)_2$, cryoscopic measurement showed that substantial dissociation occurred.[1] In addition, the solvents and temperatures of NMR spectra are different. These factors, however, were not included in making the comparisons and Figure 5.4A.

Table C2. ^{1}H NMR chemical shifts of hydride ligands in d^0 Groups 4-6 complexes following Trend 1[a]

Complexes	M = Ti	Zr	Hf	Nb	Ta	Mo	W	Refs.
Group 4								
$Cp^*_2MH_2$ (Ti analog opposite the trend)	0.28	7.46	15.57					31-33
$Cp^*_2M(OMe)(H)$ (Ti analog opposite the trend)	3.33 (THF-d_8)	5.7	9.92					33-35
$[Cp^*_2M(H)]_2O$		5.5	9.79					36
$(MeC_5H_4)_2MH_2$ (bridging and terminal)		-3.07[a] (μ-H), 3.70[a]	1.2[a]/1.35[b] (μ-H), 9.5[a]/9.67[b]					37
$(^iPrC_5H_4)_2MH_2$ (bridging and terminal)		-3.07 (μ-H), 3.75	1.14 (μ-H), 9.54					38
$(^tBuCp)_2MH_2$ (bridging and terminal)		-3.17 (μ-H), 3.65	1.25 (μ-*H*), 9.45					38
$Cp_2M(BH_4)_2$		0.78	1.56					39
Ansa-$[(SiMe_2)_2(C_5H_3)MH(\mu\text{-}H)]_2$ (bridging and terminal)		-3.21, 3.45	0.65, 8.67					40
$[(Me_2N)_3M(\mu\text{-}H)(\mu\text{-}NMe_2)_2]_2M$		5.21	9.87					41
$Cp^*_2M(H)Me$		6.15	12.97					42
$M_2H_3(BH_4)_5(PMe_3)_2$		3.96	8.53					43
$MH(BH_4)_3(Me_2PCH_2CH_2PMe_2)$		6.08	10.99					43
$MH_2(BH_4)_2(Me_2PCH_2CH_2PMe_2)_2$		3.36	6.65					43
$M_3H_6(BH_4)_6(PMe_3)_4$		3.38, 3.6	8.21, 8.29					44
$M_2H_4(BH_4)_4(Me_2PCH_2CH_2PMe_2)_2$		2.99	5.98					44
$CpCp^*M(H)Cl$		6.59	12.29					45

Table C2. Continued

Complexes	M = Ti	Zr	Hf	Nb	Ta	Mo	W	Refs.
Group 5								
Cp_2MH_3				-2.59[c]/ -3.7[d]	-1.62[c]/ -3.02[d]			46-48
Group 6								
$MH_6(P^iPr_2Ph)_3$						-4.00	-3.4	49-51

[a] Referenced to $SiMe_4$ at 0.00 ppm.

Table C3. ^{13}C NMR chemical shifts of α-C atoms in alkyl ligands of d^0 Group 3 complexes following Trend 1[a]

Complexes	M = Sc	Y	La	Lu	Refs
M(*C*H$_2$SiMe$_3$)$_3$		50.95 (THF-*d*$_8$)	75.2(methylcyclohexane-*d*$_{14}$; -30 °C)	57.35(toluene-*d*$_8$)	52-55
Cp*$_2$M[*C*H(SiMe$_3$)$_2$]		25.19	40 (solid state)	25.8 (solid state)	55,56
(Me$_3$Si*C*H$_2$)$_3$M(THF)$_2$ (THF-*d*$_8$)		33.7		41.3	57
(Ph*C*H$_2$)$_3$M(THF)$_3$ (THF-*d*$_8$)	60	54.38	67.2	59	58-60
(Ph*C*H$_2$)$_3$M(THF)$_2$	57.8			59.5 (toluene-*d*$_8$)	59
M(*C*H$_2$SiMe$_3$)$_3$(12-crown-4) (CD_2Cl_2)	40	32.5		39.6	61
(C$_5$Me$_4$SiMe$_3$)M(*C*H$_2$SiMe$_3$)$_2$(THF)	40.4	34.7			16,62
Cp*M(*C*H$_2$SiMe$_3$)$_2$(THF)	38.8			39.2	62,63
Cp*$_2$M(μ-H)(μ-η^1:η^5-*C*H$_2$C$_5$Me$_4$)MCp*		35.97		39.2	6-8
Cp$_2$M(μ-*Me*)$_2$AlMe$_2$	20.7	7.86			64
Cp$_2$M(μ-*CH$_3$CH$_2$*)$_2$AlEt$_2$	15.5	13.0			64
[o-(2,6-^{i}Pr$_2$-C$_6$H$_3$–N=C–C$_6$H$_4$)$_2$–N]M(*C*H$_2$SiMe$_3$)$_2$	44.4	38.6		44.9	65
(Flu-NHC)M(*C*H$_2$SiMe$_3$)$_2$	50.26	40.1		48.05	66
(Me$_3$Si*C*H$_2$)$_2$M-N(PPh$_2$NPh)$_2$	44.62	39.22		46.03	67
(Me$_3$Si*C*H$_2$)$_2$M-N[PPh$_2$N(2,6-^{i}Pr$_2$-phenyl)]$_2$		46.95		47.31	67
(PhNSN^{dipp})M(*C*H$_2$SiMe$_3$)$_2$(THF)$_n$	35.55 (n = 1)	35.99 (n = 2)		42.61 (n = 1)	68
(L^{Thia}Me$_2$)M(*C*H$_2$SiMe$_3$)$_2$		35.6		43.3	69,70
(L^{BnTh}Me$_2$)M(*C*H$_2$SiMe$_3$)$_2$		34.0		43.4	69,70
[(Me$_3$SiCH$_2$-L^{BnTh}Me$_2$)~S]M-*C*H$_2$SiMe$_3$		26.4		43.6	69,70
(N^{Me2}NN^{Me2}C^{Me}N$^{i\text{-}Pr2}$)M(*C*H$_2$SiMe$_3$)$_2$	45.2	37.8			71
Ap^{9Me}M(*C*H$_2$SiMe$_3$)$_2$(THF) [Ap^{9Me} = (2,4,6-trimethylphenyl)[6-(2,4,6-triisopropylphenyl)-pyridine-2-yl]amide]		39.0		46.1	72,73

Table C3. Continued

Complexes	M = Sc	Y	La	Lu	Refs
$Ap^{9Me}M(CH_2SiMe_3)_2(THF)$ [Ap^{9Me} = (2,4,6-trimethylphenyl)[6-(2,4,6-triisopropylphenyl)-pyridine-2-yl]amide]		39.0		46.1	72,73
$[LM(\mu_2\text{-}Me)]_3(\mu_3\text{-}Me)(\mu_3\text{-}PPh)$ (L = $[PhC(NC_6H_4{}^iPr_2\text{-}2,6)_2]^-$)		41.89 (μ_3-*Me*), 35.32 (μ_2-*Me*), 35.24 (μ_2-*Me*)		47.0 (μ_3-*Me*), 40.1 (μ_2-*Me*)	74
$L_3M_3(\mu_2\text{-}Me)_2(\mu_3\text{-}Me)(\mu\text{-}\eta^2\text{:}\eta^3\text{–}PC_6H_4)$ (L = $[PhC(NC_6H_4{}^iPr_2\text{-}2,6)_2]^-$)		29.9-28.6 (μ_3-*Me* and μ_2-*Me*)		33.6 (μ_2-*Me*), 33.3 (μ_2-*Me*); μ_3-Me NOT given	74
$[LM(\mu\text{-}Me)]_3(\mu_3\text{-}Me)(\mu_3\text{-}O)$ (L = $[PhC(NC_6H_4{}^iPr_2\text{-}2,6)_2]^-$)		28.0 (μ-*Me*), 21.2 (μ_3-*Me*)		32.5 (μ-Me), 22.7 (μ_3-*Me*)	74,75
$[LM(\mu_2\text{-}Me)]_3(\mu_3\text{-}Me)(\mu_3\text{-}S)$ (L = $[PhC(NC_6H_4{}^iPr_2\text{-}2,6)_2]^-$)		33.5 (μ_2-*Me*), 33.2 (μ_3-*Me*)		124.1(μ_3-*Me*), 47.9 (μ_3-*Me*), 37.9 (μ_2-*Me*)	74
$L_3M_3(\mu_2\text{-}Me)_2(\mu_3\text{-}S)[\mu\text{-}\eta^1\text{:}\eta^1\text{:}\eta^2\text{–}PhP(Me)CMeS]$ (L = $[PhC(NC_6H_4{}^iPr_2\text{-}2,6)_2]^-$)		41.8 (μ-Me)		41.7 (μ-Me)	74
$Cp^*_2M(\mu\text{-}H)(\mu\text{-}\eta^1\text{:}\eta^5\text{-}CH_2C_5Me_4)LaCp^*$ (Opposite to Trend 1)		41.7		41.7	5
$L_2MK(THF)$ {L = 1,3-bis[O-4,6-$^tBu_2C_6H_2$-2-CH_2][C(NCH_2CH_2N)]} (NHC carbene atom)		220.77, 214.61	225.57, 220.26		76
$Cp'M[CH_2\text{-}o\text{-}C_6H_3(NMe_2)]_2$ (Cp' = chiral Cp)	47.08 or 45.01 (The other peak is from NMe_2)	42.53			77

Table C3. Continued

Complexes	M = Sc	Y	La	Lu	Refs
[(3,5-$Me_2Pz)_2$CHP-$^tBu_2O$]M(*C*$H_2SiMe_3)_2$(THF)		31.08, 30.71		35.52	78
[(3,5-$Me_2Pz)_2$CHP-Cy_2O]M(*C*$H_2SiMe_3)_2$(THF)		30.27, 29.89		34.79	78
[(3,5-$Me_2Pz)_2$CHP-Cy_2NPh]M(*C*$H_2SiMe_3)_2$(THF)		32.91, 32.55		36.72	78
[(3,5-$Me_2Pz)_2$CHP-Ph_2NPh]M(*C*$H_2SiMe_3)_2$(THF) (ONE peak opposite to Trend 1)		32.77, 32.41		36.90, 31.96	78
Cp*$_2$M*C*H$(SiMe_3)_2$			44.64	25.8 (solid state)	55
M[*C*H$(SiMe_3)_2]_3$			57.35	75.2	55
[(^{t}BuC$_5$H$_4$)$_2$M(μ-*Me*)$_2$]$_2$		25.03		29.02	15
(^{t}BuC$_5$H$_4$)$_2$M*Me*(THF) (THF-d_8)		14.22		19.2	15
(^{t}BuC$_5$H$_4$)$_2$M(μ-*H*)(μ-*Me*)M(C$_5$H$_4{}^t$Bu)$_2$		26.34		32.60	15
(^{t}BuC$_5$H$_4$)2M(μ-*Me*)(μ-OMe)M(C$_5$H$_4{}^t$Bu)$_2$		20.23		23	15
(R,S)-Me2Si(^{t}BuCp)[(+)-neo-Men-Cp]M*C*H$(SiMe_3)_2$		29.8		49.4	79
[{η^5:η^1-C$_5$Me$_4$SiMe$_2$(C$_4$H$_3$O-2)}M(*C*$H_2SiMe_3)_2$(THF)] (toluene-d_8)		32.1		38.3	80
M[N($SiMe_2$*C*HPMe_2)($SiMe_2CH_2PMe_2$)]N[($SiMe_2CH_2PMe_2)_2$]		32.29 (toluene-d_8, −28 °C)		34.03(toluene-d_8, −28 °C)	81
[2,6-^{i}Pr$_2$C$_6$H$_3$NH($SiMe_3$)]M(*C*$H_2SiMe_3)_2$(THF)	44.38	38.93		46.08	82
[η^5-C$_5$Me$_4$SiMe$_2$(C$_4$H$_2$MeO-2)]M(*C*$H_2SiMe_3)_2$(THF)	39.3 (toluene-d_8, −60 °C)			38.8 (toluene-d_8, −80 °C)	83
(Me_3TACD)M(*C*$H_2SiMe_3)_2$ (Me_3TACD = 1,4,7-trimethyl-1,4,7,10-tetraazacyclododecane)		25		32	19

Table C3. Continued

Complexes	M = Sc	Y	La	Lu	Refs
LM(CH_2SiMe_3)$_3$ (L= 6-Pyrrolidinyl-1,4,6-trimethyl-1,4-diazepine)	39.7	35.5			84
LM(CH_2Ph)$_3$ (C_6D_5Br)	61.6		69.2		84
MeC(2,6-^{i}Pr$_2$C$_6$H$_3$N)CHCMe(NCH$_2$CH$_2$−NMe$_2$)M(CH_2SiMe_3)$_2$		35.6		43	85
(tbmp)M(CH_2SiMe_3)(THF)$_n$ [tbmpH$_2$ = 2,2′-thiobis(6-t-butyl-4-methylphenol]	not detected (n = 1, 2)	24.8 (n = 1, 2) (THF-d_8)			86
(etbmp)M(CH_2SiMe_3)(THF)$_n$ [etbmpH$_2$ = 1,4-dithiabutanediylbis(6-tert-butyl-4-methylphenol]	34.8 (n = 1, 2) (THF-d_8)	21.8 (n = 1, 2) (THF-d_8)			86
(mtbmp)M(CH_2SiMe_3)(THF)$_n$ [mtbmpH$_2$ = 1,3-dithiapropanediylbis(6-t-butyl-4-methylphenol)]		24.5 (n = 1)		29.2 (n = 1, 2)	86
Ap*M(CH_2SiMe_3)$_2$(THF) {Ap* = 2,6-diisopropylphenyl)[6-(2,4,6-triisopropylphenyl)pyridin-2-yl]amide}		39.6		46.1	29
(Ap*M)$_3$(μ$_2$-H)$_3$(μ$_3$-H)$_2$(CH_2SiMe_3)(THF)$_2$		41.8 (toluene-d_8)		45.8(toluene-d_8)	29
(Tp^{tBu,Me})M(CH_2SiMe_3)$_2$(THF)		39.62		46.15	21
(Tp^{Me2})M(CH_2SiMe_3)$_2$(THF)		32.43		35.89	21
[2-(2,6-^{i}Pr$_2$C$_6$H$_3$NC(H)C$_6$H$_4$-C$_9$H$_6$N)M(CH_2SiMe_3)$_2$(THF)$_n$	44.32 (n = 0)	35.32 (n = 1)		no listed	87
(η^5-2,5-^{t}Bu$_2$C$_4$H$_2$N)M(CH_2C$_6$H$_4$NMe$_2$-o)$_2$	48.1	44.2	43.5		88
M(AlMe_4)$_2$[1,3-(Me$_3$Si)$_2$C$_5$H$_3$]		0	2.3	1.5	89
M(AlMe_4)$_2$(C$_5$Me$_4$SiMe$_3$)		0.1	2.4	1.7	89

Table C3. Continued

Complexes	M = Sc	Y	La	Lu	Refs
LM(CH$_2$Ph)$_2$ (L =N-(2-pyrrolidin-1-ylethyl)-1,4-diazepan-6-amido)	52.3	51.4	62.6		[90]
[LM(C≡CPh)(μ-C≡CPh)]$_2$ (toluene-d$_8$)		148.4	162.1		[90]
[CyC(N-2,6-^{i}Pr$_2$C$_6$H$_3$)$_2$]M(CH$_2$SiMe$_3$)$_2$(THF)		44.2		45.3	[91]
[CyC(N-2,6-Me$_2$C$_6$H$_3$)$_2$]M(CH$_2$SiMe$_3$)$_2$(THF)$_2$		37.2		45.5	[91]
(NPN)^{7}M(CH$_2$SiMe$_3$)$_2$(THF) [(NPN)^7 = 2-EtC$_6$H$_4$NPPh$_2$NC$_6$H$_3$ ^{i}Pr$_2$-2,6)	42.66	33.36		41.16	[92]
(NPN)^{9}M(CH$_2$SiMe$_3$)$_2$(THF) [(NPN)^9 = NC$_5$H$_4$NPPh$_2$NC$_6$H$_2$Me$_3$-2,4,6)		34.8		42.42	[92]
(^{t}BuFlu-NHC)M(CH$_2$SiMe$_3$)$_2$	49.64			47.7	[93]
(C$_5$Me$_4$SiMe$_2$CH$_2$PPh$_2$)M(CH$_2$SiMe$_3$)$_2$(THF)		38.1		43	[94]
(C$_5$Me$_4$C$_2$H$_4$PPh$_2$)M(CH$_2$SiMe$_3$)$_2$(THF)		33.8		41.8	[94]
[(Tph)$_2$N$_3$]M(Al$Me$$_4$)$_2$ [Tph = 2-(2,4,6-^{i}Pr$_3$C$_6$H$_2$)C$_6$H$_4$] (Opposite to Trend 1)		3.5	5	-0.02	[95]
LM(CH$_2$SiMe$_3$)$_2$(THF)$_n$ (L = imidazolin-2-iminato)	34.5 (n = 1)	26.2 (n = 2)		36.3	[96]
[ONNO]M(CH$_2$SiMe$_3$)(THF) {[ONNO] = 4-bis(2-hydroxy-3,5-di-tert-butylbenzyl)piperazidine}		45.3		44.7	[97]
L$_2$M(CH$_2$SiMe$_3$)(THF) (L = 2-pyridyl-NPPh$_2$)		32.58		35.18	[98]
M(CH$_2$SiMe$_3$)$_2$(2,6-Me$_2$Ph-DAB-CH$_2$SiMe$_3$)(THF) (DAB = 1,4-diaza-1,3-butadiene)	25.7	33.6			[99]

Table C3. Continued

Complexes	M = Sc	Y	La	Lu	Refs
M(CH$_2$SiMe$_3$)$_2$(2,6-^{i}Pr$_2$Ph-DAB-CH$_2$SiMe$_3$)(THF)	25.1	33.6			99
ApLn(CH$_2$Ph)$_2$(THF) {Ap = (2,6-^{i}Pr$_2$C$_6$H$_3$)-[6-(2,4,6-^{i}Pr$_3$C$_6$H$_2$)pyridin-2-yl]amide}		54.1		59.1	100
[NON]M(CH$_2$SiMe$_3$)$_2$(THF) {[NON] = 2,2-[bis(3,5-dimethylpyrazolyl)]-1,1-diphenylethoxide	32	28.3		31.9	101
[M(CH$_2$SiMe$_3$)$_2$(pbptam)]	31.8	34.9			102
[M(CH$_2$SiMe$_3$)$_2$(tbptam)]	29.7	33.1			102
(Tp$^{i\text{Pr}2}$)M(CH$_2$SiMe$_3$)$_2$(THF)		34.9		38.39	24
[M(CH$_2$SiMe$_3$)$_3$(IPr)] (IPr = NHC = 1,3-bis(2,6-diisopropylphenyl)imidazol-2-ylidene)		47.99 (CH$_2$), 193.05 (NHC)		56.72 (CH$_2$), 205.01 (NHC)	103
[(Tp^{Me2})M(μ-C≡CPh)]$_2$(μ-PhC$_4$Ph) (dymanic behavior)		133.91 (Cinternal), 181.12 (Cterminal), 143.84 (Cbridging), 120.76 (Cbridging)		155.61 (Cinternal), 204.99 (Cterminal), 143.84 (Cbridging), 120.76 (Cbridging)	104
[(Tp^{Me2})M(μ-C≡CSiMe$_3$)]$_2$(μ-Me$_3$SiC$_4$SiMe$_3$) (dymanic behavior)		158.28 (Cinternal), 204.00 (Cterminal), 173.07 (Cbridging)		134.72 (Cinternal), 184.88 (Cterminal), 177.16 (Cbridging)	104

Table C3. Continued

Complexes	M = Sc	Y	La	Lu	Refs
[(Tp^{Me2})M(μ-*C*≡C^{t}Bu)]$_2$(μ-^{t}BuC$_4$^{t}Bu) (dymanic behavior)		195.5 ($C_{terminal}$), 127.02 ($C_{bridging}$)		198.8 ($C_{terminal}$), 132.47 ($C_{bridging}$), 128.52($C_{bridging}$)	104
[{2-(2-CH$_3$OC$_6$H$_3$NC(H)(CH$_2$SiMe$_3$)–C$_4$H$_3$N}M(*C*H$_2$SiMe$_3$)]$_2$		32.38		35.53	105
(C$_5$H$_5$BNEt$_2$)$_2$M-*C*H(SiMe$_3$)$_2$		33.8		34.1	106
(C$_5$H$_5$BNPh$_2$)$_2$M-*C*H(SiMe$_3$)$_2$		39.06		38.6	106
(C$_5$H$_5$BMe)$_2$M-*C*H(SiMe$_3$)$_2$		38.7		38.6	106
(C$_5$Me$_4$H)M(Al*Me*$_4$)$_2$		0.4		1.2	107
[NNP]M(*C*H$_2$SiMe$_3$)$_3$(THF) {[NNP] = [bis(3,5-dimethylpyrazolyl)methyl]-diphenylphosphine}	40.4, 42.6	38.1, 36.1		44.0, 41.2	108
[NNN]M(CH$_2$SiMe$_3$)$_2$(THF) (Zwitterionic) [NNN] = [bis(3,5-dimethylpyrazolyl)methyl]-(diphenyl)imino-phosphine}		33.6, 34.1		38.2	108
LM(CH$_2$C$_6$H$_4$NMe$_2$-o)$_2$ [L = 1,8-Bis(phosphino)-3,6-di-tert-butylcarbazolium]	59.1	53.98			109
[(2,6-^{i}Pr$_2$C$_6$H$_3$N−CH$_2$−C(CH$_2$SiMe$_3$)═NC$_6$H$_3$^{i}Pr$_2$-2,6)]M(CH$_2$SiMe$_3$)$_2$(THF)	37.6	33.9		40.6	110
[(2,6-Me$_2$C$_6$H$_3$N−CH$_2$−C(CH$_2$SiMe$_3$)═NC$_6$H$_3$Me$_2$-2,6)]M(*C*H$_2$SiMe$_3$)$_2$(THF)	37	33.3, 33.7		40.9	110

Table C3. Continued

Complexes	M = Sc	Y	La	Lu	Refs
M{B(NArCH)$_2$}(*C*H$_2$SiMe$_3$)$_2$(THF)$_n$	60.4 (n = 1)	33.7 (n = 2)		53.4 (n = 2)	111
(Cp$^{\#}$PN)M(*C*H$_2$SiMe$_3$)$_2$ (Cp$^{\#}$PN =C$_5$Me$_4$PMe$_2$NAd)	36.8	31.4		38.3	112,113
(Me$_3$SiC$_5$Me$_4$)M(*C*H$_2$SiMe$_3$)$_2$(THF)	40.4	34.7		39.6	22
[(NCN)M(μ$_2$-*Me*)]$_3$(μ$_3$-*Me*)(μ$_3$-*C*H$_2$) [NCN = PhC{NC$_6$H$_4$(^{i}Pr-2,6)$_2$}$_2$]$^-$	33.8 (μ$_2$-*Me*), 45.5 (μ$_3$-*Me*), 123.9 (μ$_3$-*C*H$_2$)			36.5 (μ$_2$-*Me*), 43.5 (μ$_3$-*Me*), 107.6 (μ$_3$-*C*H$_2$)	75
(NCN)M(Al*Me*$_4$)$_2$	0			3	75
[(NCN)M(μ$_2$-*Me*)]$_3$(μ$_3$-*Me*)(μ$_3$-O)	29.5 (μ$_2$-*Me*), 24.8 (μ$_3$-*Me*)			32.5 (μ$_2$-*Me*), 22.7 (μ$_3$-*Me*)	75
[2-MeOC$_6$H$_4$NC(^{t}Bu)N(2,6-Me$_2$C$_6$H$_3$)]Y(*C*H$_2$SiMe$_3$)$_2$(THF)$_n$		31.4 (n =1)		39.3 (n = 2)	114
[2-MeOC$_6$H$_4$NC(^{t}Bu)N(2,6-^{i}Pr$_2$C$_6$H$_3$)]Y(*C*H$_2$SiMe$_3$)$_2$(THF)		31.7		41.5	114
[C$_5$H$_4$N-CH(Me)-NC$_6$H$_3$ ^{i}Pr$_2$]M(*C*H$_2$SiMe$_3$)$_2$(THF)	35.93	31.32		40.1	115
[C$_6$H$_4$-1,2-{NC(^{t}Bu)N(2,6-Me$_2$C$_6$H$_3$)}$_2$]M(*C*H$_2$SiMe$_3$)(THF)		33.7		38.3	116
LM(*C*H$_2$SiMe$_3$)$_2$ [L = bis(phosphinimine)pyrrole ligand]	40.5			41.3	117
(C$_5$H$_4$−PPh$_2$=N−C$_6$H$_3$ ^{i}Pr$_2$)M(*C*H$_2$SiMe$_3$)$_2$(THF)$_n$	42.01 (n = 0)	32.09 (n = 1)		40.21 (n =1)	118
[C$_5$HMe$_3$(η^3-CH$_2$)-PPh$_2$=N-C$_6$H$_3$ ^{i}Pr$_2$]M(*C*H$_2$SiMe$_3$)$_2$(THF)		34.16		40.64	118

Table C3. Continued

Complexes	M = Sc	Y	La	Lu	Refs
(Ind−PPh_2=N-$C_6H_3Me_2$)M(*C*$H_2SiMe_3)_2$(THF) (Ind = indenyl)	45.32	36.39		44.73	118
(Ind−PPh_2=N-C_6H_3 $^iPr_2$)M(*C*$H_2SiMe_3)_2(THF)_n$	43.59 (n = 0)	37.30 (n =1)		45.58 (n = 1)	118
[(η^1-Flu)-PPh_2=N-C_6H_4Me)M(*C*$H_2SiMe_3)_2$(THF) (Flu = fluorenyl)	46.28			44.21	118
(FluCH_2-Py)M(*C*$H_2SiMe_3)_2(THF)_n$	45.27 (n = 0)	35.39 (n = 1)		40.36 (n = 1)	119
LM(*C*$H_2SiMe_3)_2(THF)_n$ {HL = 2,5-bis[(pyrrolidin-1-yl)methylene]-1*H*-pyrrole}	41.52 (n = 0)	35.2		44.61	120
LM(*C*$H_2SiMe_3)_2$ {HL = 2,5-bis[(piperidino)methylene]-1*H*-pyrrole}	43.78 (monomer)	39.91 (dimer)		46.80 (dimer)	120
(PhN=PPh_2NPh_2P=NPh)M(*C*$H_2SiMe_3)_2$	44.62	39.22		46.03	67
(2,6-$^iPr_2C_6H_3$N=PPh_2NPh_2P=N-2,6-$^iPr_2C_6H_3$)M(*C*$H_2SiMe_3)_2$		46.95		47.31	67
(2,6-$^iPr_2C_6H_3$N=PPh_2NPh_2P=N-2,6-$^iPr_2C_6H_3$)M(*C*H_2SiMe_3)[$NHC_6H_3(^iPr)_2$]		37.12		40.77	121
[PhC(N-2,6-$^iPr_2$-$C_6H_4)_2$]M(*C*$H_2C_6H_4NMe_2$-o)$_2$	47.1	47.1		51.8	122
1,4-C_6H_4[C(NR)$_2$M(o-*C*$H_2C_6H_4NMe_2)_2]_2$ (R = 2,6-$^iPr_2C_6H_3$)	47.95	47.42		51.71	123
(NCN^{dipp})$_3M_3$(μ-*Me*)$_3$(μ $_3$-*Me*)(μ-η^1:η^3-NC_6H_5)		31.2 (μ_3-Me), 29.8 (μ_2-Me)		34.3 (μ_2-Me), 33.1 (μ_3-Me)	124
(NCN^{dipp})$_3M_3$(μ -*Me*)$_3$(μ $_3$-*Me*)(μ- η^1:η^3-$NC_6H_3Me_2$-2,6)		37.1 (μ_3-Me), 29.7 (μ_2-Me)		39.3 (μ_3-Me), 34.2 (μ_2-Me)	124
(NCN^{dipp})$_3M_3$(μ -*Me*)$_3$(μ $_3$-*Me*)(μ-η^1:η^3-NC_6H_4Cl-p)		31.8 (μ_3-Me), 29.8 (μ_2-Me)		34.2 (μ_2-Me), 33.6 (μ_3-Me),	124

Table C3. Continued

Complexes	M = Sc	Y	La	Lu	Refs
$(NCN^{dipp})_3M_3(\mu\text{-}Me)_3(\mu_3\text{-}Me)(\mu\text{-}\eta^1\text{:}\eta^1\text{:}\eta^3\text{-}NC_6H_4OMe\text{-}p)$		30.6 (μ_3-Me), 29.6 (μ_2-Me)		34.0 (μ_2-Me), 32.3 (μ_3-Me),	124
$(NCN^{dipp})_3M_3(\mu\text{-}Me)_3(\mu_3\text{-}Me)(\mu\text{-}\eta^1\text{:}\eta^3\text{-}NCH_2CH_2CHMe_2)$		28.6 (μ_3-Me, μ_2-Me)		32.5 (μ_2-Me), 30.2 (μ_3-Me),	124
$(NCN^{dipp})_3M_3(\mu_2\text{-}Me)_3(\mu\text{-}\eta^1\text{:}\eta^1\text{:}\eta^3\text{-}NPh)(\mu_3\text{-}SPh)$		30.6 (μ_2-Me)		35.7 (μ_2-Me)	124
$[(2,6\text{-}{}^{i}Pr_2C_6H_3)N{=}C(Me)C(=CH_2)N(C_6H_3{}^{i}Pr_2\text{-}2,6)]M(CH_2SiMe_3)_2(THF)$		36.4		42.6	125
$M(Me_3TAMC)(CH_2SiMe_3)_2$ [(Me_3TAMC)H = 2,5,8-trimethyl-2,5,8-triaza-meta-cyclophane]	37.9	(not reported; only ^{1}H NMR)		36	126
$(DippForm)M[(\mu\text{-}Me_2)AlMe_2]_2$ (DippForm = ArNCHNAr; Ar = 2,4,6-$Me_3C_6H_2$)		2.1	4.8		127
(^{t}BuForm)$M[(\mu\text{-}Me_2)AlMe_2]_2$ (^{t}BuForm = ArNCHNAr; Ar = 2-^{t}BuC_6H_4)		2.5	4.9		127
$(OC_6H_3{}^{t}Bu_2\text{-}2,6)M(\mu\text{-}H)(\mu\text{-}\eta^1\text{:}\eta^5\text{-}C_5H_4)\{\kappa^3C,P,P'\text{-}CH_2(Me)P(CH_2)_2PMe_2\}Ru]_2$ (average of three CH_2 moieties)		32.3		32.3	28
[o-(2,6-$^{i}Pr_2C_6H_3N{=}CC_6H_4)_2N]M(CH_2SiMe_3)_2$	44.4	38.6		44.9	65
$(PNP)M(CH_2SiMe_3)_2$ [PNP^- = N(2-$^{i}Pr_2$P-4-methylphenyl)$_2$]		49.27		56.75	30,128
[o-$(PPh_2)C_6H_4CH_2NH$-1,2-$Me_2C_6H_3]M(CH_2SiMe_3)_2(THF)$		36.50		43.74	129
[o-$(PPh_2)C_6H_4CH_2NH$-1,2-$^{i}Pr_2C_6H_3]M(CH_2SiMe_3)_2(THF)$		35.48		42.39	129

[a] Referenced to $SiMe_4$ at 0.00 ppm.

Table C4. ^{13}C NMR chemical shifts of α-C atoms in alkyl ligands of d^0 Group 4 complexes following Trend 1[a]

Complexes	M = Ti	Zr	Hf	Refs.
M(*C*H$_2$Ph)$_4$	98.4	72.3	83.2	130
M(*C*H$_2$*t*Bu)$_4$	118.9	102.7	117	131-133
(Naph*C*H$_2$)$_4$M (Naph = naphenyl)	94.3	70.6	81	130
[NCO]M(*C*H$_2$Ph)$_2$ {[NCO] = (σ-aryl)-2-phenolate-6-pyridyl}	81.73	62.56	71.19	134
(1-Nor)$_4$M	106.4	88.9	105.8	135
Cp$_2$M*Me*$_2$	45.9	30.62	36.84	136,137
Cp$_2$M(*C*H$_2$Ph)$_2$	73.5 (THF-*d*$_8$)	61.15	64.97	130,136
Cp$_2$M(*C*H$_2$Ph)Cl	73.6 (THF-*d*$_8$)	59.7		130
[Cp*M*Me*[(η^2-ONMeCH$_2$)$_2$]]	26.7	17.4	43.4	138
[PhP(C$_5$Me$_4$)$_2$]M*Me*$_2$	48.6,50.2	34.9, 35.4	40.6, 41.5	139
Cp$_2$M(*C*H$_2$)$_2$MCp$_2$ (bridging CH$_2$) (Opposite of Trend 1)	235.8	205.7	193.3	140
Cp$_2$M[*C*H$_2$C(Me)$_2$*C*H$_2$] (toluene-*d*$_8$, -30 °C)	83.4	66.4	71.7	141
Cp$_2$M[*C*H$_2$Si(Me)$_2$*C*H$_2$]	70.55	45.99	47.7	142
Cp$_2$M[bicyclo[3.3.0]octadiene-l,4] (CDCl$_3$) (Opposite of Trend 1)	204.18	189.98	189.84	143
(η^5-C$_5$Me$_4$H)$_2$M*Me*$_2$	47.0	34.2 (35.3), 34.23 in (CDCl$_3$)	40.95	144-147
^{Ph}(PN$_3$)M-*C*H$_2$Ph [^{Ph}(PN$_3$) = P(CH$_2$CH$_2$CH$_2$NPh)$_3^{3-}$]	83.6	66.7	74.7	148
(PN$_3$)M*Me* (PN$_3$ = benzylene-linked trisamidophosphine)	63.5	40.0 (CD$_2$Cl$_2$)	48.1	149
(2-R-8-Ph$_2$PC$_9$H$_9$N)M(*C*H$_2$Ph)$_3$ (R = H)	93.61	72.71	83.25	150
(2-R-8-Ph$_2$PC$_9$H$_9$N)M(*C*H$_2$Ph)$_3$ (R = Me)		72.42	82.79	150
(2-R-8-Ph$_2$PC$_9$H$_9$N)M(*C*H$_2$Ph)$_3$ (R = *i*Pr)		74.85	84.07	150

Table C4. Continued

Complexes	M = Ti	Zr	Hf	Refs.
(2-R-8-$Ph_2PC_9H_9N$)M(CH_2Ph)$_3$ (R = ^{n}Bn)		73.08	83.33	150
(N-R-2-$Ph_2PC_6H_4N$)M(CH_2Ph)$_3$ (R = Me)		72.50	83.30	150
(N-R-2-$Ph_2PC_6H_4N$)M(CH_2Ph)$_3$ (R = Et)		72.26	82.67	150
[(^{i}Pr N-o-C_6H_4)$_2$O]MMe_2	56.8	41.6		151
[(^{i}Pr N-o-C_6H_4)$_2$O]M(CH_2 ^{i}Pr)$_2$	94.7	76.6		151
[(^{i}Pr N-o-C_6H_4)$_2$O]M(CH_2^{t}Bu)$_2$	103.9	84.6		151
(Cbz-P_2^{Ph}-CH)MCl(CH_2Ph) (cyclometalated, carbazole-based PNP pincer ligand)		56.4 (CH), 64.9 (CH_2)	61.8 (CH), 69.9 (CH_2)	152
(Cbz-P_2^{Ph}-CH)MI(CH_2Ph)		57.3 (CH), 66.2 (CH_2)	62.5 (CH), 72.7 (CH_2)	152
(Cbz-P_2^{Ph}-CH)M(CH_2Ph)$_2$		50.0 (CH), 66.7 (CH_2), 67.5 (CH_2)	68.8 (CH), 77.3 (CH_2), 79.2 (CH_2)	152
{[^{t}Bu(OC(CH_2Ph)O)]MCl}$_2$ {[^{t}Bu(OC(CH_2Ph)O)] = η^5-O,N,C,N,O-pentadentate trianionic ligand}	111.6	102.2		153
[^{t}Bu (OC(CH_2Ph)O)]MCl(THF) {[^{t}Bu(OC(CH_2Ph)O)] = η^5-O,N,C,N,O-pentadentate trianionic ligand} (CD_2Cl_2)	110.6	100.8	107.5	153
[^{t}BuOC(CH_2Ph)O)]M(CH_2Ph)(THF) {[^{t}Bu(OC(CH_2Ph)O)] = η^5-O,N,C,N,O-pentadentate trianionic ligand} (CD_2Cl_2)	109.6 (OCO) 58.8 (MCH_2-)	101.9 (OCO) 49.0 (MCH_2-)	109.1 (OCO) 53.0 (MCH_2-)	153
[^{t}Bu (OCO)]M(CH_2Ph)Cl ([^{t}Bu(OCO)] = N-heterocyclic carbenes) (CD_2Cl_2)		204.3 (OCO) 62.5 (MCH_2-)	209.1 (OCO) 65.9 (MCH_2-)	153
[^{t}Bu(OCO)]M(CH_2Ph)$_2$ ([^{t}Bu(OCO)] = N-heterocyclic carbenes) (CD_2Cl_2)		205.8 (OCO) 55.0 (MCH_2-)	212.6 (OCO) 63.0 (MCH_2-)	153
Me_2M([N($SiMe_3$)$_2$]$_2$		48.8	60.2	154
(CH_3CH_2)$_2$M([N($SiMe_3$)$_2$]$_2$		63.5	74.6	154,155

Table C4. Continued

Complexes	M = Ti	Zr	Hf	Refs.
$(Me_3SiCH_2)_2M([N(SiMe_3)_2]_2$		69.4	76.3	154,155
$[(Me_2N)[(Me_3Si)_2N]M(NSiMe_3SiMe_2CH_2]_2$		37.2	42.1	156
(PNP)M*Me*$_3$ [PNP$^-$ = N(2-^{i}Pr$_2$P-4-methylphenyl)$_2$]		51.7	60.6	157,158
(PNP)M*Me*$_2$(O-2,6-^{i}Pr$_2$C$_6$H$_3$)		40.95	48.30	159
$[(Me_3SiN\text{-}o\text{-}C_6H_4)_2O]M$*Me*$_2$ [L^{2-} = NON]		47.19	58.06	160
$(MeOx)_2M(CH_2Ph)_2$ (MeOx = 2-Me-8-quinolinolato)		64	73.9	161
$(MeBr_2Ox)_2M(CH_2Ph)_2$ ($MeBr_2Ox$ = 2-Me-5,7-Br_2-8-quinolinolato)		64.8	75.3	161
$(Me_8taa)M$*Me*$_2$ (Me_8taa^{2-} = octamethyldibenzotetraazaannulene)		30.4	33.3 (C2D2Cl4)	162
$(Me_8taa)M(CH_2SiMe_3)_2$ (Me_8taa^{2-} = octamethyldibenzotetraazaannulene)		43.8	47.9	162
M(imido-enamido-L-1)$(CH_2Ph)_3$		75.11	85.07 (toluene-d_8)	163
M(imido-enamido_L-1)*Me*$_3$		48.6	60.4	164
M(imido-enamido_L-2)*Me*$_3$		47	60.12	164
M(imido-enamido_L-1)*Me*$_2$(imidazolimine)		38.07	47.6	165
M(imido-enamido_L-1)*Me*$_2$(phosphinimine)		35.13	46.06	165
M(imido-enamido_L-1)*Me*$_2$(O-2,6-^{t}Bu$_2$-C$_6$H$_3$)		48.72	56.1	165
M(imido-enamido_L-1)*Me*$_2$(OR) (OR = 2,3,4-trimethyl-3-pentanolato)		35.95	45.88	165
M(imido-enamido_L-1)*Me*$_2$X(amidinate)		45	50.77	165
M(amidoquinoline)$(CH_2Ph)_3$		77.7	89.9	166
Cp_2MPh_2		183.58 (ipso)	192.32 (ipso)	136
CpCp*M[Si(SiMe$_3$)$_3$]*Me*		-0.43	54.57	45,167

Table C4. Continued

Complexes	M = Ti	Zr	Hf	Refs.
(Cp*)($C_2B_9H_{11}$)M(*C*(Me)=CMe_2)		190.6 (chlorobenzene-d_5)	197.0 (toluene-d_8)	168
[Cp*($C_2B_9H_{11}$)M]$_2$(μ-*C*H_2)		193.1(toluene-d_8)	172.5(toluene-d_8)	168
Cp*($C_2B_9H_{11}$)M(*Me*)(THF)		48.8 (THF-d_8)	50.9(THF-d_8)	168
Cp*M[*C*$H_2CH_2CH_2NMe_2$]$_3$		56.61	66.49	169
Cp*M[*C*$H_2CH_2CH_2NMe_2$]$_2$Cl		51.94, 59.95 (toluene-d_8, -65 °C)	54.98, 70.09 (toluene-d_8, -60 °C)	170
(η^5-1,2-$Me_2C_5H_3$)$_2$M*Me*(*C*H_2 ^{t}Bu)		73.0 for Zr-*C*H_2 37.5 for Zr-*Me*	74.9 for Hf-*C*H_2, 38.3 for Hf-*Me*	171
(η^5-1,2-$Me_2C_5H_3$)$_2$M*Me*Cl		31.5	33.2	171
(η^5-1,2-$Me_2C_5H_3$)$_2$M*Me*(*C*H_2SiMe$_3$)		44.5 (*C*H_2), 32.3 for Zr-*Me*	46.3 for Hf-*C*H_2; 37.4 for Hf-*Me*	171
(η^5-1,3-^{t}Bu$_2C_5H_3$)CpM*Me*$_2$		32.7	38.2	172,173
(η^5-1,3-^{t}Bu$_2C_5H_3$)M*Me*$_3$		45.6	57.3	173,174
(η^5-1,3-^{t}Bu$_2C_5H_3$)M(*C*H_2Ph)$_3$		72.3	84.2	173,174
Cp*$_2$M(H)(*C*$H_2CH_2CH_2CH_3$)		52.48	62.55	175
Cp*$_2$M(H)(*C*H_2CH_2Ph)		51.79	62.45	175
Cp*(η^5-C_5H_3-1,3-^{t}Bu$_2$)M(H)(*C*H_2CHMe$_2$)		70.44	76.44	175

Table C4. Continued

Complexes	M = Ti	Zr	Hf	Refs.
[η^5-1,3-($SiMe_3$)$_2$$C_5H_3$]M*Me*(DAD) (DAD = 1,4-diphenyl-2,3-dimethyl-1,4-diazabuta-1,3-diene)		22.71	28.48	176
[η^5-1,3-($SiMe_3$)$_2$$C_5H_3$]M(*C*$H_2$Ph)(DAD)		51.07	55.97	176
(Cp*)($C_2B_9H_{11}$)M[*C*(Me)=CMe_2], $C_2B_9H_{11}^{2-}$ = dicarbollide		190.6	197	168
^{Mes}(N*C*N)M*Me*$_2$ [^{Mes}(N*C*N) = diamido N-heterocyclic carbene (NHC)]		48.4 (Me) 189.8 (Zr-$C_{carbene}$)	54.1 (Me) 196.1 (Hf-$C_{carbene}$)	177
cis-{[Cp*M*Me*(μ-F)][(μ-F)$_2$AlMe_2]}$_2$ (Opposite of Trend 1)		45.2	43.5	178
Cp*M[*C*H_2CH_2CH_2NMe_2)Cl_2 (Opposite of Trend 1)		65.23	64.44	169
[1,2-(9-fluorenyl)$_2$(CH_2)$_2$]M*Me*$_2$ (Opposite of Trend 1)		41.1(CD_2Cl_2)	27.2 (CD_2Cl_2)	179
Cp*M*Me*$_2$[Me_3SiNS(Me)NSiMe_3] (Opposite of Trend 1)		12.5	12.39	180
cis-{[Cp*M*Me*(μ$_2$-F)][(μ$_2$-F)$_2$AlMe_2]}$_2$ (Opposite of Trend 1)		45.2	43.5	178

[a] Referenced to $SiMe_4$ at 0.00 ppm.

Table C5. ^{13}C NMR chemical shifts of α-C atoms in alkyl ligands of d^0 Group 5 complexes following Trend 1[a]

Complexes	M = Nb	Ta	Refs.
M*Me*$_3$(O-2,6-Me_2-C_6H_3)$_2$	47.1	57.4	181
M*Me*$_3$(O-2,6-Ph_2-C_6H_3)$_2$	52	58.7	182
M*Me*$_2$(O-2,6-Ph_2-C_6H_3)$_3$	62	64.8	182
M(*C*H_2-p-tolyl)$_3$(O-2,6-Ph_2-C_6H_3)$_2$	72.5	78.4	183
M*Me*(OC_6H_3Ph-C_6H_4)(O-2,6-Ph_2-C_6H_3)	62.0 (*Me*), 190.9 (Nb-*C* in C_6H_4)	64.3 (*Me*), 199.9 (Ta-*C* in C_6H_4)	184
M(*C*H_2-p-tolyl)(OC_6H_3Ph-C_6H_4)(O-2,6-Ph_2-C_6H_3)	84.3 (*C*H_2), 193.9 (Nb-*C* in C_6H_4)	86.6 (*C*H_2), 200.7 (Nb-*C* in C_6H_4)	184
[M(*C*H_2SiMe_3)$_3$(NCMe)]$_2$(μ-1,3-NC_6H_4N) (Dimer)	62.1	77	185
M(*C*H_2Ph)$_3$(=N ^{t}Bu)	53.3	67.6	186,187
[M(*C*H_2SiMe_3)(η^2-RC=NAr)]$_2$(μ-1,4-NC_6H_4N) (R = CH_2SiMe_3; Ar = 1,6-Me_2-C_6H_3) (Dimer)	21.9, 32.1 (two *C*H_2SiMe_3)	27.0, 32.6 (two *C*H_2SiMe_3)	188
[BDI^{Cl}]M*Me*$_2$(=N ^{t}Bu) [BDI^{Cl} = bis-N,N-(2,6-dichlorophenyl)-β-diketiminate]	46.63	56.5	189
Cp$_2$M*Me*(=N ^{t}Bu) ($CDCl_3$)	-6.7	4.65	190
[(η^5-C_5H_4)(η^1-*C*$_5H_4$)CMe_2]M(NMe_2)(=N-2,6-^{i}Pr$_2$$C_6H_3$)	142.8 (ipso-C_5H_4)	145.3 (ipso-C_5H_4)	191
Cp*M*Me*$_3$Cl	64.9 (benzene-*d*$_6$, 20 °C)	72.8 (toluene-*d*$_8$)	192,193
Cp*M*Me*$_2$(=N-2,6-^{i}Pr$_2$$C_6H_3$)	41	48.4	194
Cp*M*Me*$_2$(*benzyne*)	44 (*Me*), 213 (*benzyne*)	52.7 (*Me*), 230.5 (*benzyne*)	195
Tp*M*Me*Cl(=N^{t}Bu)	50	51.5	196

Table C5. Continued

Complexes	M = Nb	Ta	Refs.
Tp*M*Me*$_2$(=N^{t}Bu)	46.9	52.5	196
Tp*M*Me*(NMe$_2$)(=N^{t}Bu)	24.8	30	197
(N$_2$P*C*N)M(*C*H$_2$SiMe$_3$) (N$_2$PCN^{4-} = tetraanionic pentadentate ligand derived from a triamidophosphine)	49.8 (CH$_2$), 58.9 (CH)	62.1 (CH$_2$), 67.5 (CH)	198
(N$_2$P*C*N)M(NMe$_2$)	65.3 (CH)	69.9 (CH)	198
[NP(*C*N)$_2$]M(PMe$_3$) [NP(CN)$_2^{5-}$ = pentaanionic hexadentate ligand derived from N$_2$PCN^{4-}]	57.1 (CH), 57.7 (CH)	58.0 (CH), 58.3 (CH)	198
M(=CH^{t}Bu)(*C*H$_2$^{t}Bu)$_3$	96.9 (toluene-*d*$_8$, -50 °C)	113.7	199
M$_2$(μ-CSiMe$_3$)$_2$(*C*H$_2$SiMe$_3$)$_4$	64.2	79.3 (76.8)	200,201
Cp*M(=CHSiMe$_3$)(*C*H$_2$SiMe$_3$)$_2$	50.25	56.31	202
[(η^5-C$_5$H$_4$)$_2$CMe$_2$]M*Me*(=N^{t}Bu) (Opposite of Trend 1)	2.3	2.2	203
Tp*M(*C*H$_2$Ph)Cl(=N^{t}Bu) (Opposite of Trend 1)	78.6	76	196
Tp*M(*C*H$_2$^{t}Bu)Cl(=N^{t}Bu) (Opposite of Trend 1)	99.3	92	196
Tp*M(*C*H$_2$SiMe$_3$)Cl(=N^{t}Bu) (Opposite of Trend 1)	67	59.6	196
Tp*M(*C*H$_2$CMe$_2$Ph)Cl(=N^{t}Bu) (Opposite of Trend 1)	97.6	91.4	196

[a] Referenced to SiMe$_4$ at 0.00 ppm.

Table C6. ^{13}C NMR chemical shifts of α-C atoms in alkyl ligands of d^0 Groups 6-7 complexes following Trend 1[a]

Complexes	M = Mo	W	Tc	Re	Refs.
Group 6 Complexes					
(^{t}Bu*C*H$_2$)$_3$M≡C^{t}Bu	88.1	103.4			204,205
(Me$_3$Si*C*H$_2$)$_3$M≡CSiMe$_3$	68.8	75.85			206
M(≡C^{t}Bu)(*C*H$_2$^{t}Bu)$_2$(O-2,6-^{i}Pr$_2$-C$_6$H$_3$)	59.5	62.12			207
M(*C*H$_2$^{t}Bu)$_2$(=CH^{t}Bu)(=N-2,6-^{i}Pr$_2$C$_6$H$_3$) (Also Alkyl) (Opposite the trend)	77.9	89.9			207,208
M(≡CH^{t}Bu)(*C*H$_2$^{t}Bu)(=N-2,6-^{i}Pr$_2$-C$_6$H$_3$)(OC$_6$F$_5$)	60.4	61.8			207
M(≡CH^{t}Bu)(*C*H$_2$^{t}Bu)(=N-2,6-^{i}Pr$_2$-C$_6$H$_3$)(O^{t}Bu)	79.8	82.10			207
M(≡CH^{t}Bu)(*C*H$_2$^{t}Bu)(=N-2,6-^{i}Pr$_2$-C$_6$H$_3$)(O-2,6-^{i}Pr$_2$-C$_6$H$_3$)	59.5	62.12			207
M(*C*H$_2$^{t}Bu)$_2$(=N-2,6-^{i}Pr$_2$C$_6$H$_3$)$_2$	79.9	91.19			208,209
M(*C*H$_2$SiMe$_3$)$_2$(=N-2,6-^{i}Pr$_2$C$_6$H$_3$)$_2$	50.3	59.30			210,211
M(*C*H$_2$GeMe$_3$)$_2$(=N-2,6-^{i}Pr$_2$C$_6$H$_3$)$_2$	51.9	61.31			210,211
M(*C*H$_2$SnMe$_3$)$_2$(=N-2,6-^{i}Pr$_2$C$_6$H$_3$)$_2$	48.8	57.47			210,211
M(*C*H$_2$GeMe$_3$)$_2$(NH-2,6-^{i}Pr$_2$-C$_6$H$_3$)(=N-2,6-^{i}Pr$_2$-C$_6$H$_3$)(OTf)	76.94	79.45			211
M(*C*H$_2$^{t}Bu)$_2$(=N^{t}Bu)(NHIPT) [NHIPT^{2-} = N-2,6-(2,4,6-^{i}Pr$_3$-C$_6$H$_2$)$_2$-C$_6$H$_3$][b]	81.07	89.88			212
M[*C*H(^{t}Bu)CH$_2$CH(CONMe$_2$)](=N-2,6-^{i}Pr$_2$-C$_6$H$_3$)(O^{t}Bu)$_2$	59.1[c]	63.7 (CD$_2$Cl$_2$)[c]			213

Table C6. Continued

Complexes	M = Mo	W	Tc	Re	Refs.
M[*C*H(^{t}Bu)CH$_2$CH(CONMe$_2$)](=N-2,6-^{i}Pr$_2$-C$_6$H$_3$)[OCMe$_2$(CF$_3$)]$_2$	61.2[c]	66.4 (CD$_2$Cl$_2$)[c]			213
Cp*M*Me*$_3$(=N^{t}Bu) (Me$_2$ peak opposite of Trend 1)	23.7 (Me$_2$); 26.8 (Me)	21.2 (Me$_2$); 27.5 (Me)			214
Cp*M*Me*(=O)$_2$ (Opposite of Trend 1)	17.5 ($CDCl_3$)	13.8			214
Cp*M(*C*H$_2$Ph)(=CHPh)(=N-^{t}Bu) (Opposite of Trend 1)	35.3	35.1			214
CpM*Ph*(=N-Mes)$_2$ (ipso-C; Opposite of Trend 1)	170.8	160.1			214
Cp*M*Ph*(=N-^{t}Bu)$_2$ (ipso-C; Opposite of Trend 1)	169.3	167.8			214
Cp*M*Ph*(=N-^{t}Bu)(=O) (ipso-C; Opposite of Trend 1)	167.9	167.0			214
Group 7 Complexes					
*Me*M(=N-2,6-^{i}Pr$_2$-C$_6$H$_3$)$_3$ (Opposite of Trend 1)			30.1 (CD$_2$Cl$_2$)	9.2	215,216

[a] Referenced to SiMe$_4$ at 0.00 ppm.

[b] Unknown solvent.

[c] Second peak not observed

Table C7. ^{29}Si NMR chemical shifts of α-Si atoms in silyl ligands of d^0 complexes following Trend 1[a]

Complexes	M = Zr	Hf	Refs.
$(Me_2N)_3MSi(SiMe_3)_3$	-124.6	-103.5	217
$(Me_2N)_3M(SiPh_2{}^tBu)\bullet 0.5THF$	19.6	46.8	217
$CpCp^*M[Si(SiMe_3)_3]Cl$	-87.3	-77.87	218
$CpCp^*M(SiH_2Ph)Cl$	-14.33	1.49	218
$CpCp^*M[Si(SiMe_3)_3]Me$	-105.72	-83.59	167,218
$Cp^*{}_2M(SiPh_3)Cl$ (Opposite of Trend 1)	47.34	42.86	219
$Cp^*CpM(SiPh_3)Cl$ (Opposite of Trend 1)	42.42	39.96	219

[a] Referenced to $SiMe_4$ at 0.00 ppm.

Table C8. ^{31}P NMR chemical shifts of phosphine ligands in d^0 Groups 3-4 complexes following Trend 1[a]

Complexes	M = Sc	Y	La	Lu	Ti	Zr	Hf	Refs.
Group 3 Complexes								
(*P*N*P*)M(CH_2SiMe_3)$_2$ [PNP$^-$ = N(2-^{i}Pr$_2$P-4-methylphenyl)$_2$]		4.90		14.17				30,128
[(*P*N*P*)MH_2]$_3$		6.61		13.85				30
[(*P*N*P*)$_3$M$_3$H$_5$](BPh_4) (C_6D_5Cl)		10.71		20.35				30
[(*P*N*P*)$_2$M$_2$H$_3$(THF)$_2$](BPh_4) (THF-d_8)		9.55		17.20				30
[N($SiMe_2CH_2$*P*Me_2)$_2$]$_2$MCl (toluene-d_8) La and Lu shifts are opposite of Trend 1		-45.7	-43.51	-42.93				81,220,221
[N($SiMe_2CH_2$*P*Ph_2)$_2$]$_2$MCl (toluene-d_8)		-16.3 (29 °C)	-12.3 (80 °C)					81
[N($SiMe_2CH_2$*P*Me_2)$_2$]$_2$MPh (toluene-d_8)		-46.7		-43.58				81
{[Ph*P*($CH_2SiMe_2NSiMe_2CH_2$)$_2$*P*Ph]M}$_2$(μ-$C_{10}H_8$)		-26.00		-18.37				222
{[Ph*P*($CH_2SiMe_2NSiMe_2CH_2$)$_2$*P*Ph]M}$_2$(μ-$C_{10}H_7$Me)		-25.96		-18.28				222
{[Ph*P*($CH_2SiMe_2NSiMe_2CH_2$)$_2$*P*Ph]M}$_2$(μ-$C_{14}H_{10}$)		-27.29		-19.04				222
[Ph*P*(CH_2SiMe_2NPh)$_2$]MCl(THF)		-27.17		-22.70				223
(3,5-Me_2-C_6H_3N*P* ^{i}Pr$_2$)$_3$M(THF)	34.4	29.6						224

Table C8. Continued

Complexes	M = Sc	Y	La	Lu	Ti	Zr	Hf	Refs.
Group 4 Complexes								
$M_2H_3(BH_4)_5(PMe_3)_2$						-21.2	-14.7	43
$MH(BH_4)_3(Me_2PCH_2CH_2PMe_2)$ (Opposite to Trend 1)						0.2	-3.8	43
$MH_2(BH_4)_2(Me_2PCH_2CH_2PMe_2)_2$ (Opposite to Trend 1)						15.3, 3.5	12.4, 2.5	43
$M_3H_6(BH_4)_6(PMe_3)_4$						-21.4	-14.2	44
$M_2H_4(BH_4)_4(Me_2PCH_2CH_2PMe_2)_2$						11.3, -6.9	12.7, -4.6	44
$(PNP)MCl_3$ [PNP$^-$ = N(2-^{i}Pr$_2$P-4-methylphenyl)$_2$]					48.5	27.1 (CD_2Cl_2)	34.0	157,158,225
$(PNP)MMe_3$					20.1	13.0	17.7 (toluene)	157,158,225
$(PNP)MMe_2(O\text{-}2,6\text{-}{}^iPr_2C_6H_3)$						2.51	2.94	159
$(PNP)M(=CH_2)(O\text{-}2,6\text{-}{}^iPr_2C_6H_3)$						2.51	2.94	159
$(P_2N_2)MCl_2$ [P_2N_2 = $PhP(CH_2SiMe_2NSiMe_2CH_2)_2PPh$]						-14.3	-5.8	226
$MMe_3[N(SiMe_2CH_2P^tBu_2)_2]$						20.35 (toluene-d_8)	20.88	227
$MMe_3[N(SiMe_2CH_2P\,{}^iPr_2)_2]$ (Opposite to Trend 1)						8.7	2.4	227
$(P_2Cp)M(=CHPh)Cl$ [(P_2Cp) = η^5-C_5H_3-1,3-$(SiMe_2CH_2P\,{}^iPr_2)_2$]						18.81	23.4	228,229

Table C8. Continued

Complexes	M = Sc	Y	La	Lu	Ti	Zr	Hf	Refs.
$^{Ph}(P\mathrm{N_3})$M-CH_2Ph [$^{Ph}(PN_3)$ = $P(CH_2CH_2CH_2NPh)_3^{3-}$]					-33.7	-40.2	-34.6	148
$^{Ph}(P\mathrm{N_3})$M-NMe_2					-30.7	-37.3 (toluene-d_8)	-30.7	148
$^{Ph}(P\mathrm{N_3})$M(OTf) (CD_2Cl_2)					6.2	-17.0	-7.6	148
($P\mathrm{N_3}$)MMe (PN_3 = benzylene-linked trisamidophosphine)					-58.0	-58.5 (CD_2Cl_2)	-54.8 (CD_2Cl_2)	149
($P\mathrm{N_3}$)M-NMe_2					-47.1 (toluene-d_8)	-50.5 (toluene-d_8)	-46.9 (CD_2Cl_2)	149
($P\mathrm{N_3}$)MOTf (CD_2Cl_2)					-31.8	-42.9	-34.8	149
(2-R-8-$Ph_2PC_9H_9N$)M(CH_2Ph)$_3$ (R = H)[b]					28.90	23.44	31.03	150
(2-R-8-$Ph_2PC_9H_9N$)M(CH_2Ph)$_3$ (R = Me)[b]						25.65	33.86	150
(2-R-8-$Ph_2PC_9H_9N$)M(CH_2Ph)$_3$ (R = ^{i}Pr)[b]						16.60	19.11	150
(2-R-8-$Ph_2PC_9H_9N$)M(CH_2Ph)$_3$ (R = ^{n}Bn)[b]						24.45	31.98	150
(N-R-2-$Ph_2PC_6H_4N$)M(CH_2Ph)$_3$ (R = Me)[b]						22.46	30.16	150
(N-R-2-$Ph_2PC_6H_4N$)M(CH_2Ph)$_3$ (R = Et)[b]						24.65	32.95	150
(Cbz-P_2^{Ph}-CH)MCl(CH_2Ph) (cyclometalated, carbazole-based PNP pincer ligand) (The CHP atom next to the cyclometalated C atom is opposite to the trend)						-13.2 (CHP), 0.3 (CH_2P)	-20.8 (CHP), 3.1 (CH_2P)	152

Table C8. Continued

Complexes	M = Sc	Y	La	Lu	Ti	Zr	Hf	Refs.
(Cbz-*P*$_2^{Ph}$-CH)MI(CH$_2$Ph) (The CHP atom next to the cyclometalated C atom is opposite to the trend)						-13.3 (CHP), 0.1 (CH$_2$P)	-20.7 (CHP), 3.8 (CH$_2$P)	152
(Cbz-*P*$_2^{Ph}$-CH)M(CH$_2$Ph)$_2$						-17.3 (CHP), 3.5 (CH$_2$P)	-26.4 (CHP), 3.2 (CH$_2$P)	152

[a] Referenced to external (85%) H_3PO_4 at 0.00 ppm.

[b] Presumably the ^{31}P NMR shifts were referenced to external (85%) H_3PO_4.

Table C9. ^{31}P NMR chemical shifts of phosphine ligands in d^0 Groups 5-6 complexes following Trend 1[a]

Complexes	M = Nb	Ta	Mo	W	Refs.
Group 5 Complexes					
$Cp^*MCl_4(PH_2{}^tBu)$ ($CDCl_3$) (Opposite of Trend 1)	20	19			230
$Cp^*MCl_4(PH_2Ad)$ ($CDCl_3$) (Opposite of Trend 1)	16	15			230
$Cp^*MCl_4(PH_2Cy)$ ($CDCl_3$)	5	7			230
$Cp^*MCl_4(PH_2Ph)$ ($CDCl_3$) (Opposite of Trend 1)	-12	-12			230
$Cp^*MCl_4(PH_2Mes)$ ($CDCl_3$) (Opposite of Trend 1)	-40	-40			230
$CpMCl_3[PPh_2CH{=}C(=O)Ph]$	36.5 (CD_2Cl_2)	37.2 ($CDCl_3$)			231
$CpMCl_4[PPh_2CH_2C(O)NPh_2]$ (CD_2Cl_2) (Opposite of Trend 1)	33.1	27.9			231
$(N_2PCN)M(CH_2SiMe_3)$ (N_2PCN^{4-} = tetraanionic pentadentate ligand derived from a triamidophosphine) (Opposite of Trend 1)	-12.3	-18.8			198
$(N_2PCN)M(NMe_2)$ (Opposite of Trend 1)	-20.7	-23.2			198
$[NP(CN)_2]M(PMe_3)$ [$NP(CN)_2^{5-}$ = pentaanionic hexadentate ligand derived from N_2PCN^{4-}] (Shifts of PMe_3 follow Trend 1. However, shifts of $[NP(CN)_2]$ are opposite of Trend 1.)	45.8 $[NP(CN)_2]$, -27.8 (PMe_3)	41.5 $[NP(CN)_2]$, -19.7 (PMe_3)			198
Group 6 Complexes					
$MH_6(P{}^iPr_2Ph)_3$ (Opposite of Trend 1)			57.89	55.5 (toluene-Et_2O; high temperature .	49,51

[a] Referenced to external (85%) H_3PO_4 at 0.00 ppm.

Table C10. ^{13}C NMR chemical shifts of α-C atoms in alkylidene and alkylidyne ligands of d^0 Groups 4-6 complexes following Trend 2[a]

Complexes	M = Zr	Hf	Nb	Ta	Mo	W	Refs.
Group 4 Complexes							
{[M(μ-*C*HSi(Me)$_2$N] SiMe$_3$[N(SiMe$_3$)$_2$]}$_2$	195.7	180.3					155
(PNP)M(=*C*H$_2$)(O-2,6-^{i}Pr$_2$C$_6$H$_3$) [PNP$^-$ = N(2-^{i}Pr$_2$P-4-methylphenyl)$_2$]	230.20	224.58					159
(P$_2$Cp)M(=*C*HPh)(Cl) [(P$_2$Cp) = η^5-C$_5$H$_3$-1,3-(SiMe$_2$CH$_2$P^{i}Pr$_2$)$_2$]	229.4	210					228,229
Group 5 Complexes							
Cp$_2$M(=*C*H^{t}Bu)Cl			299	274 (CD$_2$Cl$_2$)			232
Cp*M(CH$_2$SiMe$_3$)$_2$(=*C*HSiMe$_3$)			270.97	223.94			202
M(=*C*H^{t}Bu)(THF)$_2$Cl$_3$			257 (CDCl$_3$, -20 °C)	253.8 (CDCl$_3$, -30 °C)			233
M$_2$(μ-*C*SiMe$_3$)$_2$(CH$_2$SiMe$_3$)$_4$			406	404.7 (authors' data)			200,201
M(CH$_2$^{t}Bu)$_3$(=*C*H^{t}Bu) (Opposite of Trend 2)			246 (toluene-*d*$_8$, -50 °C)	250			199

Table C10. Continued

Complexes	M = Zr	Hf	Nb	Ta	Mo	W	Refs.
M(=*C*H^{t}Bu)(PMe$_3$)$_2$Cl$_3$ (Opposite of Trend 2)			252.8 ($CDCl_3$, -30 °C)	255.9 (toluene-d_8, -50 °C)			233
Group 6 Complexes							
M(CH$_2$^{t}Bu)$_2$(=*C*H^{t}Bu)(=N-2,6-^{i}Pr$_2$C$_6$H$_3$)					255.0	247.2	208,234
M(CH$_2$^{t}Bu)(=*C*H^{t}Bu)(=N-2,6-^{i}Pr$_2$-C$_6$H$_3$)(OC$_6$F$_5$)					286.5	260.5	207
M(CH$_2$^{t}Bu)(=*C*H^{t}Bu)(=N-2,6-^{i}Pr$_2$-C$_6$H$_3$)(O^{t}Bu)					275.9	253.6	207
M(CH$_2$^{t}Bu)(=*C*H^{t}Bu)(=N-2,6-^{i}Pr$_2$-C$_6$H$_3$)[OCMe(CF$_3$)$_2$]					283.6	259.15	207
M(CH$_2$^{t}Bu)(=*C*H^{t}Bu)(=N-2,6-^{i}Pr$_2$-C$_6$H$_3$)(O-2,6-^{i}Pr$_2$-C$_6$H$_3$)					277.7	255.15	207
M(CH$_2$^{t}Bu)(=*C*H^{t}Bu)(=N-2,6-^{i}Pr$_2$-C$_6$H$_3$)(OAd) (Ad = 1-adamantyl)					275.7	253.11	207,235
Cp*M(CH$_2$Ph)(=*C*HPh)(=N-^{t}Bu)					269.6	246.8	214
M(=*C*H^{t}Bu)(=N-2,6-^{i}Pr$_2$-C$_6$H$_3$)(O^{t}Bu)$_2$					265.8 (J_{CH} = 117 Hz)	236.5 (J_{CH} = 114 Hz)	209,236
M(=*C*H^{t}Bu)(=N-2,6-^{i}Pr$_2$-C$_6$H$_3$)[OCMe$_2$(CF$_3$)]$_2$					276.8 (J_{CH} = 118 Hz)	244.9 (J_{CH} = 114 Hz)	209,236
M(=*C*H^{t}Bu)(=N-2,6-^{i}Pr$_2$-C$_6$H$_3$)[OCMe(CF$_3$)$_2$]$_2$					288.2 (J_{CH} = 117 Hz)	253.9	237

Table C10. Continued

Complexes	M = Zr	Hf	Nb	Ta	Mo	W	Refs.
M(=*C*H^{t}Bu)(=N-2,6-^{i}Pr$_2$-C$_6$H$_3$)[OCMe(CF$_3$)$_2$]$_2$(PMe$_3$)					293.2 (syn), 313.9 (anti)	270.1 (syn), 286.9 (anti)	238
M(=*C*H^{t}Bu)(=N-2,6-^{i}Pr$_2$-C$_6$H$_3$)[OCMe(CF$_3$)$_2$]$_2$(quin) (quin = quinuclidine)					296.4 (syn), 311.1 (anti)	273.5 (syn), 279.3 (anti)	238
M(=*C*HSiMe$_3$)(=N-2,6-^{i}Pr$_2$-C$_6$H$_3$)[OCMe(CF$_3$)$_2$]$_2$					289.8	242.8	237,239
M(=*C*H^{t}Bu)[NHIPT]Cl$_2$(py) ([NHIPT]$^{2-}$ = N-2,6-(2,4,6-^{i}Pr$_3$-C$_6$H$_2$)$_2$-C$_6$H$_3$)[b]					331.54	298.90	212
M(=*C*H^{t}Bu)[NHIPT]Cl$_2$ ([NHIPT]$^{2-}$ = N-2,6-(2,4,6-^{i}Pr$_3$-C$_6$H$_2$)$_2$-C$_6$H$_3$)					317.76	284.06	212
M(=*C*H^{t}Bu)(=N^{t}Bu)(O-2,6-Mesityl$_2$-C$_6$H$_3$)(Pyr)					287.72	255.02	240,241
M(=*C*HGeMe$_3$)(=N-2,6-^{i}Pr$_2$-C$_6$H$_3$)(OCMe$_2$CF$_3$)$_2$					275.5 (toluene-*d*$_8$)	231.8	242,243
M(=*C*HCMe$_2$Ph)(=N-2,6-^{i}Pr$_2$-C$_6$H$_3$)[OC(CF$_3$)$_3$]$_3$					298.6	260.6	244,245
M(=*C*HCMe$_2$Ph)(=N-2,6-dimesityl-C$_6$H$_3$)Cl$_2$(py)					329.4 (CD$_2$Cl$_2$)	298.0	246,247

Table C10. Continued

Complexes	M = Zr	Hf	Nb	Ta	Mo	W	Refs.
M(=*C*HCMe$_2$Ph)(=N-2,6-dimesityl-C$_6$H$_3$)(Me$_2$pyr)(O^{t}Bu)					283.4	256.0	246,247
M(=*C*HCMe$_2$Ph)(=N-2,6-dimesityl-C$_6$H$_3$)(Pyr)$_2$(Py) (Pyr = pyrrole)					319.1	284.6 (CD$_2$Cl$_2$)	247
(^{t}BuCH$_2$)$_3$M≡*C*^{t}Bu					323.8	316.2	204,205
(Me$_3$SiCH$_2$)$_3$M≡*C*SiMe$_3$					363.9 (toluene-*d*$_8$)	343.67 (toluene-*d*$_8$)	206
(^{t}BuO)$_3$M≡*C*^{t}Bu					296.1	271.5	205,248
M(≡*C*^{t}Bu)Cl$_3$(DME)					341.3	335.1	204,205
M(≡*C*^{t}Bu)(O-2,6-^{i}Pr$_2$-C$_6$H$_3$)$_3$					337.2	295.2	204,249
M(≡*C*^{t}Bu)[OCMe$_2$(CF$_3$)]$_3$					309.7	283.0	204,250
M(≡*C*Ph)(O^{t}Bu)$_3$					276.7	271	251,252
M(≡^{13}*C*CH$_3$)(O^{t}Bu)$_3$					279.6	254.1	253
M(≡*C*^{n}Pr)(O^{t}Bu)$_3$					286.6	261.7	204,254
M(≡^{13}*C* ^{i}Pr)(O^{t}Bu)$_3$					292.7	268.3	253
M(≡*C*H)(O^{t}Bu)$_3$(quin) (quin = quinuclidine)					267.2	247.1	251,254
M(≡*C*^{t}Bu)(O$_2$CCF$_3$)$_3$(DME)					341.3	319.7	255
M(≡*C*^{t}Bu)(O$_2$CCHMe$_2$)$_3$					311.2	298.2	255
M(≡*C*^{t}Bu)(O$_2$CCH$_3$)$_3$					312.4	286.5	255
M(≡*C*^{t}Bu)(O$_2$C^{t}Bu)$_3$					311.3	285.5	255
M(≡*C*^{t}Bu)(TIPT)$_3$ (TIPT = 2,4,6-triisopropylbenzenethiolate)					341.5 (CD$_2$Cl$_2$)	329.4 (CD$_2$Cl$_2$)	256

Table C10. Continued

Complexes	M = Zr	Hf	Nb	Ta	Mo	W	Refs.
$[M(\equiv C^tBu)(TMT)_3]_2$ (TMT = 2,4,6-trimethylbenzenethiolate)					336.0 (CD_2Cl_2)	324.3 (CD_2Cl_2)	256
$(N_3N_F)M(\equiv C^tBu)$ [$N_3N_F^{3-}$ = $(C_6F_5NCH_2CH_2)_3N^{3-}$]					312.9 (CD_2Cl_2)	296.07 (THF-d_8)	257
$(N_3N_F)M(\equiv COSiMe_3)$					212.44	216.9	258
$(F_3NMe)M(\equiv C^tBu)(CH_2{}^tBu)$ [F_3NMe^{2-} = $(C_6H_2F_3NCH_2CH_2)_2NMe^{2-}$]					307.74	295.71 (CD_2Cl_2)	259

[a] Referenced to $SiMe_4$ at 0.00 ppm.

[b] Unknown solvent.

Table C11. ^{17}O NMR chemical shifts of oxo ligands in d^0 Groups 6-8 complexes following Trend 2[a]

Complexes	M = Mo	W	Tc	Re	Ru	Os	Refs.
MO_4^{2-}	496, 524	384					260,261
MO_4^-			713	543			260,261
MO_4					1070	760	260,261

[a] Referenced to H_2O at 0.00 ppm.

Table C12. ^{19}F NMR chemical shifts of fluoride ligands in Groups 4-5 d^0 complexes following Trend 2[a]

Complexes	M = Ti	Zr	Hf	V	Nb	Ta	Refs.
Group 4 complexes							
$(NH_4)_2MF_6$ (aqueous)[b,c]	75.65	2.65	-43.55				262-264
$(NH_4)_2MF_6$ (aqueous)		-11.4	-41.4				265
Cp^*MF_3	124.0 (dimer)	97.5 (4F), -26.3 (4F), -50.7 (2F), -72.7 (2F) (tetramer)	41.8 (4F), -54.0 (4F), -77.3 (2F), -97.8 (2F) (tetramer)				266
Cp^*_2MHF (cyclohexane-d_{12})		141.4	107.8				267,268
$Cp^*_2MF_2$	74.14, 50.3 ($DCCl_3$)		49.7 (cyclohexane-d_{12})				269,270
$(Cp^*MF_2Cl)_4$ ($CDCl_3$)		-19.9 (4F), -30.9 (2F), -59.2 (2F)	-46.5 (4F), -58.5 (2F), -84.3 (2F)				271
$[Cp^*_2MF(OCOCF_3)_2]_2$		-82.1	-103.8				272
(Htmpy)[$(Cp^*MF_2)_2(m\text{-}F)_3$] (tmpy = 2,4,6-trimethylpyridine)		59.6 (2F, F_t), 20.4 (2F), -58.8 (2F), -66.5 (1F)	10.8 (2F, F_t), -17.9 (2F), -81.1 (2F), -91.6 (1F)				273
cis-{[Cp*MMe(m_2-F)][(m_2-F)$_2$AlMe$_2$]}$_2$		-32.5 (MFM), -69.5 (MFM), -108.2 (MFAl)	-56.7 (MFM), -87.3 (MFM), -109.8 (MFAl)				178

Table C12. Continued

Complexes	M = Ti	Zr	Hf	V	Nb	Ta	Refs.
Group 5 complexes							
M*F*$_5$					162 (CH_2Cl_2)*	99.6 (SO_2)*	274
M*F*$_5$(THF) ($CDCl_3$)					156.3	71.8	275
M*F*$_5$(Me_2CO) ($CDCl_3$)					114.4	78.4	275
M*F*$_5$[$(Me_2N)_2CO$] (CD_2Cl_2)					126.8	81.7	275
M*F*$_5$(Ph_2CO) ($CDCl_3$)					142.6	72.2	275
M*F*$_5$[O=P(SEt)Ph_2][c,d] (CH_2Cl_2)					159.5, 128.0	85.2, 58.4	276
M*F*$_5$[O=P(OEt)Ph_2][c,d] (CH_2Cl_2)					163.9, 129.5	87.1, 58.9	276
M*F*$_5$(O=PPh_3)[c,d] (CH_2Cl_2)					156.0, 125.5	81.6, 56.8	276
M*F*$_5$(PMe_3) (toluene-*d*$_8$)					156.7	70.3	277
M*F*$_5$(PMe_3) (toluene-*d*$_8$), -80 °C					155.2 (1F), 108.7 (4F)	82.4 (1F), 43.1 (4F)	277
M*F*$_5$(PPh_3) (CH_2Cl_2)					104.2	38	277
M*F*$_5$($AsMe_3$) (toluene-*d*$_8$, -80 °C)					135.1 (1F), 98.9 (4F)	70.2 (1F), 27.2 (4F)	277

Table C12. Continued

Complexes	M = Ti	Zr	Hf	V	Nb	Ta	Refs.
M*F*$_5$(AsEt$_3$) (toluene-*d*$_8$, -80 °C)					143.9 (1F), 103.3 (4F)	69.2 (1F), 34.6 (4F)	277
[M*F*$_4$(PMe$_3$)$_2$](M*F*$_6$) (CD_2Cl_2)					118.5 (4F), 103.4 (6F)	56.2 (4F), 39.5 (6F)	277
[M*F*$_4$(PMe$_3$)$_2$](M*F*$_6$) (CD_2Cl_2), -80 °C					112.9 (4F), 103.5 (6F)	55.0 (4F), 39.5 (6F)	277
M(=O)*F*$_3$				211 (CH_3CN)	196.3, -10.4 (solid state)	124.2, -51.5 (solid state)	278,279
M$_2$*F*$_{10}$[O=P(SEt)Ph$_2$][c,d] (CH_2Cl_2)					223.1, 193.7, 184.8, 167.2, 149.2, -52.4	130.4, 119.4, 110.0, 87.2, 73.6, -78.7	276

Table C12. Continued

Complexes	M = Ti	Zr	Hf	V	Nb	Ta	Refs.
$M_2F_{10}[O=P(OEt)Ph_2]^{c,d}$ (CH_2Cl_2)					223.9, 194.5, 185.0, 168.8, 149.5, -51.9	131.4, 119.7, 111.1, 88.0, 78.4, -78.4	276
$[S(NMe_2)_3](MF_6)$ $(CDCl_3)$					103.5	39.1	275
$[S(NMe_2)_3](M_2F_{11})$ $(CDCl_3)$					135.2	77.6	275
$(N^nBu_4)(MF_6)$					103.1 $(CH_2Cl_2)^b$	40.4 $(SO_2)^b$	274
$(N^nBu_4)(M_2F_{11})$					191.0, 145.9, -56.0 (CH_2Cl_2)*	115.1, 72.0, -80.8 (SO_2)*	274
$[2,4\text{-}(OMe)_2C_6H_5](M_2F_{11})$ (CD_2Cl_2)					132.6	69.3	280
$\{MF_4[o\text{-}C_6H_4(PMe_2)_2]_2\}(MF_6)$ (CD_3CN)					102.3 (6F), -7.8 (4F)	37.4 (6F), -39.8 (4F)	281
$\{MF_4[o\text{-}C_6H_4(AsMe_2)_2]_2\}(MF_6)$ (CD_2Cl_2)					103.6 (6F), 27.1 (4F)	39.5 (6F), -28.0 (4F)	281

Table C12. Continued

Complexes	M = Ti	Zr	Hf	V	Nb	Ta	Refs.
{M*F*$_4$[Me$_2$P(CH$_2$)$_2$PMe$_2$]$_2$}(M*F*$_6$) (CD$_3$CN)					102.0 (6F), -10.9 (4F)	38.3 (6F), -40.8 (4F)	281
{M*F*$_4$[o-C$_6$H$_4$(PPh$_2$)$_2$]$_2$}(M*F*$_6$) (CD$_3$CN)					102.8 (6F), 54.8 (4F)	38.6 (6F), 16.8 (4F)	281
[M*F*$_4$(THF)$_4$](M*F*$_6$) (CDCl$_3$)					180.1 (4F), 103.1 (6F)	80.0 (4F), 39.6 (6F)	275
[M*F*$_4$(DMF)$_4$](M*F*$_6$) (CDCl$_3$)					144.1 (4F), 103.7 (6F)	64.9 (4F), 39.6 (6F)	275
(M*F*$_5$)$_2$[κ^2-1,3-(OMe)$_2$C$_6$H$_4$] (CD$_2$Cl$_2$, -85 °C)					199.1 (1F, *trans*-F), 156.3 (4F, cis-F)	100.4 (1F, *trans*-F), 79.9 (4F, cis-F)	280
[M*F*$_4$(κ^2-DME)$_2$](M*F*$_6$) (CD$_2$Cl$_2$)					182.0 (4F), 103.8 (6F)	93.2 (4F), 39.7 (6F)	282

Table C12. Continued

Complexes	M = Ti	Zr	Hf	V	Nb	Ta	Refs.
[M*F*$_4$(κ^2-DME)$_2$](M$_2$*F*$_{11}$)(CD_2Cl_2)					183.7 (4F), 153.3 (11F)	94.7 (4F), 72.2 (11F)	282
{M*F*$_4$[κ^2-$MeOCH_2CH(Me)OMe]_2$}(M*F*$_6$)(CD_2Cl_2)					189.1 (2F), 174.1 (2F), 104.1 (6F)	99.8 (2F), 87.3 (2F), 38.9 (6F)	282
{M*F*$_4$[κ^2-$MeOCH_2CH(Me)OMe]_2$}(M$_2$*F*$_{11}$)(CD_2Cl_2)					190.7 (2F), 168.1 (2F), 143.8 (11F)	101.7 (2F), 90.0 (2F), 70.2 (11F)	282
M{*cis*-*F*$_4$[O=P(SEt)Ph_2]$_2$}(M$_2$*F*$_{11}$)[b,c] (CH_2Cl_2)					179.5 and 151.0 (4F), 191.3, 145.6 and -56.4 (11F)	101.0 and 75.2 (4F), 115.7, 71.5 and -80.9 (11F)	276

Table C12. Continued

Complexes	M = Ti	Zr	Hf	V	Nb	Ta	Refs.
$[V(acac)_3](MF_6)$ ($CDCl_3$)					103.2 (-90 °C)	42.6	[283]

[a] Unless noted, referenced to $CFCl_3$ at 0.00 ppm.

[b] The data in the original paper, referenced to CF_3COOH, have been converted with $CFCl_3$ as reference (and ^{19}F NMR of CF_3COOH at -76.55 ppm according to ^{19}F NMR Reference Standards.[263]).

[c] The signs of the chemical shifts in the original paper have been converted, using the current system.

[d] The data in the original paper, referenced to F_2, have been converted to using $CFCl_3$ as reference (and ^{19}F NMR of F_2 at 430.6 ppm as the authors indicated)

Table C13. ^{19}F NMR chemical shifts of fluoride ligands in Groups 6-7 d^0 complexes following Trend 2[a]

Complexes	M = Mo	W	Tc	Re	Refs
M*F*$_6$ (unknown solvent)	282.1	167.0, 169.2			264,284,285
M(=O)*F*$_4$[b] (propylene carbonate solutions)	145.9	65.2			286
*F*Kr*F*-M(=O)*F*$_4$ (SO_2ClF, -121 °C)	148.6 (Mo-F), -12.4 (Mo-F-Kr), 70.4 (Kr-F)	67.9 (W-F), -26.1 (W-F-Kr), 67.7 (Kr-F)			287
*F*Xe*F*-M(=O)*F*$_4$ (BrF_5)	141.8 (Mo-F), -170.0 (Mo-F-Kr), -223.1 (Xe-F) (-84 °C)	135.8 (W-F), -168.8 (W-F-Xe), -228.9 (Xe-F) (-62 °C)			288
M(=O)*F*$_5$			50.6 (pure liquid; whether +50.6 or -50.6 ppm is not clear)	199 (equatorial), -3.7 (axial) (1:4 in WF_6)	285,289

[a] Unless noted, ref. to $CFCl_3$.

[b] The signs of the chemical shifts in the original paper have been converted using the current system.

Table C14. DFT calculations for ^{13}C shift of Me ligands in Cp_2MMe_2 complexes[290-299]

Complexes	Exp.	TZP	QZ4P
$Cp_2Ti\mathit{Me}_2$	45.9[137]	51.78	52.17
$Cp_2Zr\mathit{Me}_2$	30.62[136]	35.48	34.44
$Cp_2Hf\mathit{Me}_2$	36.84[136]	37.53	37.26

References

1. Jeske, G.; Lauke, H.; Mauermann, H.; Swepston, P. N.; Schumann, H.; Marks, T. J. *J. Am. Chem. Soc.* **1985**, *107*, 8091.
2. Booij, M.; Deelman, B. J.; Duchateau, R.; Postma, D. S.; Meetsma, A.; Teuben, J. H. *Organometallics* **1993**, *12*, 3531.
3. Thompson, M. E.; Baxter, S. M.; Bulls, A. R.; Burger, B. J.; Nolan, M. C.; Santarsiero, B. D.; Schaefer, W. P.; Bercaw, J. E. *J. Am. Chem. Soc.* **1987**, *109*, 203.
4. Watson, P. L.; Roe, D. C. *J. Am. Chem. Soc.* **1982**, *104*, 6471.
5. Fieser, M. E.; Mueller, T. J.; Bates, J. E.; Ziller, J. W.; Furche, F.; Evans, W. J. *Organometallics* **2014**, *33*, 3882.
6. den Haan, K. H.; Teuben, J. H. *J. Chem. Soc. Chem. Comm.* **1986**, 682.
7. Evans, W. J.; Perotti, J. M.; Ziller, J. W. *Inorg. Chem.* **2005**, *44*, 5820.
8. Evans, W. J.; Champagne, T. M.; Ziller, J. W. *J. Am. Chem. Soc.* **2006**, *128*, 14270.
9. Lorenz, S. E.; Schmiege, B. M.; Lee, D. S.; Ziller, J. W.; Evans, W. J. *Inorg. Chem.* **2010**, *49*, 6655.
10. Busch, M. A.; Harlow, R.; Watson, P. L. *Inorg. Chim. Acta* **1987**, *140*, 15.
11. Ye, C.; Qian, C.; Yang, X. *J. Organomet. Chem.* **1991**, *407*, 329.
12. Xie, Z.; Qian, C.; Huang, Y. *J. Organomet. Chem.* **1991**, *412*, 61.
13. Deng, D.; Jiang, Y.; Qian, C.; Wu, G.; Zheng, P. *J. Organomet. Chem.* **1994**, *470*, 99.
14. Alvarez, D.; Caulton, K. G.; Evans, W. J.; Ziller, J. W. *Inorg. Chem.* **1992**, *31*,

5500.

15. Voskoboynikov, A. Z.; Parshina, I. N.; Shestakova, A. K.; Butin, K. P.; Beletskaya, I. P.; Kuz'mina, L. G.; Howard, J. A. K. *Organometallics* **1997**, *16*, 4041.

16. (16) Hultzsch, K. C.; Spaniol, T. P.; Okuda, J. *Angew. Chem. Int. Ed.* **1999**, *38*, 227.

17. Arndt, S.; Voth, P.; Spaniol, T. P.; Okuda, J. *Organometallics* **2000**, *19*, 4690.

18. Qian, C.-T.; Zou, G.; Nie, W.-L.; Sun, J.; Lemenovskii, D. A.; Borzov, M. V. *Polyhedron* **2000**, *19*, 1955.

19. Ohashi, M.; Konkol, M.; Del Rosal, I.; Poteau, R.; Maron, L.; Okuda, J. *J. Am. Chem. Soc.* **2008**, *130*, 6920.

20. Cui, D.; Nishiura, M.; Tardif, O.; Hou, Z. *Organometallics* **2008**, *27*, 2428.

21. Cheng, J.; Saliu, K.; Kiel, G. Y.; Ferguson, M. J.; McDonald, R.; Takats, J. *Angew. Chem. Int. Ed.* **2008**, *47*, 4910.

22. Nishiura, M.; Baldamus, J.; Shima, T.; Mori, K.; Hou, Z. *Chem. Eur. J.* **2011**, *17*, 5033.

23. Shima, T.; Hou, Z. *Dalton Trans.* **2010**, *39*, 6858.

24. Cheng, J.; Ferguson, M. J.; Takats, J. *J. Am. Chem. Soc.* **2010**, *132*, 2.

25. Cheng, J.; Wang, H.; Nishiura, M.; Hou, Z. *Chem. Sci.* **2012**, *3*, 2230.

26. Cui, P.; Spaniol, T. P.; Maron, L.; Okuda, J. *Chem. Eur. J.* **2013**, *19*, 13437.

27. Schädle, C.; Schädle, D.; Eichele, K.; Anwander, R. *Angew. Chem. Int. Ed.* **2013**, *52*, 13238.

28. Sobaczynski, A. P.; Bauer, T.; Kempe, R. *Organometallics* **2013**, *32*, 1363.

29. Lyubov, D. M.; Döring, C.; Fukin, G. K.; Cherkasov, A. V.; Shavyrin, A. S.; Kempe, R.; Trifonov, A. A. *Organometallics* **2008**, *27*, 2905.

30. Cheng, J.; Shima, T.; Hou, Z. *Angew. Chem. Int. Ed.* **2011**, *50*, 1857.

31. Baldwin, S. M.; Bercaw, J. E.; Brintzinger, H. H. *J. Am. Chem. Soc.* **2008**, *130*, 17423.

32. Manriquez, J. M.; McAlister, D. R.; Sanner, R. D.; Bercaw, J. E. *J. Am. Chem. Soc.* **1978**, *100*, 2716.

33. Roddick, D. M.; Fryzuk, M. D.; Seidler, P. F.; Hillhouse, G. L.; Bercaw, J. E. *Organometallics* **1985**, *4*, 97.

34. Beckhaus, R.; Wagner, M.; Burlakov, V. V.; Baumann, W.; Peulecke, N.; Spannenberg, A.; Kempe, R.; Rosenthal, U. *Z. Anorg. Allg. Chem.* **1998**, *624*, 129.

35. Manriquez, J. M.; McAlister, D. R.; Sanner, R. D.; Bercaw, J. E. *J. Am. Chem. Soc.* **1976**, *98*, 6733.

36. Hillhouse, G. L.; Bercaw, J. E. *J. Am. Chem. Soc.* **1984**, *106*, 5472.

37. Erker, G.; Schlund, R.; Krueger, C. *Organometallics* **1989**, *8*, 2349.

38. Couturier, S.; Tainturier, G.; Gautheron, B. *J. Organomet. Chem.* **1980**, *195*, 291.

39. Marks, T. J.; Kolb, J. R. *J. Am. Chem. Soc ty* **1975**, *97*, 3397.

40. Cuenca, T.; Galakhov, M.; Royo, E.; Royo, P. *J. Organomet. Chem.* **1996**, *515*, 33.

41. Liu, X.; Wu, Z.; Cai, H.; Yang, Y.; Chen, T.; Vallet, C. E.; Zuhr, R. A.; Beach, D. B.; Peng, Z.-H.; Wu, Y.-D.; Concolino, T. E.; Rheingold, A. L.; Xue, Z. *J. Am. Chem. Soc.* **2001**, *123*, 8011.

42. Moore, E. J.; California Institute of Technology: 1984.

43. Gozum, J. E.; Girolami, G. S. *J. Am. Chem. Soc.* **1991**, *113*, 3829.

44. Gozum, J. E.; Wilson, S. R.; Girolami, G. S. *J. Am. Chem. Soc.* **1992**, *114*, 9483.

45. Woo, H. G.; Walzer, J. F.; Tilley, T. D. *J. Am. Chem. Soc.* **1992**, *114*, 7047.

46. Lemenovskii, D. A.; Nikonov, G. I.; Brusova, G. P.; Kuzmina, L. G.; Stankoviè, E.; Putala, M. *J. Organomet. Chem.* **1995**, *496*, 227.

47. Reynoud, J. F.; Leblanc, J. C.; Moise, C. *Organometallics* **1985**, *4*, 1059.

48. Deutsch, P. P.; Maguire, J. A.; Jones, W. D.; Eisenberg, R. *Inorg. Chem.* **1990**, *29*, 686.

49. Crabtree, R. H.; Hlatky, G. G. *J. Organomet. Chem.* **1982**, *238*, C21.

50. Crabtree, R. H.; Hlatky, G. G. *Inorg. Chem.* **1984**, *23*, 2388.

51. Gregson, D.; Howard, J. A. K.; Nicholls, J. N.; Spencer, J. L.; Turner, D. G. *J. Chem. Soc. Chem. Comm.* **1980**, 572.

52. Westerhausen, M.; Hartmann, M.; Schwarz, W. *Inorg. Chim. Acta* **1998**, *269*, 91.

53. Hitchcock, P. B.; Lappert, M. F.; Smith, R. G.; Bartlett, R. A.; Power, P. P. *J. Chem. Soc. Chem. Comm.* **1988**, 1007.

54. Schaverien, C. J.; Orpen, A. G. *Inorg. Chem.* **1991**, *30*, 4968.

55. Schaverien, C. J.; Nesbitt, G. J. *J. Chem. Soc. Dalton Trans.* **1992**, 157.

56. Den Haan, K. H.; De Boer, J. L.; Teuben, J. H.; Spek, A. L.; Kojic-Prodic, B.; Hays, G. R.; Huis, R. *Organometallics* **1986**, *5*, 1726.

57. Hultzsch, K. C.; Voth, P.; Beckerle, K.; Spaniol, T. P.; Okuda, J. *Organometallics* **2000**, *19*, 228.

58. Bambirra, S.; Meetsma, A.; Hessen, B. *Organometallics* **2006**, *25*, 3454.

59. Meyer, N.; Roesky, P. W.; Bambirra, S.; Meetsma, A.; Hessen, B.; Saliu, K.; Takats, J. *Organometallics* **2008**, *27*, 1501.

60. Mills, D. P.; Cooper, O. J.; McMaster, J.; Lewis, W.; Liddle, S. T. *Dalton Trans.* **2009**, 4547.

61. Arndt, S.; Zeimentz, P. M.; Spaniol, T. P.; Okuda, J.; Honda, M.; Tatsumi, K. *Dalton Trans.* **2003**, 3622.

62. Li, X.; Nishiura, M.; Hu, L.; Mori, K.; Hou, Z. *J. Am. Chem. Soc.* **2009**, *131*, 13870.

63. Cameron, T. M.; Gordon, J. C.; Scott, B. L. *Organometallics* **2004**, *23*, 2995.

64. Holton, J.; Lappert, M. F.; Ballard, D. G. H.; Pearce, R.; Atwood, J. L.; Hunter, W. E. *J. Chem. Soc. Dalton Trans.* **1979**, 45.

65. Du, G.; Wei, Y.; Zhang, W.; Dong, Y.; Lin, Z.; He, H.; Zhang, S.; Li, X. *Dalton Trans.* **2013**, *42*, 1278.

66. Wang, B.; Cui, D.; Lv, K. *Macromolecules* **2008**, *41*, 1983.

67. Rong, W.; Liu, D.; Zuo, H.; Pan, Y.; Jian, Z.; Li, S.; Cui, D. *Organometallics* **2013**, *32*, 1166.

68. Liu, B.; Li, L.; Sun, G.; Liu, J.; Wang, M.; Li, S.; Cui, D. *Macromolecules* **2014**, *47*, 4971.

69. Luconi, L.; Lyubov, D. M.; Rossin, A.; Glukhova, T. A.; Cherkasov, A. V.; Tuci, G.; Fukin, G. K.; Trifonov, A. A.; Giambastiani, G. *Organometallics* **2014**, *33*, 7125.

70. Lyubov, D. M.; Luconi, L.; Rossin, A.; Tuci, G.; Cherkasov, A. V.; Fukin, G. K.; Giambastiani, G.; Trifonov, A. A. *Chem. Eur. J.* **2014**, *20*, 3487.

71. Rad'kov, V.; Roisnel, T.; Trifonov, A.; Carpentier, J.-F.; Kirillov, E. *Eur. J. Inorg. Chem.* **2014**, *2014*, 4168.

72. Kretschmer, W. P.; Meetsma, A.; Hessen, B.; Schmalz, T.; Qayyum, S.; Kempe, R. *Chem. Eur. J.* **2006**, *12*, 8969.

73. Lyubov, D. M.; Cherkasov, A. V.; Fukin, G. K.; Ketkov, S. Y.; Shavyrin, A. S.; Trifonov, A. A. *Dalton Trans.* **2014**, *43*, 14450.

74. Wang, K.; Luo, G.; Hong, J.; Zhou, X.; Weng, L.; Luo, Y.; Zhang, L. *Angew. Chem. Int. Ed. Engl.* **2014**, *53*, 1053.

75. Hong, J.; Zhang, L.; Yu, X.; Li, M.; Zhang, Z.; Zheng, P.; Nishiura, M.; Hou, Z.; Zhou, X. *Chem. Eur. J.* **2011**, *17*, 2130.

76. Zhang, M.; Ni, X.; Shen, Z. *Organometallics* **2014**, *33*, 6861.

77. Song, G.; O, W. W. N.; Hou, Z. *J. Am. Chem. Soc.* **2014**, *136*, 12209.

78. Mou, Z.; Liu, B.; Liu, X.; Xie, H.; Rong, W.; Li, L.; Li, S.; Cui, D. *Macromolecules* **2014**, *47*, 2233.

79. Roesky, P. W.; Denninger, U.; Stern, C. L.; Marks, T. J. *Organometallics* **1997**, *16*, 4486.

80. Arndt, S.; Spaniol, T. P.; Okuda, J. *Organometallics* **2003**, *22*, 775.

81. Fryzuk, M. D.; Haddad, T. S.; Rettig, S. J. *Organometallics* **1991**, *10*, 2026.

82. Luo, Y.; Nishiura, M.; Hou, Z. *J. Organomet. Chem.* **2007**, *692*, 536.

83. Hitzbleck, J.; Okuda, J. *Organometallics* **2007**, *26*, 3227.

84. Ge, S.; Meetsma, A.; Hessen, B. *Organometallics* **2008**, *27*, 5339.

85. Xu, X.; Xu, X.; Chen, Y.; Sun, J. *Organometallics* **2008**, *27*, 758.

86. Konkol, M.; Kondracka, M.; Voth, P.; Spaniol, T. P.; Okuda, J. *Organometallics*

2008, *27*, 3774.

87. Gao, W.; Cui, D.; Liu, X.; Zhang, Y.; Mu, Y. *Organometallics* **2008**, *27*, 5889.

88. Nishiura, M.; Mashiko, T.; Hou, Z. *Chem. Comm.* **2008**, 2019.

89. Zimmermann, M.; Törnroos, K. W.; Sitzmann, H.; Anwander, R. *Chem. Eur. J.* **2008**, *14*, 7266.

90. Ge, S.; Meetsma, A.; Hessen, B. *Organometallics* **2009**, *28*, 719.

91. Luo, Y.; Wang, X.; Chen, J.; Luo, C.; Zhang, Y.; Yao, Y. *J. Organomet. Chem.* **2009**, *694*, 1289.

92. Li, S.; Cui, D.; Li, D.; Hou, Z. *Organometallics* **2009**, *28*, 4814.

93. Wang, B.; Tang, T.; Li, Y.; Cui, D. *Dalton Trans.* **2009**, 8963.

94. Nakajima, Y.; Hou, Z. *Organometallics* **2009**, *28*, 6861.

95. Litlabo, R.; Lee, H. S.; Niemeyer, M.; Tornroos, K. W.; Anwander, R. *Dalton Trans.* **2010**, *39*, 6815.

96. Trambitas, A. G.; Panda, T. K.; Jenter, J.; Roesky, P. W.; Daniliuc, C.; Hrib, C. G.; Jones, P. G.; Tamm, M. *Inorg. Chem.* **2010**, *49*, 2435.

97. Luo, Y.; Li, W.; Lin, D.; Yao, Y.; Zhang, Y.; Shen, Q. *Organometallics* **2010**, *29*, 3507.

98. Yang, Y.; Lv, K.; Wang, L.; Wang, Y.; Cui, D. *Chem. Comm.* **2010**, *46*, 6150.

99. Kaneko, H.; Tsurugi, H.; Panda, T. K.; Mashima, K. *Organometallics* **2010**, *29*, 3463.

100. Döring, C.; Kretschmer, W. P.; Kempe, R. *Eur. J. Inorg. Chem.* **2010**, *2010*, 2853.

101. Zhang, Z.; Cui, D.; Trifonov, A. A. *Eur. J. Inorg. Chem.* **2010**, *2010*, 2861.

102. Otero, A.; Lara-Sanchez, A.; Fernandez-Baeza, J.; Martinez-Caballero, E.; Marquez-Segovia, I.; Alonso-Moreno, C.; Sanchez-Barba, L. F.; Rodriguez, A. M.; Lopez -Solera, I. *Dalton Trans.* **2010**, *39*, 930.

103. Fegler, W.; Spaniol, T. P.; Okuda, J. *Dalton Trans.* **2010**, *39*, 6774.

104. Saliu, K. O.; Cheng, J.; McDonald, R.; Ferguson, M. J.; Takats, J. *Organometallics* **2010**, *29*, 4950.

105. Yang, Y.; Cui, D.; Chen, X. *Dalton Trans.* **2010**, *39*, 3959.

106. Yuan, Y.; Chen, Y.; Li, G.; Xia, W. *Organometallics* **2010**, *29*, 3722.

107. Zimmermann, M.; Volbeda, J.; Törnroos, K. W.; Anwander, R. *C. R. Chimie* **2010**, *13*, 651.

108. Zhang, Z.; Cui, D. *Chem. Eur. J.* **2011**, *17*, 11520.

109. Wang, L.; Cui, D.; Hou, Z.; Li, W.; Li, Y. *Organometallics* **2011**, *30*, 760.

110. Du, G.; Wei, Y.; Ai, L.; Chen, Y.; Xu, Q.; Liu, X.; Zhang, S.; Hou, Z.; Li, X. *Organometallics* **2011**, *30*, 160.

111. Saleh, L. M. A.; Birjkumar, K. H.; Protchenko, A. V.; Schwarz, A. D.; Aldridge, S.; Jones, C.; Kaltsoyannis, N.; Mountford, P. *J. Am. Chem. Soc.* **2011**, *133*, 3836.

112. Hangaly, N. K.; Petrov, A. R.; Rufanov, K. A.; Harms, K.; Elfferding, M.; Sundermeyer, J. *Organometallics* **2011**, *30*, 4544.

113. Rufanov, K. A.; Petrov, A. R.; Kotov, V. V.; Laquai, F.; Sundermeyer, J. *Eur. J. Inorg. Chem.* **2005**, *2005*, 3805.

114. Rad'kov, V. Y.; Skvortsov, G. G.; Lyubov, D. M.; Cherkasov, A. V.; Fukin, G. K.; Shavyrin, A. S.; Cui, D.; Trifonov, A. A. *Eur. J. Inorg. Chem.* **2012**, *2012*, 2289.

115. Jian, Z.; Cui, D. *Dalton Trans.* **2012**, *41*, 2367.

116. Tolpygin, A. O.; Shavyrin, A. S.; Cherkasov, A. V.; Fukin, G. K.; Trifonov, A. A. *Organometallics* **2012**, *31*, 5405.

117. Johnson, K. R. D.; Hannon, M. A.; Ritch, J. S.; Hayes, P. G. *Dalton Trans.* **2012**, *41*, 7873.

118. Jian, Z.; Petrov, A. R.; Hangaly, N. K.; Li, S.; Rong, W.; Mou, Z.; Rufanov, K. A.; Harms, K.; Sundermeyer, J.; Cui, D. *Organometallics* **2012**, *31*, 4267.

119. Pan, Y.; Rong, W.; Jian, Z.; Cui, D. *Macromolecules* **2012**, *45*, 1248.

120. Wang, L.; Liu, D.; Cui, D. *Organometallics* **2012**, *31*, 6014.

121. Rong, W.; Cheng, J.; Mou, Z.; Xie, H.; Cui, D. *Organometallics* **2013**, *32*, 5523.

122. Hong, J.; Zhang, L.; Wang, K.; Chen, Z.; Wu, L.; Zhou, X. *Organometallics* **2013**, *32*, 7312.

123. Li, M.; Hong, J.; Chen, Z.; Zhou, X.; Zhang, L. *Dalton Trans.* **2013**, *42*, 8288.

124. Hong, J.; Zhang, L.; Wang, K.; Zhang, Y.; Weng, L.; Zhou, X. *Chem. Eur. J.* **2013**, *19*, 7865.

125. Kissel, A. A.; Lyubov, D. M.; Mahrova, T. V.; Fukin, G. K.; Cherkasov, A. V.; Glukhova, T. A.; Cui, D.; Trifonov, A. A. *Dalton Trans.* **2013**, *42*, 9211.

126. Kulinna, H.; Spaniol, T. P.; Okuda, J. *J. Organomet. Chem.* **2013**, *744*, 49.

127. Hamidi, S.; Jende, L. N.; Martin Dietrich, H.; Maichle-Mössmer, C.; Törnroos, K. W.; Deacon, G. B.; Junk, P. C.; Anwander, R. *Organometallics* **2013**, *32*, 1209.

128. Masuda, J. D.; Jantunen, K. C.; Ozerov, O. V.; Noonan, K. J. T.; Gates, D. P.; Scott, B. L.; Kiplinger, J. L. *J. Am. Chem. Soc.* **2008**, *130*, 2408.

129. Liu, B.; Cui, D.; Ma, J.; Chen, X.; Jing, X. *Chem. Eur. J.* **2007**, *13*, 834.

130. Scholz, J.; Schlegel, M.; Thiele, K.-H. *Chemische Berichte* **1987**, *120*, 1369.

131. Miller, J. B.; Schwartz, J.; Carroll, K. M. *Organometallics* **1993**, *12*, 4204.

132. Tosin, G.; Santini, C. C.; Taoufik, M.; Mallmann, A. D.; Basset, J.-M. *Organometallics* **2006**, *25*, 3324.

133. Cheon, J.; Rogers, D. M.; Girolami, G. S. *J. Am. Chem. Soc.* **1997**, *119*, 6804.

134. So, L.-C.; Liu, C.-C.; Chan, M. C. W.; Lo, J. C. Y.; Sze, K.-H.; Zhu, N. *Chem. Eur. J.* **2012**, *18*, 565.

135. Dimitrov, V.; Thiele, K. H.; Schenke, D. *Z. Anorg. Allg. Chem.* **1985**, *527*, 85.

136. Jantunen, K. C.; Scott, B. L.; Kiplinger, J. L. *J. Alloys Compd.* **2007**, *444–445*, 363.

137. Kobeissi, M.; Cherry, K.; Jomaa, W. *Synthetic Commun.* **2013**, *43*, 2955.

138. Willner, A.; Niemeyer, J.; Mitzel, N. W. *Dalton Trans.* **2009**, 4473.

139. Shin, J. H.; Hascall, T.; Parkin, G. *Organometallics* **1999**, *18*, 6.

140. Van de Heisteeg, B. J. J.; Schat, G.; Akkerman, O. S.; Bickelhaupt, F. *Organometallics* **1985**, *4*, 1141.

141. Seetz, J. W. F. L.; Schat, G.; Akkerman, O. S.; Bickelhaupt, F. *Angew. Chem.* **1983**, *95*, 242.

142. Tikkanen, W. R.; Liu, J. Z.; Egan, J. W.; Petersen, J. L. *Organometallics* **1984**, *3*, 825.

143. Yousaf, S. M.; Farona, M. F.; Shively, R. J.; Youngs, W. J. *J. Organomet. Chem.* **1989**, *363*, 281.

144. Zachmanoglou, C. E.; Docrat, A.; Bridgewater, B. M.; Parkin, G.; Brandow, C. G.; Bercaw, J. E.; Jardine, C. N.; Lyall, M.; Green, J. C.; Keister, J. B. *J. Am. Chem. Soc.* **2002**, *124*, 9525.

145. Chirik, P. J.; Day, M. W.; Bercaw, J. E. *Organometallics* **1999**, *18*, 1873.

146. Courtot, P.; Pichon, R.; Salaun, J. Y.; Toupet, L. *J. Can. Chem.* **1991**, *69*, 661.

147. Benito-Garagorri, D.; Bernskoetter, W. H.; Lobkovsky, E.; Chirik, P. J. *Organometallics* **2009**, *28*, 4807.

148. Sietzen, M.; Batke, S.; Merz, L.; Wadepohl, H.; Ballmann, J. *Organometallics* **2015**, *34*, 1118.

149. Sietzen, M.; Wadepohl, H.; Ballmann, J. *Organometallics* **2014**, *33*, 612.

150. Jun, S. H.; Park, J. H.; Lee, C. S.; Park, S. Y.; Go, M. J.; Lee, J.; Lee, B. Y. *Organometallics* **2013**, *32*, 7357.

151. Baumann, R.; Stumpf, R.; Davis, W. M.; Liang, L.-C.; Schrock, R. R. *J. Am. Chem. Soc.* **1999**, *121*, 7822.

152. Plundrich, G. T.; Wadepohl, H.; Gade, L. H. *Inorg. Chem.* **2016**, *55*, 353.

153. Romain, C.; Specklin, D.; Miqueu, K.; Sotiropoulos, J.-M.; Fliedel, C.; Bellemin-Laponnaz, S.; Dagorne, S. *Organometallics* **2015**, *34*, 4854.

154. Andersen, R. A. *Inorg. Chem.* **1979**, *18*, 2928.

155. Planalp, R. P.; Andersen, R. A.; Zalkin, A. *Organometallics* **1983**, *2*, 16.

156. Yu, X.; Bi, S.; Guzei, I. A.; Lin, Z.; Xue, Z.-L. *Inorg. Chem.* **2004**, *43*, 7111.

157. Weng, W.; Yang, L.; Foxman, B. M.; Ozerov, O. V. *Organometallics* **2004**, *23*, 4700.

158. Brammell, C. M.; Pelton, E. J.; Chen, C.-H.; Yakovenko, A. A.; Weng, W.; Foxman, B. M.; Ozerov, O. V. *J. Organomet. Chem.* **2011**, *696*, 4132.

159. Kamitani, M.; Pinter, B.; Chen, C.-H.; Pink, M.; Mindiola, D. J. *Angew. Chem. Int. Ed.* **2014**, *53*, 10913.

160. Schrock, R. R.; Liang, L.-C.; Baumann, R.; Davis, W. M. *J. Organomet. Chem.* **1999**, *591*, 163.

161. Bei, X.; Swenson, D. C.; Jordan, R. F. *Organometallics* **1997**, *16*, 3282.

162. Martin, A.; Uhrhammer, R.; Gardner, T. G.; Jordan, R. F.; Rogers, R. D. *Organometallics* **1998**, *17*, 382.

163. Figueroa, R.; Froese, R. D.; He, Y.; Klosin, J.; Theriault, C. N.; Abboud, K. A. *Organometallics* **2011**, *30*, 1695.

164. Fontaine, P. P.; Figueroa, R.; McCann, S. D.; Mort, D.; Klosin, J. *Organometallics* **2013**, *32*, 2963.

165. Klosin, J.; Fontaine, P. P.; Figueroa, R.; McCann, S. D.; Mort, D. *Organometallics* **2013**, *32*, 6488.

166. Fontaine, P. P.; Ueligger, S.; Klosin, J.; Hazari, A.; Daller, J.; Hou, J. *Organometallics* **2015**, *34*, 1354.

167. Elsner, F. H.; Tilley, T. D.; Rheingold, A. L.; Geib, S. J. *J. Organomet. Chem.* **1988**, *358*, 169.

168. Crowther, D. J.; Baenziger, N. C.; Jordan, R. F. *J. Am. Chem. Soc.* **1991**, *113*, 1455.

169. Visser, C. Doctoral Thesis, University of Groningen, 2003.

170. Visser, C.; van den Hende, J. R.; Meetsma, A.; Hessen, B.; Teuben, J. H. *Organometallics* **2001**, *20*, 1620.

171. (171) Beswick, C. L.; Marks, T. J. *J. Am. Chem. Soc.* **2000**, *122*, 10358.

172. Amor, J. I.; Cuenca, T.; Galakhov, M.; Gómez-Sal, P.; Manzanero, A.; Royo, P. *J. Organomet. Chem.* **1997**, *535*, 155.

173. Cuenca, T.; Montejano, C.; Royo, P. *J. Organomet. Chem.* **1996**, *514*, 93.

174. Amor, J.; Cuenca, T.; Galakhov, M.; Royo, P. *J. Organomet. Chem.* **1995**, *497*, 127.

175. Chirik, P. J.; Bercaw, J. E. *Organometallics* **2005**, *24*, 5407.

176. Jimenez Pindado, G.; Thornton-Pett, M.; Bochmann, M. *J. Chem. Soc. Dalton Trans.* **1998**, 393.

177. Spencer, L. P.; Fryzuk, M. D. *J. Organomet. Chem.* **2005**, *690*, 5788.

178. Herzog, A.; Roesky, H. W.; Jäger, F.; Steiner, A.; Noltemeyer, M. *Organometallics* **1996**, *15*, 909.

179. Siedle, A. R.; Newmark, R. A. *J. Organomet. Chem.* **1995**, *497*, 119.

180. Bayram, M.; Bläser, D.; Wölper, C.; Schulz, S. *Organometallics* **2015**, *34*, 3421.

181. Chamberlain, L. R.; Rothwell, I. P.; Folting, K.; Huffman, J. C. *J. Chem. Soc. Dalton Trans.* **1987**, 155.

182. Chesnut, R. W.; Durfee, L. D.; Fanwick, P. E.; Rothwell, I. P.; Folting, K.; Huffman, J. C. *Polyhedron* **1987**, *6*, 2019.

183. Chesnut, R. W.; Jacob, G. G.; Yu, J. S.; Fanwick, P. E.; Rothwell, I. P. *Organometallics* **1991**, *10*, 321.

184. Chesnut, R. W.; Yu, J. S.; Fanwick, P. E.; Rothwell, I. P.; Huffman, J. C. *Polyhedron* **1990**, *9*, 1051.

185. Antinolo, A.; Dorado, I.; Fajardo, M.; Garces, A.; Kubicki, M. M.; Lopez-Mardomingo, C.; Otero, A. *Dalton Trans.* **2003**, 910.

186. Arteaga-Müller, R.; Sánchez-Nieves, J.; Ramos, J.; Royo, P.; Mosquera, M. E. G. *Organometallics* **2008**, *27*, 1417.

187. Anderson, L. L.; Schmidt, J. A. R.; Arnold, J.; Bergman, R. G. *Organometallics* **2006**, *25*, 3394.

188. Prashar, S.; Fajardo, M.; Garcés, A.; Dorado, I.; Antiñolo, A.; Otero, A.; López-Solera, I.; López-Mardomingo, C. *J. Organomet. Chem.* **2004**, *689*, 1304.

189. Nechayev, M.; Kriegel, B. M.; Gianetti, T. L.; Bergman, R. G.; Arnold, J. *Inorg. Chim. Acta* **2014**, *422*, 114.

190. Schmidt, S.; Sundermeyer, J. *J. Organomet. Chem.* **1994**, *472*, 127.

191. Herrmann, W. A.; Baratta, W.; Herdtweck, E. *J. Organomet. Chem.* **1997**, *541*, 445.

192. McLain, S. J.; Wood, C. D.; Schrock, R. R. *J. Am. Chem. Soc.* **1979**, *101*, 4558.

193. Castro, A.; Galakhov, Mikhail V.; Gómez, M.; Gómez-Sal, P.; Martín, A.; Sánchez, F.; Velasco, P. *Eur. J. Inorg. Chem.* **2000**, *2000*, 2047.

194. Gibson, V. C.; Poole, A. D.; Siemeling, U.; Williams, D. N.; Clegg, W.; Hockless, D. C. R. *J. Organomet. Chem.* **1993**, *462*, C12.

195. McLain, S. J.; Schrock, R. R.; Sharp, P. R.; Churchill, M. R.; Youngs, W. J. *J. Am. Chem. Soc.* **1979**, *101*, 263.

196. Galajov, M.; Garcia, C.; Gomez, M.; Gomez-Sal, P. *Dalton Trans.* **2014**, *43*, 5747.

197. Elorriaga, D.; Galajov, M.; García, C.; Gómez, M.; Gómez-Sal, P. *Organometallics* **2012**, *31*, 5089.

198. Sietzen, M.; Wadepohl, H.; Ballmann, J. *Inorg. Chem.* **2015**, *54*, 4094.

199. Schrock, R. R.; Fellmann, J. D. *J. Am. Chem. Soc.* **1978**, *100*, 3359.

200. Andersen, R. A.; Galyer, A. L.; Wilkinson, G. *Angew. Chem. Int. Ed.* **1976**, *15*,

609.

201. Fanwick, P. E.; Ogilvy, A. E.; Rothwell, I. P. *Organometallics* **1987**, *6*, 73.

202. de Castro, I.; de la Mata, J.; Gómez, M.; Gómez-Sal, P.; Royo, P.; Selas, J. M. *Polyhedron* **1992**, *11*, 1023.

203. J. Bailey, N.; A. Cooper, J.; Gailus, H.; L. H. Green, M.; Thomas James, J.; A. Leech, M. *J. Chem. Soc. Dalton Trans.* **1997**, 3579.

204. McCullough, L. G.; Schrock, R. R.; Dewan, J. C.; Murdzek, J. C. *J. Am. Chem. Soc.* **1985**, *107*, 5987.

205. Schrock, R. R.; Clark, D. N.; Sancho, J.; Wengrovius, J. H.; Rocklage, S. M.; Pedersen, S. F. *Organometallics* **1982**, *1*, 1645.

206. Andersen, R. A.; Chisholm, M. H.; Gibson, J. F.; Reichert, W. W.; Rothwell, I. P.; Wilkinson, G. *Inorg. Chem.* **1981**, *20*, 3934.

207. Sinha, A.; Lopez, L. P. H.; Schrock, R. R.; Hock, A. S.; Müller, P. *Organometallics* **2006**, *25*, 1412.

208. Schrock, R. R.; DePue, R. T.; Feldman, J.; Yap, K. B.; Yang, D. C.; Davis, W. M.; Park, L.; DiMare, M.; Schofield, M. *Organometallics* **1990**, *9*, 2262.

209. Schrock, R. R.; Murdzek, J. S.; Bazan, G. C.; Robbins, J.; DiMare, M.; O'Regan, M. *J. Am. Chem. Soc.* **1990**, *112*, 3875.

210. Bochkarev, L. N.; Skatova, A. A.; Begantsova, Yu. E.; Shcherbakov, V. I.; Malysheva, I. P.; Basova, G. V.; Fukin, G. K.; Kurskii, Yu. A.; Khorshev, S. Ya.; Barinova, Yu. P.; Abakumov G. A. *Russ. Chem. Bull.* **2005**, *54*, 606.

211. Bochkarev, L. N.; Scherbakov, V. I.; Malysheva, I. P.; Basova, G. V.; Stolyarova, N. E.; Grigorieva, I. K.; Bochkarev, A. L.; Fukin, G. K.; Kurskii, Y. A.; Abakumov,

G. A. *J. Organomet. Chem.* **2006**, *691*, 983.

212. Axtell, J. C.; Schrock, R. R.; Müller, P.; Hoveyda, A. H. *Organometallics* **2015**, *34*, 2110.

213. Feldman, J.; Murdzek, J. S.; Davis, W. M.; Schrock, R. R. *Organometallics* **1989**, *8*, 2260.

214. Radius, U.; Wahl, G.; Sundermeyer, J. *Z. Anorg. Allg. Chem.* **2004**, *630*, 848.

215. Wang, W.-D.; Guzei, I. A.; Espenson, J. H. *Inorg. Chem.* **2000**, *39*, 4107.

216. Bryan, J. C.; Burrell, A. K.; Miller, M. M.; Smith, W. H.; Burns, C. J.; Sattelberger, A. P. *Polyhedron* **1993**, *12*, 1769.

217. Wu, Z.; Diminnie, J. B.; Xue, Z. *Inorg. Chem.* **1998**, *37*, 6366.

218. Woo, H. G.; Heyn, R. H.; Tilley, T. D. *J. Am. Chem. Soc.* **1992**, *114*, 5698.

219. Woo, H. G.; Freeman, W. P.; Tilley, T. D. *Organometallics* **1992**, *11*, 2198.

220. Fryzuk, M. D.; Haddad, T. S. *J. Am. Chem. Soc.* **1988**, *110*, 8263.

221. Fryzuk, M. D.; Haddad, T. S. *J. Chem. Soci. Chem. Comm.* **1990**, 1088.

222. Fryzuk, M. D.; Jafarpour, L.; Kerton, F. M.; Love, J. B.; Rettig, S. J. *Angew. Chem. Int. Ed.* **2000**, *39*, 767.

223. Fryzuk, M. D.; Yu, P.; Patrick, B. O. *Can. J. Chem.* **2001**, *79*, 1194.

224. Halcovitch, N. R.; Fryzuk, M. D. *Dalton Trans.* **2012**, *41*, 1524.

225. Bailey, B. C.; Huffman, J. C.; Mindiola, D. J.; Weng, W.; Ozerov, O. V. *Organometallics* **2005**, *24*, 1390.

226. Fryzuk, M. D.; Corkin, J. R.; Patrick, B. O. *Can. J. Chem.* **2003**, *81*, 1376.

227. Fryzuk, M. D.; Carter, A.; Rettig, S. J. *Organometallics* **1992**, *11*, 469.

228. Fryzuk, M. D.; Mao, S. S. H.; Zaworotko, M. J.; MacGillivray, L. R. *J. Am. Chem.*

Soc. **1993**, *115*, 5336.

229. Fryzuk, M. D.; Duval, P. B.; Patrick, B. O.; Rettig, S. J. *Organometallics* **2001**, *20*, 1608.

230. Blaurock, S.; Hey-Hawkins, E. *Z. Anorg. Allg. Chem.* **2002**, *628*, 2515.

231. Morise, X.; Green, M. L. H.; Braunstein, P.; Rees, L. H.; Vei, I. C. *New J. Chem.* **2003**, *27*, 32.

232. Schrock, R. R.; Messerle, L. W.; Wood, C. D.; Guggenberger, L. J. *J. Am. Chem. Soc.* **1978**, *100*, 3793.

233. Rupprecht, G. A.; Messerle, L. W.; Fellmann, J. D.; Schrock, R. R. *J. Am. Chem. Soc.* **1980**, *102*, 6236.

234. Sinha, A.; Schrock, R. R. *Organometallics* **2004**, *23*, 1643.

235. Lopez, L. P. H.; Schrock, R. R. *J. Am. Chem. Soc.* **2004**, *126*, 9526.

236. Schrock, R. R.; Feldman, J.; Cannizzo, L. F.; Grubbs, R. H. *Macromolecules* **1987**, *20*, 1169.

237. Murdzek, J. S.; Schrock, R. R. *Organometallics* **1987**, *6*, 1373.

238. Schrock, R. R.; Crowe, W. E.; Bazan, G. C.; DiMare, M.; O'Regan, M. B.; Schofield, M. H. *Organometallics* **1991**, *10*, 1832.

239. Schrock, R. R.; DePue, R. T.; Feldman, J.; Schaverien, C. J.; Dewan, J. C.; Liu, A. H. *J. Am. Chem. Soc.* **1988**, *110*, 1423.

240. Jeong, H.; Kozera, D. J.; Schrock, R. R.; Smith, S. J.; Zhang, J.; Ren, N.; Hillmyer, M. A. *Organometallics* **2013**, *32*, 4843.

241. Jeong, H.; Axtell, J. C.; Török, B.; Schrock, R. R.; Müller, P. *Organometallics* **2012**, *31*, 6522.

242. Bochkarev, L. N.; Nikitinskii, A. V.; Begantsova, Y. E.; Shcherbakov, V. I.; Stolyarova, N. E.; Grigorieva, I. K.; Malysheva, I. P.; Basova, G. V.; Fukin, G. K.; Baranov, E. V.; Kurskii, Y. A.; Abakumov, G. A. *J. Organomet. Chem.* **2005**, *690*, 3212.

243. Bochkarev, L. N.; Begantsova, Y. E.; Bochkarev, A. L.; Stolyarova, N. E.; Grigorieva, I. K.; Malysheva, I. P.; Basova, G. V.; Platonova, E. O.; Fukin, G. K.; Baranov, E. V.; Kurskii, Y. A.; Abakumov, G. A. *J. Organomet. Chem.* **2006**, *691*, 5240.

244. Bailey, B. C.; Schrock, R. R.; Kundu, S.; Goldman, A. S.; Huang, Z.; Brookhart, M. *Organometallics* **2009**, *28*, 355.

245. Oskam, J. H.; Fox, H. H.; Yap, K. B.; McConville, D. H.; O`Dell, R.; Lichtenstein, B. J.; Schrock, R. R. *J. Organomet. Chem.* **1993**, *459*, 185.

246. Gerber, L. C. H.; Schrock, R. R.; Müller, P.; Takase, M. K. *J. Am. Chem. Soc.* **2011**, *133*, 18142.

247. Gerber, L. C. H.; Schrock, R. R.; Müller, P. *Organometallics* **2013**, *32*, 2373.

248. McCullough, L. G.; Schrock, R. R. *J. Am. Chem. Soc.* **1984**, *106*, 4067.

249. Churchill, M. R.; Ziller, J. W.; Freudenberger, J. H.; Schrock, R. R. *Organometallics* **1984**, *3*, 1554.

250. Freudenberger, J. H.; Pedersen, S. F.; Schrock, R. R. *Bull. Soc. Chim. Fr.* **1985**, 349.

251. Strutz, H.; Schrock, R. R. *Organometallics* **1984**, *3*, 1600.

252. Wengrovius, J. H.; Sancho, J.; Schrock, R. R. *J. Am. Chem. Soc.* **1981**, *103*, 3932.

253. Chisholm, M. H.; Delbridge, E. E.; Kidwell; A. R.; Quinlan, K. B. *Chem. Comm.* **2003**, 126.

254. Listemann, M. L.; Schrock, R. R. *Organometallics* **1985**, *4*, 74.

255. Schrock, R. R.; Murdzek, J. S.; Freudenberger, J. H.; Churchill, M. R.; Ziller, J. W. *Organometallics* **1986**, *5*, 25.

256. Murdzek, J. S.; Blum, L.; Schrock, R. R. *Organometallics* **1988**, *7*, 436.

257. Seidel, S. W.; Schrock, R. R.; Davis, W. M. *Organometallics* **1998**, *17*, 1058.

258. Greco, G. E.; O'Donoghue, M. B.; Seidel, S. W.; Davis, W. M.; Schrock, R. R. *Organometallics* **2000**, *19*, 1132.

259. Cochran, F. V.; Hock, A. S.; Schrock, R. R. *Organometallics* **2004**, *23*, 665.

260. Figgis, B. N.; Kidd, R. G.; Nyholm, R. S. *Proc. R. Soc. A* **1962**, *269*, 469.

261. Kaupp, M.; Malkin, V. G.; Malkina, O. L.; Salahub, D. R. *J. Am. Chem. Soc.* **1995**, *117*, 1851.

262. Dean, P. A. W.; Evans, D. F. *J. Chem. Soc. A: Inorg. Phys. Theo.* **1967**, 698.

263. Dungan, C. H.; Van Wazer, J. R. *Compilation of Reported F^{19} NMR Chemical Shifts*; Wiley, 1970.

264. Muetterties, E. L.; Phillips, W. D. *J. Am. Chem. Soc.* **1959**, *81*, 1084.

265. Buslaev, Y. A.; Tarasov, V. P.; Petrosyants, S. P. *J. Struct. Chem. (Translation of Zh. Strukt. Khim.)* **1968**, *9*, 146.

266. Herzog, A.; Liu, F.-Q.; Roesky, H. W.; Demsar, A.; Keller, K.; Noltemeyer, M.; Pauer, F. *Organometallics* **1994**, *13*, 1251.

267. (Kraft, B. M.; Lachicotte, R. J.; Jones, W. D. *J. Am. Chem. Soc.* **2001**, *123*, 10973.

268. Rieth, R. D.; Brennessel, W. W.; Jones, W. D. *Eur. J. Inorg. Chem.* **2007**, *2007*, 2839.

269. Piglosiewicz, I. M.; Kraft, S.; Beckhaus, R.; Haase, D.; Saak, W. *Eur. J. Inorg. Chem.* **2005**, *2005*, 938.

270. Murphy, E. F.; Yu, P.; Dietrich, S.; Roesky, H. W.; Parisini, E.; Noltemeyer, M. *J. Chem. Soc. Dalton Trans.* **1996**, 1983.

271. Murphy, E. F.; Lübben, T.; Herzog, A.; Roesky, H. W.; Demsar, A.; Noltemeyer, M.; Schmidt, H.-G. *Inorg. Chem.* **1996**, *35*, 23.

272. Dorn, H.; Shah, S. A. A.; Parisini, E.; Noltemeyer, M.; Schmidt, H.-G.; Roesky, H. W. *Inorg. Chem.* **1996**, *35*, 7181.

273. Herzog, A.; Roesky, H. W.; Jager, F.; Steiner, A. *Chem. Comm.* **1996**, 29.

274. Brownstein, S. *Inorg. Chem.* **1973**, *12*, 584.

275. Marchetti, F.; Pampaloni, G.; Zacchini, S. *J. Fluorine Chem.* **2010**, *131*, 21.

276. Buslayev, Y. A.; Ilyin, E. G.; Ignatov, M. E.; Butorina, L. S.; Mastryukova, T. A. *J. Fluorine Chem.* **1978**, *12*, 387.

277. Levason, W.; Reid, G.; Zhang, W. *J. Fluorine Chem.* **2015**, *172*, 62.

278. Hibbert, R. C. *J. Chem. Soc. Dalton Trans.* **1986**, 751.

279. Köhler, J.; Simon, A.; van Wüllen, L.; Cordier, S.; Roisnel, T.; Poulain, M.; Somer, M. *Z. Anorg. Allg. Chem.* **2002**, *628*, 2683.

280. Marchetti, F.; Pampaloni, G.; Pinzino, C.; Zacchini, S. *Eur. J. Inorg. Chem.* **2013**, *2013*, 5755.

281. Levason, W.; Light, M. E.; Reid, G.; Zhang, W. *Dalton Trans.* **2014**, *43*, 9557.

282. Bini, R.; Chiappe, C.; Marchetti, F.; Pampaloni, G.; Zacchini, S. *Inorg. Chem.*

2010, *49*, 339.

283. Funaioli, T.; Marchetti, F.; Pampaloni, G.; Zacchini, S. *Dalton Trans.* **2013**, *42*, 14168.

284. Brownstein, S.; Christian, B. H.; Latremouille, G.; Steigel, A. *Can. J. Chem.* **1976**, *54*, 2343.

285. Bartlett, N.; Beaton, S.; Reeves, L. W.; Wells, E. J. *Can. J. Chem.* **1964**, *42*, 2531.

286. Bougon, R.; Bui Huy, T.; Charpin, P. *Inorg. Chem.* **1975**, *14*, 1822.

287. Holloway, J. H.; Schrobilgen, G. J. *Inorg. Chem.* **1981**, *20*, 3363.

288. Holloway, J. H.; Schrobilgen, G. J. *Inorg. Chem.* **1980**, *19*, 2632.

289. Binenboym, J.; El-Gad, U.; Selig, H. *Inorg. Chem.* **1974**, *13*, 319.

290. The DFT calculations were carried out with ADF[291-293] by Prof. Michael G. Richmond and Dr. David A. Hrovat (University of North Texas) using Becke's three-parameter hybrid exchange functional[294] and the correlation functional of Lee-Yang-Parr (B3LYP).[295] Relativistic effects were treated by the 2-component zeroth-order regular approximation (ZORA)[296-298] with spin-orbit coupling included. Geometries were optimized with the polarized triple-ζ basis set (TZP)[299] and NMR shielding calculations were carried out with the polarized quadruple-ζ basis set (QZ4P)[299] at these geometries.

291. ADF2016, SCM, Theoretical Chemistry, Vrije Universiteit, Amsterdam, The Netherlands, http://www.scm.com

292. te Velde, G.; Bickelhaupt, F. M.; Baerends, E. J.; Fonseca Guerra, C.; van Gisbergen, S. J. A.; Snijders, J. G.; Ziegler, T. *J. Comp. Chem.* **2001**, *22*, 931.

293. Fonseca Guerra, C.; Snijders, J. G.; te Velde, G.; Baerends, E. J. *Theor. Chem. Acc.* **1998**, *99*, 391.

294. Becke, A. D. *J. Chem. Phys.* **1993**, *98*, 5648.

295. Lee, C.; Yang, W.; Parr, R. G. *Phys. Rev. B*. **1988**, *37*, 785.

296. van Lenthe, E.; Ehlers, A. E.; Baerends, E. J. *J. Chem. Phys.* **1999**, *110*, 8943.

297. van Lenthe, E.; Baerends, E. J.; Snijders, J. G. *J. Chem. Phys.* **1994**, *101*, 9783.

298. van Lenthe, E.; Baerends, E. J.; Snijders, J. G. *J. Chem. Phys*. **1993**, *99*, 4597.

299. van Lenthe, E.; Baerends, E. J. *J. Comp. Chem.* **2003**, *24*, 1142.

Vita

Tabitha Marie Cook (née Callaway) was born on September 15, 1988 in Warner Robins, Georgia to Michael and Heidi Callaway. Her adolescence education was though Houston County public school systems. She graduated from Warner Robins High School in June 2007. The following fall, she enrolled at Berry College in Rome, Ga. She conducted undergraduate research at Berry College under Dr. Kenneth Martin studying crystallography of phenol and phenolate compounds. She graduated in 2011 with a B.S. in chemistry and a minor in biology. In August 2011, she enrolled at the University of Tennessee and joined Dr. Zi-Ling Xue's group.